Optimization of Loudspeakers using Material and Shape Optimization.

Nielsen, Daniel Gert

Publication date:
2021

Document Version
Publisher's PDF, also known as Version of record

DTU Electrical Engineering
Department of Electrical Engineering

Optimization of loudspeakers using material and shape optimization

Daniel Gert Nielsen - PhD Thesis

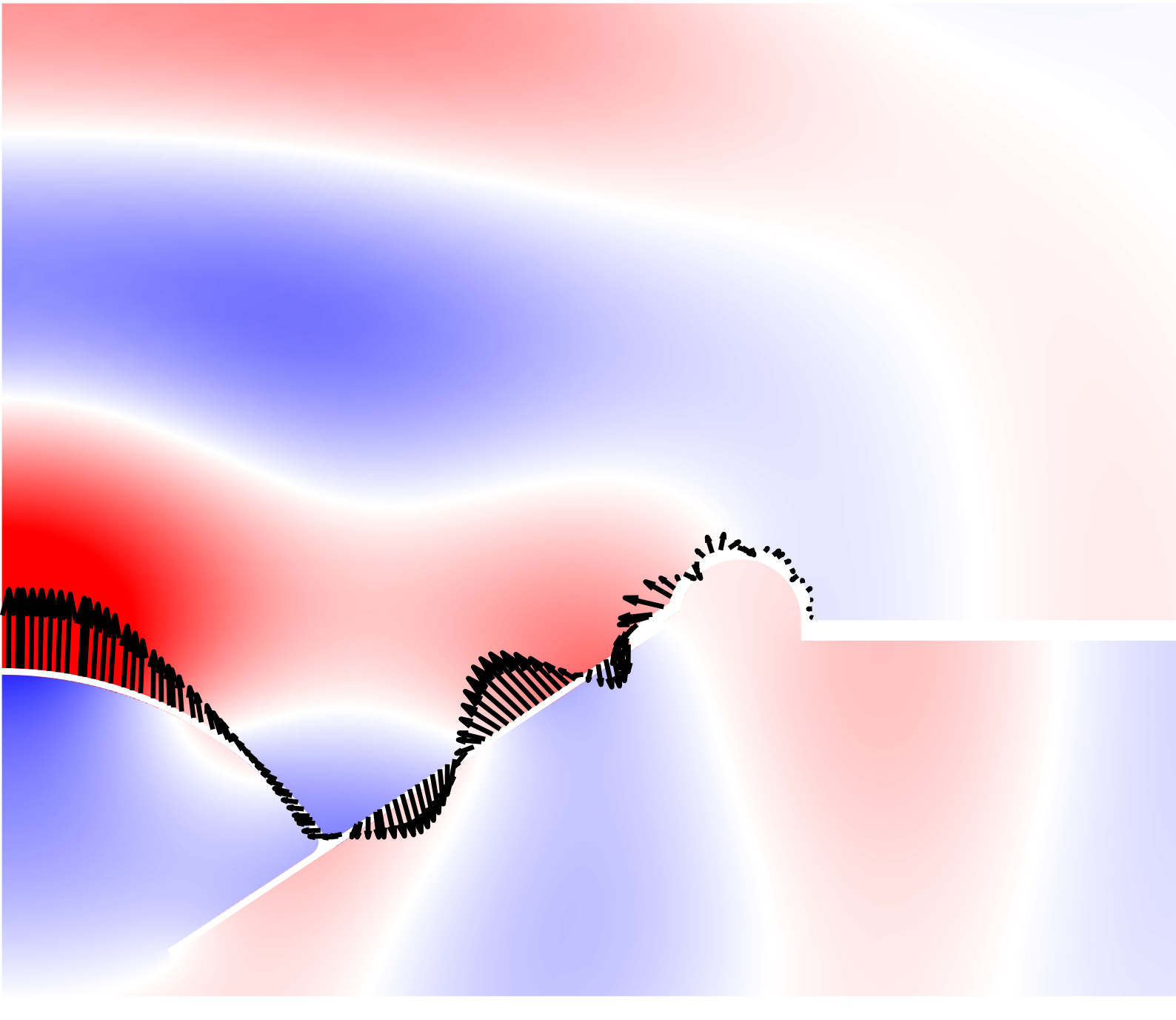

Optimization of Loudspeakers using Material and Shape Optimization

PhD Thesis
Feb, 2021

Author
Daniel Gert Nielsen

Supervisors
Assoc. Prof. Finn Thomas Agerkvist
Prof. MSO Jakob Søndergaard Jensen

Preface: This thesis was submitted to the Technical University of Denmark (DTU) in partial fulfillment of the requirements for the degree of Doctor of Philosophy (Ph.D.) in Electronics and Communication. The project is a part of the Signature Project, which was founded as a strategic partnership between DTU and Korea Advanced Institute of Science and Technology (KAIST). This project is funded by DTU. The work presented in this thesis was completed between March 1, 2018, and February 28, 2021, at the Acoustic Technology Group of the Department of Electrical Engineering, DTU, under the supervision of Associate Professor Finn T. Agerkvist and Professor MSO Jakob Søndergaard Jensen.

Published by: DTU, Acoustic Technology Group, Ørsteds Plads, Building 352, 2800 Kgs. Lyngby Denmark
www.https://www.act.elektro.dtu.dk/

Abstract

Loudspeakers are an integral part of modern-day society, and their applications are many. It is a technology that has matured over many decades and is used in a wide range of products with diverse use cases. The maturity of the technology also means that there are no obvious improvements to be made to the existing technology in most instances. Therefore, this work is centered around utilizing numerical optimization techniques, as they can generate new designs, ideas, or concepts that have yet to be introduced by more conventional design methods.

Firstly, the thesis concerns the modeling aspect of loudspeakers. Here, a hybrid approach is developed where a fully coupled finite element model is coupled to a lumped parameter model. The model is able to mimic a reference model of a full loudspeaker, even at very high frequencies.

Subsequently, the work is centered around improving the quality of sound radiated from loudspeaker drivers and compact speakers. The design problems considered are formulated to be applicable in broad frequency ranges. This thesis investigates the positive influence on the frequency response and directivity that can be gained from optimizing the material layout in the speaker diaphragm and surround. The design of the material layout is determined with a density-based optimization approach. A generic 5-inch loudspeaker unit is considered in a target frequency range of 600 Hz up to 10 kHz; here, a completely flat on-axis response is achieved with the proposed optimization method. It is also shown that the method can be used to control the directivity of the loudspeaker unit to obtain a wider listening window where both the on-axis and off-axis response is reasonably flat and aligned. The method is also applied to determine the homogeneous material properties of a passive radiator to enhance the low frequency performance of a smart speaker significantly. Furthermore, the application of shape optimization relying on the principles of free form deformation with nonlinear element constraints is developed. The suggested approach uses element constraints to ensure that the quality of the mesh is not degraded during the optimization. The design problem considers a compact speaker consisting of a down-firing woofer and an acoustic lens. The suggested approach can produce smooth and uncomplicated designs that are able to yield a well-behaved horizontal frequency response in the frequency range from 90 Hz to 10 kHz.

Resumé

Højttalere er en integreret del af det moderne samfund, og deres applikationer er mange. Det er en teknologi, der er modnet over mange årtier og bruges i en bred vifte af produkter med forskellige anvendelsesområder. Modenheden af teknologien betyder også, at der i de fleste tilfælde ikke er nogen åbenlyse forbedringer af den eksisterende teknologi. Derfor er dette arbejde centreret omkring anvendelse af numeriske optimeringsmetoder, da de kan generere nye designs, ideer eller koncepter, som endnu ikke er opdaget med mere konventionelle designmetoder.

For det første omhandler afhandlingen modelleringsaspektet af højttalere. Her udvikles en hybrid model, hvor en fuldt koblet finite element model er koblet til et ækvivalent diagram. Modellen er i stand til at efterligne en referencemodel af en usimplificeret højttaler, selv ved meget høje frekvenser.

Herefter bruges modellen til at forbedre lydkvaliteten fra højttalerenheder og kompakte højttalere. De fleste af de betragtede designproblemer er formuleret til at være anvendelige i brede frekvensområder. Denne afhandling undersøger den positive indflydelse på frekvensresponset og direktiviteten, som kan opnås ved at optimere materialefordelingen i højttalermembranen og det ydre ophæng. Designet af materialefordelingen bestemmes med en densitetsbaseret optimeringsmetode. En generisk 5-tommer højttalerenhed betragtes i et frekvensområde fra 600 Hz op til 10 kHz; her opnås en fuldstændig flad respons on-axis med den udviklede optimeringsmetode. Det er også vist, at metoden kan bruges til at styre højttalerenhedens direktivitet for at opnå et bredere lyttevindue, hvor både on-axis og off-axis respons er tilnærmelsesvist flade og på samme niveau. Metoden anvendes også til at bestemme de homogene materialegenskaber for en passiv radiator inkorporeret i en kompakt højtaler for at forbedre dens output ved lave frekvenser. Desuden udvikles en metode til brug af formoptimering, der bygger på principperne fra free form deformation med ikke-lineære elementbegrænsninger. Den udviklede metode bruger elementbegrænsninger for at sikre, at kvaliteten af meshet ikke forringes under optimeringen. Designproblemet omhandler en kompakt højttaler, der består af en nedad-strålende bashøjttaler og en akustisk linse. Den foreslåede tilgang kan producere glatte og ukomplicerede designs, der er i stand til at give et forholdsvist fladt frekvensrespons i frekvensområdet fra 90 Hz til 10 kHz.

Acknowledgements

Firstly, I would like to thank my two supervisors Finn and Jakob, I am grateful for your help and support throughout my PhD study. Thank you for embracing my ideas and helping me bring them to life. Your suggestions for improving things in the development phase, your help with a physical understanding of the problems-at-hand and your knowledge about mechanics, acoustics, numerical methods, and loudspeaker design have been invaluable to this project.

It has been a great pleasure to be a part of the DTU Acoustic technology group, I have enjoyed being part of an ambitious, inspiring, and cheerful department. A special thanks to my office mates and colleagues in the signature project and the CAMM group members for the many useful discussions and support.

In particular, I want to thank Peter Risby Andersen for the many fruitful discussions we have had throughout this project. You have also kept my spirits high during difficult times, and I am very grateful for that. I would also like to thank Jonas Brunskog and Peter Risby Andersen for reading my thesis. Your comments and suggestions have been very thoughtful and valuable to this work.

Part of this work was carried out in collaboration with Professor Yong-Hwa Park and Gyeong-Tae Lee at KAIST in South Korea during my visit in February 2020. The exchange was facilitated through the Signature project, which was a project founded as strategic partnership between DTU and KAIST. Although my time there was cut short due to the pandemic, I felt very welcome when I was there. A special thanks to Gyeong-Tae Lee for showing me around campus, helping me mesh into the group, and also for our valuable discussions and collaboration.

Finally, I would like to thank my friends and family for your moral support and fun times. Thank you, Andreas, for always being up for a hunting trip; that has often cleared my mind. A special thanks to my fiancee Emilie for always believing in me, I am grateful for your love, support, and encouragement.

Publications

The thesis is based on the following papers:

Paper 1 Nielsen, D. G., Andersen, P. R., Jensen, J. S., and Agerkvist, F. T. (2020). *Estimation of Optimal Values for Lumped Elements in a Finite Element - Lumped Parameter Model of a Loudspeaker*. Journal of Computational Acoustics, 28(2), 2050012.
https://doi.org/10.1142/S2591728520500127

Paper 2 Nielsen, D. G., Agerkvist, F. T., and Jensen, J. S. (2019). *Optimization of realistic loudspeaker models with respect to basic response characteristics*. Proceedings of 23rd International Congress on Acoustics, 2019-, 6219–6226.
https://doi.org/10.18154/RWTH-CONV-239709

Paper 3 Nielsen, D. G., Lee, G-T., Park, Y-H., Jensen, J. S., and Agerkvist, F. T.(2020). *Optimization of the Performance of Small Speaker Systems with Passive Radiators*. In Proceedings of 49th International Congress and Exposition on Noise Control Engineering

Paper 4 Nielsen, D. G., Agerkvist, F. T., and Jensen, J. S. (2021). *Achieving a flat wideband frequency response by numerical optimization of a loudspeaker unit with requirements for its directivity*. Submitted to JASA (Under revision)

Paper 5 Nielsen, D. G., Andersen, P. R., and Agerkvist, F. T (2021). *Shape optimization of compact loudspeakers using free form deformation and the finite element method*. (Manuscript)

A conference publication was also written during the PhD but is not included in this thesis due to content overlap with **Paper 1**.

Nielsen, D. G., Jensen, J. S., Cutanda Henriquez, V., and Agerkvist, F. T. (2019). *Finite element model coupled with lumped parameter elements*. Proceedings of 14th International Conference on Theoretical and Computational Acoustics, 291–198.

Contents

List of Symbols

r	Radial position
z	Axial position
Ω_s	Solid domain
Ω_a	Acoustic domain
Ω_A	Acoustic domain - PML layer
Γ_{as}	Interface between mechanical and acoustic domain
Γ_s	Clamped boundary
Γ_{sym}	Boundary subject to symmetry boundary conditions
Γ_A	Outer boundary of acoustic domain
$\delta\Omega_s$	Boundary of Ω_s
$\delta\Omega_a$	Boundary of Ω_a
z^*	Axial position of PML
r^*	Radial position of PML
z_{PML}	Axial position of current element in PML
r_{PML}	Radial position of current element in PML
e	Element number e
ρ_s	Density of solid structure
ω	Excitation frequency in radians
$\mathbf{u}$	Nodal displacement vector
∇	Divergence operator
$\boldsymbol{\sigma}$	Cauchy stress tensor
$\mathbf{f}$	Nodal force vector
v	Test function
$\boldsymbol{\epsilon}$	Strain vector
ν	Poisson's ratio
$\mathbf{D}$	Constitutive matrix
$\mathbf{N}$	Structural shape function matrix
$\mathbf{K}$	Structural stiffness matrix
$\mathbf{M}$	Structural mass matrix
$\mathbf{B}$	Strain-displacement matrix
η	Isotropic loss factor
c	Speed of sound
p	Pressure
$\mathbf{n}$	Surface normal
$\mathbf{N}_a$	Acoustic shape function matrix
$\mathbf{p}$	Nodal Pressure
$\mathbf{K}_a$	Acoustic stiffness matrix
$\mathbf{M}_a$	Acoustic mass matrix
γ_r	PML coefficient in the radial direction
γ_z	PML coefficient in the axial direction
κ	Absorption coefficient in the PML
$\mathbf{S}$	Coupling matrix

e_g	Appliad voltage
i_c	Current
R_E	DC resistance
L_E	Inductance
Bl	Force factor
$M_{p,lump}$	Mass of lumped structural components
$R_{p,lump}$	Damping in lumped structural components
$C_{p,lump}$	Compliance of lumped structural components
$\widetilde{\mathbf{K}}$	Augmented coupled stiffness matrix
$\widetilde{\mathbf{M}}$	Augmented coupled mass matrix
$\widetilde{\mathbf{C}}$	Velocity proportional terms from lumped model
$\tilde{\mathbf{S}}$	System matrix of state equation
$\tilde{\mathbf{u}}$	Nodal solution vector containing $\mathbf{u}$, $\mathbf{p}$ and i_c
$\mathbf{z}$	Impedance
$\tilde{\mathbf{f}}$	Excitation vector containing e_g
$\mathbf{x}$	Vector containing design variables
x_j	Design variable number j
$\phi_0(\mathbf{x})$	Objective function
α_e	Element design variable controlling element stiffness
β_e	Element design variable controlling element mass
ζ_e	Element design variable controlling element damping
$(\ldots)_{min}$	Lower bound on material property
$(\ldots)_{max}$	Upper bound on material property
E_e	Element stiffness
ρ_e	Element density
η_e	Element damping
x_e	Element design variable
$\mathbf{d}_{i,j}$	Control point
$\mathbf{q}_{i,j}$	Coordinate of control point
$b_i(s)$	Bernstein polynomial
$b_j(t)$	Bernstein polynomial
x_l	Design variable related to control point
L_l	Lower bound of box constraint
L_h	Upper bound of box constraint
b	Total number of frequencies included in design problem
q	Total number of constraints included in the design problem
a	Total number of design variables included in the design problem
$g_i(\mathbf{x})$	Inequality constraint number i
T_L	Target line
$\boldsymbol{\lambda}_k$	Lagrange multiplier for frequency number k
$\mathbf{L}$	Indicator matrix
$\boldsymbol{\tau}_n$	Indicator vector for angle number n

1 Introduction

1.1 Motivation and Goal

Loudspeakers have been used for many years for a wide range of applications. They have made it possible to enjoy music at home effortlessly, create the illusion of almost being present in the movie you are watching in a cinema, or provide loud and clear stage sound from a concert, to name but a few. The invention of the loudspeaker by Johann Philipp Reis in 1861 and its refined version in 1876 invented by Alexander Graham Bell opened up a whole new world for the people living in the 19th century. The loudspeaker was invented as a part of the telephone and made it possible for people to communicate in new ways, something we today take for granted. Continuous effort eventually led to the discovery of the moving-coil loudspeaker in 1898, and in 1924 the moving-coil-loudspeaker we know today was discovered. Further improvements to the loudspeaker's components made the speaker cheaper to a point where it could be produced in larger numbers and be affordable to more people. The demands to the quality of speakers have not slowed down; Colloms and Darlington [1] gives a historical overview of the specifications on the frequency response of ideal two-way domestic loudspeaker systems as a function of time. In 1965 ±6dB between 100Hz to 10 kHz was acceptable, in 1985 it was ±3dB between 50Hz and 18kHz and finally in 2012 the authors suggest ±2dB within ±10° vertical and ±4dB within ±30° vertical. This development emphasizes that the loudspeaker technology today has matured over time.

The quality of sound is often regarded as subjective, and thus the perceived quality of sound may differ between individuals. While it is true that two different people can perceive sound differently, one might question whether it is possible, at least to some degree, to quantify the quality of sound. Toole [2] states that quantification of sound quality should not be disregarded as a design parameter for loudspeakers. This is backed up by a comprehensive study carried out in [3] where the main conclusion is that a smooth, flat and wide-band frequency response with a similarly well-behaved off-axis response is the key aspect of a loudspeaker.

The improvements of loudspeakers can, to some extend, be attributed to trial-and-error type of research where different materials, shapes, and designs of the individual loudspeaker components have been implemented and listened to. The evaluation of the quality is often performed by expert listeners and accompanied by measurements. Another popular design approach uses lumped parameter models (LPM)s [4, 5]. Lumped parameter models are essentially equivalent circuits representing electric, mechanical and acoustic components, they are convenient to use and accurately capture the movement of the dynamic speaker at low frequencies. By simulating the LPM in the time domain, one can also include some of the many nonlinearities that are present in loudspeakers [6, 7].

As predicted by Moore's law [8], the available computational power continuously increases. This has allowed for the use of more computationally heavy methods, such as the finite element method (FEM), to compute the response of loudspeakers. The advantage of using numerical methods is that it allows for calculating the frequency response at frequencies

where higher-order mechanical resonances in the diaphragm play a significant role. Furthermore, it allows for more advanced numerical optimization techniques that can aid in the design process of loudspeakers with respect to an objective function based on a quantitative evaluation of sound quality. Christensen and Olhoff [9] optimizes a flat loudspeaker diaphragm with respect to uniform directivity. They optimize discrete ring masses in a 2D-axisymmetric model with the intention of having a piston-like movement in a wide frequency range. The paper also considers shape optimization of the loudspeaker diaphragm. The optimization problems include single frequency optimization and a problem with three discrete frequencies. The frequency range is wide, but the frequency resolution included in the design problem is not very dense. It is shown that uniform radiation can be achieved for the three discrete frequencies. However, more frequencies are needed to be included in the optimization problem to see whether the solutions are applicable in a broad frequency range. Work has been done on purely acoustic problems where the goal was to improve the performance of an acoustic horn; here the excitation is a plane wave and the simulated geometry was in 2D, the shape was optimized using topology optimization [10]. A more recent example with a similar setup uses shape optimization to design the interior of the acoustic horn, and the exterior lens is designed with topology optimization [11]. In [11] the widest frequency range examined is two octaves. The boundary element method has been used to simulate and design an acoustic lens improving the sound quality of a domestic speaker system [12]. In hearing-aids, topology optimization is also used to reduce the amount of trial-and-error research associated with building physical models and testing new suspension designs used for reducing the feedback between the microphone and the receiver[13, 14, 15]. These models are often fully coupled as to bring the numerical model as close to the physical model as possible. To the author's knowledge, the literature available for similar optimization strategies for fully coupled numerical models of loudspeakers is more scarce. With the ever-growing capabilities of commercial software packages, the author believes that these tools are indeed used for product development within the loudspeaker industry. However, this is not reflected in scientific publications. These techniques might be able to take loudspeaker design to the next level and bring new and novel ideas for shape and material configurations. Very recently a surge in published material on this particular subject has happened. In [16] several numerical optimization strategies for loudspeakers are discussed. In [17] optimal port designs for loudspeaker cabinets are created with numerical methods and [18] uses topology and shape optimization to design loudspeaker components such as the magnet and the basket. In [19] a metamaterial inspired from causal-optimal acoustic absorbers were proposed to reduce the influence from the cabinet on the frequency response.

In general, most people enjoying music do so within the comfort of their own home and when they are commuting. In that sense, the amount of research spent within the different listening areas is a bit skewed. This is pointed out by Toole in [2], where he gives an estimate of how much research time is spent on different listening areas compared to how much time is spent listening in these areas. This overview can be seen in Fig. 1.1. This thesis deals with a vital part of the listening experience in homes, namely the loudspeaker. Toole claims in [2] that loudspeakers are the single most important factor in sound reproduction. However, it must be acknowledged that there are many other facets and nuances to achieve high fidelity sound from a domestic loudspeaker, such as cabinet design and the influence of the room.

This thesis's main scope is to optimize the frequency response and directivity of loudspeakers. This is accomplished by applying numerical methods and gradient-based optimization techniques to improve the wide-band performance of loudspeakers. Specifically, the me-

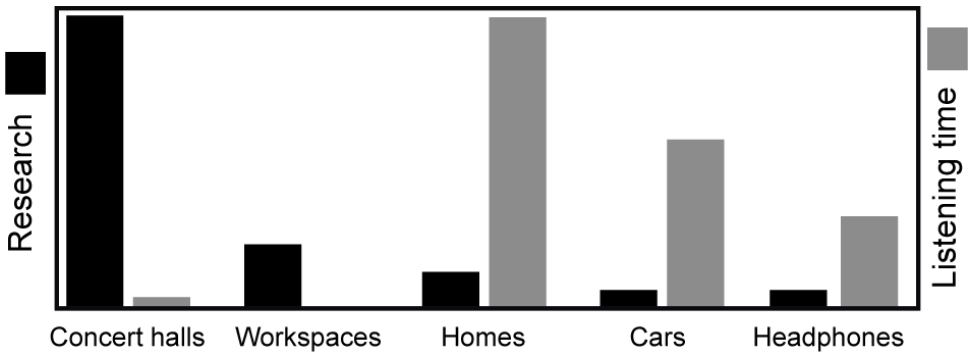

Figure 1.1: A crude comparison between the amount of research for a certain listening space and the amount of listening time spend in each space. The figure is from [2] and the rights to use it was kindly provided by Floyd E. Toole.

chanical parts of the dynamic speaker are subject to improvements. This work has been carried out in sequential order; first, the method and the computational tools necessary to model the problem has been developed, secondly, optimization methods have been build upon this method. Two types of optimization techniques are applied to the loudspeaker; a density-based approach is used to optimize the materials in the speaker diaphragm and outer suspension. Shape optimization is utilized to optimize the speaker diaphragm and an acoustic lens of a compact speaker. These optimization methods rely on a discretized model domain, and therefore parts of the thesis are also concerned with the modeling aspect of loudspeakers.

1.2 Structure

The thesis is structured in the following way. Chapter 2 introduces the equations and finite element theory required to solve a fully coupled vibro-acoustic problem. Chapter 3 provides an overview of lumped parameter models and how they can be coupled to the finite element model in order to reduce the complexity of the numerical model, this work constitutes [P1]. Chapter 4 gives an introduction to numerical optimization techniques, especially density-based methods and shape optimization is explained. The chapter also summarizes the objective functions used in this work and the associated adjoint problem. Chapter 5 presents the work done with the density-based material optimization approach. The method is used to optimize an initial example concerning a flat disk [P2], the low frequency performance of a smart speaker [P3], and also for customizing directivity and obtaining a flat frequency response [P4]. Chapter 6 contains results from [P5], here an acoustic lens has been added to the smart speaker example, and both the shape of the lens and the speaker is optimized to achieve a flat horizontal frequency response. Finally, Chapter 7 present a brief summary, conclusions, and suggestions for expanding on the work done in this thesis.

The chapters including papers end with a contribution section. This section highlights the major contributions to the known literature from the paper(s).

1.3 A Reader's Guide

This thesis uses abbreviations; the first time an abbreviation is introduced, the words to be abbreviated are written out, followed by the abbreviation in parenthesis, e.g. finite element method (FEM). Subsequent uses of the abbreviation are used without explanation. Similarly, nontrivial mathematical symbols are defined the first time they are used in a

formula, successive uses follow the introduced notation. Scalar values are written in italics, vectors are bold letters, and matrices are bold capital letters, e.g. L_E, $\mathbf{f}$ and $\mathbf{M}$.

2 Finite Element Theory for Coupled Acoustic-Structure Problems

Solving partial differential equations (PDE)s are a part of many engineering disciplines, in some cases, it is possible to derive analytical solutions to the PDEs and thereby obtain exact solutions. However, in many practical examples, it is not possible to solve the PDEs analytically, and it is, as a consequence, necessary to approximate the solution of the PDEs with numerical methods. The FEM[20, 21] used in this work was introduced in the 1940s [22, 23] and has since then evolved into a popular method covering a vast field of engineering disciplines. Other methods for solving PDEs exist; such as the boundary element method [24, 25], the finite volume method [26] and the finite difference method [27].

The general FE theory presented in this Chapter is expanded in Chapter 3 by coupling the acoustic-structure model to a lumped model of the electric motor system, the spider, and the voice coil. This method is then applied to design problems in Chapters 5-6. Besides reducing the complexity of the numerical model by coupling it to a lumped model, it is chosen to consider the design problems as 2D-axisymmetric. The general shape of loudspeaker units suggests that the shapes considered generally are symmetric. However, several features on loudspeakers are asymmetric, and some loudspeaker designs are also asymmetric. It should be noted that at very high frequencies our modeling choice implies that the implemented approach does not capture a-symmetric and rocking modes. These modes are generally not considered to yield a high quality of sound and the exclusion of them is therefore a limitation in the current model approach. However, it was shown in [28] that an axisymmetric FE model is able to match measurements accurately up to 10 kHz. Efficiency and reduced complexity is a necessity. The optimizations carried out in chapter 5-6 generally runs 50-300 iterations where most of the computation cost can be attributed to solving the numerical model and computing the design sensitivities.

2.1 The Finite Element Method

The following sections provide an overview of the FEM used to solve the unbounded coupled acoustic-structure problem. A sketch of the model domains with an arbitrarily shaped mechanical domain is shown in Fig. 2.1. For an in-depth explanation of the FEM see [20].

2.1.1 Mechanical Finite Elements

Fig. 2.2 shows an arbitrary mechanical domain that is discretized into a finite number of non-overlapping elements connected in the element nodes. In this work, quadratic iso-parametric six node triangular elements are used for the structure and acoustic domain, except for [P2] where 9 node iso-parametric rectangular elements were used. The advantage of using higher-order elements is that they are better at approximating the solution and therefore fewer elements can be used in the mesh. Triangular elements are also an advantage when meshing curved, thin, and complex geometries as they are better at resolving complex geometries than square elements. For the rectangular region, Ω_a representing the perfectly matched layer (PML) iso-parametric nine node elements have

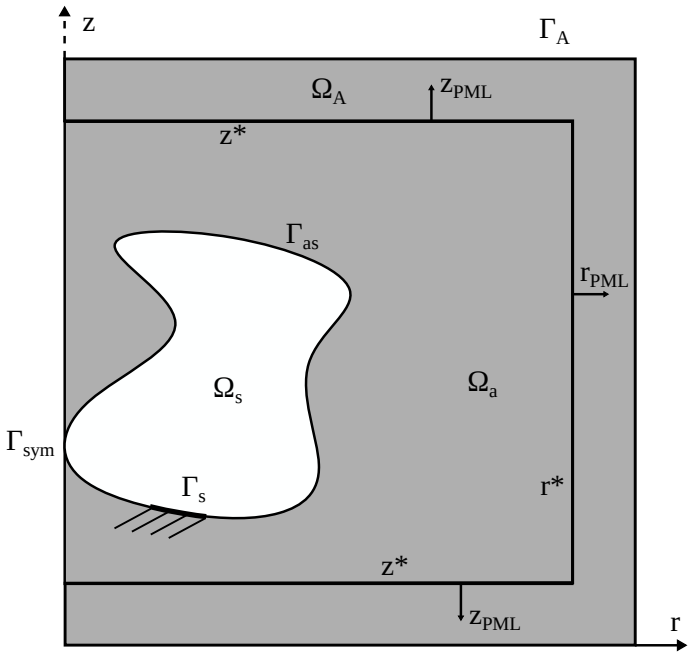

Figure 2.1: Sketch of a general axisymmetric acoustic-structure coupled problem including the perfectly matched layer. Ω_s is the structural domain, Ω_a is the acoustic domain, Ω_A is the perfectly matched layer, Γ_{as} denotes the interface between the acoustic and structural domain, Γ_{sym} is the surface subject to axisymmetric boundary conditions, on Γ_s the structure is clamped and Γ_A denotes the outer boundary.

been used. The resolution of the mesh is determined by the wavelength; in this work, 6 elements per wavelength is used.

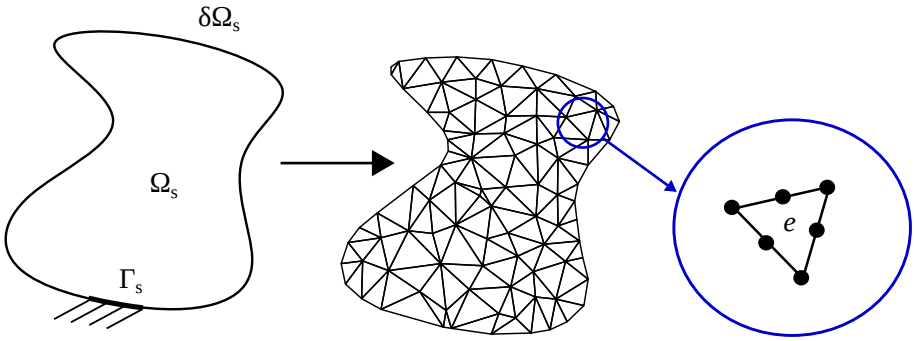

Figure 2.2: Sketch of a mechanical domain Ω_s, its outer boundary $\delta\Omega_s$ and clamped boundary Γ_s. The discretization of the domain into triangular elements is shown together with close up of element e.

The governing equations for the time-harmonic motion assuming a linear elastic isotropic body with small deformations and where body forces has been neglected are

$$\rho_s \omega^2 \mathbf{u} + \nabla \cdot \boldsymbol{\sigma}(\mathbf{u}) = \mathbf{0} \qquad \text{in} \quad \Omega_s \tag{2.1}$$

here ρ is the mass density of the material, ω is the excitation frequency in radians, $\mathbf{u}$ is the structural displacements, $\boldsymbol{\sigma}$ is the Cauchy stress tensor, Ω_s is the structural domain with the boundary $\delta\Omega_s$.

A forcing term, $\mathbf{f}$, is added on the boundary, $\delta\Omega_s$, of the PDE in Eq. (2.1). The weak form of the PDE can is derived with the Galerkin method. The PDE is first multiplied with an admissible test function, v, and then integrated over the model domain and then Greens theorem is applied to obtain the weak form of the equation

$$-\omega^2\rho_s\int_{\Omega_s} v\mathbf{u}\,\mathrm{dV}+\int_{\Omega_s}\nabla v\cdot\boldsymbol{\sigma}\,\mathrm{dV}=\int_{\delta\Omega_s} v\mathbf{f}\,\mathrm{dS}. \tag{2.2}$$

Hook's law $\boldsymbol{\sigma}=\mathbf{D}\boldsymbol{\epsilon}$, relates the stresses to the strains via a constitutive matrix $\mathbf{C}$ [20]

$$\mathbf{D}=\frac{(1-\nu)E}{(1+\nu)(1-2\nu)}\begin{bmatrix}1 & f & f & 0\\ f & 1 & f & 0\\ f & f & 1 & 0\\ 0 & 0 & 0 & g\end{bmatrix}\quad\text{with}\quad f=\frac{\nu}{1-\nu}\quad\text{and}\quad g=\frac{1-2\nu}{2(1-\nu)} \tag{2.3}$$

where the strains for a 2D axisymmetric structure needs to take into account the circumferential strain, such that we have the following relation

$$\begin{Bmatrix}\epsilon_r\\ \epsilon_\theta\\ \epsilon_z\\ \gamma_{zr}\end{Bmatrix}=\boldsymbol{\partial}\begin{Bmatrix}u_r\\ u_z\end{Bmatrix}\quad\text{with}\quad\boldsymbol{\partial}=\begin{bmatrix}\frac{\partial}{\partial r} & 0\\ 1/r & 0\\ 0 & \frac{\partial}{\partial z}\\ \frac{\partial}{\partial z} & \frac{\partial}{\partial r}\end{bmatrix}. \tag{2.4}$$

Replacing the test functions in Eq. (2.2) with $\mathbf{N}$, where $\mathbf{N}$ is a matrix consisting of the quadratic iso-parametric shape functions and inserting Hook's law instead of $\boldsymbol{\sigma}$ yields

$$\int_{\Omega_s}\int_{-\pi}^{\pi}\boldsymbol{\partial}\mathbf{N}^T\mathbf{D}\boldsymbol{\partial}\mathbf{N}r\,\mathrm{d}\theta\mathrm{d}\Omega_s\mathbf{u}-\omega^2\rho_s\int_{\Omega_s}\int_{-\pi}^{\pi}\mathbf{N}^T\mathbf{N}r\,\mathrm{d}\theta\mathrm{d}\Omega_s\mathbf{u}=\int_{\delta\Omega_s}\int_{-\pi}^{\pi}\mathbf{N}^T\mathbf{f}r\,\mathrm{d}\theta\mathrm{d}\delta\Omega_s. \tag{2.5}$$

Here r is the radial distance from the center axis. Equation (2.5) can be posed as the more well known matrix equation

$$\left(\mathbf{K}-\omega^2\mathbf{M}\right)\mathbf{u}=\mathbf{f}, \tag{2.6}$$

with $\mathbf{B}=\boldsymbol{\partial}\mathbf{N}$ being the strain-displacement matrix we can identify the FE matrices for the mechanical system on element level as

$$\mathbf{K}=\int_{\Omega_s}\int_{-\pi}^{\pi}\mathbf{B}^T\mathbf{D}\mathbf{B}r\,\mathrm{d}\theta\mathrm{d}\Omega_s \tag{2.7}$$

$$\mathbf{M}=\int_{\Omega_s}\int_{-\pi}^{\pi}\rho\mathbf{N}^T\mathbf{N}r\,\mathrm{d}\theta\mathrm{d}\Omega_s \tag{2.8}$$

$$\mathbf{f}=\int_{\delta\Omega_s}\int_{-\pi}^{\pi}\mathbf{N}^T\mathbf{f}\,\mathrm{d}\theta\mathrm{d}\delta\Omega_s. \tag{2.9}$$

Damping in the mechanical components are often considered as an isotropic structural loss factor [28], denoted η, such that the stiffness becomes complex $\mathbf{K}=\mathbf{K}\,(1+j\eta)$, where j is the imaginary number, this formulation assumes homogeneous distribution of damping.

Boundary Conditions
Due to the nature of Eq. (2.5), it is not necessary to specify a specific boundary condition on free surfaces since this particular boundary condition is self-fulfilling by setting $\mathbf{f}$ equal to zero on all free surfaces.

For 2D-axisymmetric structures it is imperative to impose symmetry boundary conditions on the surfaces at $r = 0$. This boundary condition essentially ensures that the structure cannot move in a non-physical sense. This means that displacements in the r-direction at $r = 0$ is prohibited

$$u_r = 0 \quad \text{on} \quad \Gamma_{sym}. \tag{2.10}$$

A principal boundary condition often used in this work is the clamped boundary condition. This boundary condition is shown as Γ_s on Fig. 2.2. The boundary conditions prescribes that all nodal DOFs on the surface are equal to 0

$$u = 0 \quad \text{on} \quad \Gamma_s. \tag{2.11}$$

2.1.2 Acoustic Finite Elements

Under the assumption that the fluid is perfectly elastic, isotropic, homogeneous, inviscid and that it is perturbed with small amplitudes the pressure in the acoustic domain can be computed using the Helmholtz equation. Using time-harmonic analysis the Helmholtz equation in the frequency domain can be posed as

$$\nabla^2 p + \frac{\omega^2}{c^2} p = 0 \quad \text{in} \quad \Omega_a \tag{2.12}$$

here ∇^2 is the Laplace operator in cylindrical coordinates, p is the pressure and c is the speed of sound in air and Ω_a is the acoustic domain with the boundary $\delta\Omega_a$. Equation (2.12) is multiplied with an admissible test function, v, and integrated over the volume

$$\int_{\Omega_a} \left(v\nabla^2 p + v\frac{\omega^2}{c^2} p \right) \, \mathrm{dV} = 0, \tag{2.13}$$

Greens first identity is used to get rid of the second order term in eq. (2.13)

$$\int_{\Omega_a} \left(v\nabla^2 p + \nabla v \nabla p \right) \, \mathrm{dV} = \int_{\delta\Omega_a} v \left(\nabla p \cdot \mathbf{n} \right) \, \mathrm{dS}$$
$$\int_{\Omega_a} v\nabla^2 p \, \mathrm{dV} = \int_{\delta\Omega_a} v \left(\nabla p \cdot \mathbf{n} \right) \, \mathrm{dS} - \int_{\Omega_a} \nabla v \nabla p \, \mathrm{dV}.$$

A hard wall boundary condition can be imposed on the surface $\delta\Omega_a$

$$\mathbf{n} \cdot \nabla p = 0 \quad \text{on} \quad \delta\Omega_a,$$

which implies that the term $\int_{\delta\Omega_a} v \left(\nabla p \cdot \mathbf{n} \right) \, \mathrm{dS}$ vanishes and the second order term in Eq. (2.13) can be substituted with $-\int_{\Omega_a} \nabla v \nabla p \, \mathrm{dV}$ to obtain the weak formulation of the Helmholtz equation

$$\int_{\Omega_a} \left(\nabla v \nabla p - v\frac{\omega^2}{c^2} p \right) \, \mathrm{dV} = 0. \tag{2.14}$$

The weak formulation is discretized in the domain and the shape functions $\mathbf{N}_a$ is introduced. The shape functions are used to describe the pressure field, such that $p = \mathbf{N}_a \mathbf{p}$, where $\mathbf{p}$ is the FE solution of the pressure in each node. Galerkin finite elements are used and the test function v is now substituted with $\mathbf{N}_a$ and p with $\mathbf{N}_a \mathbf{p}$ in Eq. (2.14) to obtain the discretized Helmholtz equation

$$\int_{\Omega_a}\int_{-\pi}^{\pi}\left(\nabla\mathbf{N}_a^T\nabla\mathbf{N}_a-\frac{\omega^2}{c^2}\mathbf{N}_a^T\mathbf{N}_a\right)\mathbf{p}\,\mathrm{d}\theta\mathrm{d}\Omega_a=\mathbf{0}. \tag{2.15}$$

Equation (2.15) can be written in matrix form as

$$\left(\mathbf{K}_a-\omega^2\mathbf{M}_a\right)\mathbf{p}=\mathbf{0}, \tag{2.16}$$

where the acoustic stiffness and mass matrix[1] is

$$\mathbf{K}_a=\int_{\Omega_a}\int_{-\pi}^{\pi}\left(\mathbf{N}_{a,r}^T\mathbf{N}_{a,r}+\mathbf{N}_{a,z}^T\mathbf{N}_{a,z}\right)r\,\mathrm{d}\theta\mathrm{d}\Omega_a \tag{2.17}$$

$$\mathbf{M}_a=\int_{\Omega_a}\int_{-\pi}^{\pi}\frac{1}{c^2}\mathbf{N}_a^T\mathbf{N}_a r\,\mathrm{d}\theta\mathrm{d}\Omega_a. \tag{2.18}$$

Subscript r and z refers to the derivative with respect to the r and z direction, respectively.

Perfectly Matched Layers

The primary purpose of the PML is to give the approximate effect of an infinite domain even though the simulation domain is always finite. The PML is an artificial absorbing layer added around the computational acoustic domain to absorb propagating waves. The first formulation of a PML was developed by Bérenger [30] to simulate Maxwell's equations in an unbounded domain. The method developed by Bérenger relied on the so-called split-field PML. Bérenger's approach proved useful in many different disciplines in which propagating waves should be damped instead of reflected. Collino and Monk [31] showed how the PML could be applied to the Helmholtz equation to truncate an acoustic domain. This approach, among many others following Bérenger, relies on stretched-coordinate PML, where the coordinates inside the PML are mapped to complex numbers. This mapping allows for replacing the propagating waves with exponentially decaying waves within the PML. Inside the PML a modified Helmholtz equation is solved

$$\frac{1}{\gamma_r}\frac{\partial}{\partial r}\left(\frac{1}{\gamma_r}\frac{\partial p}{\partial r}\right)+\frac{1}{\gamma_z}\frac{\partial}{\partial z}\left(\frac{1}{\gamma_z}\frac{\partial p}{\partial z}\right)+\frac{\omega^2}{c^2}p=0\quad\text{in}\quad\Omega_A, \tag{2.19}$$

here γ_r and γ_z are complex numbers that scales with the position inside the PML in the r and z direction

$$\gamma_r(r_{PML})=1-j\kappa\left(\frac{r_{PML}-r^*}{t}\right)^2 \tag{2.20}$$

$$\gamma_z(z_{PML})=1-j\kappa\left(\frac{z_{PML}-z^*}{t}\right)^2. \tag{2.21}$$

Where r^* and z^*, are the interface coordinates between the PML/acoustic domain and r_{PML} and z_{PML} are the positions within the PML, κ is the absorption coefficient which is a tune-able parameter and t is half the thickness of the PML. These parameters are illustrated on Fig. 2.1.

Generally, papers regarding PML methods use frequency dependent γ coefficients because it gives the lowest error. The frequency scaling of the coefficients accounts for the different

[1] The acoustic stiffness matrix is not related to stiffness instead it can be understood as an inverse mass. Similarly, the acoustic mass matrix is not related to the mass but it is a compressibility matrix relating displacement to presssure [29]. The naming of the matrices is based on the name-conventions used for structural finite elements.

wavelengths of the propagating waves, thus almost completely eliminating reflections from the PML. Our coefficients are not frequency dependent, and they are adapted from Ref. [32] and extended to 2D axisymmetry. This implies that we sacrifice some accuracy and rely on the tuning of the κ parameter and the thickness of the PML. This is a viable approach and the κ can be tuned such that reflections from the PML are minimal in the frequency range of interest. As we will show in Chapters 5 and 6, the optimization problems to be solved are computationally heavy. Evaluating and assembling parts of the acoustic stiffness and mass matrix for each frequency for each optimization step was deemed to be prohibitively high. A frequency dependent approach was used in [P2] where the unbounded integral from Ref. [33] was used. Other interesting and optimized approaches for PMLs in acoustics are discussed in [34, 35]. Infinite elements can also be used to absorb incident waves [36, 37].

With the same approach used in Sec. 2.1.2 we can discretize Eq. (2.19) into acoustic stiffness and mass matrix and combine it with the matrices from Eq. (2.17) and (2.18)

$$\begin{aligned}\mathbf{K}_a = &\int_{\Omega_a}\int_{-\pi}^{\pi}\left(\mathbf{N}_{a,r}^T\mathbf{N}_{a,r}+\mathbf{N}_{a,z}^T\mathbf{N}_{a,z}\right) r\ \mathrm{d}\theta\mathrm{d}\Omega_a \\ &+\int_{\Omega_A}\int_{-\pi}^{\pi}\left(\frac{\gamma_z}{\gamma_r}\mathbf{N}_{a,r}^T\mathbf{N}_{a,r}+\frac{\gamma_r}{\gamma_z}\mathbf{N}_{a,z}^T\mathbf{N}_{a,z}\right) r\ \mathrm{d}\theta\mathrm{d}\Omega_A \qquad (2.22)\\ \mathbf{M}_a = &\int_{\Omega_a}\int_{-\pi}^{\pi}\frac{1}{c^2}\mathbf{N}_a^T\mathbf{N}_a r\ \mathrm{d}\theta\mathrm{d}\Omega_a+\int_{\Omega_A}\int_{-\pi}^{\pi}\frac{1}{c^2}\gamma_r\gamma_z\mathbf{N}_a^T\mathbf{N}_a r\ \mathrm{d}\theta\mathrm{d}\Omega_A. \qquad (2.23)\end{aligned}$$

The outer boundary of the acoustic domain is denoted Γ_A, this boundary marks the end of the PML layer, on this boundary we apply a Dirichlecht boundary condition [31]

$$p = 0 \quad \text{on} \quad \Gamma_A. \qquad (2.24)$$

2.1.3 Coupling of Mechanical and Acoustic Finite Elements

Loudspeaker units often feature a thin diaphragm, and as a consequence, the fluid load on the structure must be included; this is known as a two-way-coupling or strong coupling. At the interface between the mechanical structure and the acoustic domain, the boundary conditions are defined such that the structure acts as an acoustic source, and the back-induced pressure from the air is acting on the surface of the structure.

The boundary condition on Γ_{as} for the mechanical domain is relating the incident pressure to the stresses in the structure

$$\mathbf{n}\boldsymbol{\sigma} = p \quad \text{on} \quad \Gamma_{as}. \qquad (2.25)$$

The boundary condition on Γ_{as} for the acoustic domain is using the relation between the acrostic field velocity and the acoustic pressure evaluated on the boundary. Here it assumed that the structural velocity and the acoustic velocity is equal in the interface between the two computational domains

$$\mathbf{n}\cdot\nabla p = -\omega^2\rho_a\mathbf{n}^T\mathbf{u} \quad \text{on} \quad \Gamma_{as}. \qquad (2.26)$$

These boundary conditions can be described with a coupling matrix [20]

$$\mathbf{S} = \int_{\Gamma_{as}}\int_{-\pi}^{\pi}\mathbf{N}^T\mathbf{n}\mathbf{N}_a r\ \mathrm{d}\theta\mathrm{d}\Gamma_{as}. \qquad (2.27)$$

Here $\mathbf{n}$ is the normal vector of the interface between the acoustic and structural boundary pointing outwards from the acoustic boundary.

Combining the mechanical, acoustic and coupling matrices yields the entire system of equations used for solving vibro-acoustic problems

$$\left(\begin{bmatrix} \mathbf{K} & -\mathbf{S}^T \\ \mathbf{0} & \mathbf{K}_a \end{bmatrix} - \omega^2 \begin{bmatrix} \mathbf{M} & \mathbf{0} \\ \rho_a \mathbf{S} & \mathbf{M}_a \end{bmatrix} \right) \begin{Bmatrix} \mathbf{u} \\ \mathbf{p} \end{Bmatrix} = \begin{Bmatrix} \mathbf{f} \\ \mathbf{0} \end{Bmatrix}. \tag{2.28}$$

To test and validate the implementation of the FEM the developed code is compared with the commercial software COMSOL [38]. The example considered is from [P3]. To get a direct comparison, the example is excited with a harmonically varying force of 1 N. This validation example is nontrivial as the geometry is quite complex and features undamped cavity resonances. Fig. 2.3 displays the real and imaginary part of the pressure, calculated 1 m away from the speaker as also shown in the model problem in [P3]. The frequency sweep consists of 3001 linearly spaced frequencies. The figure shows excellent agreement in both magnitude and phase between the developed FE model and Comsol.

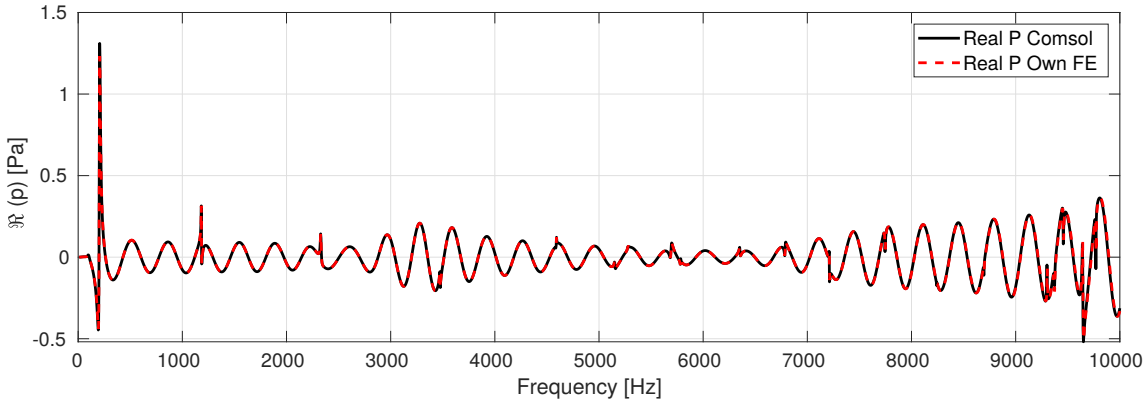

(a) Real part of the pressure

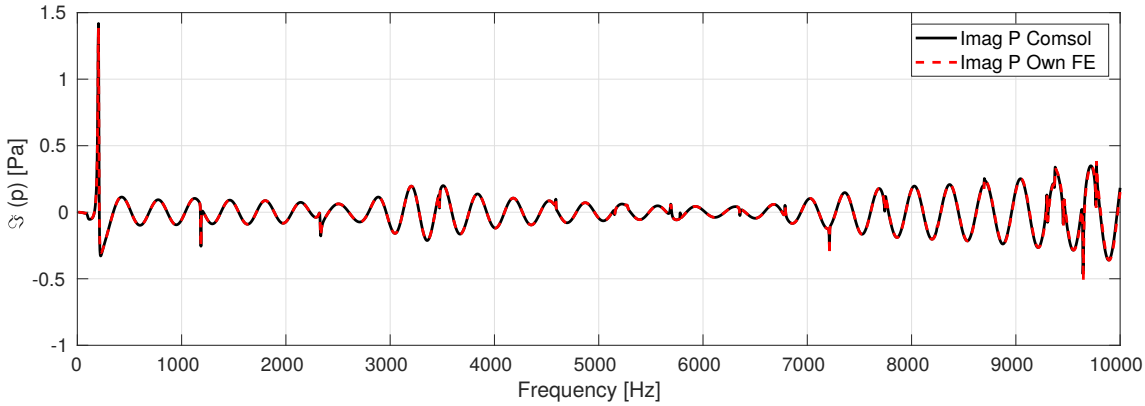

(b) Imaginary part of the pressure

Figure 2.3: Comparison of simulated pressure between the developed FE model and Comsol. The pressure is measured 1 m away from the speaker. The model problem solved follows the model problem in [P3]. Here the excitation is a harmonically varying force of 1 N.

3 Lumped Model Coupled to the FEM

A loudspeaker is often called a transducer due to the fact that it converts an electrical input signal into an acoustic output. The speaker radiates sound via the vertical movements of the diaphragm. The outer suspension, here called the surround, and the spider supports the speaker by limiting movement in the radial direction. The dust cap is attached to the diaphragm, and as the name suggests, it prevents dust from entering the speaker and deteriorate the performance of the electric motor system. Glued to the diaphragm is a cylinder, this is the voice coil former. A wire is wound around the former in order to create the voice coil. Current flows through the voice coil which generates a force due to the interaction between the magnetic field of the voice coil and the magnetic field generated by the permanent magnet. The top plate focuses the magnetic field in the air gap due to its high permeability. The AC source reverses its direction and magnitude with time which also changes the direction of the force applied and thereby making the speaker oscillate. The cross section of a typical moving-coil loudspeaker is shown in Fig 3.1.

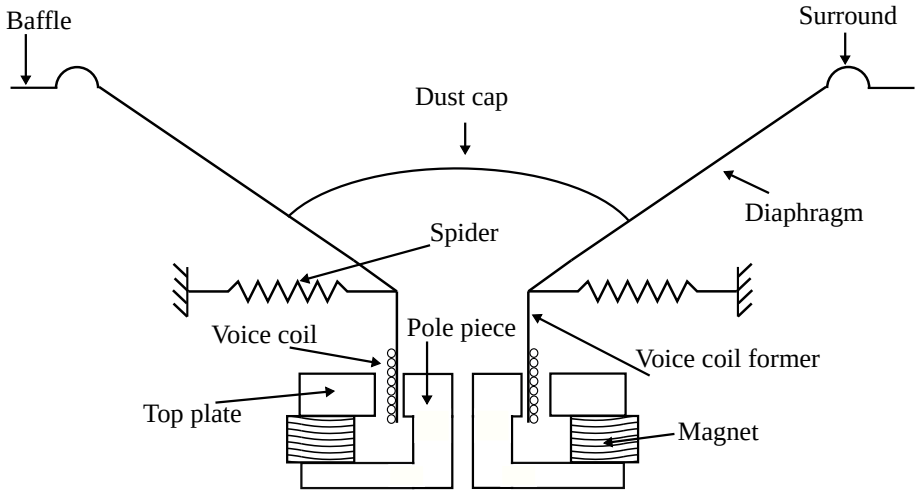

Figure 3.1: Sketch of the cross section of a moving-coil loudspeaker driver.

Equivalent analog circuits are used to obtain low-frequency solutions for loudspeakers. In the equivalent circuit approach, mechanical lumped elements such as stiffness, mass, and damping have their equivalent electrical counterparts in capacitance, inductance, and resistance. The assumption limiting the frequency range of analog circuits is that the loudspeaker cone is assumed to be a flat rigid piston. This assumption holds as long as the velocity distribution on the surface of the loudspeaker is uniform. This implies that the frequency should also be low enough such that the piston mode dominates the vibration of the loudspeaker, i.e. no break-up modes should be present in the dynamic speaker. The wavelength should also be larger than the circumference of the assumed piston as should it be significantly larger than the depth of the speaker cone. This is due to the fact that at higher frequencies the dynamic speaker will become directional. The concepts of analog circuits and the usage of LPMs for loudspeaker modeling are very well described in [4]. An

extension of the LPM with e.g. mode decomposition techniques can be used to account for higher-order vibration modes in the diaphragm [39, 1].

3.1 Partly Lumped Model of a Loudspeaker Unit [P1]

It is generally advantageous to simplify numerical models to reduce the complexity and thereby the computational time. One approach is to lump certain parts of the model that is not directly related to or are severely influencing the aspect of the model that is being studied. This section considers the results published in [P1], the specific target of the paper is to reduce the complexity of the FE model while preserving a FE model of the structural regions that are to be optimized with regards to material layout and shape. The need for a hybrid finite element - lumped parameter model (FE-LPM) comes from the fact that the optimization methods applied in the later chapters of this thesis require a FE model of the model domains. With the optimization methods we can improve the design of speakers by optimizing the material that constitutes the speaker and also the shape of loudspeaker units and acoustic lenses. The focus on optimizing the mechanical parts of the speaker unit also leads to the question of whether it is necessary to spend a considerable amount of computational time solving complex FE models of the electric motor system when it is possible to simplify it. This is a common practice throughout literature, constructing specific hybrid FE-LPMs depending on the aspect studied.

In [40] the surface pattern of a microspeaker diaphragm is optimized; here a FE model of the diaphragm is converted into a mechanical impedance and coupled to a lumped model of the electric motor system and the acoustic enclosure. Schrag et al. [41] uses the FEM to predict eigenfrequencies and eigenmodes for the mechanical parts of MEMS devices such that modal superposition techniques can be used to create a LPM that accounts for multiple flexural vibration modes. This LPM is then coupled to a FE model of the electrostatic contribution and the damping model for the fluid domain. Sun and Hu [42] simplifies a balanced-armature receiver (BAR) and compares the accuracy and computational speed of a lumped acoustic domain connected to a mechanical FE model of the BAR and vice versa. The excitation of the BAR does not come from an electric motor system it is a constant force applied. Panzer [43] uses a lumped model of the electrical and mechanical components coupled to the boundary element method (BEM). BEM is used to model the waveguide, enclosures, and acoustic radiation from the speaker. In [44] a hybrid FE-LPM is implicitly described. The model consists of a FE model of the diaphragm and outer suspension together with an acoustic domain, the electric motor system is lumped. The computations and coupling are done through the COMSOL multiphysics software [38], which features the possibility of combining lumped circuits and FE models. In [28] an axisymmetric FE model of a speaker is considered. The electric motor system is lumped and is applied as a postprocessing step, good agreement between the numerical model and a measured loudspeaker is achieved. Very recently, an approach that lumps a subwoofer entirely but uses a FE model to compute the acoustic frequency response was presented in [45]. The proposed method also pre-computes the frequency response in some of the acoustic regions to gain a feasible computational time for a 3D model of the subwoofer.

3.1.1 Lumped Parameter Model

Fig. 3.2 shows the equivalent circuit for the lumped components of the loudspeaker unit, which is the electric motor system, the spider, voice coil, and voice coil former. The circuit relies on the impedance analogy and is inspired from [4, chap. 6]. The left circuit in Fig. 3.2 represents the electrical motor system, e_g is the applied voltage from an AC source, i_c is the current, R_E is the DC resistance in the wire of the voice coil, the complex impedance block $(j\omega)^n L_E$ represents an inductor with frequency dependent inductance and losses,

Bl is the force factor, $\dot{u}$ is the velocity, $M_{p,lump}$ is the mass of the lumped mechanical components, $R_{p,lump}$ is the damping and $C_{p,lump}$ is the compliance. Unconventional names have been chosen for the lumped mechanical components to emphasize the partly lumped aspect of the model.

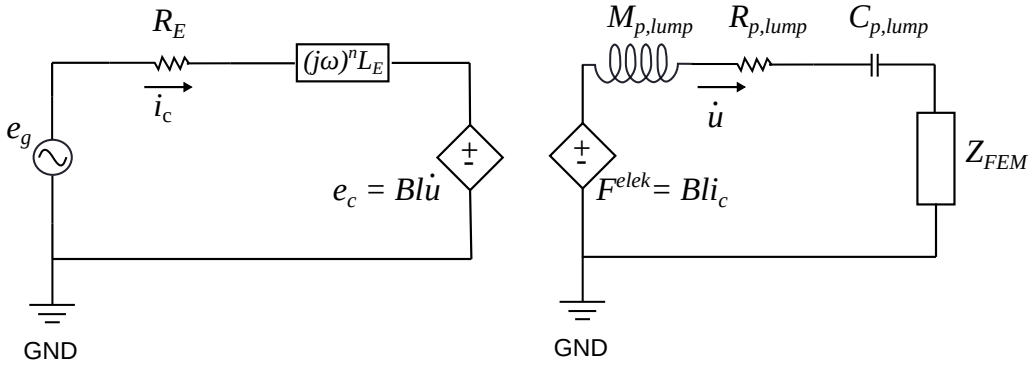

Figure 3.2: Equivalent circuit representing the lumped parts of the loudspeaker unit.

The equation for the electric motor system taking into account the eddy currents in the voice coil is [4]

$$e_g = R_E i_c + (j\omega)^n L_E i_c + j\omega Blu_i, \tag{3.1}$$

where n is the fractional order and u_i is the displacement in the coupling DOF in node i.

Similarly the scalar equation for lumped mechanical system can be derived from the analogue circuit in Fig. 3.2, the FE model is included as an impedance $Z_{FEM} = \frac{F_i}{j\omega u_i}$

$$Bli_c = -\omega^2 M_{p,lump} u_i + j\omega R_{p,lump} u_i + \frac{1}{C_{p,lump}} u_i + j\omega Z_{FEM} u_i. \tag{3.2}$$

The scalar equations are now ready to be added to the FE model of the remaining parts of the loudspeaker unit and acoustic domain. The coupling is formulated in the above equations such that the contribution from the lumped system excites the FE model, and the back-induced electromotive force from the FE model is also accounted for.

3.1.2 Coupling the Lumped Parameter Model to the FEM

Fig. 3.3 shows the components of the loudspeaker unit that is included in the lumped model, furthermore, it shows the placement of the coupling node. This node defines the DOF where the lumped system is coupled to the FE model.

Adding the lumped components into the FE model requires a set of indicator matrices, these represent the relevant DOF for the coupling node. The lumped values are multiplied with these matrices

$$\mathbf{I}_{ir} = \mathbf{e}_{idofr}\mathbf{e}_{idofr}^T \quad , \quad \mathbf{I}_{iz} = \mathbf{e}_{idofz}\mathbf{e}_{idofz}^T \quad , \quad \mathbf{I_l} = \mathbf{e}_l\mathbf{e}_l^T, \tag{3.3}$$

where $\mathbf{e}_{idofr}$ and $\mathbf{e}_{idofz}$ are zero vectors except with a unit entry corresponding to the r and z DOF of the coupling node i and $\mathbf{e}_l$ is a zero vector with a unit entry in the last component. An indicator matrix, $\mathbf{J}_{iz}$, is also created which has a unit entry in the bottom row corresponding to the z DOF of node i.

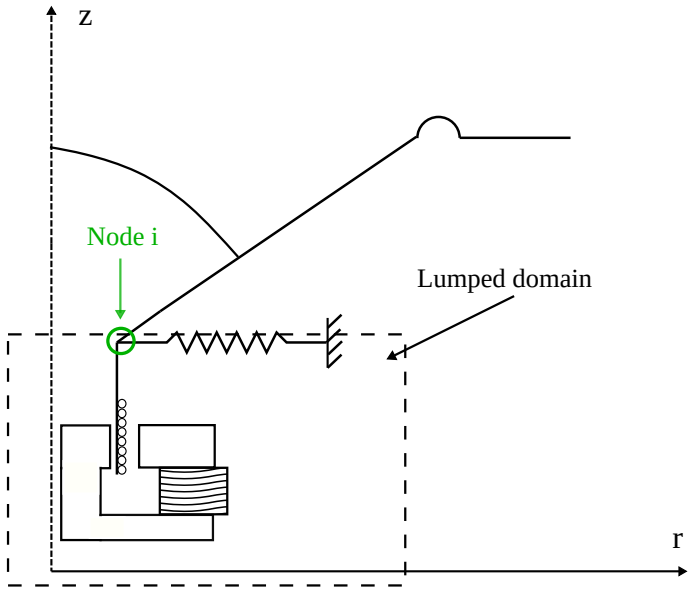

Figure 3.3: Sketch of the cross section of a moving-coil loudspeaker driver, the dashed box shows the components of the speaker that are contained in the LPM and the green circle indicates the placement of coupling node i.

This yields the following system of equation for the hybrid FE-LPM

$$\begin{aligned}\Bigg(\begin{bmatrix}\widetilde{\mathbf{K}} & \mathbf{0}\\ \mathbf{0} & 0\end{bmatrix} + \frac{1}{C_{p,lump,r}}\mathbf{I}_{ir} + \frac{1}{C_{p,lump,z}}\mathbf{I}_{iz} + R_E\mathbf{I}_l - Bl\mathbf{J}_{iz}^T \\ +j\omega\left(R_{p,lump}\mathbf{I}_{iz} + Bl\mathbf{J}_{iz}\right) + (j\omega)^n L_E\mathbf{I}_l \\ -\omega^2\left(\begin{bmatrix}\widetilde{\mathbf{M}} & \mathbf{0}\\ \mathbf{0} & 0\end{bmatrix} + M_{p,lump}\mathbf{I}_{iz}\right)\Bigg)\begin{Bmatrix}\mathbf{u}\\ \mathbf{p}\\ i_c\end{Bmatrix} = \begin{Bmatrix}\mathbf{0}\\ \mathbf{0}\\ e_g\end{Bmatrix}.\end{aligned} \tag{3.4}$$

Here $\mathbf{J}_{iz}^T$ is the transpose of $\mathbf{J}_{iz}$, $C_{p,lump,r}$ and $C_{p,lump,z}$ refers, respectively, to the lumped compliance in the r and z direction. All other lumped elements are added only to the DOF in the z-direction of the coupling node.

Equation (3.4) can be written in a compact form

$$\left(\widetilde{\mathbf{K}} + j\omega\widetilde{\mathbf{C}} - \omega^2\widetilde{\mathbf{M}}\right)\begin{Bmatrix}\mathbf{u}\\ \mathbf{p}\\ i_c\end{Bmatrix} = \begin{Bmatrix}\mathbf{0}\\ \mathbf{0}\\ e_g\end{Bmatrix}, \tag{3.5}$$

where $\widetilde{\mathbf{C}}$ contains the velocity proportional terms from the lumped model, $\widetilde{\mathbf{K}}$ and $\widetilde{\mathbf{M}}$ are augmented coupled stiffness and mass matrices.

The state equation in Eq. (3.5) is for the remainder of this thesis written with compact notation as

$$\tilde{\mathbf{S}}\tilde{\mathbf{u}} = \tilde{\mathbf{f}}. \tag{3.6}$$

Here $\tilde{\mathbf{S}}$ is the system matrix, $\tilde{\mathbf{u}}$ is the solution vector containing $\mathbf{u}$, $\mathbf{p}$ and i_c and $\tilde{\mathbf{f}}$ is the excitation containing e_g.

By lumping the mechanical components we assume that they behave as a 1 DOF system in the entire frequency range. This simplification means that the higher-order vibration

modes of both the spider and the voice coil former are not accounted for at higher frequencies. These modes can cause changes in the response. Furthermore, by lumping the components we remove the geometry such that the radiated pressure from the spider and reflections and scattering from sound waves hitting the motor system is not accounted for. However, as seen in the subsequent section, it is possible to achieve a feasible fit of the hybrid FE-LPM model when compared to a full reference model.

3.1.3 Fitting the Model to Measured Results

It is desired to be able to model a loudspeaker as realistic as possible. In this work this has been accomplished by fitting the frequency response and impedance curve of the FE-LPM to the frequency response and impedance curve of a reference model. The fit is achieved by solving an optimization problem where the error between the two curves should be minimized by tuning the lumped parameters. By doing so, it is made sure that adequate physical values for the lumped parameters are used, furthermore it allows for a more general model where different loudspeaker drivers could be considered. System identification methods that estimate the small-signal-parameters of dynamic loudspeakers such as the Klippel system also rely on fitting parameters to LPMs. [46, 47]. The details describing the specific reference model used in this work are explained in [P1]. The objective function takes into account both the magnitude and phase of both the pressure and the impedance

$$\phi = \frac{||\mathbf{p}_{meas} - \mathbf{p}||_2^2}{||\mathbf{p}_{meas}||_2^2} + \frac{||\mathbf{z}_{meas} - \mathbf{z}||_2^2}{||\mathbf{z}_{meas}||_2^2}. \tag{3.7}$$

The objective function is ϕ, the measured pressure at different frequencies 1m away from the loudspeaker unit is denoted $\mathbf{p}_{meas}$, $\mathbf{p}$ is the computed pressure, $\mathbf{z}_{meas}$ and $\mathbf{z}$ is the measured and simulated voice coil impedance, respectively. Equation (3.8) states the optimization problem together with the associated constraints, L_l and L_h are the lower and upper limits on the lumped elements and x_j is the value of lumped component number j

$$\begin{aligned} \min_{\mathbf{x}} \quad & \phi(\mathbf{x}) \ , \\ \text{s.t.} \quad & \text{Eq. (3.5)} \ , \\ & L_l \leq x_j \leq L_h \ , \quad j = 1, \ldots, 6 \ , \end{aligned} \tag{3.8}$$

The optimization problem is solved with *fmincon* in Matlab using sequential quadratic programming and computing the gradients with finite difference. The results shown in Fig 3.4 and Fig. 3.5 stems from the optimization carried out in [P1], however, some improvements have been made in this thesis. On the reference model there is a narrow slit around the voice coil and voice coil former where losses were not originally added. This meant that the back cavity was acting as a Helmholtz resonator. This resonance caused a spike in the frequency response, and this behavior has been remedied by adding losses to the reference model in the narrow slit. As a consequence, the frequency response is now more well behaved. However, the added losses also meant that the electric impedance around the first resonance of the reference loudspeaker driver is reduced. This effect is included in the FE-LPM by adding more mechanical damping to the lumped model, therefore $R_{p,lump}$ has the value $1.53\text{N} \cdot \text{s/m}$ in Fig 3.4 and Fig. 3.5. Furthermore, the PML in the presented FE-LPM model has been tuned to yield a better solution for the mid frequencies. The slight discrepancies at low frequencies can be attributed to the choice of absorption coefficient in the PML. Here a value of 0.9 is used, which yields a better agreement for the mid-to-high frequencies. In [P1] the absorption coefficient had a value of 10, and here excellent agreement at low frequencies was obtained. It should be stressed that the models used in this work are validated for the frequency range in which they are used as the choice of the absorption coefficient can, in some cases, affect the results. This is a limitation in the method due to using frequency-independent PMLs.

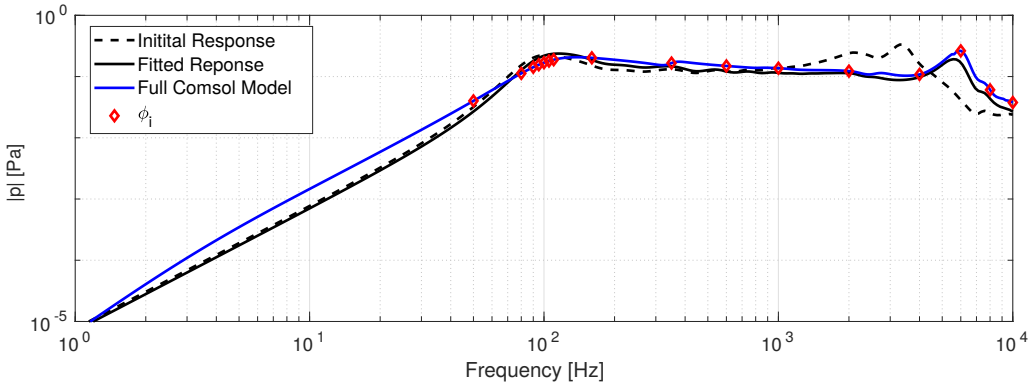

Figure 3.4: Pressure response between 1 Hz and 10 kHz. The solid black line is the result of the optimization, the solid blue line is the full loudspeaker model, the dashed black line is the starting guess and the red diamond-shaped discrete points are the frequencies which are used in the optimization. Caption is from [P1].

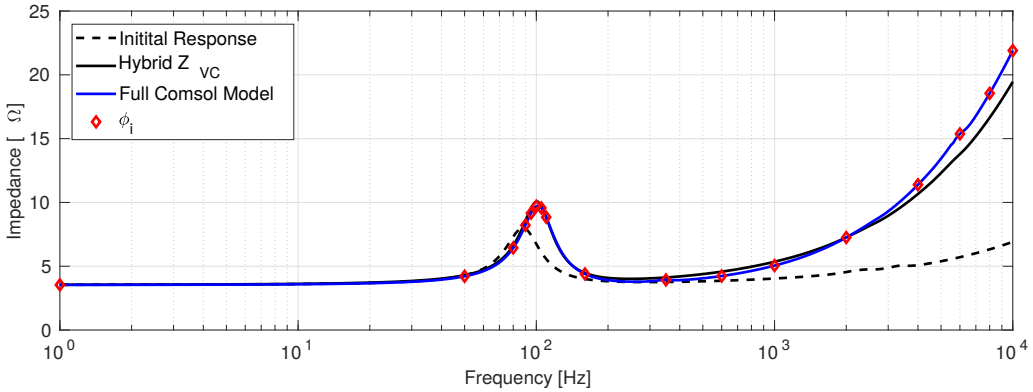

Figure 3.5: Impedance between 1 Hz and 10 kHz. The solid black line is the result of the optimization, the solid blue line is the full loudspeaker model, the dashed black line is the starting guess and the red diamond-shaped discrete points are the frequencies which are used in the optimization. Caption is from [P1].

3.2 Contribution

A particular aspect studied in this thesis is the optimization of the loudspeaker diaphragm and outer suspension. The FE-LPM approach is therefore essential to reduce the complexity of the model while preserving the geometry of the parts of the loudspeaker that is subject to numerical optimization. The paper describes and derives the necessary steps required to lump the electric motor system and parts of the mechanical system. The paper uses optimization to fit the frequency response and impedance curve of the FE-LPM to a reference loudspeaker unit. This allows for the simulation of measured loudspeakers with a FE model with reduced complexity. The detail and the explicit description of the method allow for implementing the approach into an in-house vibro-acoustic FE software. The method can be used to lump other parts of the loudspeaker unit than the ones discussed in the paper, such as the outer suspension or just the electric motor system. As described in the literature review, the idea of combining FE models and LPM is not novel, and it is also available in commercial software. The main contribution of this paper is to explicitly and in detail describe the FE-LPM approach within loudspeaker modeling and combining the approach with model fitting such that the model can be used to model a specific loudspeaker.

4 Optimization Methods

This thesis considers two different optimization techniques. They are both used to find optimal configurations of either material properties or shapes to improve the sound quality of loudspeakers. A density-based design approach is used to optimize the material properties, whereas the principles from free form deformation [48] (FFD) is used to optimize the shape. It was deemed important for this project to develop an in-house code that gives a solid foundation for developing optimization methods such as those presented in this chapter. With an in-house code, total access to design sensitivities etc. are available, which is essential when method development is carried out. Optimization methods such as the ones presented here are in recent years continuously being added into commercial software packages such as Comsol [38].

The density-based approach in this work is heavily influenced from the Solid Isotropic Material with Penalization (SIMP) [49] approach used for topology optimization [50]. Topology optimization is a method that has been increasing in popularity ever since the discovery of the method for elasticity problems by Bendsøe and Kikuchi [51]. Topology optimization on linear elasticity is still a major research topic with many applications e.g. very large-scale problems with billions of DOF [52, 53], and within the design of microstructures [54, 55]. The method is able to cover a wide range of engineering disciplines and has also successfully been employed in scientific fields such as fluid dynamics [56, 57], heat conduction [58, 59] and wave problems such as electromagnetics [60], optics [61, 62], elastic wave propagation [63] and acoustics [64].

This work features the optimization of the local material properties of fixed geometries i.e. no changes to the structure's topology. This work does not consider the materials on a microscale level, i.e. the microstructure and the material phases are not considered. Instead, the focus of this work is what could be classified as optimization on a macroscale, where the material properties of each element, in the FE model, in defined design domains can be altered by changes in the element design variables. By restricting the design problem to purely consider the material properties, it is possible to visualize the impact they have on the sound quality and how much the optimized material configuration can improve the performance of loudspeakers.

Optimizing the material properties is a strong tool. It can lead to well-performing conceptual designs that can provide benchmark examples or aid with generating new ideas for the selection of materials. There are many different methods throughout the literature that deal with the topic of optimizing material properties. This paragraph serves to give an overview of other methods than the one used in this thesis. The common ground is that they also rely on element design variables to determine the optimal material layout and, in many cases, also the topology. One approach is the so-called free material optimization. Here the elastic stiffness tensor is the design variable which implies that the method is well equipped for designing an-isotropic materials. It was introduced by Bendsøe and Diaz [65] and was later adapted to maximization of the first fundamental frequency of a sheet to improve the frequency response, here co-dependency of mass and stiffness is assumed [66]. The method has also been used to design layered shell structures

[67], a leading edge rib of A380 [68] and for glass-reinforced composites [69]. Traditional topology optimization has also been extended to account for two materials [70, 71]. In [72] a damping layer is designed to increase the maximum energy that can be dissipated from a disk that is excited by burst-tones. Many other methods also exist. Such as the design of graded multi-phase infill structures for additive manufacturing that is based on density-based topology optimization that relies on the SIMP approach [73]. In [74] multi-material structures with graded interfaces is designed, the design technique caters to very sophisticated manufacturing methods. In [75] shape and topology optimization is used to design graded materials; here, the level set approach is utilized to track the material interfaces. There is also research concerning graded material design which relies on the phase-field method [76] and using a SIMP based material model, which interpolates between three states, solid, air, and fibrous material for the design of a porous media for increased sound absorption [77].

The use of shape optimization for multiphysics problems such as acoustic-structure interaction eliminates the issue with a non-physical design field that is present for intermediate element design variables in topology optimization. The sacrifice is that we limit our design freedom, and the optimized results are often dependent on a good starting guess. In this work, shape optimization is carried out based on the work of Sederberg and Parry in 1986 [48]. Their work describes a method in which trivariate Bernstein polynomials are mapped to a geometry. By moving/pertubating the polynomials the underlying geometry changes accordingly. Derivative continuity is ensured, which makes the method ideal for gradient-based optimization. The method is applied to a diverse range of problems but is also used for shape optimization, often with relation to aerodynamics [78, 79, 80], to the authors knowledge FFD has not been used within the field of acoustics as of yet. Shape optimization can be performed with different approaches than FFD. Cubic splines have been applied as a parametrization tool to optimize absorbers in 2D using the BEM [81]. Acoustic shape optimization has been investigated for acoustic horns and brass wind instruments by Udawalpola in [82] and in [15] Dilgen uses an immersed boundary cutFEM method. Shape optimization is also applied in fluid mechanics [83] and electromagnetics [84].

The general idea of numerical optimization on structures in FE frameworks is that a design domain, Ω_d, is defined for a solid region. In Ω_d there are design variables, $\mathbf{x}$, which in this work controls either the material properties or the shape of the solid region. An optimization problem is solved iteratively where the design variables are changed in order to minimize an objective function $\phi_0(\mathbf{x})$. The design variables for both the density-based method and shape optimization with FFD are continuous in a specified interval. This allows for calculating the gradients of $\phi_0(\mathbf{x})$ with respect to the design variables. The motivation for calculating the gradients is that in general it is the most efficient way of solving PDE-constrained optimization problems [85]. In this work, the method of moving asymptotes (MMA) [86] is used to update the design variables after each iteration. Other concepts and optimization algorithms for both convex and non-convex optimization problems can be found in [87].

4.1 Design Variables in the Density-Based Method

In density-based methods, design variables are defined in each element in the design domain. These design variables are traditionally continuous in the interval between 0 and 1, but in principle, the interval range can be arbitrarily defined. The requirement for continuity is due to the fact that gradient-based optimization is used. In this work, each element in the design domain has 1, 2, or 3 design variables as illustrated in Fig. 4.1.

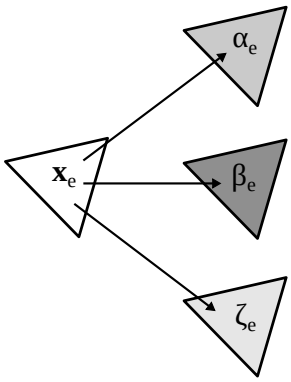

Figure 4.1: Illustration of an element within the design domain having three design variables with three different values.

The design variables α_e, β_e and η_e are related to the element stiffness, mass and damping, respectively.

In Fig. 4.1 we consider element e located in the design domain. The element has three different design variables. The design variables are used in interpolation functions. Most of the interpolation functions are based on the SIMP method in this work. This method originates from topology optimization, where binary designs with either solid or void material are often required. The major difference between material optimization and traditional topology optimization is that there are no geometry changes in this work. If a design variable reaches zero in traditional topology optimization, that element is considered a void region. In this work, that case will result in the element being assigned to a specified lower bound. Traditional topology optimization favors binary designs, the material state should either be solid or void. In this work, binary designs are not sought after, here the material of the loudspeaker is allowed to vary continuously within the design domain. As a consequence, there is no penalization in the interpolation functions used in this work. A set of linear interpolation functions used in [P2],[P3] and [P4] are shown below

$$\begin{aligned} \rho_e &= \rho_{min} + \beta_e \left(\rho_{max} - \rho_{min}\right) \\ E_e &= E_{min} + \alpha_e \left(E_{max} - E_{min}\right) \\ \eta_e &= \eta_{min} + \zeta_e \left(\eta_{max} - \eta_{min}\right). \end{aligned} \tag{4.1}$$

Here, ρ_e, E_e and η_e is the element mass, stiffness and damping, respectively, and β_e, α_e and ζ_e are the associated element design variables. Subscript min and max refers to the upper and lower bound of the material property, respectively

Different strategies have been applied for the interpolation functions. In [P2] the stiffness and mass were considered to be co-dependent, in [P3] stiffness, mass, and damping was considered independently and in [P4] stiffness, mass, and damping was varying independently in the surround of the speaker, but in the diaphragm, a more sophisticated interpolation function for the element stiffness was proposed. The idea was to essentially capture the co-dependence of stiffness and mass based on a study of the available materials for loudspeaker diaphragms. Thereby recognizing that materials with artificially high stiffness to mass ratio should not be included in the optimization. This lead to a new interpolation function, where the element stiffness is also dependent on the design variable controlling the element density

$$E_e = E_{min} + 1.8 \cdot (0.5\beta_e)^{2.6-2.1\alpha_e} \left(E_{max} - E_{min}\right) \tag{4.2}$$

The exact formulation of Eq. (4.2) is based on the range of material properties available for paper pulp, plastics, composites and metals. The study is carried out using [88] and the full details are present in [P4].

4.1.1 Filtering

It is generally advantageous to restrict density-based optimization problems by applying a filter to either smooth the design sensitivities or the design variables. This is done in order to avoid designs with small and finely detailed features. The primary motivation for applying a filter to the design problems considered in this work is to avoid very thin and detailed aspects of an optimized design that is hard to materialize from a manufacturing point-of-view. Applying a filter also prevents the designs from forming checkerboard patterns [89]. The issue with checkerboard patterns is that very stiff materials are connected only at the corner nodes and thus creating an artificial hinge. The hinge and the high contrast between neighboring elements mean that the FE analysis of the design is not trustworthy. In this work, the motivation for using a sensitivity filter is strictly related to avoiding thin and detailed aspects in the optimized designs, since the solid elements are higher-order elements and are therefore not prone to form checkerboard patterns [89]. A sensitivity filter from Ref. [90] is implemented to avoid a high level of detail in the optimized designs. The sensitivity filter modifies the sensitivity of each element based on the value of the neighboring elements inside the filter radius. The filter is formulated such that it accommodates for the unstructured mesh

$$\frac{\widehat{\partial \Phi_0}}{\partial x_e} = \frac{\sum_{i \in N_e} w\left(\mathbf{c}_i\right) x_i \frac{\partial \Phi_0}{\partial x_i} / v_i}{\max\left(\gamma, x_e\right) / v_e \sum_{i \in N_e} w\left(\mathbf{c}_i\right)}. \tag{4.3}$$

Where N_e is the neighbourhood of a given element, defined by the filter radius R, such that $N_e = \{i \mid ||\mathbf{c}_i - \mathbf{c}_e|| \leq R\}$, $\mathbf{c}_i$ is the center coordinates of element i, $\mathbf{c}_e$ is the center coordinates of the current element, here the center is determined with the incenter triangle method, $w\left(\mathbf{c}_i\right) = R - ||\mathbf{c}_i - \mathbf{c}_e||$ is linearly decaying weight function, R is the filter size which equals 1 mm, x_i is the value of the design variable in element i, $\frac{\partial \Phi_0}{\partial x_i}$ is the design sensitivity of element i, v_i is the surface area of element i, x_e is the value of the design variable in the current element and $\gamma = 10^{-3}$ is used to avoid division with zero.

In the case of multiple design domains, the filter is formulated such that it only influences a single domain at a time. This is due to the fact that the two domains consist of different ranges of material properties. The associated design sensitivities are therefore likely to be independent in the two domains and should therefore be considered independently by the sensitivity filter.

With the introduction of the sensitivity filter the design sensitivities used to solve the optimization problem are changed. This implies that the optimization problem that is actually solved is different from the one specified. This is also pointed out in [90] and later on it was theoretically justified by Sigmund and Maute [91].

Alternatively the density filter [92, 93] can be used to filter the design variables. Convergence from intermediate densities can be enforced with projection filters such as Heaviside projection [94].

4.2 Shape Optimization using FFD

The part of the computational domain which includes the solid parts that should be optimized is mapped in a rectangular region to bivariate Bernstein polynomials following the approach in [48]. Essentially the idea is to relate a set of coordinates, here the nodal

coordinates are used, to a local coordinate system. Any point $\mathbf{q}$ is related to the local coordinate system by

$$\mathbf{q} = \mathbf{q}_0 + s\mathbf{e}_s + t\mathbf{e}_t \tag{4.4}$$

where $\mathbf{q}_0$ is the origin of the local coordinate system in global mesh coordinates, s and t are the local coordinates restricted to $0 \leq s \leq 1$ and $0 \leq t \leq 1$ in the horizontal and vertical direction, respectively and $\mathbf{e}_s$ and $\mathbf{e}_t$ are in this case orthogonal basis vector in the horizontal and vertical plane, respectively. The local coordinates s and t can be found by solving the inverse problem of Eq. (4.4).

The control points are shown in Fig. 4.2 and are defined by

$$\mathbf{d}_{i,j} = \mathbf{q}_0 + \frac{i}{l}\mathbf{e}_s + \frac{j}{m}\mathbf{e}_t, \tag{4.5}$$

here l and m are the order of the Bernstein polynomials, and i and j defines a specific control point, $\mathbf{d}_{i,j}$, location in a lattice structure. In the dummy example in Fig. 4.2 l = 4 and m = 4. The deformation of the mesh is accomplished by moving $\mathbf{d}_{i,j}$. The resulting deformation is defined by a bivariate tensor product Bernstein polynomial. The coordinates within this rectangular region are denoted $\mathbf{q}_{i,j}(s,t)$ and are given by the following expression

$$\mathbf{q}_{i,j}(s,t) = \sum_{i}^{l}\sum_{j}^{m} b_i(s)b_j(t)\mathbf{d}_{i,j} \tag{4.6}$$

The Bernstein basis polynomials used in Eq. (4.6) are defined as

$$b_i(s) = \binom{l}{i} s^i \left(1-s\right)^{l-s} \quad \text{with} \quad \binom{l}{i} = \frac{l!}{i!(l-i)!} \tag{4.7}$$

$$b_j(t) = \binom{m}{j} t^j \left(1-t\right)^{m-t} \quad \text{with} \quad \binom{m}{j} = \frac{m!}{j!(m-j)!} \tag{4.8}$$

An example of how the design domain is subdivided into a rectangular region with bivariate Bernstein polynomials is shown in Fig. 4.2 In Fig. 4.2a an initial configuration is shown, the red dots are the control points. The control points placed directly onto the z-axis are restricted to only move in the z-direction. This avoids a non-physical mesh and unwanted holes in the design region. The shape of the solid regions is altered by changing the coordinates of $\mathbf{d}_{i,j}$ as demonstrated in Fig. 4.2b. Each control point is subject to a box constraint to prevent very large deformations.

The design variables are scaled using a linear change of variables such that they lie in a continuous interval between 0 and 1 instead of the range of the box constraints at each individual design variable

$$x_l = \frac{d_{i,j} - L_l}{L_h - L_l}. \tag{4.9}$$

Here L_h and L_l are the upper and lower bound values of the box constraints of the control points.

4.2.1 Nonlinear Constraints on Mesh Quality

Generally, with shape optimization, it is necessary to take precautions with regards to ensuring the quality of the mesh. This is done in order to prevent distorted elements or even flipped elements that can cause numerical errors. One approach is to use regularization in terms of filtering. Here, a filter is applied to the local coordinates in the mesh to

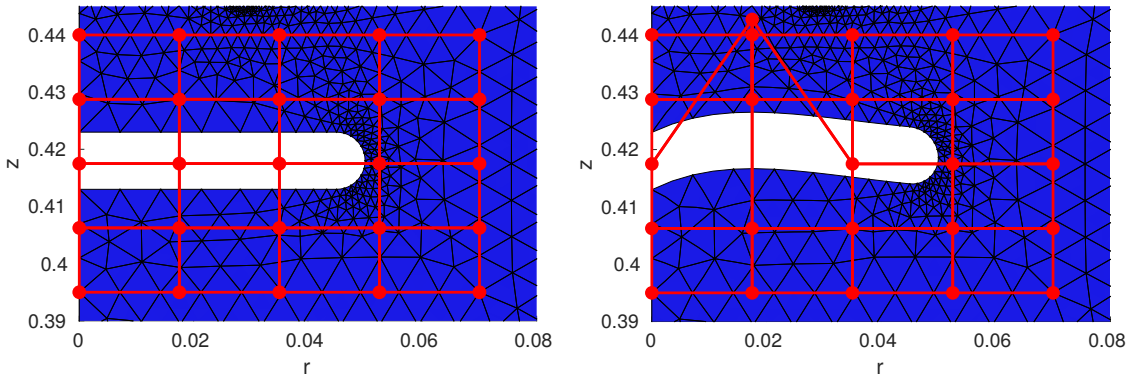

(a) Unperturbed design (b) Perturbed design

Figure 4.2: An example of the design region of the one FFD region located around a flat acoustic lens. The location of the control points are indicated with red dots. In this particular example $\mathbf{q}_0 = (0.0, 0.395)$. In the figure a) is the initial configuration of the Bernstein polynomials and b) is an example of a change in a control point in the z-direction. Figure and caption are from [P5].

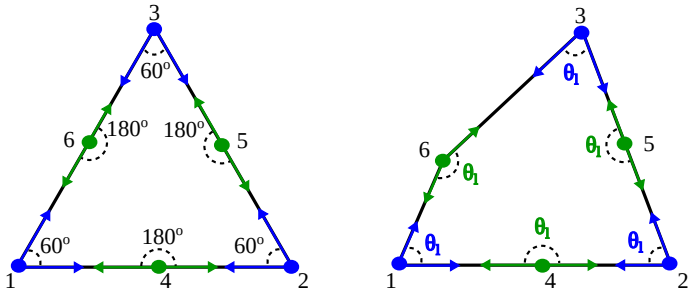

Figure 4.3: Sketch of an ideal 2nd order triangular element on the left hand side, right hand side shows a slightly deformed element due to a movement in the geometry. The angles that are measured to ensure element quality is shown, blue indicate angles with reference to 60°as and ideal angle and green has a reference angle of 180°. Figure and caption are from [P5]

avoid highly distorted elements. Examples of such filters are Laplace smoothers [21], a moving average Gauss filter [95], or for FE mesh-based shape optimization filters based on convolution integrals have been successfully applied [96]. Remeshing can be utilized to reconstruct the mesh such that good element quality can be ensured. This could be done after a certain amount of iterations or when an implemented measure of the quality of the mesh reaches a certain threshold. In this work, nonlinear element quality constraints are proposed, the constraints compare the angle deviation in each element to the angles in an equilateral triangle, this is shown for a single element in Fig. 4.3.

There are two constraints for each element, one for the angles that in the ideal case would be 60° and one for the ideal angles equal to 180° as the allowed deviation from the ideal angle is different between the two cases. There are many elements present in the design region and it is not desired to feed hundreds or even thousands of constraints to the optimizer. Instead, angles of the same type and in the same computational domain are summed using the generalized mean, and that value is then penalized with the factor p_L

such that elements with large angle deviations are dominant

$$\left(\frac{1}{N_{60}}\sum_{l=1}^{N_{60}}\theta_{60,l}^{p_L}\right)^{1/p_L} - c_{60,\max} \leq 0, \tag{4.10}$$

where $\theta_{60,l} = |\theta_l - 60°|$, with θ_l being the angle at a specific node, N_{60} is the total number of angles included in the summation, $p_L = 15$ and $c_{60,\max}$ is the allowed deviation from the ideal angle of 60°. In this work $c_{60,\max} = 25°$.

$$\left(\frac{1}{N_{180}}\sum_{l=1}^{N_{180}}\theta_{180,l}^{p_L}\right)^{1/p_L} - c_{180,\max} \leq 0, \tag{4.11}$$

here $\theta_{180,l} = |\theta_l - 180°|$, N_{180} is the total number of angles included in the summation and $c_{180,\max}$ is the allowed deviation from the ideal angle of 180°. In this work $c_{180,\max} = 10°$.

4.3 Design Problem

The design problems considered in the subsequent chapters are mainly the so-called minimax problems. This formulation is utilized since the goal is to consider design problems over broad frequency ranges. The minimax optimization problem will minimize the maximum value, which in our case is an error estimate given by the difference between the desired target line and the frequency response evaluated at a number of frequencies. This is seen as an advantage due to the deep valleys present in the considered frequency responses. Another method that could be applied to multi-frequency optimization problems is the integral of the objective function over a specified frequency range. However, this method was not used as it does not prioritize the worst-performing parts of the objective function. Therefore, it was unsure whether the integral formulation would be able to yield the same results as the minimax formulation for the problems considered in this thesis.

The objective function is denoted $\phi_{0_k}(\mathbf{x})$ where k is an integer from 1 to b, with b being the total amount of frequencies considered in the optimization. The objective function is minimized by changes in the design variables $\mathbf{x}$, the individual design variable is denoted x_j, where j is an integer from 1 to a, with a being the total amount of design variables. The formulated minimax problem is subject to a number of constraints, $g_i(\mathbf{x}) \leq 0$, with i being an integer in the interval from 1 to q, where q is the number of constraints. It is then possible to state the continuous optimization problem as

$$\begin{array}{lll} \min\limits_{\mathbf{x}} \quad \max & \phi_{0_k}(\mathbf{x}) \,, & k = 1, \ldots, b \\ \text{s.t.} & \tilde{\mathbf{S}}_k\tilde{\mathbf{u}}_k - \tilde{\mathbf{f}} = 0 \,, & k = 1, \ldots, b \\ & g_i(\mathbf{x}) \leq 0 \,, & i = 1, \ldots, q \\ & 0 \leq x_j \leq 1 \,, & j = 1, \ldots, a \end{array} \tag{4.12}$$

We transform the minimax problem in Eq. (4.12) into a bound formulation such that it is more convenient to solve with gradient-based optimization programs. This implies that an additional variable, z, should be minimized. This optimization formulation is also known as a bound formulation, here $\phi_{0_k}(\mathbf{x})$ is used as a constraint. Essentially, z can be viewed as a bound which ideally is aligned with the highest value of $\phi_{0_k}(\mathbf{x})$. All the design problems considered in this work use the residual of the state equation in Eq. (3.5) as an equality constraint. The general minimax optimization problem in Eq. (4.12) can then be

stated as

$$\begin{aligned} \min_{\mathbf{x},z} \quad & z\,, && z \geq 0 \\ \text{s.t.} \quad & \tilde{\mathbf{S}}_k \tilde{\mathbf{u}}_k - \tilde{\mathbf{f}} = 0\,, && k = 1,\ldots,b \\ & \phi_{0_k}(\mathbf{x}) - z \leq 0\,, && k = 1,\ldots,b \\ & g_i(\mathbf{x}) \leq 0\,, && i = 1,\ldots,q \\ & 0 \leq x_j \leq 1\,, && j = 1,\ldots,a \end{aligned} \tag{4.13}$$

here the equality constraint on the state equation is automatically fulfilled by solving the state equation. The solution to the state equation also provides the necessary input to compute $\phi_{0_k}(\mathbf{x})$ at the desired frequencies.

4.3.1 Objective Functions

During this work, several different objective functions have been investigated. In the early stages, the goal was to have a working optimization algorithm, and therefore [P2] seeks to maximize the pressure output from a flat panel speaker at single frequencies. The pressure formulation is also used in [P3], however, it is expanded to include a target line. The design problem is formulated such that it minimizes the difference between the target line and the computed frequency response over a range of frequencies. This addition is a key aspect as it allows for the control of the frequency response in a targeted frequency range

$$\phi_{0_k} = \left(T_L - \tilde{\mathbf{u}}_\mathbf{k}^\mathbf{T} \mathbf{L} \bar{\tilde{\mathbf{u}}}_\mathbf{k}\right)^2, \tag{4.14}$$

here T_L is the value of the target line, $(\cdot)_k$ refers to the value computed for frequency number k, $\bar{(\cdot)}$ means that it is a complex conjugate, $\tilde{\mathbf{u}}$ is the solution to Eq. (3.5) and $\mathbf{L}$ is a zero matrix with ones in the diagonal corresponding to the DOF that are to be included in the objective function.

There are many aspects of a loudspeaker that is important, and asking different professionals or audio aficionados will yield different answers. However, as mentioned in the introduction of this thesis, there is one aspect of a loudspeaker's response that is often present both in scientific literature and specification sheets of loudspeakers. That is the flatness of the frequency response over a wide frequency range and a well-behaved off-axis response. This will ensure that the optimized speaker is able to yield a listening window with high clarity and excellent sound reproduction where the speaker is not coloring the sound but instead reproduces the recorded sound as close to the original as possible. In reality sound from domestic speakers is often listened to off-axis, it is therefore important to improve the off-axis response such that a wider listening window can be achieved. Another quantitative measure of good sound quality is a flat sound power response as a function of frequency. This is confirmed by Linkwitz in [97] and by Olive's comprehensive study in [98, 99]. A flat sound power response in a wide frequency range would mean that sound is radiated evenly in all directions from the speaker. If a speaker with frequency-independent sound power is placed in a different room than the listener, the sound quality will be much better than a directional loudspeaker placed in the same room. It is also stated by Linkwitz in [100] that in-order to hide the room, then the loudspeakers must illuminate the room uniformly for all frequencies. To achieve this two stereo loudspeakers with multiple drivers should be placed in a feasible position in a listening room. Obtaining a flat power response over a broad frequency range from a single loudspeaker unit is not physically possible; instead, a loudspeaker with multiple units is required. If sound power should be formulated as an objective function for a single unit, one should optimize for smoothness and relax the requirements on the flatness of the response.

In this work, it is chosen to consider the optimization of a single loudspeaker unit. It is desired to be able to pose requirements on the sound pressure level both on-axis and off-

axis. By including directivity control in the optimization problem, it is possible to achieve a flat on-axis response but also create a wider listening window that offers a reasonable flat off-axis response that is aligned with the on-axis sound pressure level. These requirements are encapsulated in the following objective function

$$\phi_{0_k} = \sum_{i=1}^{n} \left(T_L - \mathbf{spl}_k \boldsymbol{\tau}_n \right)^2, \tag{4.15}$$

here $\boldsymbol{\tau}_n$ is a zero vector with ones at the DOF corresponding to the values that is included in the objective function and **spl** is the sound pressure level for all DOF. By choosing multiple $\boldsymbol{\tau}_n$ it is possible to specify the target response at multiple angles in the objective function, here n is the total number of measuring points. In [P3] it is desired to achieve a flat horizontal frequency response. The objective function in Eq. (4.15) is used in the design problem, but only one angle is included. If angles up to 90° are included in the objective function in Eq. (4.15) then that would correspond to optimizing for a frequency independent power response.

The adjoint approach [101] is applied since it is a fast method for obtaining design sensitivities for problems with many design variables. First, the adjoint equation is solved for each frequency to obtain the Lagrange multipliers

$$\tilde{\mathbf{S}}_k^T \boldsymbol{\lambda}_k = - \left(\frac{\partial \phi_{0_k}}{\partial \tilde{\mathbf{u}}_{r_k}} - j \frac{\partial \phi_{0_k}}{\partial \tilde{\mathbf{u}}_{i_k}} \right)^T. \tag{4.16}$$

Here $\tilde{\mathbf{S}}_k^T$ is the system matrix of the state equation and $\boldsymbol{\lambda}_k$ is the lagrange multipliers, $\tilde{\mathbf{u}}_{r_k}$ and $\tilde{\mathbf{u}}_{i_k}$ are the real and imaginary part of the solution vector of the state equation, respectively. More details regarding the derivation of the analytical gradients can be found in the appendix of [P4].

With the adjoint solution the design sensitivities can be computed for each frequency k as

$$\frac{\partial \Phi_{0_k}}{\partial x_j} = \mathrm{Re} \left(\boldsymbol{\lambda}_k^T \frac{\partial \tilde{\mathbf{S}}_k}{\partial x_j} \tilde{\mathbf{u}}_k \right),$$

where $\frac{\partial \tilde{\mathbf{S}}}{\partial x_j}$ is the derivative of the system matrix. For the density based method this expression is derived analytically and the design sensitivities are computed with respect to the element design variable. For the FFD method the design sensitivities are computed with respect to the control points, and this expression is computed with finite difference [95]

$$\frac{\partial \tilde{\mathbf{S}}_k}{\partial x_j} = \frac{\tilde{\mathbf{S}}_k(x_j + h) - \tilde{\mathbf{S}}_k(x_j)}{h} \tag{4.17}$$

where h is a small number, in this work $h = 10^{-5}$ based on a study of the step size.

4.3.2 Solving the Optimization Problem

This section serves to give a crude outline of how the optimization problem is solved and the design variables updated. In this work, two different optimization approaches are used, density-based optimization and shape optimization based on FFD. The problem is solved by specifying the desired frequency interval, and in this interval, a series of logarithmically spaced frequencies are defined. A gradient-based optimization algorithm is used to solve the optimization problem and update the design variables in each iteration step. The design sensitivities are obtained by solving an adjoint problem [101]. In this work, the nonlinear mathematical program MMA [86] is used, this method solves a convex

subproblem for each design iteration. The implementation of the minimax design problem into the MMA program follows [102]. The optimization routine is terminated once a specified stopping criterion is reached, here the change in design variables between the current and the previous step is used. In Alg. 1 one can see the outline of the program for optimizing the material properties with a density-based approach. The FFD method follows the same general structure and is therefore not presented here.

Preprocessing: Setup model problem, select design domains and objective function, initialize start configuration of α_e, β_e and η_e ;
Discretize PDEs for fully coupled system; Compute neighbourhood matrix $\mathbf{N}_e$;
while $\max(|\mathbf{x}_{new} - \mathbf{x}_{old}|) < 0.005$ **do**
  Assemble $\mathbf{K}$ and $\mathbf{M}$;
  for *k=1 to number of frequencies* **do**
    Solve state eq. $\tilde{\mathbf{S}}_k \tilde{\mathbf{u}}_k = \tilde{\mathbf{f}}$;
    Compute Φ_{0_k} from state eq.;
    Solve adjoint eq. $\mathbf{S}_k^T \boldsymbol{\lambda}_k = -\left(\frac{\partial \phi_{0_k}}{\partial \tilde{\mathbf{u}}_{r_k}} - j\frac{\partial \phi_{0_k}}{\partial \tilde{\mathbf{u}}_{i_k}}\right)^T$;
    Compute design sensitivities $\frac{\partial \Phi_{0_k}}{\partial x_j} = \mathrm{Re}\left(\boldsymbol{\lambda}_k^T \frac{\partial \tilde{\mathbf{S}}_k}{\partial x_j} \tilde{\mathbf{u}}_k\right)$;
  end
  Apply sensitivity filter $\widehat{\frac{\partial \Phi_0}{\partial x_j}}$;
  Define ϕ_0 as $\max(\phi_{0_k})$;
  Update $\mathbf{x}$ with MMA;
end
Postprocessing: Evaluate optimized design;

Algorithm 1: Outline of the program used to optimize the density based problems.

This chapter presented the methods used and developed during this work. In subsequent chapters the methods will be applied to design problems. The contributions from this chapter will be summarized together with the contribution sections present in Chapters 5 and 6.

5 Density Based Material Optimization

This chapter is concerned with the optimization of the material properties of loudspeakers. The results produced in this chapter rely on the density-based optimization method introduced in chapter 4. The main results of each paper are discussed, and for the full overview, the relevant paper should be consulted. The contents of this chapter are organized as follows. First, the initial investigation of the applicability of changing material properties and how that can affect the output of a circular disk is presented. A practical example is then investigated where the homogeneous material distribution in a passive radiator is optimized to enhance the low frequency performance of a smart speaker. Finally, the frequency response and directivity of a 5-inch generic loudspeaker are optimized by controlling the material properties in each element.

5.1 Maximizing the Output of a Oscillating Circular Disk [P2]

This research initiated a deeper investigation into optimization on fixed geometries where no changes to the topology occur. The research shows that the output can be heavily affected by changing the material properties of a given structure. As it is based on early work in this thesis, the excitation of the structure is a constant force, and the optimization considers only a single frequency. The work can be viewed as a proof-of-concept that has continuously been expanded during this project. Here, the density and stiffness are directly linked, so only a single design variable is used in each element. The damping of the structure is not considered

$$\rho^e = \rho_{min} + \alpha^e \left(\rho_{max} - \rho_{min}\right) \tag{5.1}$$

$$E^e = E_{min} + \alpha^e \left(E_{max} - E_{min}\right), \tag{5.2}$$

here ρ_e is the element density, ρ_{min} and ρ_{max} is the lower and upper bound of the element density, respectively, α_e is the element design variable, E^e is the element stiffness, and E_{min} and E_{max} is the lower and upper bound of the element stiffness.

Fig. 5.1 shows an example from the paper. Here the pressure is maximized[1] in the area marked with the red square at a single frequency. The increase in pressure for the optimized designs is visible compared to the original design. One design is meshed with a single element in the vertical direction, and the other has five elements. The two designs have similar layout tendencies. However, the design with five elements in the vertical direction utilizes the increased design freedom. This design has a stiff and heavy core at several locations, where a soft and light material is surrounding the core. The presented approach has limited applicability as it only considers a single frequency in the optimization. The design freedom of the example is limited by the fact that only one design variable for each element is used. The presented results have rigorous bounds enforced on the element

[1] This is a dummy objective function made to test the approach in the early stages of the project. The maximization of pressure is generally not a design problem that is considered.

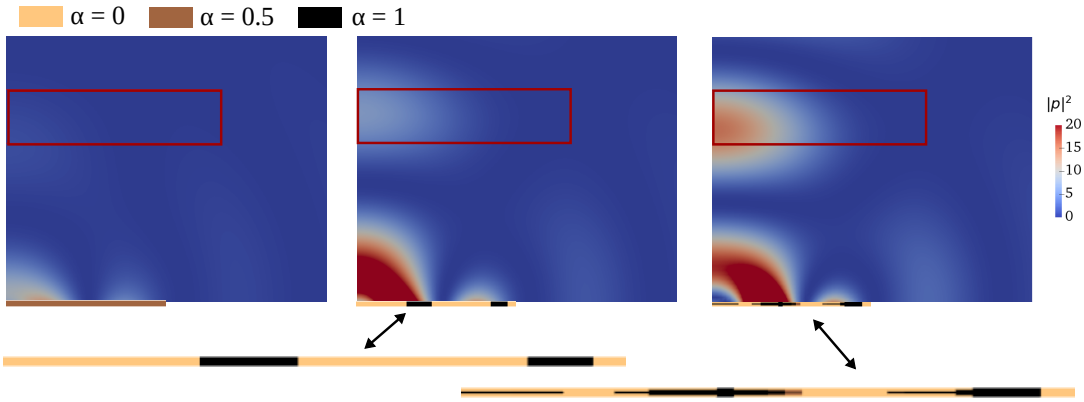

Figure 5.1: 1500Hz excitation frequency, $|p|^2$ evaluated for the starting guess (left), optimized design with 1 element in the vertical direction (middle) and optimized design with 5 elements in the vertical direction (right). The figure and caption is from [P2].

stiffness. In this paper, there is only a factor of three between the lower and upper bound of the stiffness. A similar relationship is present between the lower and upper bound of the density. However, that is far less restrictive as this range spans almost the entire range density that is to be expected from materials used for loudspeaker units.

5.2 Optimizing the Low Frequency Performance of a Smart Speaker [P3]

Smart speakers are becoming more popular in many households, and as a consequence, it is increasing in popularity for music listening [103]. This gadget is often quite costly, and therefore many expect it to provide superior sound reproduction. However, the small size of the speaker units and the loudspeaker in general makes this difficult. Especially the reproduction of low frequencies can be problematic. It is beneficial to add either digital signal processing, a vent/port or a passive radiator to the loudspeaker to boost the output at low frequencies. The research in [P3] deals with the optimization of the materials used in a passive radiator and this section will give a brief overview of this work.

The model problem for the smart speaker can be seen in Fig. 5.2. The cabinet walls are assumed to be rigid, and the hybrid FE-LPM approach from [P1] is applied to model the loudspeaker, the lumped values for this particular model problem are presented in [P3]. As illustrated in Fig. 5.2 there are two design domains $\Omega_{d,1}$ and $\Omega_{d,2}$ corresponding to the diaphragm and surround, respectively. The material properties in each design domain are assumed to be homogeneous.

The assumption of a homogeneous material in each design domain implies that in $\Omega_{d,1}$ and $\Omega_{d,2}$ all the element design variables controlling the stiffness has the same value, the same goes for mass and damping. The interpolation functions are assumed to be linear

$$\begin{aligned} E &= E_{min} + \alpha \left(E_{max} - E_{min}\right) \\ \rho &= \rho_{min} + \beta \left(\rho_{max} - \rho_{min}\right) \\ \eta &= \eta_{min} + \zeta \left(\eta_{max} - \eta_{min}\right). \end{aligned} \tag{5.3}$$

The upper and lower bounds on the material properties are shown in Tab. 5.1.

Furthermore, the author has decided to re-run the optimization with the knowledge gained from the study of available materials for loudspeakers from [P4]. This was done in order

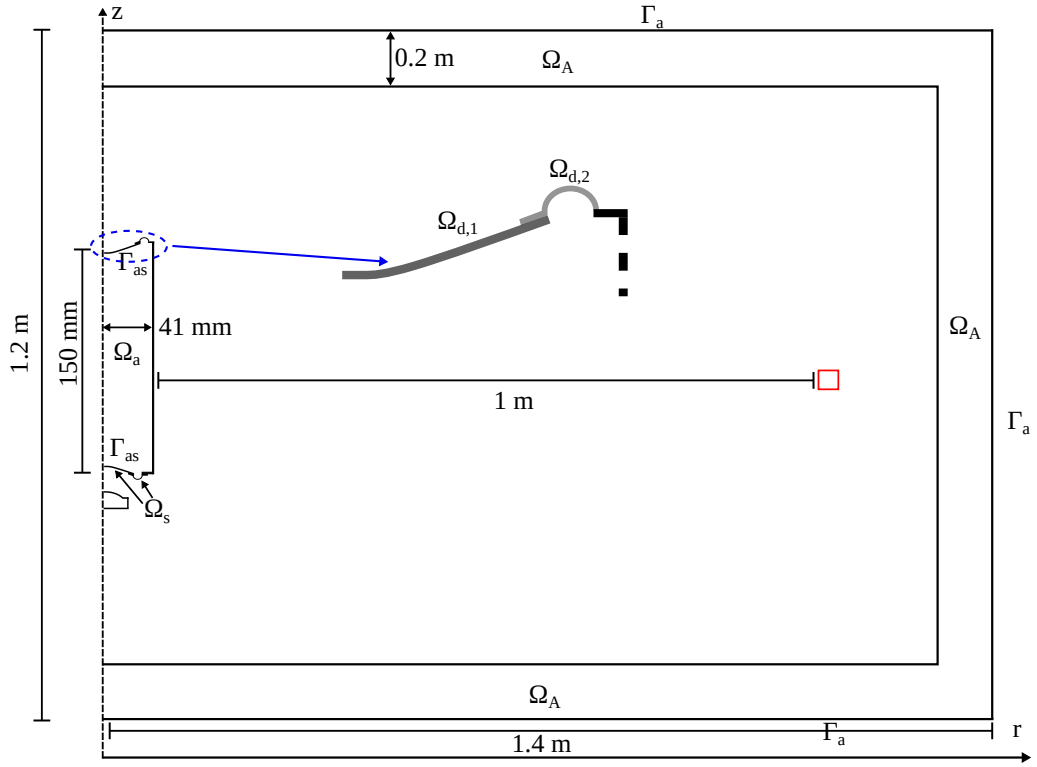

Figure 5.2: Sketch of the problem to be solved, with definitions of the different domains, interfaces and boundaries. The figure is inspired from [P3] and the caption is from [P3].

Table 5.1: Bounds on the physical values. Table and caption are from [P3].

	E_{min} [Pa]	E_{max} [Pa]	ρ_{min} [kg/m^3]	ρ_{max} [kg/m^3]	η_{min} [−]	η_{max} [−]
Diaphragm	10^8	$40 \cdot 10^9$	1000	4500	0.05	0.9
Surround	$40 \cdot 10^3$	$16 \cdot 10^6$	1000	4500	0.05	0.9

to run the optimization with more realistic choices of materials and apply the gained knowledge to new problems. The major change is that the stiffness and mass are assumed to be co-dependent in the diaphragm of the passive radiator as seen in Eq. (4.2). The bounds on the material properties are changed according to [P4] and can be seen in Tab. 5.2.

Table 5.2: Bounds on the physical values for the new third optimization case. Table is from [P4].

	E_{min} [Pa]	E_{max} [Pa]	ρ_{min} [kg/m^3]	ρ_{max} [kg/m^3]	η_{min} [−]	η_{max} [−]
Diaphragm	$1 \cdot 10^9$	$140 \cdot 10^9$	700	5000	0.05	0.3
Surround	$1 \cdot 10^6$	$10 \cdot 10^9$	850	1900	0.01	0.3

The design problem is cast as a minimax formulation introduced in Chapter 4. For this particular optimization setup, the disadvantage of using the minimax formulation is related to the desire to enhance the low frequency performance. Due to the design of the speaker, there are physical limits on how low the frequency range can go. This means that some trial-and-error is involved in including the right frequency range in the optimization

problem. If the range is specified for too low frequencies the result will converge to a sub-optimal solution. The reason for that lies in the nature of the minimax formulation as it will always minimize the maximum value, and in this case, that will be the lowest frequency in the specified range. If it is not possible to improve the design for this specific frequency due to e.g. physical limitations, the optimization will stop.

The objective function is the difference between the pressure squared in a small area of 5x5 cm 1 m away from the speaker as indicated in Fig. 5.2 and the desired target squared. The frequency range is 100 Hz - 170 Hz and is included in the optimization by 20 logarithmic spaced evaluation frequencies.

$$\begin{array}{lll} \min\limits_{\mathbf{x}} \quad \max & \Phi_{0_k} = \left(T_L - \tilde{\mathbf{u}}_k^T \mathbf{L} \tilde{\tilde{\mathbf{u}}}_k\right)^2 \ , & k = 1, \ldots, b \\ \text{s.t.} & \tilde{\mathbf{S}_k} \tilde{\mathbf{u}}_k - \tilde{\mathbf{f}} = 0 \ , & k = 1, \ldots, b \\ & 0 \leq x_j \leq 1 \ , & j = 1, \ldots, a \end{array} \tag{5.4}$$

In [P3] two optimization cases are examined. The first case considers the mass of the diaphragm and the damping of the surround. This is based on the fact that extending the frequency range towards lower frequencies is governed by the first resonance frequency of the passive radiator. The mass of the passive radiator is one of the major contributions to the value of the first fundamental frequency, and the damping of the surround controls the amplitude of the response at the resonance. In the second case we allow the optimizer to tune stiffness, mass, and damping independently in both the diaphragm and the surround of the passive radiator. The third case is a new case introduced in this thesis only. It relies on the interpolation function introduced in [P4]. The third case will only consider the 6 variable case. The iteration history for the mass tuned and 6 variable case can be seen in Fig. 5.3.

In Fig. 5.3a it is observed that the mass is increased, as one would expect, while the damping is continuously lowered to the minimum allowed value. Fig. 5.3b shows the design history for the 6 variable case. Here the mass is again increased while the stiffness and damping is decreased. The ability to reduce the stiffness of the surround leads to a smaller increase in mass compared to Fig. 5.3a. In Fig. 5.3c the design history for the new 6 variable approach is shown. The starting guess looks different since the bounds on the isotropic loss factor have been made significantly smaller. Besides, α for the diaphragm is no longer linearly related to the stiffness. It is evident that the surround should be as compliant as possible. The material properties obtained from the optimization for the three cases are shown in Tab. 5.3.

Fig. 5.4 shows the frequency response of the three optimized designs and the initial design. The initial design has the same material properties in both the woofer and the passive radiator. The blue curve is the mass tuned case; it is evident that the optimization algorithm has been able to tune the resonance of the passive radiator such that low frequency performance of the smart speaker has been enhanced. The red curve shows the frequency response of the 6 variable case from [P3]. In this case, the optimized design is also better than the initial configuration and slightly better than the mass-tuned case. There is a 1 dB difference between the red and blue curves. The magenta curve is the new 6 variable approach with interpolation functions and bounds on the material properties based on [P4]. It is shown that this case performs as well as the 6 variable case from [P3] in the specified frequency range. A derived effect that is not included in the design problem is that the red curve initially displays a less steep roll-off than the blue curve. This is due to the changes in the stiffness and mass ratio. Here a more beneficial relationship between the stiffness of the surround and the stiffness of the air inside the cabinet has been obtained.

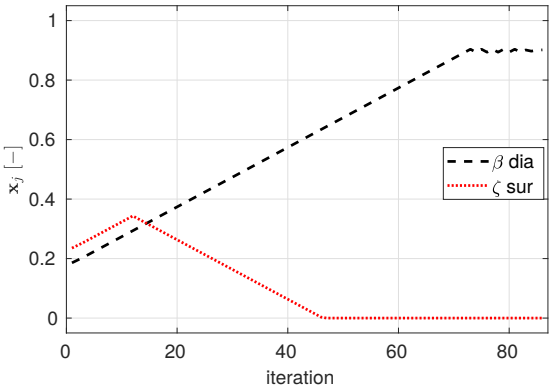

(a) Design history mass tuned

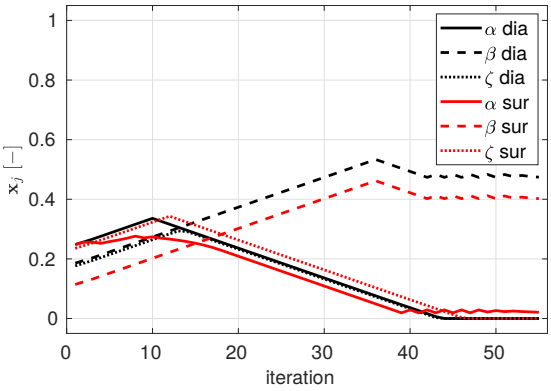

(b) Design history 6 variable case

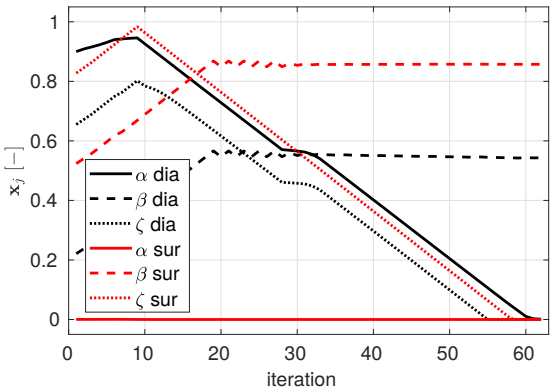

(c) Design history 6 variable case new interpolation functions

Figure 5.3: Shows the design history, here, the black curves relates to the design variables in the diaphragm and the red curves are associated with the surround. (a) is for the mass tuned case (b) is the 6 variable case (c) is for the 6 variable case with new interpolation functions and bound on the material properties. The figures (a) and (b) and caption are from [P3].

Table 5.3: Material properties obtained with optimization, (a) is the results in Fig. 5.3a and (b) is the results from Fig. 5.3b. Table (a) and (b) and corresponding captions are from [P3].

	ρ [kg/m^3]	η [−]
Diaphragm	4155	-
Surround	-	0.05

(a) Mass and damping.

	E [Pa]	ρ [kg/m^3]	η [−]
Diaphragm	10^8	2660	0.05
Surround	$37.2 \cdot 10^4$	2408	0.05

(b) All 6 variables.

	E [Pa]	ρ [kg/m^3]	η [−]
Diaphragm	1.04^{10}	3036	0.01
Surround	$1.00 \cdot 10^6$	1750	0.01

(c) All 6 variables for the new optimization case.

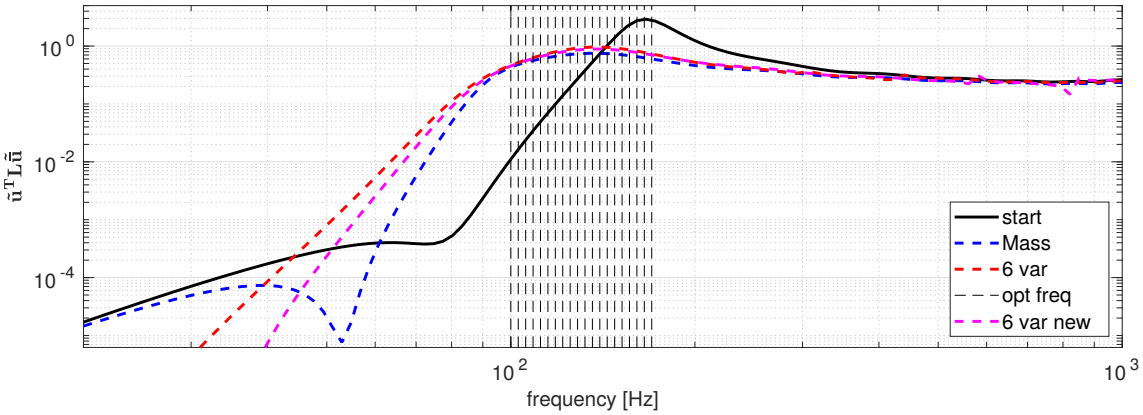

Figure 5.4: Frequency response function for the initial guess (solid black line), mass tuned passive radiator (dashed blue line) and the 6 variable optimization (dashed red line). The dashed vertical lines indicates the 20 logarithmic spaced discrete frequencies between 100-170Hz. Figure and caption are from [P3].

This effect is much less pronounced for the magenta curve as it is less compliant, and the air stiffness inside the cabinet is, therefore, less dominant. Passive radiators are often based on the textbook design of vented boxes, which relies on equivalent circuit models. This means that the stiffness of the surround is traditionally not included in the design of the passive radiator. The presented research shows that the stiffness of the surround seems to influence the frequency response. Therefore, it should be included in the design of passive radiators as the correct choice of the stiffness of the surround is beneficial to the low frequency output of the passive radiator.

5.3 Optimization for Flat Frequency Response with Directivity Control [P4]

In earlier chapters some of the quantitative measures that describe a high-quality loudspeaker was discussed. It was highlighted that either the sound pressure level or the sound power is a good measure of a speaker's ability to yield high-quality sound reproduction. It is well-established that the frequency response should be flat on-axis, and ideally, the off-axis response should be aligned with the on-axis response [3, 104]. Therefore, this

section investigates in what frequency range this can be achieved and how wide the listening window can be made for the single loudspeaker unit from [P1]. The optimization is density-based and relies on controlling the materiel properties in each individual element. The results produced in [P4] assume that unconditional design and production freedom is accessible. This implies that the presented designs might not currently be produced with conventional techniques, even though the design is made of commercially available materials. Knowledge and inspiration can be gained from the suggested designs. The designs can indicate what is theoretically achievable. With the ongoing rapid development within the scientific research fields of additive manufacturing of elastomers [105, 106] and functionally graded materials [107], it is plausible that these designs could be produced in the future. This section explains the model problem and the results briefly. The design method is described in Chapter 4 and in [P4]. For an in-depth dive into the finer details, the reader is referred to [P4], here the approach is explained in detail, and the initial configurations, the layout of the optimized designs etc. are presented.

The model problem can be seen in Fig. 5.5. The 5-inch speaker is mounted in an infinite baffle. The computational domain for the solid region is denoted Ω_s, the acoustic domain is Ω_a and the PML region is Ω_A. In this work, there are two design domains $\Omega_{d,1}$ and $\Omega_{d,2}$ corresponding to the diaphragm and the surround, respectively. The sketch also shows the placement of measuring points used to evaluate the objective function. The measuring points are spaced 2 degrees apart and they are all 1 m away from the loudspeaker driver.

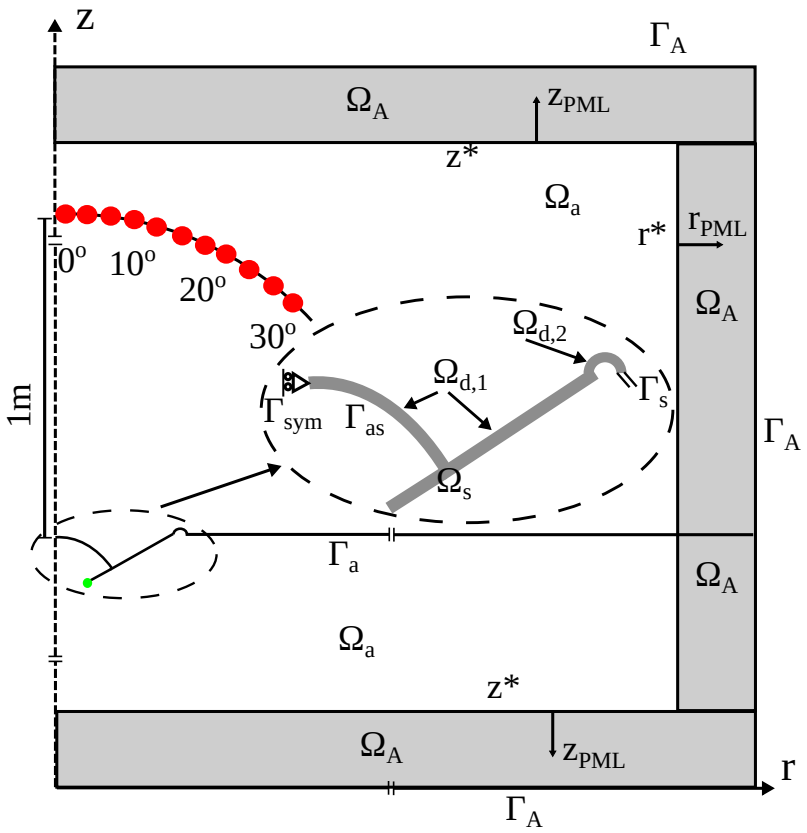

Figure 5.5: 2D sketch of the 5-inch loudspeaker driver with boundary conditions. The green circle indicates where the LPM is coupled to the FE model. The red dots indicate where the objective function is measured. Figure and caption are a combination of the figures from [P4].

This work has compiled the materials that could be used for loudspeaker manufacturing using the program Ansys Granta EduPack [88]. It is assumed that the surround can be made from elastomers and soft plastics as seen in Fig. 5.6a. Here, the red areas are thermoplastic elastomers, and the light blue color is thermoset elastomers and soft plastics are indicated with a dark blue color. The materials that can constitute the loudspeaker diaphragm are shown in Fig. 5.6b. For the diaphragm, a more comprehensive range of materials can be used, such as paper, plastic reinforced with Kevlar, glass or aramid fibers, a ceramic matrix with metal, or metals such as aluminum, magnesium, and titanium.

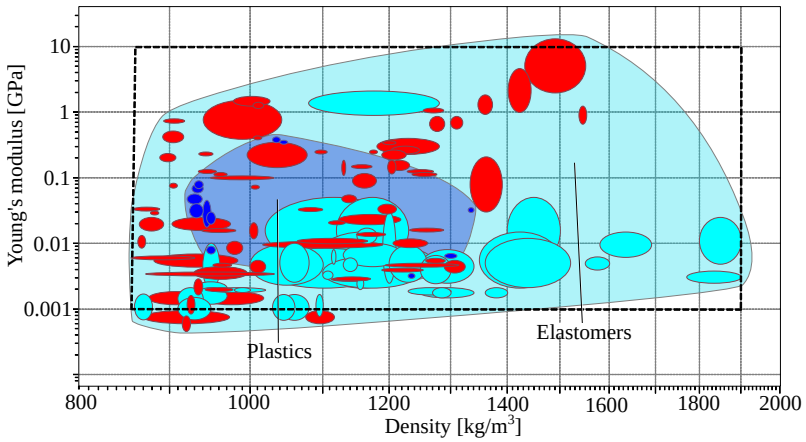

(a) Surround

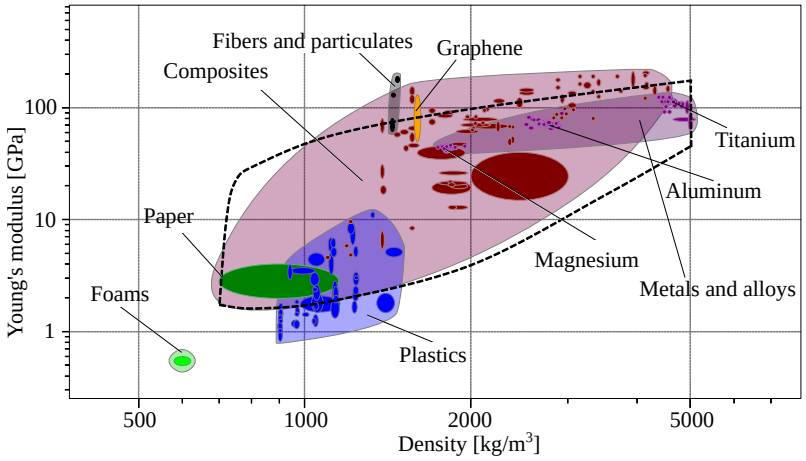

(b) Diaphragm

Figure 5.6: The available materials that can be used to manufacture the surround and diaphragm for a dynamic loudspeaker, created with GRANTA EduPack [88]. The figures are from [P4].

Based on the findings in Fig. 5.6 a series of interpolation functions with corresponding bounds were posed. The interpolation functions approximate the span of the available materials. The range covered by the interpolation functions is indicated with the dashed line in Fig. 5.6. These lines are represented by the interpolation functions presented in Eq. (5.5) which governs the material optimization in the surround and Eq. (5.6) which are concerned with the materials in the diaphragm. The interpolation functions are limited

by the bounds shown in Tab. 5.4.

$$\begin{aligned} \rho_e^s &= \rho_{min} + \beta_e \left(\rho_{max} - \rho_{min}\right) \\ E_e^s &= E_{min} + \alpha_e \left(E_{max} - E_{min}\right) \\ \eta_e^s &= \eta_{min} + \zeta_e \left(\eta_{max} - \eta_{min}\right). \end{aligned} \tag{5.5}$$

Here subscript *min* and *max* refers, respectively, to the lower and upper bound of the material property, α_e, β_e and ζ_e are three independent element design variables, and superscript s indicates that the material properties here are defined for the surround.

$$\begin{aligned} \rho_e^d &= \rho_{min} + \beta_e \left(\rho_{max} - \rho_{min}\right) \\ E_e^d &= E_{min} + 1.8 \cdot (0.5\beta_e)^{2.6-2.1\alpha_e} \left(E_{max} - E_{min}\right) \\ \eta_e^d &= \eta_{min} + \zeta_e \left(\eta_{max} - \eta_{min}\right). \end{aligned} \tag{5.6}$$

Here superscript d express that the material properties are defined for the diaphragm.

Table 5.4: Bounds on the physical values. Table and caption are from [P4].

	E_{min} [Pa]	E_{max} [Pa]	ρ_{min} [kg/m^3]	ρ_{max} [kg/m^3]	η_{min} [−]	η_{max} [−]
Diaphragm	$1 \cdot 10^9$	$140 \cdot 10^9$	700	5000	0.01	0.3
Surround	$1 \cdot 10^6$	$10 \cdot 10^9$	850	1900	0.01	0.3

The design problem is formulated as a minimax formulation. In this study, the objective function is based on the sound pressure level 1 m away from the loudspeaker unit at different angles as illustrated in Fig. 5.5. The objective function is formulated to impose a target level for the sound pressure level. If the objective function is successfully minimized, the resulting frequency response should be flat in the specified frequency range for the angles included in the optimization. The lower bound of the frequency range is always 600 Hz. Different upper bounds are used to see how wide a frequency range this design problem can be applied to. The upper bounds on the frequency range are 5 kHz, 6 kHz, 7kHz, 8 kHz, 9 kHz, and 10 kHz. This implies that the frequency range spans at least 3 octaves and the widest span is over 4 octaves. The response is measured at different angles to allow for the control of the off-axis response in order to make it more well behaved. The angles included vary from purely considering the on-axis response to considering the off-axis response up to 30°. If off-axis angles are included, they are summed as indicated in the design problem below, e.g if the angle 18° is included the objective function would contain the response for 0°, 2°, 4°, 6°,..., 18°.

The target is specified based on the initial response of the dynamic speaker. In this case $T_L = 74$ dB is chosen as it aligns the target frequency range with the low frequency response of the dynamic speaker.

$$\begin{aligned} \min_{\mathbf{x}} \quad \max \quad & \phi_{0_k} = \textstyle\sum_{i=1}^{n} \left(T_L - \mathbf{spl}_k \boldsymbol{\tau}_n \right)^2 , && k = 1, \ldots, b \\ \text{s.t.} \quad & \tilde{\mathbf{S}}_k \tilde{\mathbf{u}}_k - \tilde{\mathbf{f}} = 0 , && k = 1, \ldots, b \\ & 0 \leq x_j \leq 1 , && j = 1, \ldots, a \end{aligned} \tag{5.7}$$

The initial design used for the optimization is based on a paper pulp diaphragm and a sufficiently compliant surround both with adequate levels of damping. The decent initial guess serves two purposes. The high damping values and feasible materials mean that there

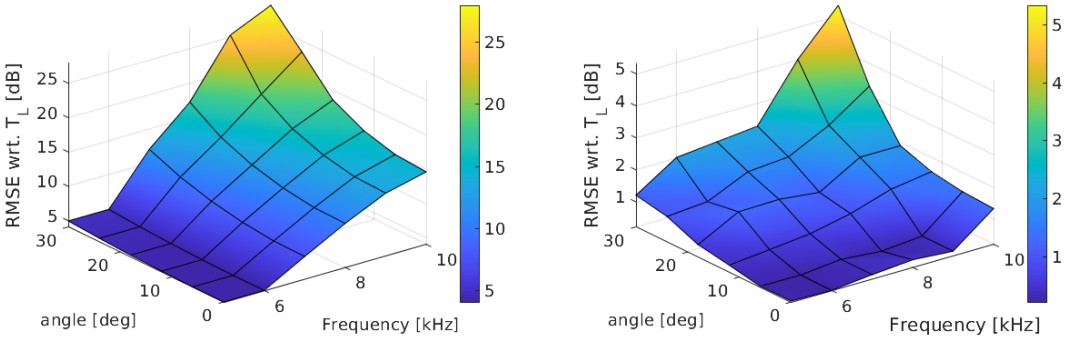

(a) Initial design (b) Optimized designs

Figure 5.7: The RMSE with respect to the target, T_L, for the original design and optimized designs. The figures and captions are from [P4].

are no trivial solutions to the optimization problem i.e. just increasing the damping and thus flattening the response is not an option. Secondly, a good initial guess simply yields the best optimized solutions. Many different starting configurations such as a uniform starting guess with all design variables equal to 0.5 or a completely random distribution of design variables, have been tried. In most cases, these starting guesses have not been able to yield as good results as just using the material properties of a decent loudspeaker driver. This can mainly be attributed to the fact that by changing the material configuration drastically, the fundamental frequency of the speaker unit is changed. The author has also experimented with keeping the initial material properties of the outer suspension intact and then either enforcing a uniform or randomized starting guess in the diaphragm. These results are improved and are in many cases close to obtaining similar results as using the baseline configuration of the speaker unit as a starting point for the optimization.

The optimization utilizes a sensitivity filter in each design domain as presented in Eq. (4.3). The sensitivity filter smooths the design sensitivities, reducing the level of thin details of the layout of stiffness mass and damping. The filter is applied to ensure that the optimized designs could be realized from a manufacturing point-of-view. The filter radius is equal to 1 mm.

The results from the 36 optimization runs are summarized in Fig. 5.7. Here the x and y-axis represent the upper bound for frequency and angle, respectively, and the z-axis is the root-mean-square error (RMSE) between the specified target, T_L and the objective function of the optimized designs. The computational cost is between 50-200 CPU hours for each design, depending on how many design iterations are necessary before convergence is reached. The optimized designs in Fig. 5.7b are improved for all design cases with at least a factor of 5 when compared to the performance of the initial configuration in Fig. 5.7a. Fig. 5.7b indicates that a reasonably flat response is achievable for a wide frequency range and directivity. The very directional loudspeaker unit designs with a narrow listening window seem to yield an entirely flat frequency response in almost all of the frequency ranges investigated.

One of the key aspects of the paper is achieving a completely flat frequency response over a very broad frequency range for a loudspeaker unit with a narrow listening window. In Fig. 5.8 the frequency response for the optimized design with the angles 0°, 2°, 4° and 6° and the frequency range of 600 Hz to 8 kHz is shown. For this design, the RMSE is only 0.26 dB compared to the target line. The largest deviation from the target line in

the entire frequency range of interest is only 0.4 dB.

The steep roll-off in the frequency response at 8 kHz illustrates that the loudspeaker unit is purely optimized for specific conditions formulated in the design problem.

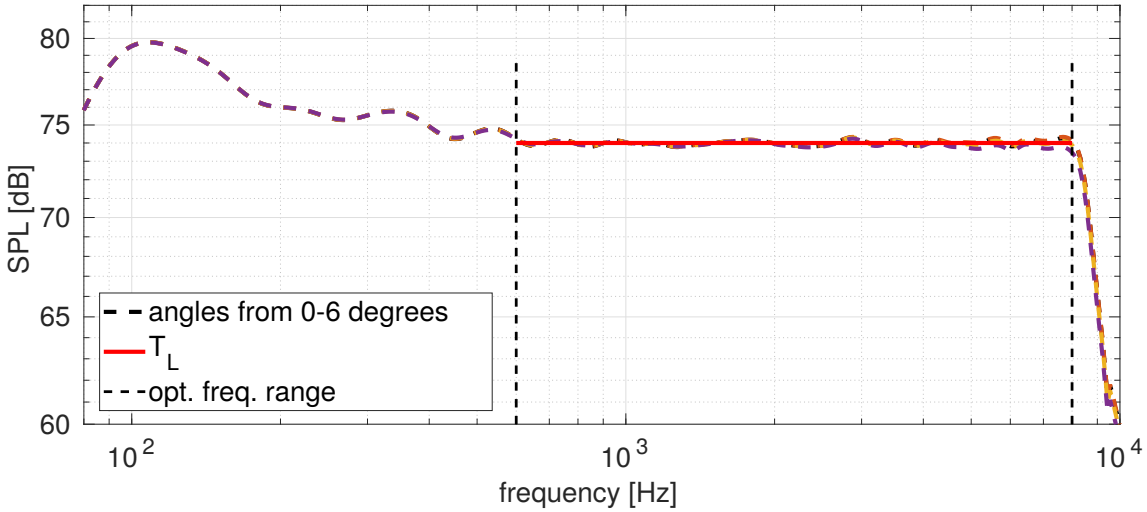

Figure 5.8: Frequency response for the optimized design between 600Hz and 8kHz up to an angle of 6 degrees away from the center axis. The figure and caption are from [P4].

Fig. 5.9 shows the surface velocity vectors representing magnitude and direction for the real part of the surface velocity, and the plot also shows the real part of the pressure field at 7600 Hz. In Fig. 5.9a the motion at this frequency is shown for the original design. The plot shows that the majority of the motion is present in the diaphragm of the speaker, where a break-up mode is present. This results in a far from optimal pressure field with a severely reduced magnitude compared to Fig. 5.9b. Fig. 5.9b shows field variables for the optimized design with a narrow listening window from Fig. 5.8 at 7600 Hz. The vibration pattern has changed due to the optimization. As it is also pointed out in [P4] the wavelength at high frequencies is short. In this case, the depth of the speaker cone corresponds to roughly a half wavelength. This means that to create a spherical wavefront, the surface velocity of the diaphragm should not be uniform. The effect of this can be seen in the optimized speaker, here, a negative pressure is situated where the dust cap and diaphragm intersect. The tuning of the break-up mode allows the speaker to generate an output with a higher magnitude and is, therefore, able to keep the pressure constant over a large frequency range.

5.4 Discussion of Methods and Results

The multi-frequency optimization examples rely on the minimax formulation. It is a strong optimization tool for multi-frequency optimization as it is forced to minimize the outliers and thereby create significant improvements to the frequency response. However, it also has its weaknesses as pointed out in the section about enhancing the low frequency performance of the passive radiator. Here, some trial-and-error adjustments are required to get the optimization algorithm to work. With these adjustments, it is possible to achieve excellent results. However, the behavior of the response below the specified frequency range is not controlled by the optimization algorithm. Similarly, for the 5-inch speaker, it is clearly shown that the frequency-response has a very steep roll-off above the frequency range included in the design problem. It would be beneficial to formulate the design problem such that the calculated objective function value could be weighted. For example,

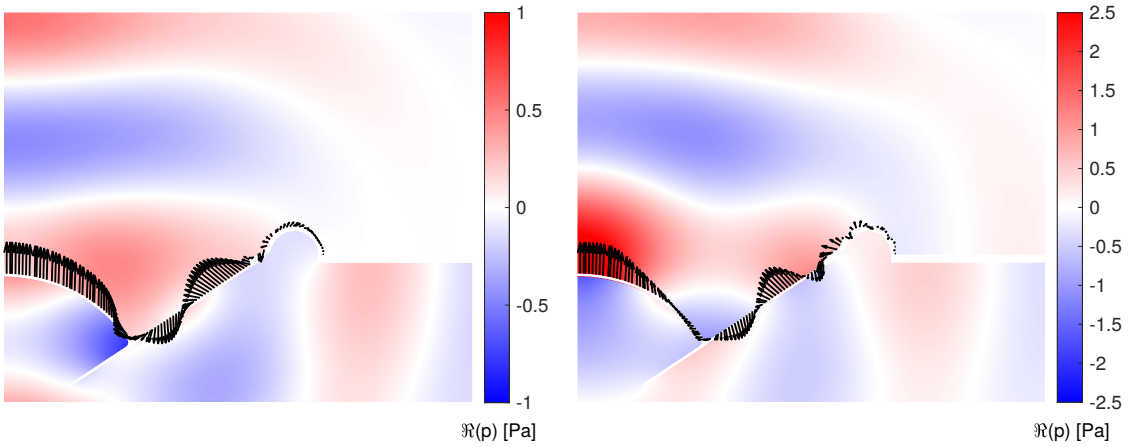

(a) Initial design (b) Optimized design

Figure 5.9: Arrow plot for the surface velocity of the loudspeaker unit and the real part of the pressure field at 7600 Hz. (a) is the initial design (b) is the optimized design. The figures and captions are from [P4].

the current specified frequency range would have a weight equal to one. For the passive radiator example, one could include frequencies below the specified range and then apply a decaying weight function to control the frequency response better. A similar feature could be implemented for the 5-inch loudspeaker unit; here a decaying weight function could be applied to the objective function calculated above the current specified range. This would enforce a control on the frequency response that could improve the results even more.

This section has shown that it is indeed possible to improve the frequency response of loudspeakers. Both low and mid-to-high frequencies have been considered in the design problems. These improvements are encouraging, and the applied approach shows that significant improvements to the frequency response are achievable. It was shown that directivity control could be included in the optimization problem. Based on these findings, it would be interesting to expand the objective function to minimize unwanted sound radiation. Therefore, an addition to the current objective function would be to minimize sound radiated towards either the floor or the ceiling. One could also imagine that further optimization constraints could be added to the 5-inch speaker example. The constraints should be concerned with the manufacturing of the design. Either an approach where different parts of the speaker are assumed homogeneous, similar to [P3], or one could impose projection filters to force convergence towards predefined materials. An anisotropic material model could also be adapted to consider composite materials in detail. The considered interpolation functions are in most cases based on rather simple bounds. The method is formulated such that these bounds can be changed, thus restricting the material choices available for the optimization algorithm. A deeper investigation into manufacturing limitations could yield more realistic and strict bounds.

5.5 Contribution

Paper 2 shows that altering the material properties of a flat disc is able to change the acoustic output of the vibrating disc. The design is using only one design variable in each element meaning that element stiffness and mass are directly linked. The objective of the paper is to maximize the output at single frequencies, here three individual frequencies are investigated. The paper shows that the output can be significantly affected by changes in the material properties. This inspired further work into optimizing the material properties

of actual loudspeakers over broad frequency ranges.

Paper 3 presents a numerical model of a cylindrical smart speaker with a passive radiator. The paper deals with the enhancement of the low frequency performance of the speaker by optimizing the materials of the passive radiator. Two approaches were investigated in the paper, one case restricted the optimization to only consider the mass of the diaphragm and the damping of the surround. In the second case the optimizer could change stiffness, mass and damping in both the diaphragm and surround. The design problem is formulated as a minimax problem with 20 frequencies. The results show that it is indeed possible to boost the output at low frequencies, for both of the presented methods. By including stiffness, mass and damping of both the surround and diaphragm the impact on the frequency response from these parameters was clear. It was shown that the stiffness of the surround has a major impact on the low frequency output, here and adequately tuned stiffness yielded a less steep roll-off.

Paper 4 investigates what is theoretically possible if almost complete design freedom is assumed. The paper focus on the optimization of a loudspeaker unit. The key aspect of the paper is to obtain a flat wide band frequency response for different range of directions. This is achieved by optimizing the local material properties in each individual element in the loudspeaker diaphragm and surround. The range of material properties that the elements can attain are based on a study of available materials for loudspeakers. The study concerns numerous different frequency ranges and directivities in-order to map the limits of the proposed design method. It is shown that for loudspeaker units with a narrow directivity it is possible to achieve an almost perfectly flat response from 600 Hz to 9 kHz. The study investigates the performance of the optimized solutions as demands on a wider directivity for the solutions are imposed. These results show that a flat response with ± 2.5dB in a wide frequency range in many cases are achievable with the proposed optimization technique.

6 Shape Optimization of Speakers [P5]

Earlier in this thesis and in [P3] a cylindrical smart speaker was considered as a design problem. The goal was to extend the low frequency range by optimizing a passive radiator. This chapter presents the work done in [P5], here the same smart speaker is considered. However, the goal is now to improve the speaker's performance at mid-to-high frequencies. The speaker is down-firing, so the key aspect would be to design an acoustic lens that can create a flat horizontal frequency response. Moreover, the shape of the speaker itself is also considered. The use of numerical simulation tools (without optimization) have in [12] been used to compute the response of an acoustic lens, the lens was later installed in several domestic loudspeakers. Before numerical tools became available analytical solutions and geometric considerations were used to design lenses as seen in e.g. [108, 109]. The research presented in this chapter uses numerical optimization techniques to optimize the shape of the lens and woofer based on the desired response characteristic included in the objective function. This chapter presents a brief overview of the contents of [P5] for a more detailed description of the problem-at-hand, the initial configurations, and the complete set of results the paper should be consulted.

The model problem is seen in Fig. 6.1 consists of a cylindrical smart speaker with a 3-inch down-firing woofer and a passive radiator. The woofer is partly lumped following the principles presented in [P1], and the lumped values used in this numerical setup can be found in [P5]. It is desired to improve the horizontal frequency response of the smart speaker. This is achieved by optimizing the shape of both the woofer and an acoustic lens. Shape optimization relies on a decent starting guess for the optimization; therefore, several initial configurations are examined. The three shapes used are shown in Fig. 6.1. The shapes are flat, spatidate-shaped, and triangular-shaped from top to bottom. The lens is initially situated with the distance L_D from the woofer. The design region referring to the woofer is denoted $\Omega_{d,w}$, and $\Omega_{d,l}$ is the design region associated with the lens.

Fig. 6.2 shows how the design domain is subdivided into two rectangular regions with bivariate Bernstein polynomials. In this figure, one region controls the shape of the woofer, and another region is governing the shape of the acoustically rigid lens. In Fig. 6.2 an initial configuration is shown; the red and green dots are the control points. The red color indicates an inactive control point, and the green-colored control points are active during the optimization. The control points placed directly onto the z-axis are restricted to only move in the z-direction. This avoids a nonphysical mesh and unwanted holes in the design region. The shape of the solid regions is altered by changing the coordinates of $\mathbf{d}_{i,j}$. Each control point is subject to a box constraint to prevent extensive deformations. In the upper and lower FFD regions, the control points are allowed to move ± 15 mm and ± 50 mm in both r and z-directions from their initial location, respectively.

To extend the speaker's frequency range, a design problem is formulated. The design problem minimizes the error between the speaker's sound pressure level and the desired target line T_L. The design problem is a minimax problem that uses the r and z-directions of the control points as design variables. If the speaker is considered without any lens, the sound pressure level drops above 5 kHz as shown in [P5]. Therefore, the design problem's

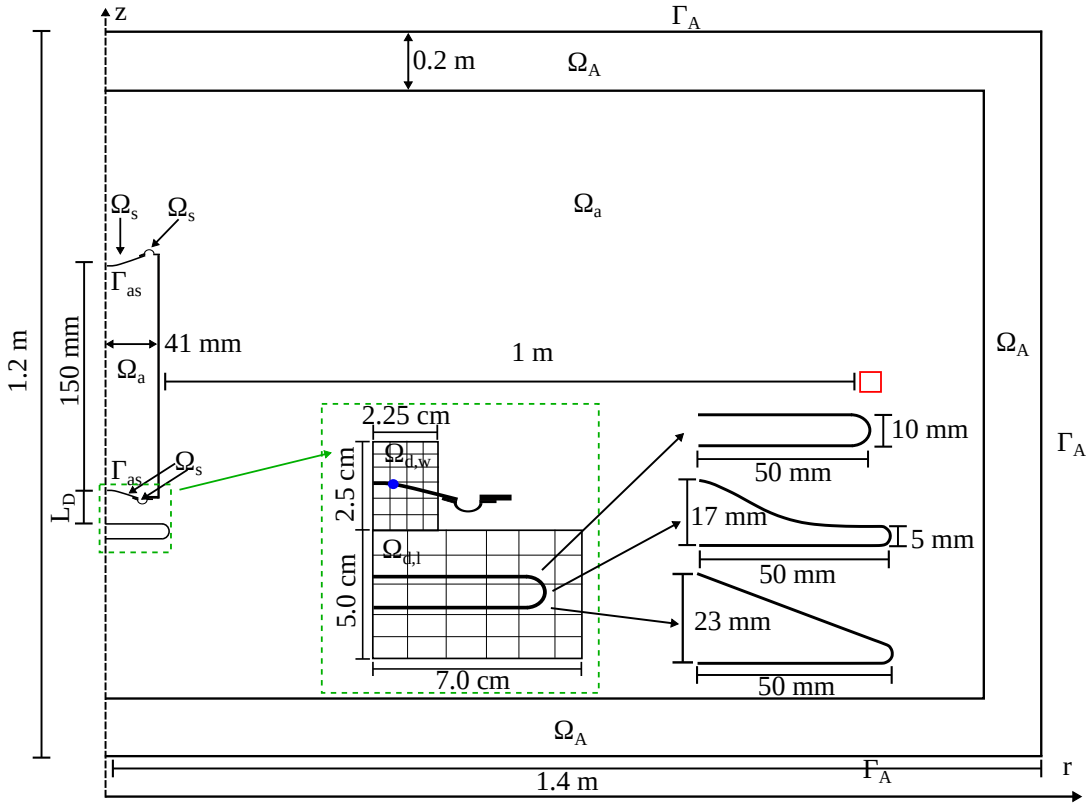

Figure 6.1: 2D sketch of the compact speaker with domain names and boundary conditions and dimensions The blue circle indicates where the LPM is coupled to the FE model. The red square is the measurement point where the objective function is evaluated. The two design domains $\Omega_{d,w}$ and $\Omega_{d,l}$ contain the grid of Bernstein Polynomials. The three lens designs used as a starting guess is also shown. They are placed with the distance L_D to the woofer. Figure and caption are from [P5].

frequency range has the lower bound of 1 kHz and upper bound equal to either 6 kHz, 7 kHz, or 8 kHz. The frequency range is included in the optimization problem by 30 logarithmic spaced frequencies.

$$\begin{array}{lll} \min\limits_{\mathbf{x}} \quad \max & \phi_{0_k}(\mathbf{x}) = \left(T_L - \mathbf{spl}_k \boldsymbol{\tau}\right)^2 \ , & k = 1, \ldots, b \\ \text{s.t.} & \tilde{\mathbf{S}}_k \tilde{\mathbf{u}}_k - \tilde{\mathbf{f}} = 0 \ , & k = 1, \ldots, b \\ & 0 \leq \ x_l \leq 1 \ , & l = 1, \ldots, a \\ & c_i(\mathbf{x}) \leq 0 & i = 1, \ldots, q, \end{array} \tag{6.1}$$

where $c_i(\mathbf{x})$ is the nonlinear element constraints introduced in Chapter 4.

In [P5] a comprehensive study was carried out in order to assess the improvement on the frequency response that could arise from optimizing the shape of the acoustic lens and the woofer. The three lens geometries were used with three different values of L_D (21.5 mm, 26.5 mm, and 31.5 mm) as it was expected that the initial distance to the woofer would influence the outcome of the optimization. Furthermore, it was unclear how far the frequency range could be extended; thus, three different frequency ranges for each starting guess were investigated. This amounts to 9 optimization runs for each initial lens geometry, 27 runs in total. In [P5] the outcome of this study is presented. In this thesis, the best design for each frequency range is presented. The optimized designs can be seen in Fig. 6.3.

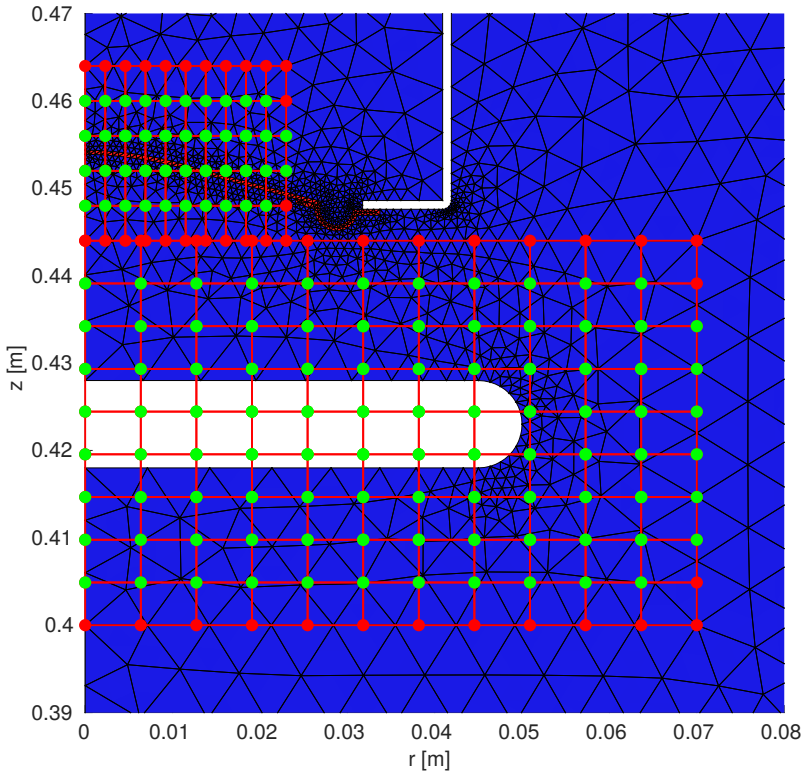

Figure 6.2: The initial configuration of the Bernstein polynomials and control points for an actual starting configuration. The top FFD region controls the woofer's shape, and the bottom region is concerning the shape of the acoustic lens. The active control points' location is indicated with green dots and the inactive with red dots.

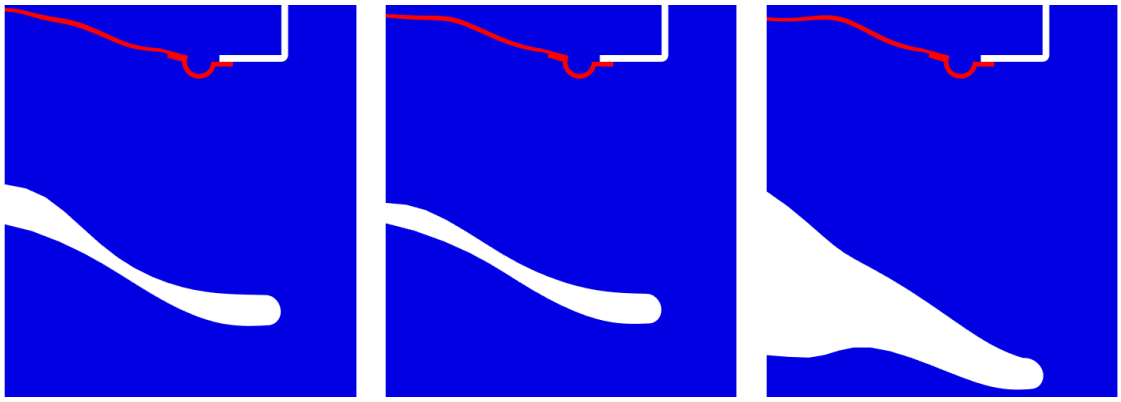

(a) 1 kHz to 6 kHz (b) 1 kHz to 7 kHz (c) 1 kHz to 8 kHz

Figure 6.3: The best performing optimized designs in the three frequency ranges. (a) has a frequency range of 1 kHz to 6 kHz, the initial designs was spatidate-shaped and with L_D equal to 26.5 mm (b) has a frequency range of 1 kHz to 7 kHz, the initial designs was spatidate-shaped and with L_D equal to 26.5 mm (c) has a frequency range of 1 kHz to 8 kHz, the initial designs was triangular-shaped and with L_D equal to 31.5 mm. The figures are from [P5].

In [P5] several designs were collapsing, meaning that the bottom of the lens surpassed the top of the lens, creating a nonphysical solution. This problem was especially pronounced for the flat lens with low values of L_D and was also seen for the spatidate-shaped lens with L_D equal to 21.5 mm and 26.5 mm with the frequency range of 1 kHz to 8 kHz. Fig. 6.4 shows an example of a collapsed lens; here, the green line represents the top surface of the lens, and the red line is the bottom surface of the lens. The elements have not been degraded, but there are no formulated constraints in the design problem to the collapse of the lens geometry. To circumvent this behavior the internal void region of the lens is meshed in the cases that collapse. The nonlinear element constraints can now be enforced in the lens due to the void mesh, which prevents the optimization problem from converging to something nonphysical. Only the collapsed designs have a meshed lens, as this further limits the design freedom.

The three optimized designs from Fig. 6.3 are evaluated by performing a frequency sweep. The results are shown in Fig. 6.5, here the frequency response of the smart speaker without a lens is represented by the dashed red curve. The low frequency range has been excluded from the plot as the introduction of the lens does not alter the response significantly. The black curve corresponds to the frequency response of the optimized design in Fig. 6.3a. As the black curve reaches its upper frequency bound indicated with a dashed black line, the sound pressure level drops. This design is able to extend the frequency range and that a maximum deviation from the target line of ± 2.0 dB is achieved. The blue curve is the frequency response of the optimized design in Fig. 6.3b. This design performs very well in the specified range from 1 kHz to 7 kHz, where it is within ± 2.5 dB of the target line. One can note that the frequency response is also well behaved and flat beyond the specified upper bound. The blue curve has the same initial guess as the black curve, and it shows the full potential of this starting configuration. The magenta curve has a specified frequency range in the design problem that spans 3 octaves (1 kHz to 8 kHz). Interestingly the magenta curve is quite similar to the blue curve's response up to around 2.5 kHz. This could be attributed to the similarities in the optimized shape of the woofer. The largest deviation from the target line is ± 2.5 dB in the specified frequency range.

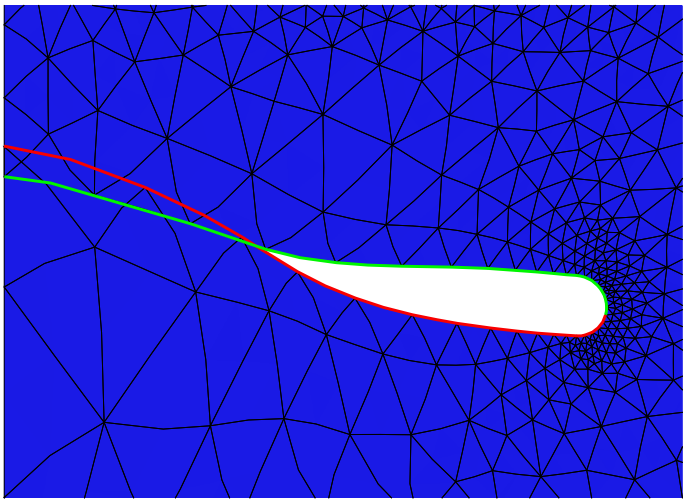

Figure 6.4: Collapsed lens for the spatidate-shaped design with $L_D = 21.5$ mm and the frequency range 1 kHz to 8 kHz. The red and green line belongs to the top and bottom of the lens, respectively.

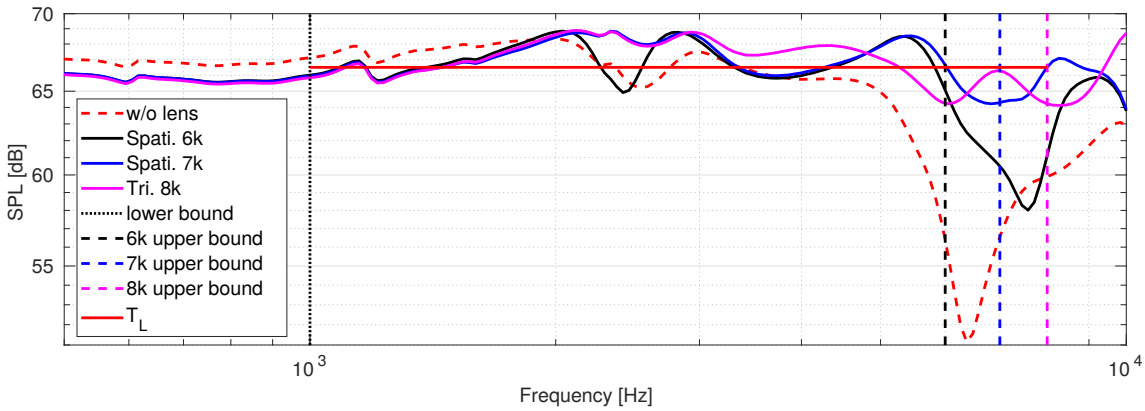

Figure 6.5: Frequency response of the optimized lenses. The frequency range of the plot is from 500 Hz to 10 kHz. The black curve is the best performing design in the frequency range 1 kHz to 6 kHz, the red curve is the best performing design in the frequency range 1 kHz to 7 kHz, and the magenta curve is the best performing design in the frequency range 1 kHz to 8 kHz. The upper bound of each optimization is indicated with the same color scheme as the response curve. The target line used in the objective function is indicated with the red line. Figure and caption are from [P5].

6.1 Discussion of Methods and Results

The proposed method uses FFD to control the movement of the underlying geometry. This approach has been shown to yield smooth and uncomplicated geometries that are able to provide feasible solutions to the posed design problem. The FFD approach relies on a global map between the control points and the geometry that is to be optimized. This means that the movement of one control point, to some degree, affects the entire geometry encapsulated in the FFD region. This reduces the method's design freedom and prevents the method from creating sharp local features. If sharp design features are wanted, other shape optimization methods should be consulted. The use of cutFEM has proven to yield designs with a high level of detail. Furthermore, the geometry can be parameterized with e.g. B-splines, which will enable more design freedom. Increased design freedom would

enhance the demands for controlling the quality of the mesh. In cases with extreme design freedom frequent remeshing or mesh regularization would be necessary.

In some cases, the acoustic lens was exhibiting an unwanted behavior where the geometry collapsed, meaning that the bottom of the lens surpassed the top of the lens. This was remedied by meshing the lens and enforcing the nonlinear element constraints inside the lens. This approached fixed the problem, however, as the affected designs show in [P5], the design freedom is severely limited, and that is reflected in the performance of the optimized designs. The issue should be further investigated to obtain maximum design freedom. One approach would be to relax the current constraints for the void mesh inside the lens geometry. Another approach would involve a new set of constraints that detects whether the bottom and top of the lens are close to intersecting. Fortunately, this behavior is not present in the most promising optimized designs. However, if this method's full potential should be unlocked, further investigation is necessary.

6.2 Contribution

This research presents a method for optimizing the shape of acoustic devices. In this example, the shape of a down-firing woofer and an acoustic lens is simultaneously optimized. The method relies on controlling the geometry with FFD, and nonlinear element constraints are implemented in order to ensure the quality of the mesh. Using FFD to optimize acoustic devices is to the author's knowledge a novel concept, and so is the use of nonlinear element constraints. The implemented method is best used to optimize existing structures where the method can be used to improve the design based on an objective function. In this work the goal is to achieve a flat horizontal frequency response in a wide frequency range. This is obtained by considering a diverse range of initial configurations in three different frequency ranges. Applying the proposed method to these configurations has led to numerous well-performing designs that are able to extend the frequency response of the speaker. It is shown that good performance can be achieved even for very high frequencies. The designs are smooth and uncomplicated, thus ideal for manufacturing. The comprehensive study carried out in the paper also shows the importance of the initial configuration. It is exemplified that not all the optimized designs perform equally well in comparable frequency ranges. Generally, the flat lens cannot achieve as good performance as the other configurations that are partly or entirely inclined.

7 Summary, Conclusions and Suggestion for Future Work

Different challenges associated with the modeling and optimization of loudspeakers have been investigated in this thesis. The study has been divided into three topics, all related to loudspeakers; modeling, optimizing the material properties, and optimizing the shape. Relevant objective functions have been created and the design problems are formulated such that they are applicable in very broad frequency intervals. This is a vital aspect of this work as loudspeakers must work in broad frequency intervals. Two different optimization methods have been implemented and the results show that improvements on the frequency response are achievable. The optimized designs have innovative design features produced by applying the presented numerical optimization techniques. This shows that numerical optimization can be a powerful tool that can be used either directly or to provide inspiration to improve the design of loudspeakers. The work has lead to six scientific papers, where five of them have been the foundation of this thesis. This chapter will summarize these results, and suggestions for future work will be presented.

Modeling loudspeakers are a complex task due to the multiphysics nature of the problem. A full model of the loudspeaker would mean that a large amount of computational time would be spent on solving the state equation. The state equation is solved for numerous frequencies during the iterative optimization procedure. Therefore, it is convenient to build a reliable model with reduced complexity that allows for applying numerical optimization techniques to specific parts of the loudspeaker, in this case the diaphragm and the surround. Furthermore, the modeled loudspeaker should be able to mimic a reference loudspeaker's response. This was the motivation for the work presented in [P1]. Here the loudspeaker diaphragm and surround together with the acoustic domain is modeled with FE, whereas a LPM represents the electric motor system, spider, voice coil, and voice coil former. This approach reduced the complexity of the numerical model significantly. Model fitting is adapted such that the modeled loudspeaker can approximate the response of a given reference speaker by tuning the lumped components. The hybrid FE-LPM model can mimic the reference model's pressure and electrical impedance even at very high frequencies. The paper describes and explicitly derives the necessary equations, making them straightforward to include in vibro-acoustic FE models. The method can be expanded to lump different parts of loudspeakers.

In [P3] a smart speaker was considered. The paper uses the developed material optimization method to extend the speaker's low frequency range by optimizing the material properties of the passive radiator. A minimax formulation is used for the multi-frequency optimization problem. The material properties are assumed to be homogeneous in the passive radiator's diaphragm and surround. The motivation for investigating this particular problem stems from the increasing number of compact speakers in the consumer market, where the reduced size of the loudspeaker influences the sound quality. Besides, many of the speakers are battery-driven, which means that a passive component that can increase the output is highly beneficial. The paper investigates two cases. In one case, the mass of the diaphragm and the damping in the surround can be tuned. For the other case, stiffness, mass, and damping can be controlled in both the diaphragm and surround

by the optimization algorithm. The two cases improve the low frequency performance significantly, and they display an almost identical performance in the frequency range of interest. However, the choice of material properties is very different. In the case with stiffness, mass, and damping, the optimization predicts a lower mass of the diaphragm than for the mass tuned case. To compensate for the lower mass, the stiffness of the surround is reduced. This leads to an interesting discovery that the more compliant surround seems to yield a substantially less steep roll-off than the mass-tuned case. The advantage of a less steep roll-off is that higher output at lower frequencies is achieved. Furthermore, the less steep roll-off also means that the ringing from the passive radiator present in the time domain is reduced. In this thesis, a third optimization case is introduced. It takes into account the study on available materials for loudspeakers from [P4]. It is shown that this setup performs equally well in the frequency range of interest. In this instance, the surround is less compliant due to the bounds on the material properties. As a consequence, the roll-off towards lower frequencies is steeper than for the similar optimization example from [P3].

In [P4] a generic 5-inch speaker is considered. In this example, it is desired to control the on-axis and off-axis frequency response. This is achieved by constructing an objective function that minimizes the difference between the loudspeaker unit's sound pressure level and the desired target line. A comprehensive study is carried out where the loudspeaker driver is optimized for a flat frequency response in different frequency ranges and for different directivities. The results section of the paper consist of 36 optimization runs that maps the limits of the proposed method. It is shown that a flat on-axis frequency response is achievable in a broad frequency range. In this thesis an example was shown where the optimized design only deviated 0.4 dB from the specified target line in the frequency range from 600 Hz to 8 kHz. The paper also investigates the limits of aligning the off-axis response with the on-axis response. Here it is shown that for increasing demands on angles included in the off-axis response, the frequency range in which the response can be assumed reasonably flat is shortened. However, many of the designs are able to produce a reasonably flat and well-aligned off-axis response. The proposed designs may not be directly realizable with conventional manufacturing techniques even though the materials used exists. However, the proposed designs show clear similarities, and the layout of stiffness, mass, and damping could inspire new designs that follow the overall design trends produced with this optimization method.

A shape optimization method for vibro-acoustic problems using FFD and nonlinear element constraints was developed in [P5]. The problem considered is the smart speaker introduced in [P3]. In [P5] the shape of the down-firing woofer and the acoustic lens is determined by shape optimization. The goal of the optimization is to create a flat horizontal frequency response that extends the current frequency range of the speaker. The method uses bivariate Bernstein polynomials and control points mapped to the underlying geometry. The control points are used as design variables in the optimization. The paper investigates three different lens geometries at three distinct distances from the woofer for three different frequency ranges. The comprehensive study is carried out as the feasibility of the end result of the optimization has proven to depend on the starting configuration. The paper shows that by optimizing the shape of the acoustic lens and the speaker unit's shape, the frequency response of the loudspeaker can be extended. The best optimized designs are able to yield a frequency response that is ± 2.5 dB from the target line in the frequency range of 90 Hz to 10 kHz with only one active speaker. The practical example shows the capabilities of the method. That is, to provide rather simple geometries as a solution to a complex problem, these geometries have a highly positive effect on the

frequency response. The approach could also consider the shape of loudspeaker units such as the one from [P4] or waveguides.

7.1 Future Work

The methods applied in this thesis aim to optimize the performance of loudspeakers. A considerable amount of time has been spent on implementing the FE-LPM method and the optimization algorithms used. This section serves to suggest additions to the current implementation that could lead to new results or improve the implemented method.

In this work, the model problem has been simplified by using a 2D-axisymmetric model. This is, in many cases, a reasonable assumption. However, it would be beneficial to consider the design problem in a full 3D model. That would include the non-symmetric vibration modes in the numerical model. These modes are in general poor radiators but they can influence the frequency response, especially at high frequencies. A 3D-model would yield the possibility to include non-symmetric features such as the basket or a lens mount. Furthermore, it would allow for more advanced objective functions which could lead to some interesting designs. The extension to 3D would, however, increase the computational cost significantly.

The work in this thesis is concerned solely with the frequency domain. Extending the numerical model to capture the behavior of the loudspeaker in the time domain would open up for a range of interesting problems to be solved. By simulating the model in the time domain, one could estimate the distortion of a given speaker. Based on these computations, a design problem could be formulated to minimize the distortion. Time domain simulation would also mean that more nonlinearities could be included. For example, the LPM could be extended to include a position-dependent force factor. Modeling in the time domain would mean that the model should perform discrete time steps, which will increase the solution time.

The main focus has been to achieve a desired target for the frequency response and, in some cases, also the off-axis response. The methods presented show some of the possibilities that can be exploited by utilizing numerical optimization to design loudspeakers. However, it is an approach that could be expanded upon. An interesting objective would be to achieve a flat on-axis response while minimizing the off-axis response and thereby minimizing the undesired reflections from the ceiling and the floor. It would also be interesting to consider the phase and the roll-off of the frequency response to design loudspeaker units that are easy to design crossover filters for. One could also consider the sound power as an objective function, here the sound power should ideally be flat as a function of frequency. To obtain a flat power response the loudspeaker considered should consists of multiple loudspeaker units. If a single unit is considered an interesting objective function would be a very smooth power response.

Instead of assuming a continuously varying material as in [P4] one could consider a finite range of materials. Another approach would be to use the results from [P4] to estimate the optimal material properties. This could be coupled with an in-depth look at composite material design optimization to design the local material properties and fiber orientation with consideration of how to produce the results.

The combination of the proposed methods could also be investigated. It would be interesting to see what happens if both shape and material optimization is applied simultaneously. It is unsure if this is viable, but it would be interesting to investigate. One could set up a study where material and shape optimization is applied to a design problem simultaneously. The same initial problem should then have shape optimization applied and after

that material optimization and vice versa. This could answer whether it is feasible to utilize the entire optimization package or the methods should be applied sequentially.

The lumped parameters have only been used as a modeling tool. Including the lumped parameters in the optimization would yield the possibility of optimizing the components of the electric motor system with respect to a given objective function.

It would be interesting to conduct experiments to analyze and verify the results obtained with the numerical optimization techniques. The smart speaker example from [P5] would make an ideal setup. It would be straightforward to manufacture the lens designs with additive manufacturing. Furthermore, one could also investigate the results from [P3] as the material properties in the diaphragm and surround are homogeneous.

Bibliography

[1] Martin Colloms and Paul Darlington. *High Performance Loudspeakers: Sixth Edition*. eng. London: Wiley Blackwell, 2013, pp. 1–532. ISBN: 0470094303. DOI: 10.1002/9780470094327.

[2] Floyd E. Toole. *Sound reproduction: The acoustics and psychoacoustics of loudspeakers and rooms: Third edition*. eng. Routledge: Taylor and Francis, 2017, pp. 1–490. ISBN: 9781315686424. DOI: 10.4324/9781315686424.

[3] Floyd E. Toole. "Loudspeaker Measurements and their Relationship to Listener Preferences .1". eng. In: *Journal of the Audio Engineering Society* 34.4 (1986), pp. 227–235. ISSN: 15494950.

[4] W. Marshall Leach Jr. *Introduction to Electroacoustics & Audio Amplifier Design*. eng. 3rd. Dubuque: Kendal/Hunt Publishing Company, 2003.

[5] Leo L. Beranek and Tim Mellow. *Acoustics: Sound Fields and Transducers*. eng. Academic Press, 2012. DOI: 10.1016/C2011-0-05897-0.

[6] Alexander Weider King. "Nonlinear fractional order derivative models of components and materials in hearing aids and transducers". eng. PhD thesis. Technical University of Denmark, 2019.

[7] Wolfgang Klippel. "Tutorial: Loudspeaker nonlinearities - Causes, parameters, symptoms". eng. In: *Aes: Journal of the Audio Engineering Society* 54.10 (2006), pp. 907–939. ISSN: 15494950.

[8] Gordon E. Moore. "Cramming more components onto integrated circuits". eng. In: *Proceedings of the IEEE* 86.1 (1998), pp. 82–85. ISSN: 15582256, 00189219. DOI: 10.1109/JPROC.1998.658762.

[9] Søren T. Christensen and Niels Olhoff. "Shape optimization of a loudspeaker diaphragm with respect to sound directivity properties". eng. In: *Control and Cybernetics* 27.2 (1998), pp. 177–198. ISSN: 04848569, 03248569.

[10] Eddie Wadbro and Martin Berggren. "Topology optimization of an acoustic horn". eng. In: *Computer Methods in Applied Mechanics and Engineering* 196.1-3 (2006), pp. 420–436. ISSN: 18792138, 00457825. DOI: 10.1016/j.cma.2006.05.005.

[11] Eddie Wadbro, Rajitha Udawalpola, and Martin Berggren. "Shape and topology optimization of an acoustic horn-lens combination". eng. In: *Journal of Computational and Applied Mathematics* 234.6 (2010), pp. 1781–1787. ISSN: 18791778, 03770427. DOI: 10.1016/j.cam.2009.08.028.

[12] Jan Abildgaard Pedersen and Gert Munch. "Driver Directivity Control by Sound Redistribution". eng. In: *Audio Engineering Society Convention 113*. Oct. 2002. URL: http://www.aes.org/e-lib/browse.cfm?elib=11277.

[13] Ester Creixell Mediante. "Computational reduction techniques for numerical vibro-acoustic analysis of hearing aids". eng. PhD thesis. Technical University of Denmark, Department of Electrical Engineering, 2018.

[14] Morten Birkmose Søndergaard and Claus B.W. Pedersen. "Applied topology optimization of vibro-acoustic hearing instrument models". eng. In: *Journal of Sound and Vibration* 333.3 (2014), pp. 683–692. ISSN: 10958568, 0022460x. DOI: 10.1016/j.jsv.2013.09.029.

[15] Sümer Bartug Dilgen. "Topology and advanced shape optimization of multiphysics problems". eng. PhD thesis. Technical University of Denmark, 2020.

[16] Andri Bezzola. “Numerical optimization strategies for acoustic elements in loudspeaker design”. eng. In: *145th Audio Engineering Society International Convention* (2018).

[17] Andri Bezzola, Allan Devantier, and Elisabeth McMullin. “Loudspeaker port design for optimal performance and listening experience”. eng. In: *147th Audio Engineering Society International Convention* (2019).

[18] Rene Christensen. “Shape and Topology Optimization of Loudspeaker Drivers”. eng. In: *Comsol Conference Europe 2020* (2020).

[19] Sebastien Degraeve and Jack Oclee-Brown. “Metamaterial absorber for loudspeaker enclosures”. eng. In: *148th Audio Engineering Society International Convention* (2020).

[20] Robert D Cook et al. *Concepts and Applications of Finite Element Analysis*. eng. 4th ed. John Wiley & Sons, 2002. ISBN: 9780471356059.

[21] Olek Zienkiewicz, Robert Taylor, and J. Z. Zhu. *The Finite Element Method: its Basis and Fundamentals: Seventh Edition*. eng. Elsevier Ltd, 2013, pp. 1–714. ISBN: 1299833454. DOI: 10.1016/C2009-0-24909-9.

[22] Alexander Hrennikoff. “Solution of problems of elasticity by the framework method”. jpn. In: *Journal of Applied Mechanics* 8 (1941), A169–A175.

[23] Richard Courant. “Variational methods for the solution of problems of equilibrium and vibrations”. eng. In: *Bulletin of the American Mathematical Society* 49.1 (1943), pp. 1–23. ISSN: 1936881x, 00029904. DOI: 10.1090/S0002-9904-1943-07818-4.

[24] Robert D. Ciskowski and Carlos Alberto Brebbia. *Boundary element methods in acoustics*. eng. Computational Mechanics Publ. [u.a.], 1991. ISBN: 0945824874.

[25] Peter Møller Juhl. “The boundary element method for sound field calculations”. eng. PhD thesis. Department of Acoustics Laboratory, Technical University of Denmark, 1993.

[26] Randall J. LeVeque. *Finite volume methods for hyperbolic problems*. eng. Cambridge Univ. Press, 2002, vol. 31. ISBN: 0521009243.

[27] Randall J. LeVeque. *Finite difference methods for ordinary and partial differential equations : steady-state and time-dependent problems*. eng. Society for Industrial and Applied Mathematics, 2007. ISBN: 9780898716290.

[28] David Henwood and Gary Geaves. “Finite element modelling of a loudspeaker part 1: Theory and validation”. eng. In: *Audio Engineering Society - 119th Convention Fall Preprints 2005* 1 (2005), pp. 242–255.

[29] W. Desmet and D. Vandepitte. “Finite Element Modeling for Acoustics”. In: *ISAAC13-International Seminar on Applied Acoustics, Leuven*. 2002. ISBN: 9073802733.

[30] Jean-Pierre Berenger. “A perfectly matched layer for the absorption of electromagnetic waves”. eng. In: *Journal of Computational Physics* 114.2 (1994), pp. 185–200. ISSN: 10902716, 00219991. DOI: 10.1006/jcph.1994.1159.

[31] Francis Collino and Peter Monk. “The perfectly matched layer in curvilinear coordinates”. eng. In: *Siam Journal of Scientific Computing* 19.6 (1998), pp. 2061–2090. ISSN: 10957197, 10648275. DOI: 10.1137/s1064827596301406.

[32] Jakob Søndergaard Jensen. “Topology optimization problems for reflection and dissipation of elastic waves”. eng. In: *Journal of Sound and Vibration* 301.1-2 (2007), pp. 319–340. ISSN: 10958568, 0022460x. DOI: 10.1016/j.jsv.2006.10.004.

[33] Alfredo Bermúdez et al. “An optimal finite-element/pml method for the simulation of acoustic wave propagation phenomena”. In: *Variational Formulations in Mechanics: Theory and Applications* January (2006).

[34] Mario Zampolli et al. “A computationally efficient finite element model with perfectly matched layers applied to scattering from axially symmetric objects”. eng.

In: *Journal of the Acoustical Society of America* 122.3 (2007), pp. 1472–1485. ISSN: 15208524, 00014966. DOI: 10.1121/1.2764471.

[35] Francis Collino and Peter B. Monk. "Optimizing the perfectly matched layer". eng. In: *Computer Methods in Applied Mechanics and Engineering* 164.1-2 (1998), pp. 157–171. ISSN: 18792138, 00457825. DOI: 10.1016/S0045-7825(98)00052-8.

[36] David S. Burnett. "A three-dimensional acoustic infinite element based on a prolate spheroidal multipole expansion". eng. In: *Journal of the Acoustical Society of America* 96.5 (1994), pp. 2798–816. ISSN: 15208524, 00014966. DOI: 10.1121/1.411286.

[37] Jean Christophe Autrique and Frédéric Magoulès. "Studies of an infinite element method for acoustical radiation". eng. In: *Applied Mathematical Modelling* 30.7 (2006), pp. 641–655. ISSN: 0307904x, 18728480. DOI: 10.1016/j.apm.2005.08.022.

[38] *COMSOL Multiphysics 5.6*. URL: http://www.comsol.com.

[39] Wei Sun and Wenxiang Hu. "Lumped element multimode modeling of balanced-armature receiver using modal analysis". eng. In: *Journal of Vibration and Acoustics, Transactions of the ASME* 138.6 (2016), p. 061017. ISSN: 15288927, 10489002. DOI: 10.1115/1.4034535.

[40] Mingsain R. Bai, Ching Yu Liu, and Rong Liang Chen. "Optimization of microspeaker diaphragm pattern using combined finite element-lumped parameter models". eng. In: *IEEE Transactions on Magnetics* 44.8 (2008), pp. 2049–2057. ISSN: 00189464, 19410069. DOI: 10.1109/TMAG.2008.923316.

[41] Gabriele Schrag, Thomas Kunzig, and Alfons Dehe. "Enhanced design of microsystems by combining lumped and distributed system-level models". eng. In: *2016 Symposium on Design, Test, Integration and Packaging of Mems/moems (DTIP)* (2016). DOI: 10.1109/DTIP.2016.7514839.

[42] Wei Sun and Wenxiang Hu. "Integrated FE-LE modelling method for a simplified balanced-armature receiver". eng. In: *International Journal of Acoustics and Vibrations* 22.3 (2017), pp. 377–383. ISSN: 24151408, 10275851. DOI: 10.20855/ijav.2017.22.3483.

[43] Joerg Panzer. "Coupling lumped and boundary element methods using superposition". eng. In: *Audio Engineering Society Convention 133* 1 (2012), pp. 132–140.

[44] Pasi Marttila and Mads J. Herring Jensen. "A Hybrid Electroacoustic Lumped and Finite Element Model for Modeling Loudspeaker Drivers". In: *Audio Engineering Society Conference: 51st International Conference: Loudspeakers and Headphones*. Aug. 2013. URL: http://www.aes.org/e-lib/browse.cfm?elib=16880.

[45] Ahmad H. Bokhari et al. "A computationally efficient hybrid 2D–3D subwoofer model". eng. In: *Scientific Reports* 11.1 (2021), p. 255. ISSN: 20452322. DOI: 10.1038/s41598-020-80092-9.

[46] Klippel Gmbh. *Specification of the KLIPPEL Analyzer System*. www.klippel.de. Accessed 12-02-2020.

[47] Wolfgang Klippel and Joachim Schlechter. "Distributed Mechanical Parameters of Loudspeakers Part 1: Measurements". eng. In: *Journal of the Audio Engineering Society* 57.7-8 (2009), pp. 500–511. ISSN: 15494950, 00047554.

[48] Thomas W. Sederberg and Scott R. Parry. "Free-form deformation of solid geometric models". eng. In: *ACM SIGGRAPH Computer Graphics* 20.4 (1986), pp. 151–160. ISSN: 15584569, 00978930. DOI: 10.1145/15886.15903.

[49] Martin P. Bendsøe. "Optimal shape design as a material distribution problem". eng. In: *Structural Optimization* 1.4 (1989), pp. 193–202. ISSN: 16151488, 09344373, 1615147x, 14362503. DOI: 10.1007/BF01650949.

[50] Martin P. Bendsøe and Ole Sigmund. *Topology Optimization - Theory, Methods, and Applications*. eng. Springer Verlag, 2003. ISBN: 3540429921.

[51] Martin P. Bendsøe and Noboru Kikuchi. "Generating optimal topologies in structural design using a homogenization method". eng. In: *Computer Methods in Applied Mechanics and Engineering* 71.2 (1988), pp. 197–224. ISSN: 18792138, 00457825. DOI: 10.1016/0045-7825(88)90086-2.

[52] Niels Aage et al. "Giga-voxel computational morphogenesis for structural design". eng. In: *Nature* 550.7674 (2017), pp. 84–86. ISSN: 14764687, 00280836. DOI: 10.1038/nature23911.

[53] Mads Jacob Baandrup et al. "Closing the gap towards super-long suspension bridges using computational morphogenesis". eng. In: *Nature Communications* 11.1 (2020), p. 2735. ISSN: 20411723. DOI: 10.1038/s41467-020-16599-6.

[54] Joe Alexandersen and Boyan Stefanov Lazarov. "Topology optimisation of manufacturable microstructural details without length scale separation using a spectral coarse basis preconditioner". eng. In: *Computer Methods in Applied Mechanics and Engineering* 290 (2015), pp. 156–182. ISSN: 18792138, 00457825. DOI: 10.1016/j.cma.2015.02.028.

[55] Christian Rye Thomsen, Fengwen Wang, and Ole Sigmund. "Buckling strength topology optimization of 2D periodic materials based on linearized bifurcation analysis". eng. In: *Computer Methods in Applied Mechanics and Engineering* 339 (2018), pp. 115–136. ISSN: 18792138, 00457825. DOI: 10.1016/j.cma.2018.04.031.

[56] Casper Schousboe Andreasen, Allan Roulund Gersborg, and Ole Sigmund. "Topology optimization of microfluidic mixers". eng. In: *International Journal for Numerical Methods in Fluids* 61.5 (2009), pp. 498–513. ISSN: 10970363, 02712091. DOI: 10.1002/fld.1964.

[57] Joe Alexandersen and Casper Schousboe Andreasen. "A Review of Topology Optimisation for Fluid-Based Problems". eng. In: *Fluids* 5.1 (2020), p. 29. ISSN: 23115521, 14321114, 07234864. DOI: 10.3390/fluids5010029.

[58] Sümer Bartug Dilgen et al. "Density based topology optimization of turbulent flow heat transfer systems". eng. In: *Structural and Multidisciplinary Optimization* 57.5 (2018), pp. 1905–1918. ISSN: 16151488, 1615147x. DOI: 10.1007/s00158-018-1967-6.

[59] Joe Alexandersen et al. "Design of passive coolers for light-emitting diode lamps using topology optimisation". eng. In: *International Journal of Heat and Mass Transfer* 122 (2018), pp. 138–149. ISSN: 18792189, 00179310. DOI: 10.1016/j.ijheatmasstransfer.2018.01.103.

[60] Daniel Gert Nielsen et al. "Topology optimization and experimental verification of compact E-plane waveguide filters". eng. In: *Microwave and Optical Technology Letters* 61.5 (2019), pp. 1208–1215. ISSN: 10982760, 08952477. DOI: 10.1002/mop.31741.

[61] Jakob Søndergaard Jensen and Ole Sigmund. "Topology optimization of photonic crystal structures: a high-bandwidth low-loss T-junction waveguide". eng. In: *Journal of the Optical Society of America B* 22.6 (2005), pp. 1191–1198. ISSN: 15208540, 07403224. DOI: 10.1364/JOSAB.22.001191.

[62] Fengwen Wang et al. "Maximizing the quality factor to mode volume ratio for ultra-small photonic crystal cavities". eng. In: *Applied Physics Letters* 113.24 (2018), p. 241101. ISSN: 10773118, 00036951. DOI: 10.1063/1.5064468.

[63] Erik Andreassen and Jakob Søndergaard Jensen. "Topology optimization of periodic microstructures for enhanced dynamic properties of viscoelastic composite materials". eng. In: *Structural and Multidisciplinary Optimization* 49.5 (2014), pp. 695–705. ISSN: 16151488, 1615147x. DOI: 10.1007/s00158-013-1018-2.

[64] Gil Ho Yoon, Jens Stissing Jensen, and Ole Sigmund. "Topology optimization of acoustic-structure interaction problems using a mixed finite element formulation".

eng. In: *International Journal for Numerical Methods in Engineering* 70.9 (2007), pp. 1049–1075. ISSN: 10970207, 00295981. DOI: 10.1002/nme.1900.

[65] Martin P. Bendsøe and Alejandro R. Díaz. "Optimization of material properties for Mindlin plate design". eng. In: *Structural Optimization* 6.4 (1993), pp. 268–270. ISSN: 16151488, 09344373, 1615147x. DOI: 10.1007/BF01743387.

[66] Martin P. Bendsøe and Alejandro R. Diaz. "Optimization of Material Properties for Improved Frequency Response". eng. In: *Structural Optimization* 7.1-2 (1994), pp. 138–140. ISSN: 14362503, 09344373, 16151488, 1615147x. DOI: 10.1007/BF01742519.

[67] Alemseged Gebrehiwot Weldeyesus and Mathias Stolpe. "Free material optimization for laminated plates and shells". eng. In: *Structural and Multidisciplinary Optimization* 53.6 (2016), pp. 1335–1347. ISSN: 16151488, 1615147x. DOI: 10.1007/s00158-016-1416-3.

[68] Michal Kocvara, Michael Stingl, and Jochem Zowe. "Free material optimization: Recent progress". eng. In: *Optimization* 57.1 (2008), pp. 79–100. ISSN: 10294945, 02331934. DOI: 10.1080/02331930701778908.

[69] Herbert R.E.M. Hörnlein, Michal Kočvara, and Ralf Werner. "Material optimization: Bridging the gap between conceptual and preliminary design". eng. In: *Aerospace Science and Technology* 5.8 (2001), pp. 541–554. ISSN: 16263219, 12709638. DOI: 10.1016/S1270-9638(01)01125-7.

[70] J. Thomsen. "Topology optimization of structures composed of one or two materials". eng. In: *Structural Optimization* 5.1-2 (1992), pp. 108–115. ISSN: 16151488, 09344373, 1615147x. DOI: 10.1007/BF01744703.

[71] Martin P. Bendsøe and Ole Sigmund. "Material Interpolation Schemes in Topology Optimization". eng. In: *Archive of Applied Mechanics* 69.9-10 (1999), pp. 635–654. ISSN: 09391533, 14320681. DOI: 10.1007/s004190050248.

[72] Wei Huang et al. "Optimal design of the damping layer in plate with imperfect Acoustic Black Hole for wave energy dissipation". eng. In: *INTER-NOISE and NOISE-CON Congress and Conference Proceedings* 259.2 (2019), pp. 7763–7771.

[73] Hang Li et al. "Spatial-varying multi-phase infill design using density-based topology optimization". eng. In: *Computer Methods in Applied Mechanics and Engineering* 372 (2020), p. 113354. ISSN: 18792138, 00457825. DOI: 10.1016/j.cma.2020.113354.

[74] Sheng Chu et al. "Topology optimization of multi-material structures with graded interfaces". eng. In: *Computer Methods in Applied Mechanics and Engineering* 346 (2019), pp. 1096–1117. ISSN: 18792138, 00457825. DOI: 10.1016/j.cma.2018.09.040.

[75] Zhan Kang et al. "Robust topology optimization of multi-material structures considering uncertain graded interface". eng. In: *Composite Structures* 208 (2019), pp. 395–406. ISSN: 18791085, 02638223. DOI: 10.1016/j.compstruct.2018.10.034.

[76] Massimo Carraturo et al. "Graded-material design based on phase-field and topology optimization". eng. In: *Computational Mechanics* 64.6 (2019), pp. 1589–1600. ISSN: 14320924, 01787675. DOI: 10.1007/s00466-019-01736-w.

[77] Gil Ho Yoon. "Acoustic topology optimization of fibrous material with Delany-Bazley empirical material formulation". eng. In: *Journal of Sound and Vibration* 332.5 (2013), pp. 1172–1187. ISSN: 10958568, 0022460x. DOI: 10.1016/j.jsv.2012.10.018.

[78] Gaetan K.W. Kenway, Graeme J. Kennedy, and Joaquim R.R.A. Martins. "A CAD-free approach to high-fidelity aerostructural optimization". eng. In: *13th AIAA/ISSMO Multidisciplinary Analysis and Optimization Conference* (2010). DOI: 10.2514/6.2010-9231.

[79] Toni Lassila and Gianluigi Rozza. “Parametric free-form shape design with PDE models and reduced basis method”. eng. In: *Computer Methods in Applied Mechanics and Engineering* 199.23-24 (2010), pp. 1583–1592. ISSN: 18792138, 00457825. DOI: 10.1016/j.cma.2010.01.007.

[80] Rui Li et al. “Multi-objective optimization of a high-speed train head based on the FFD method”. eng. In: *Journal of Wind Engineering and Industrial Aerodynamics* 152 (2016), pp. 41–49. ISSN: 18728197, 01676105. DOI: 10.1016/j.jweia.2016.03.003.

[81] Peter Risby Andersen, Vicente Cutanda Henríquez, and Niels Aage. “Shape optimization of micro-acoustic devices including viscous and thermal losses”. eng. In: *Journal of Sound and Vibration* 447 (2019), pp. 120–136. ISSN: 10958568, 0022460x. DOI: 10.1016/j.jsv.2019.01.047.

[82] Rajitha Udawalpola. “Shape Optimization for Acoustic Wave Propagation Problems”. eng. PhD thesis. Acta Universitatis Upsaliensis, 2010.

[83] Bijan Mohammadi and Olivier Pironneau. *Applied Shape Optimization for Fluids*. eng. Vol. 9780199546909. Oxford University Press, 2010, pp. 1–292. ISBN: 9780191720482. DOI: 10.1093/acprof:oso/9780199546909.001.0001.

[84] Johannes Semmler et al. “Shape Optimization in Electromagnetic Applications”. eng. In: *New Trends in Shape Optimization* 166 (2015), pp. 251–269. DOI: 10.1007/978-3-319-17563-8_11.

[85] Ole Sigmund. “On the usefulness of non-gradient approaches in topology optimization”. eng. In: *Structural and Multidisciplinary Optimization* 43.5 (2011), pp. 589–596. ISSN: 16151488, 1615147x. DOI: 10.1007/s00158-011-0638-7.

[86] Krister Svanberg. “The Method of Moving Asymptotes - A New Method for Structural Optimization”. In: *International Journal for Numerical Methods in Engineering* 24.2 (1987), pp. 359–373.

[87] Jorge Nocedal and Stephen J. Wright. *Numerical Optimization*. eng. Springer New York, 2006. ISBN: 9780387400655.

[88] *GRANTA EduPack*. URL: https://www.ansys.com/products/materials/granta-edupack.

[89] Ole Sigmund and Joakim Petersson. “Numerical instabilities in topology optimization: A survey on procedures dealing with checkerboards, mesh-dependencies and local minima”. eng. In: *Structural Optimization* 16.1 (1998), pp. 68–75. ISSN: 14362503, 09344373, 16151488, 1615147x. DOI: 10.1007/BF01214002.

[90] Ole Sigmund. “Morphology-based black and white filters for topology optimization”. eng. In: *Structural and Multidisciplinary Optimization* 33.4-5 (2007), pp. 401–424. ISSN: 16151488, 1615147x. DOI: 10.1007/s00158-006-0087-x.

[91] Ole Sigmund and Kurt Maute. “Sensitivity filtering from a continuum mechanics perspective”. eng. In: *Structural and Multidisciplinary Optimization* 46.4 (2012), pp. 471–475. ISSN: 16151488, 1615147x. DOI: 10.1007/s00158-012-0814-4.

[92] Tyler E. Bruns and Daniel A. Tortorelli. “Topology optimization of non-linear elastic structures and compliant mechanisms”. eng. In: *Computer Methods in Applied Mechanics and Engineering* 190.26-27 (2001), pp. 3443–3459. ISSN: 18792138, 00457825. DOI: 10.1016/S0045-7825(00)00278-4.

[93] Blaise Bourdin. “Filters in topology optimization”. eng. In: *International Journal for Numerical Methods in Engineering* 50.9 (2001), pp. 2143–2158. ISSN: 10970207, 00295981. DOI: 10.1002/nme.116.

[94] Ole Sigmund and Kurt Maute. “Topology optimization approaches: A comparative review”. eng. In: *Structural and Multidisciplinary Optimization* 48.6 (2013), pp. 1031–1055. ISSN: 16151488, 1615147x. DOI: 10.1007/s00158-013-0978-6.

[95] Peter Risby Andersen et al. “Towards large-scale acoustic shape optimization for industrial applications using the Boundary Element Method”. eng. In: *INTER-NOISE and NOISE-CON Congress and Conference Proceedings* 261.1 (2020), pp. 5763–5773. ISSN: 07362935.

[96] Matthias Firl, Roland Wüchner, and Kai Uwe Bletzinger. “Regularization of shape optimization problems using FE-based parametrization”. eng. In: *Structural and Multidisciplinary Optimization* 47.4 (2013), pp. 507–521. ISSN: 16151488, 1615147x. DOI: 10.1007/s00158-012-0843-z.

[97] Siegfried Linkwitz. “Which Loudspeaker Parameters are Important to Create the Illusion of a Live Performance in the Living Room?” In: *Audio Engineering Society Convention 113*. Oct. 2002. URL: http://www.aes.org/e-lib/browse.cfm?elib=11289.

[98] Sean E. Olive. “A multiple regression model for predicting loudspeaker preference using objective measurements: part I - listening test results”. eng. In: *Audio Engineering Society Convention 116* (2004).

[99] Sean E. Olive. “A multiple regression model for predicting loudspeaker preference using objective measurements: part II - development of the model”. eng. In: *Audio Engineering Society Convention 117* (2004).

[100] Siegfried Linkwitz. “Hearing Spatial Detail in Stereo Recordings”. eng. In: *26th Tonmeistertagung-VDT International Convention* (2010).

[101] Daniel A. Tortorelli and Panagiotis Michaleris. “Design sensitivity analysis: Overview and review”. eng. In: *Inverse Problems in Engineering* 1.1 (1994), pp. 71–105. ISSN: 10290281, 10682767. DOI: 10.1080/174159794088027573.

[102] K Svanberg. “The method of moving asymptotes (MMA) with some extensions”. eng. In: *Optimization of large structural systems. NATO ASI Series (Series E: Applied Sciences)*. Vol. 231. Springer, 1993, pp. 555–566. ISBN: 0792321308.

[103] Edison Research and NPR. *The Smart Audio Report*. Tech. rep. Feb. 2020.

[104] Floyd E. Toole. “Loudspeaker measurements and their relationship to listener preferences: Part 2”. eng. In: *Journal of the Audio Engineering Society* 34.5 (1986), pp. 323–348. ISSN: 15494950, 00047554.

[105] Jana Herzberger et al. “Polymer Design for 3D Printing Elastomers: Recent Advances in Structure, Properties, and Printing”. eng. In: *Progress in Polymer Science* 97 (2019), p. 101144. ISSN: 18731619, 00796700. DOI: 10.1016/j.progpolymsci.2019.101144.

[106] M. Saari et al. “Additive manufacturing of soft and composite parts from thermoplastic elastomers”. eng. In: *Proceedings - 26th Annual International Solid Freeform Fabrication Symposium - an Additive Manufacturing Conference, SFFS 2015* (2020), pp. 949–958.

[107] Abdolreza Toudehdehghan et al. “A brief review of functionally graded materials”. eng. In: *Matec Web of Conferences* 131 (2017), p. 03010. ISSN: 2261236x. DOI: 10.1051/matecconf/201713103010.

[108] Earl Geddes. “Acoustic Lens, Their Design and Application”. eng. In: *Audio Eng Soc Prepr for 61st Conv* (1978).

[109] Michael W. Ferralli et al. “Wide Dispersion Frequency Invariant Acoustic Lens”. eng. In: *Audio Engineering Society Convention 79* (1985).

Paper 1

Estimation of Optimal Values for Lumped Elements in a Finite Element - Lumped Parameter Model of a Loudspeaker

Daniel Gert Nielsen, Peter Risby Andersen, Jakob Søndergaard Jensen, Finn Thomas Agerkvist

December 14, 2020

Abstract

Finite element methods are progressively being utilized to assist in the continuous development of loudspeakers. The core of this paper is the method of lumping certain parts of the finite element model, creating a significant reduction in the model complexity that allows for e.g. faster structural optimization. This is illustrated in the paper with a loudspeaker example where the electromagnetic parts are lumped as well as the spider. It is shown that the simplified model still matches the complex response of the full FE model at very high frequencies.

1 Introduction

Loudspeakers have been an essential part of society for over a century, the performance requirements vary depending on the situation and environment in which said loudspeaker is operating in. Therefore, a great effort is made in order to analyse and predict the behaviour of loudspeakers. Simulating a loudspeaker in a numerical model is a complex task with respect to modelling the physics in a finite element (FE) model and the associated long computational times. When considering a particular aspect of the loudspeaker performance, one may simplify and lump those parts of the speaker that have little influence in the aspect studied, for the linear response at high frequencies, the electromagnetic part may be lumped as the diaphragm and surround are the most substantial parts. This approach can be beneficial in many cases, for instance when optimizing mechanical structures where many calculations are carried out repeatedly, in-order to find an optimized design. Optimization of acoustic-structure problems is a rapidly growing research field, examples of the applicability can be seen in Refs. [1, 2, 3, 4, 5] and in Refs. [6, 7] examples of loudspeaker optimization can be found. Therefore, we propose a numerical method for predicting the behaviour of a loudspeaker in its linear operating range in a simple and efficient manner. The proposed method combines two well known techniques, namely the FE method [8] and a lumped parameter model (LPM) [9].

The combination of the FE method and LPM is made such that structural optimization ultimately can be performed on the diaphragm of the loudspeaker, therefore, this part must be considered with a FE-model. A LPM is then utilized to model the entire electric motor system together with the voice-coil (VC), VC former and the spider in order to reduce the complexity of the modelling task and the calculation time.

Utilizing a combination of FE and Lumped Elements (LE) is not novel. It is especially common within the research topics regarding balanced-armature receivers and MEMS microphones. Recently Sun et. al. presented a modelling technique where a FE-LE model was used to model a simplified balanced-armature receiver [10]. Schrag et. al. enhances the design of microsystems by combining a lumped model with a distributed system level model [11]. A computational example in which a balanced-armature receiver itself is represented by a LPM that is then coupled to a FE model of the vibration isolation system is shown in Ref. [12]. Marttila and Jensen [13] briefly presents an approach for incorporating a LPM in conjunction with a FE-model.

If the amplitude of the movement of the speaker is small, the loudspeaker is in its linear operating range, which simplifies the required measurement technique. The small-signal parameters can be measured dynamically in conjunction with a system identification technique such as the Klippel system described in Ref. [14]. This measurement technique will yield the Thiele/Small parameters which can be used in a LPM of the loudspeaker. Klippel describes a measuring technique using a laser scanner to obtain the distributed mechanical parameters

which could be used in a FE model of e.g. the loudspeaker cone[15]. Furthermore, Cardenas and Klippel estimated an effective frequency dependent and complex Young's modulus by fitting FE simulations to measurements of a loudspeaker [16].

The method disclosed in this paper can be used to fit a numerical model to measurements of a loudspeaker. Ideally the measurements would contain values of the impedance as a function of frequency and/or measurements of the magnitude and phase of the pressure 1 meter away from the unit. The measured data is then used to optimally configure the parameters in the LPM, such that the impedance and radiated sound from the loudspeaker unit in the numerical model resemble the authentic unit.

This paper is a continuation of the work presented in Ref. [17], but here we study the geometry of an actual 5 inch loudspeaker instead of a flat panel loudspeaker. The lumped circuit model is extended to include eddy currents by considering the inductor with a fractional order derivative model. Furthermore, an optimization algorithm has been implemented, which can fit the lumped components in the proposed numerical model to represent an actual loudspeaker either with parameters from a data sheet or actual measurements.

The paper is structured such that the theory required to combine the FE method with the LPM is presented together with the optimization problem used for estimating the optimal lumped parameters. Succeeding sections will contain relevant numerical results and comparisons together with a discussion and conclusion about the results.

2 Theory

Figure 1 shows a sketch of the model problem, which is a loudspeaker mounted in a baffle. The dashed box in the figure show the components that are contained in the LPM. Namely, the entire electric motor system, the VC, VC former and the spider. The rest of the geometry and the surrounding unbounded acoustic domain are modelled with a FE-model. The two models are linked together in "coupling node i", referring to a specific node in the FE-model. This section serves to establish a system of equations that can readily be used to solve an unbounded acoustic-mechanical interaction problem, then couple it to a LPM model, in which the values of the lumped components are estimated based on measurements.

2.1 Finite element model

The numerical model is used to simulate the acoustic wave propagation in an unbounded domain caused by a moving coil loudspeaker. The modelling setup can be seen in Fig. 2, note that the loudspeaker geometry is exaggerated for explanatory purposes. The loudspeaker geometry and acoustic domain is studied by utilizing an axisymmetric FE model, which implies that the geometry in Fig. 2 is revolved around the z-axis. Perfectly Matched Layers (PMLs) have been used to truncate the unbounded domain into a finite domain [18].

The governing equation for the time-harmonic motion of a linear elastic body where body forces has been neglected can be written as

$$-\rho\omega^2\mathbf{u} - \nabla\cdot\boldsymbol{\sigma}(\mathbf{u}) = 0 \qquad \text{in} \quad \Omega_s \tag{1}$$

$$\boldsymbol{\sigma} = \mathbf{C}\boldsymbol{\epsilon} \tag{2}$$

$$\epsilon = \{\epsilon_r\ \epsilon_\theta\ \epsilon_z\ \gamma_{zr}\}^T \qquad \text{(2D Axisymmetric)} \tag{3}$$

$$\epsilon_r = \frac{\partial u_r}{\partial r},\ \epsilon_\theta = \frac{u_r}{r},\ \epsilon_z = \frac{\partial u_z}{\partial z},\ \gamma_{zr} = \left(\frac{\partial u_r}{\partial z} + \frac{\partial u_z}{\partial r}\right) \tag{4}$$

here ρ is the mass density of the material, $\mathbf{u}$ is the structural displacements, $\boldsymbol{\sigma}$ is the stress tensor, ω is the excitation frequency in radians, Ω_s is the structural domain $\mathbf{C}$ is the constitutive matrix for an axisymmetric structure, $\boldsymbol{\epsilon}$ is the strain tensor, u_r is the structural displacement in the r-direction and u_z is the displacement in the z-direction. Applying the Galerkin method to Eq. (2) and transformation into the frequency domain, yields the following FE equation

$$\left(\mathbf{K} - \omega^2\mathbf{M}\right)\mathbf{u} = \mathbf{f}, \tag{5}$$

where the capital bold letters specifies a matrix, small bold letters implies a vector, non bold letters are scalars. The externally applied time harmonic force is denoted $\mathbf{f}$, $\mathbf{K}$ is the structural stiffness matrix and $\mathbf{M}$ is the structural

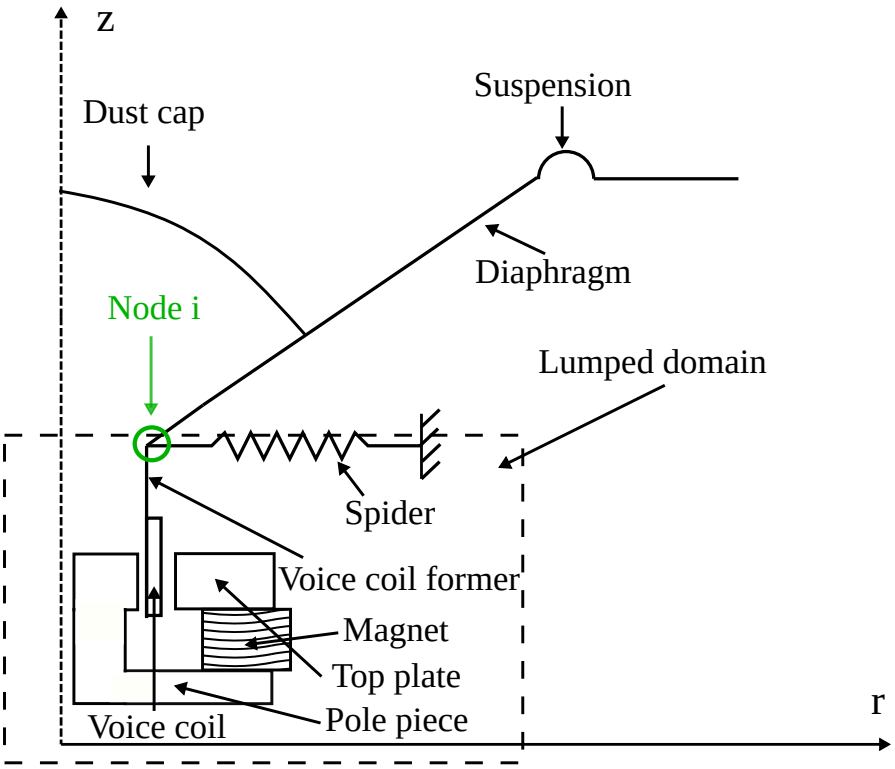

Figure 1: 2D sketch of a loudspeaker placed in an infinite baffle

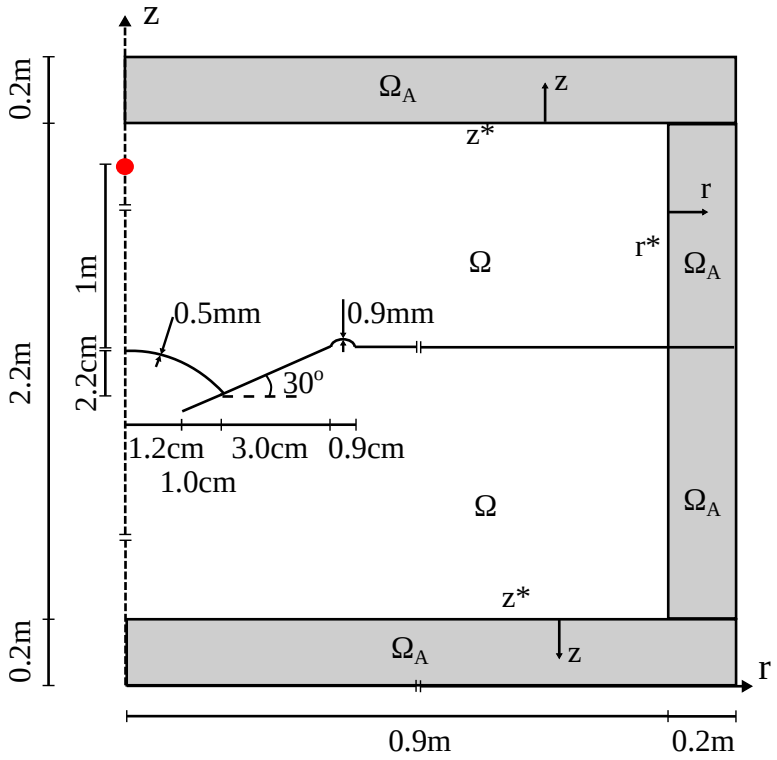

Figure 2: Sketch of the loudspeaker geometry, PML regions, the acoustic domain and the location of the measuring point for the pressure.

mass matrix which can be written as

$$\mathbf{K} = \int_{\Omega_s} \int_{-\pi}^{\pi} \mathbf{B}^T \mathbf{C} \mathbf{B} r \, \mathrm{d}\Omega_s \, , \; \mathbf{M} = \int_{\Omega_s} \int_{-\pi}^{\pi} \rho \mathbf{N}^T \mathbf{N} r \, \mathrm{d}\Omega_s. \tag{6}$$

Here $\mathbf{B}$ is the strain-displacement matrix, r is the radial distance to the Gauss point and $\mathbf{N}$ is a matrix consisting of the quadratic iso-parametric shape functions.

In this paper damping is considered as an isotropic structural loss factor, denoted η, such that $\mathbf{K} = \mathbf{K}\,(1 + j\eta)$, where j is the imaginary number, η equals 0.25 in the rubber surround of the speaker and 0.2 in the diaphragm and dust cap.

In the acoustic domain the Helmholtz equation is solved in the frequency domain

$$\Delta p + \frac{\omega^2}{c^2} p = 0, \tag{7}$$

here Δ is the Laplace operator in cylindrical coordinates, p is the pressure and c is the speed of sound in air.

A modified Helmholtz equation[19, 20] is solved in a truncated PML region (Ω_A), as shown in Fig. 2.

$$\frac{1}{\gamma_r} \frac{\partial}{\partial r} \left(\frac{1}{\gamma_r} \frac{\partial p_A}{\partial r} \right) + \frac{1}{\gamma_z} \frac{\partial}{\partial z} \left(\frac{1}{\gamma_z} \frac{\partial p_A}{\partial z} \right) + k^2 p_A = 0, \tag{8}$$

where p_A is the pressure in the PML region, the formulation of γ is from [21], here extended to accommodate for a

PML in both the r- and z direction

$$\gamma_r(r) = 1 - j\alpha \left(\frac{r - r^*}{t} \right)^2 \tag{9}$$

$$\gamma_z(z) = 1 - j\alpha \left(\frac{z - z^*}{t} \right)^2. \tag{10}$$

Where r^* and z^*, indicate the interface coordinate between the PML/acoustic domain and r and z are the position within the PML as shown in Fig. 2. α is the absorption coefficient with a constant value of 10 and t is half the thickness of the PML which equates to 0.1m.

Equations (7) and (8) are written in the usual FE equations in the frequency domain

$$\left(\mathbf{K}_a - \omega^2 \mathbf{M}_a \right) \mathbf{p} = 0. \tag{11}$$

Here $\mathbf{p}$ is the solution vector containing the nodal pressures, $\mathbf{M}_a$ is the acoustic mass matrix and $\mathbf{K}_a$ is the acoustic stiffness matrix which can be computed as

$$\mathbf{K}_a = \int_\Omega \int_{-\pi}^{\pi} \left(\mathbf{N}_{a,r}^T \mathbf{N}_{a,r} + \mathbf{N}_{a,z}^T \mathbf{N}_{a,z} \right) r \, \mathrm{d}\Omega + \int_{\Omega_A} \int_{-\pi}^{\pi} \left(\frac{\gamma_z}{\gamma_r} \mathbf{N}_{a,r}^T \mathbf{N}_{a,r} + \frac{\gamma_r}{\gamma_z} \mathbf{N}_{a,z}^T \mathbf{N}_{a,z} \right) r \, \mathrm{d}\Omega_A \tag{12}$$

$$\mathbf{M}_a = \int_\Omega \int_{-\pi}^{\pi} \frac{1}{c^2} \mathbf{N}_a^T \mathbf{N}_a r \, \mathrm{d}\Omega + \int_{\Omega_A} \int_{-\pi}^{\pi} \frac{1}{c^2} \gamma_r \gamma_z \mathbf{N}_a^T \mathbf{N}_a r \, \mathrm{d}\Omega_A, \tag{13}$$

where subscript r and z refers, respectively, to the differential operator with respect to global r- and z-coordinates, $\mathbf{N}_a$ is a row vector consisting of the quadratic acoustic shape functions, Ω and Ω_A refers to the acoustic domain and the PML, respectively.

The acoustic and mechanical domains are fully coupled at the shared interfaces such that when the mechanical structure vibrates it acts as an acoustic source, furthermore the surface pressure acting on the mechanical structure is accounted for. This is included in the coupling matrix $\mathbf{S}$

$$\mathbf{S} = \int_\Gamma \int_{-\pi}^{\pi} \mathbf{N}^T \mathbf{n}_a \mathbf{N}_a r \, \mathrm{d}\Gamma, \tag{14}$$

where $\mathbf{n}_a$ is the normal vector of the interface between the acoustic and structural boundary pointing outwards from the acoustic boundary and Γ refers to the interface between the acoustic and structural domain.

Combining Eq. 5 and 11 yields the entire system of equations for the FE-model[8]

$$\left(\begin{bmatrix} \mathbf{K} & -\mathbf{S}^T \\ \mathbf{0} & \mathbf{K}_a \end{bmatrix} - \omega^2 \begin{bmatrix} \mathbf{M} & \mathbf{0} \\ \rho \mathbf{S} & \mathbf{M}_a \end{bmatrix} \right) \begin{Bmatrix} \mathbf{u} \\ \mathbf{p} \end{Bmatrix} = \begin{Bmatrix} \mathbf{f} \\ \mathbf{0} \end{Bmatrix}. \tag{15}$$

For the remainder of this paper Eq. (15) is written in a compact format

$$\left(\tilde{\mathbf{K}} - \omega^2 \tilde{\mathbf{M}} \right) \begin{Bmatrix} \mathbf{u} \\ \mathbf{p} \end{Bmatrix} = \begin{Bmatrix} \mathbf{f} \\ \mathbf{0} \end{Bmatrix}. \tag{16}$$

2.2 Coupled system

Figure 3 is a schematic drawing of the lumped circuit model representing the entire electric motor system and the VC, VC former and spider of the mechanical system. Information is passed between the LPM and the FE model in the coupling node i located as shown on Fig. 1. The left circuit in Fig. 3 is a representation of the electrical motor system, where e_g is the applied voltage from an AC source, i_c is the current, R_E is the DC resistance in the wire of the VC, L_E is the inductance of the VC and e_c is the back-induced voltage caused by the movement of the loudspeaker. In the expression describing e_c, Bl is the force factor and $\dot{u}$ is the velocity of the movement.

The right circuit on Fig. 3 represents the material properties of the partly lumped mechanical components, the force applied from the electric motor system is F^{elek}, $M_{p,lump}$ is the total mass of the lumped components, $R_{p,lump}$

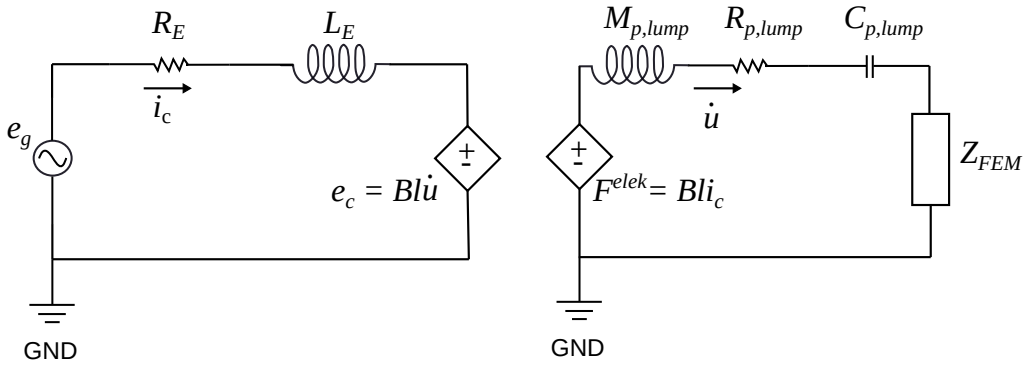

Figure 3: Lumped circuit model with partly lumped mechanical components

is the damping coefficient, $C_{p,lump}$ is the compliance and the impedance block, Z_{FEM}, represents the contribution from the FE model.

The equation for the electric motor system is represented in the frequency domain, in which the eddy currents in the inductor are included with a fractional order derivative model [22, 23]

$$e_g = R_E i_c + (j\omega)^n L_E i_c + Bl\dot{u}_i, \tag{17}$$

where n is the fractional order. The scalar equation for the mechanical components in Fig. 3 including the contribution from the FE-model via the impedance $Z_{FEM} = \frac{F_i}{j\omega u_i}$, where sub-index i refers to the value in the coupling node i is

$$Bli_c = -\omega^2 M_{p,lump} u_i + j\omega R_{p,lump} u_i + \frac{1}{C_{p,lump}} u_i + j\omega Z_{FEM} u_i. \tag{18}$$

As shown in Fig. 1 the coupling node i defines which node in the FE system the LPM should couple to. In order to identify the degree of freedom (DOF) the contribution from the LPM should be added to, a set of indicator matrices are created

$$\mathbf{I}_{ir} = \mathbf{e}_{idofr}\mathbf{e}_{idofr}^T \quad , \quad \mathbf{I}_{iz} = \mathbf{e}_{idofz}\mathbf{e}_{idofz}^T \quad , \quad \mathbf{L} = \mathbf{e}_l\mathbf{e}_l^T, \tag{19}$$

where $\mathbf{e}_{idofr}$ and $\mathbf{e}_{idofz}$ are zero vectors except with a unit entry corresponding to the r and z DOF of the coupling node i and $\mathbf{e}_l$ is a zero vector with a unit entry in the last component. An indicator matrix, $\mathbf{J}_{iz}$, is also created which has a unit entry in the bottom row corresponding to the z DOF.

The scalar equation (18) is added to Eq. (16) by multiplying the lumped components onto the indicator matrices in Eq. (19). This yields the system of equations for the hybrid FE-LPM model

$$\begin{aligned}\left(\begin{bmatrix}\tilde{\mathbf{K}} & \mathbf{0}\\ \mathbf{0} & 0\end{bmatrix} + \frac{1}{C_{p,lump,r}}\mathbf{I}_{ir} + \frac{1}{C_{p,lump,z}}\mathbf{I}_{iz} + R_E\mathbf{L} - Bl\mathbf{J}_{iz}^T \right.\\ +j\omega\left(R_{p,lump}\mathbf{I}_{iz} + Bl\mathbf{J}_{iz}\right) + (j\omega)^n L_E\mathbf{L}\\ \left. -\omega^2\left(\begin{bmatrix}\tilde{\mathbf{M}} & \mathbf{0}\\ \mathbf{0} & 0\end{bmatrix} + M_{p,lump}\mathbf{I}_{iz}\right)\right)\begin{Bmatrix}\mathbf{u}\\ \mathbf{p}\\ i_c\end{Bmatrix} = \begin{Bmatrix}\mathbf{0}\\ \mathbf{0}\\ e_g\end{Bmatrix},\end{aligned} \tag{20}$$

where $\mathbf{J}_{iz}^T$ is the transpose of $\mathbf{J}_{iz}$, $C_{p,lump,r}$ and $C_{p,lump,z}$ refers, respectively, to the lumped compliance in the r and z direction. The rest of the lumped parameters are only applied in the z-direction, which is the direction of the applied force. The FE equations in Eq. 20 are solved with an in-house Matlab code.

2.3 Estimation of optimal lumped parameters

Two of the most distinctive parameters used to identify the performance of a given loudspeaker are the pressure 1 meter away from the speaker and the electrical impedance of the VC. These physical quantities are used to formulate an objective function, such that the measured speaker response can be matched with the numerical model. The following objective function considers the absolute error squared, meaning the square of the norm of the complex difference between the numerical model and the measured data, which is normalized with respect to the square of the norm of the measured data, which in this paper comes from a numerical experiment carried out on a full model of a loudspeaker

$$\phi = \frac{||\mathbf{p}_{meas} - \mathbf{p}||_2^2}{||\mathbf{p}_{meas}||_2^2} + \frac{||\mathbf{z}_{meas} - \mathbf{z}||_2^2}{||\mathbf{z}_{meas}||_2^2}. \tag{21}$$

Here ϕ is the value of the objective function, $\mathbf{p}_{meas}$ is the measured pressure 1m away from the speaker at different frequencies, $\mathbf{p}$ is the computed pressure, $\mathbf{z}_{meas}$ is the measured VC impedance and $\mathbf{z}$ is the simulated VC impedance. The optimization problem is stated in Eq. (22), the associated constraints, L_l and L_h are defined in Tab 1.

$$\begin{aligned} \min_{\mathbf{x}} \quad & \phi\left(\mathbf{x}\right) \ , \\ \text{s.t.} \quad & \text{Eq. (13)} \ , \\ & L_l \leq x_k \leq L_h \ , \quad k = 1, \ldots, 6 \ , \end{aligned} \tag{22}$$

2.3.1 Adapting the proposed method for an experimental setup

The proposed method takes into account both the magnitude and phase of both the pressure and the impedance. This is done such that the motion of the speaker in the numerical model can match the motion of a measured speaker. In this work we match our numerical model with a numerical reference model from Comsol. The objective function is, however, constructed in such a way that the data obtained from Comsol in principle could be replaced with measurements. These measurements should be done in an anechoic chamber with a pressure microphone and electrical equipment to measure the impedance. From these measurements one can extract the magnitude and phase from the pressure and impedance measurements, respectively.

If an anechoic chamber is not readily available another physical quantity that describes the motion of the speaker, such as the velocity of the diaphragm, could be used. The measurement of the velocity could be carried out with e.g. the Klippel system that utilizes a system identification technique based on impedance- and velocity measurements.

2.4 Numerical setup of reference examples

The goal is to match the FE-LPM model with a reference loudspeaker. In this paper it is chosen to carry out a numerical experiment by simulating a full loudspeaker in Comsol Multiphysics. The reference model constitutes of the loudspeaker in Fig. 2 and the system in Fig. 4, here, the loudspeaker diaphragm is attached to the VC former as indicated with the dashed line. The system on Fig. 4 consists of the electric motor system, VC, VC former and spider which is exactly the system in the dashed box on Fig. 1. The VC consists of 100 windings, the wire has a thickness of 0.3 mm and it is made of copper. The VC-former is made of aluminum.

The reference model is a 2D axisymmetric model, where linear elasticity is assumed, the acoustics are computed without including viscous losses, the pole piece is made of iron with non-linear magnetic material properties. The solution procedure follows that of the example in Ref. [24]. First, the problem is considered static and solved in-order to extract the driving force factor and local permeability. The subsequent full analysis considers the stationary response of the loudspeaker and utilizes the former stationary solution as a linearization point. This numerical analysis includes fully coupled physics, which means that Lorentz coupling is used to describe the electromagnetic force acting on the moving VC in a magnetic field and acoustic-structure interaction is used to model the sound propagation from the moving loudspeaker.

The reference model is a full model including the entire magnet system which means that this model consists of 584072 DOF. This is computationally heavier compared to our proposed FE-LP method which has 217309 DOF. The discrepancy in complexity between the two models can mainly be attributed to the entire magnet system that

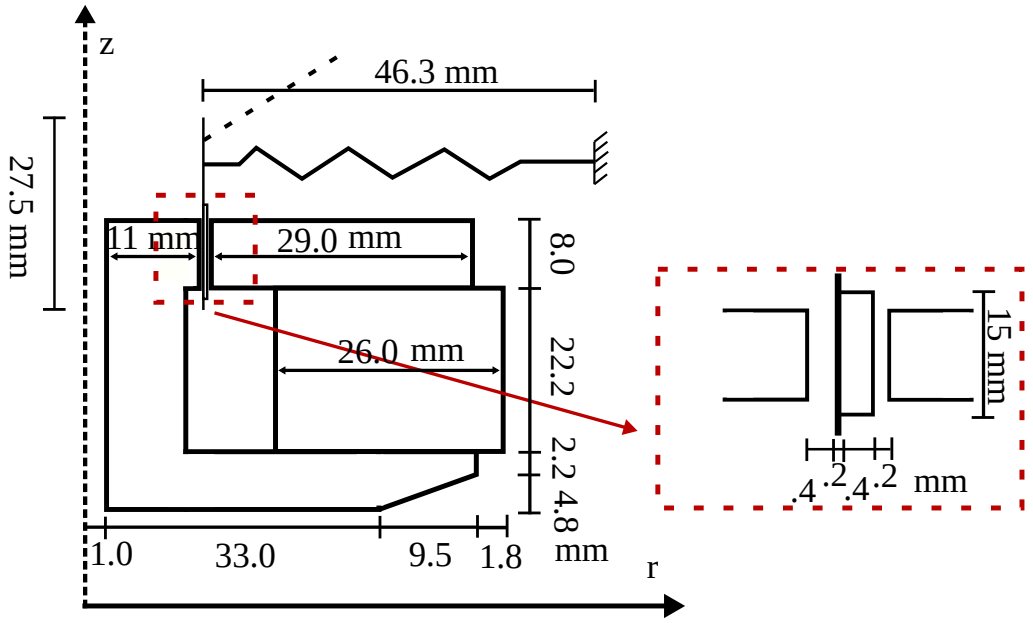

Figure 4: Sketch of the electric motor system, VC and VC-former which is included in the FE reference model.

Table 1: Table of values used as a starting guess for the optimization together with the constraint of each individual variable

x_k	L_E[mH]	n[−]	$C_{p,lump,z}$[m/N]	$C_{p,lump,r}$[m/N]	$R_{p,lump}$[Ns/m]	Bl[Tm]
Start	2.0	0.7	$4{\cdot}10^{-3}$	$4{\cdot}10^{-6}$	1.2	4.0
$[L_l; L_h]$	[0.1;6.0]	[0.2;0.9]	$4{\cdot}[10^{-6}; 10^{-1}]$	$4{\cdot}[10^{-9}; 10^{-4}]$	[0.24;6]	[3.5;7.5]

needs to be meshed. The mesh for the reference model contains many small details such as the gap between the VC and the pole piece or the very thin VC former.

3 Results

The target for the optimization is to find a set of suitable values for the lumped parameter elements in Eq. (20). An initial guess of the value of the lumped parameters is required, these values are shown together with the constraints used for each variable during the optimization in Tab. 1.

Two of the lumped parameters are not included in the optimization, one of them is the DC resistance, R_E, of the VC which can be found from the impedance measurement. The value of R_E is 3.54 Ω. The second is $M_{p,lump}$ which can be found by weighing the spider and VC components, $M_{p,lump}$ has a value of 0.006 kg. Due to the fact that a numerical experiment is used we know the force factor, however, this would not be the case for an experimental set-up of a authentic loudspeaker. Therefore we consider Bl as unknown and as a consequence of that it is included in the optimization. The input into the electrical motor system is an AC voltage source with the value of 1V.

We apply sequential quadratic programming (SQP) to solve the optimization problem in Eq. (22). The SQP algorithm is used by calling the internal Matlab function fmincon. The gradients used in the optimization is computed with finite difference using the default step length $\sqrt{\epsilon}$. Using the SQP algorithm to minimize Eq. (21), on the system of equations in Eq. (20), using the starting guess in Tab. 1 yields the design history in Fig. 5.

The values of the LPM that minimizes the objective function the most are presented in Tab. 2. We note that the value found for the force factor is 4.83 T · m which is only 3 % deviation from the calculated value of 4.67 T · m.

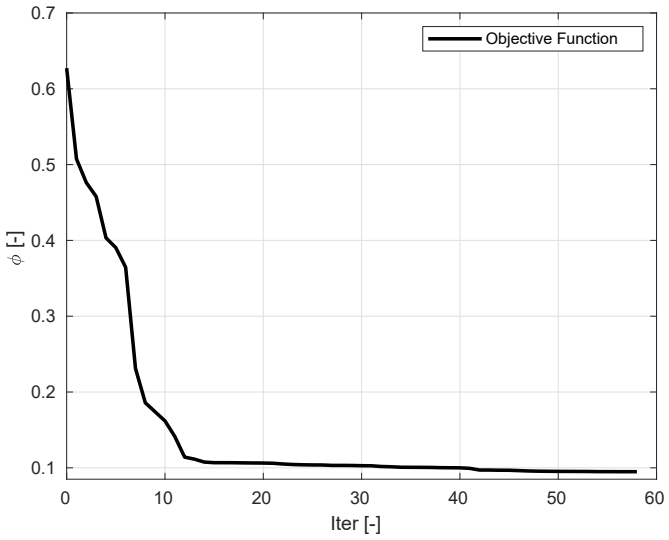

Figure 5: The history of the optimization, where the y-axis represents the value of ϕ for each iteration step.

Table 2: Table containing the optimally estimated lumped parameters

L_E[mH]	n[−]	$C_{p,lump,z}$[m/N]	$C_{p,lump,r}$[m/N]	$R_{p,lump}$[N · s/m]	Bl[T · m]
3.63	0.77	$4.81{\cdot}10^{-4}$	$4{\cdot}10^{-9}$	0.53	4.83

We can also observe that the compliance in the r direction reaches its lower bound, if this bound is lowered even further the compliance will also reach that. This finding makes sense since the compliance in the r direction keeps the loudspeaker centred, ideally, the stiffness in this direction would be infinite.

The optimal values of Tab. 2 are analysed by computing the pressure response 1 meter away from the speaker as a function of frequency. These results are compared with results for a full loudspeaker model and results for the values of the starting guess in Tab. 1. This is shown in Fig. 6.

From Fig. 6 one can observe that the optimization algorithm is able to tune the lumped parameters such that the the FE-LPM model matches the numerical experiment. A discrepancy between the two models at 316 Hz can be observed. The discrepancy can be attributed to the lack of viscous and thermal losses in the reference model in the small slits between the VC and the pole piece and the tube near the z-axis, these features are shown in Fig. 4. It is expected that viscous and thermal losses can have an effect on the actual response, which is to reduce the cavity resonance effect compared to the lossless counterpart. The cavity resonance at 316 Hz manifests itself in both the pressure and impedance response. In practice this resonance will hardly be present, this is mainly due to losses being present but also due to air-vents in the VC former, which prevents a pressure build-up. The discrepancy is mainly due to model simplifications in the reference loudspeaker and are therefore not considered important.

The values of Tab. 2 are used to simulate the impedance of the VC as a function of frequency. Again, the obtained response is compared with the reference values from the numerical experiment and the initial guess. This comparison can be seen in Fig. 7.

Figure 7 shows that the FE-LPM and the numerical experiment has a good agreement from 1 Hz to approximately 4 kHz, above 4 kHz the FE-LPM model starts to deviate from the reference as the frequency increases. No immediate explanation exist for this deviation, however, some deviation is to be expected due to high-frequency effects that are present in the full model but not in our simplified approach with lumped mechanical and electrical components. The full model includes the spider and VC former, where break-up modes will be present at high frequencies, besides this difference the two FE models have identical mechanical components.

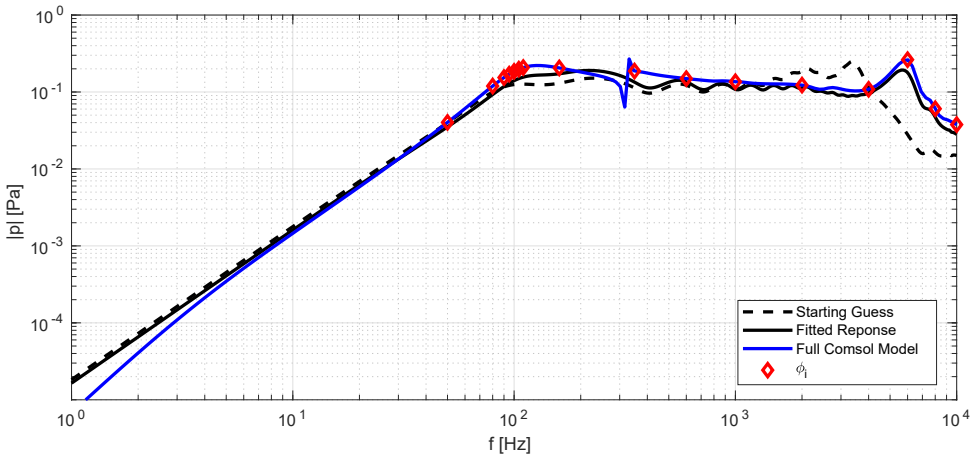

Figure 6: Pressure response between 1 Hz and 10 kHz. The solid black line is the result of the optimization, the solid blue line is the full loudspeaker model, the dashed black line is the starting guess and the red diamond-shaped discrete points are the frequencies which are used in the optimization.

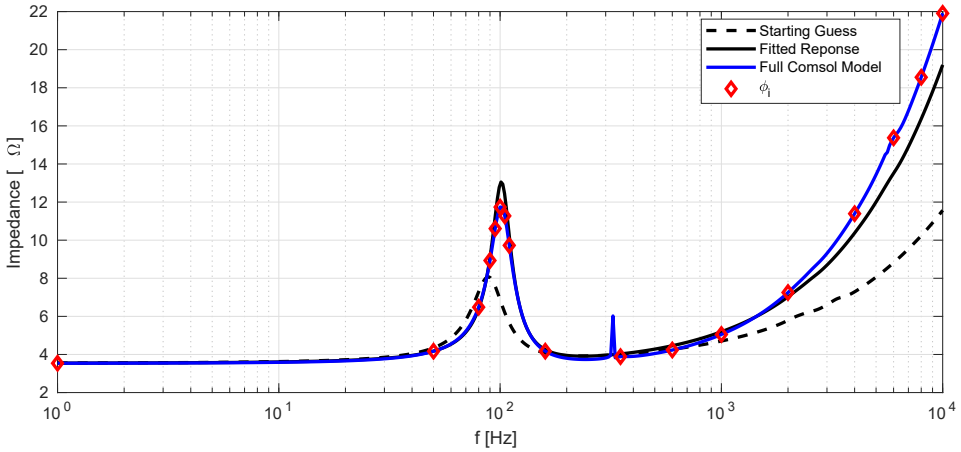

Figure 7: Impedance between 1 Hz and 10 kHz. The solid black line is the result of the optimization, the solid blue line is the full loudspeaker model, the dashed black line is the starting guess and the red diamond-shaped discrete points are the frequencies which are used in the optimization.

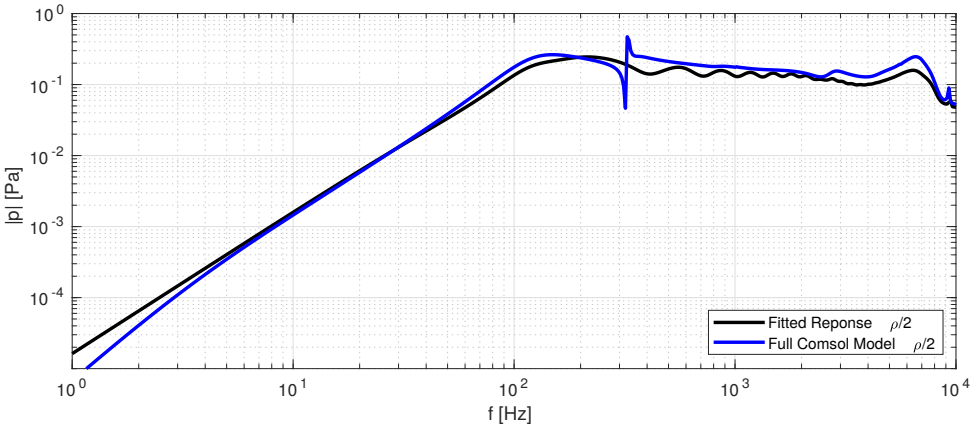

Figure 8: Pressure response between 1 Hz and 10 kHz. The solid black line is the result of the optimization, the solid blue line is the full loudspeaker model.

3.1 Robustness of the method

This section presents a test case which demonstrates the robustness of the proposed method. It is necessary to test whether the results obtained in the above section rely on a very specific tuning of the lumped parameters. Ideally changes to the baseline configuration of the reference loudspeaker and the FE-LPM should not cause a deviation between the two models. However, if the above results are a product of a fortunate tuning of the lumped parameters that only works in this specific case, the results will be very sensitive to changes in the baseline configuration. That means that one should observe a major deviation between the output of the reference loudspeaker compared to the proposed FE-LPM. The change in the models will be a change of the density of the loudspeaker diaphragm and dust cap. The density will be halved in these structural regions in both the reference loudspeaker and in the FE-LPM model. The rest of the material parameters in the FE-model will remain unchanged as will the values in the LP-model.

Figure 8 shows the pressure response of the test case. It is observed that the trends from Fig. 6 is preserved and an overall satisfactory agreements is reached between the two models. One can observe a spike in the pressure at 9.2 kHz which is attributed to a breakup mode that is now present due to the lower density of the diaphragm.

Figure 9 shows the impedance as a function of frequency. Again, the trends from Fig. 7 is also present for the test case. Figure 9 demonstrates that the FE-LPM accurately captures that the first eigenfrequency of the structure is slightly higher than that of Fig. 9. This shift of the natural resonance frequency is to be expected since the mass of the diaphragm and dust cap is lower.

Generally the test case shows that the FE-LPM adapts well to changes. When comparing the FE-LPM model with the reference loudspeaker we see the same trends as in the previous section. We note the the FE-LPM captures the break-up mode at high frequencies and the shift in the fundamental resonance frequency of the loudspeaker.

4 Discussion

This paper presents a method that can be utilized together with structural optimization. The method lumps certain parts of the loudspeaker to create a computational speedup. However, this method is not limited to the model problem in this paper. The presented method can be extended, such that it can be applied on different model problems.

In this paper we find values for the lumped components, that works well in the frequency range from 1 Hz to 10 kHz, in reality the components are frequency dependent. Therefore, the presented model could be used to solve several optimization problems at different frequencies and thus obtaining a frequency dependent mechanical stiffness

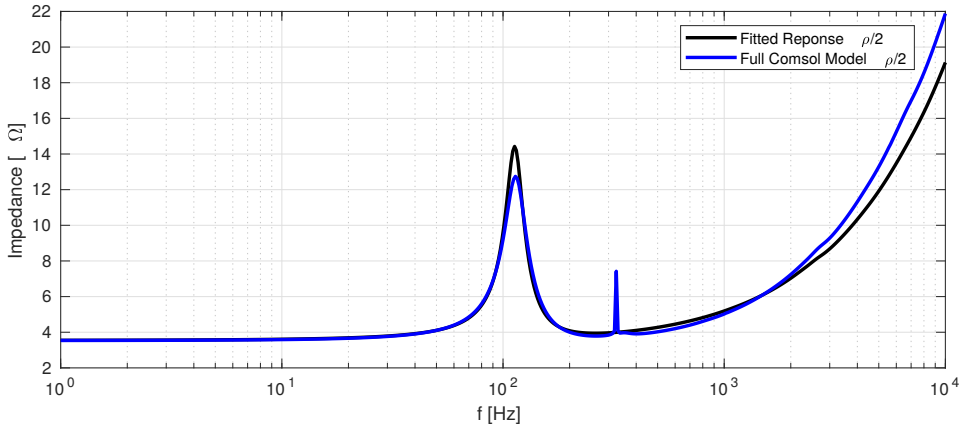

Figure 9: Impedance between 1 Hz and 10 kHz. The solid black line is the result of the optimization, the solid blue line is the full loudspeaker model.

and damping. Taking this approach one step further would include lumping the surround as well and establishing a fractional order derivative model of the surround and by that account for the viscoelastic effects in the rubber.

One could consider lumping only the electrical system and therefore include the spider, VC and VC former in the FE model. This approach could be used to optimize the electrical components of a loudspeaker.

Currently 17 discrete points are used to evaluate the objective function, as shown in Fig. 6 and 7. The amount of points are limited to 17 due to the computational effort required to carry out the optimization. This can be attributed to the fact that finite difference is used to calculate the gradients used in the optimization. A more efficient way would be to compute the gradients with the adjoint approach. Another approach than the one presented in this paper would be to compute the mechanical impedance of the FE model together with a transfer function related to the pressure 1 meter away from the speaker, these quantities would replace the FE model. This will greatly reduce the DOF in the model, which will allow for more discrete points in the optimization. This will be a very relevant approach if the end goal is only to consider lumped parameter estimation.

The objective function in Eq. (21) considers the pressure generated by the loudspeaker and the impedance of the VC. However, if there is no reliable way of obtaining the pressure one could possibly use a laser to measure the velocity of the diaphragm and use that quantity in the objective function.

5 Conclusion

This paper presents a methodology for improving the computational efficiency of FE models of loudspeaker while preserving the accuracy of the model for a specific purpose. This is illustrated by lumping the motor system and parts of the mechanical components. We demonstrate that the approach is able to closely mimic the pressure and impedance response of a full loudspeaker model even at high frequencies. The presented method can be used together with structural optimization of the diaphragm, dust cap and surround. Simple model effects such as mechanical damping and electrical inductance were used but more sophisticated models are straightforward to include.

References

[1] J. Kook and J. S. Jensen, Topology optimization of periodic microstructures for enhanced loss factor using acoustic–structure interaction, *International Journal of Solids and Structures* **122-123** (2017) 59–68.

[2] L. Shu, M. Yu Wang and Z. Ma, Level set based topology optimization of vibrating structures for coupled acoustic-structural dynamics, *Computers and Structures* **132** (2014) 34–42.

[3] S. Marburg, Developments in structural-acoustic optimization for passive noise control, *Archives of Computational Methods in Engineering* **9** (2002) 291–370.

[4] G. H. Yoon, J. S. Jensen and O. Sigmund, Topology optimization of acoustic-structure interaction problems using a mixed finite element formulation, *International Journal for Numerical Methods in Engineering* **70** (2007) 1049–1075.

[5] M. P. Bendsøe and O. Sigmund, *Topology optimization Theory, Methods and Applications* (Springer, Berlin, Heidelberg, New York, 2004), 2 edition.

[6] A. Bezzola, Numerical optimization strategies for acoustic elements in loudspeaker design, *145th Audio Engineering Society International Convention, Aes 2018* .

[7] P. Macey and K. Griffiths, Automated design of loudspeaker diaphragm profile by optimising the simulated radiated sound field with experimental validation, *128th Audio Engineering Society Convention 2010* **3** (2010) 1777–1788.

[8] R. D. Cook, D. S. Malkus, M. E. Plesha and R. J. Witt, *Concepts and Applications of Finite Element Analysis* (John Wiley & Sons, 2002), 4 edition.

[9] W. M. Leach Jr., *Introduction to Electroacoustics & Audio Amplifier Design* (Kendal/Hunt Publishing Company, 2003), 3rd edition.

[10] W. Sun and W. Hu, Integrated fe-le modelling method for a simplified balanced-armature receiver, *International Journal of Acoustics and Vibrations* **22** (2017) 377–383.

[11] G. Schrag, T. Kunzig and A. Dehe, Enhanced design of microsystems by combining lumped and distributed system-level models, *Symposium on Design, Test, Integration and Packaging of Mems/moems, Dtip 2016* (2016) 7514839.

[12] Comsol Multiphysics, Lumped receiver with full vibroacoustic coupling, https://www.comsol.com/model/lumped-receiver-with-full-vibroacoustic-coupling-61751, accesed 27-1-2020.

[13] P. Marttila and M. J. H. Jensen, A hybrid electroacoustic lumped and finite element model for modeling loudspeaker drivers, in *Audio Engineering Society Conference: 51st International Conference: Loudspeakers and Headphones* (2013).

[14] Klippel Gmbh, Specification of the klippel analyzer system, www.klippel.de, accesed 12-02-2020.

[15] W. Klippel and J. Schlechter, Distributed mechanical parameters of loudspeakers part 1: Measurements, *Journal of the Audio Engineering Society* **57** (2009) 500–511.

[16] W. Cardenas and W. Klippel, Optimal material parameter estimation by fitting finite element simulations to loudspeaker measurements, *144th Audio Engineering Society Convention 2018* .

[17] D. G. Nielsen, J. S. Jensen, V. Cutanda Henriquez and F. T. Agerkvist, Finite element model coupled with lumped parameter elements, *Proceedings of 14th International Conference on Theoretical and Computational Acoustics* (2019) 297–304.

[18] J. P. Bérenger, Perfectly matched layer for the fdtd solution of wave-structure interaction problems, *Ieee Transactions on Antennas and Propagation* **44** (1996) 110–117.

[19] J. N. Li, S. X. Wang, H. J. Yin, C. H. Dong and H. M. Chen, Acoustic wave equation modeling in cylindrical coordinates with convolutional pml, *77th Eage Conference and Exhibition 2015: Earth Science for Energy and Environment* (2015) 4546–4548.

[20] F. Collino and P. Monk, The perfectly matched layer in curvilinear coordinates, *Siam Journal of Scientific Computing* **19** (1998) 2061–2090.

[21] J. S. Jensen, Topology optimization problems for reflection and dissipation of elastic waves, *Journal of Sound and Vibration* **301** (2007) 319–340.

[22] A. W. King and F. T. Agerkvist, Fractional derivative loudspeaker models for nonlinear suspensions and voice coils, *Journal of Audio Engineering Society* **66** (2018) 525–536.

[23] P. Brunet and B. Shafai, Identification of loudspeakers using fractional derivatives, *Aes: Journal of the Audio Engineering Society* **62** (2014) 505–515.

[24] Comsol Multiphysics, Loudspeaker driver — frequency-domain analysis, https://www.comsol.com/model/loudspeaker-driver-8212-frequency-domain-analysis-1369, accesed 27-1-2020.

Paper 2

PROCEEDINGS of the
23rd International Congress on Acoustics
9 to 13 September 2019 in Aachen, Germany

Optimization of realistic loudspeaker models with respect to basic response characteristics

Daniel Gert NIELSEN[(1)], Finn T. AGERKVIST[(2)], Jakob S. JENSEN[(3)]

[(1)]Department of Electrical Engineering Technical University of Denmark , Denmark, dgniel@elektro.dtu.dk
[(2)]Department of Electrical Engineering Technical University of Denmark , Denmark, fa@elektro.dtu.dk
[(3)]Department of Mechanical Engineering Technical University of Denmark , Denmark, jsj@mek.dtu.dk

Abstract
A numerical model for optimization of loudspeakers mounted in infinite baffles is presented in this paper. The optimization is carried out by using objective functions based on basic response characteristics for loudspeakers such as the on axis frequency response. In-order to create a realistic model of the speaker we include the excitation of the speaker from the motor system. The interaction between acoustic medium and structure is modelled with the finite element method. As most loudspeaker drivers are nearly symmetric, the presented model is a 2D axisymmetric finite element model. The exterior domain is modelled with perfectly matched layers, which ensure free-field radiation conditions. Optimized designs for a selection of objective functions are presented and discussed.
Keywords: Optimization, FEM, Loudspeaker, Materials

1 INTRODUCTION

Since its discovery three decades ago [2], structural topology optimization has increased in popularity [3] and is now widely used as a design tool to for improving a wide range of engineering structures such as airplane fuselages [1], waveguide filters [10] and periodic microstructures [8]. The usage of optimization techniques has over the years expanded to many different scientific disciplines, including acoustic-structure problems [9].

Topology optimization has previously been used when performing structural-acoustic optimization. One of the pitfalls of using structural topology optimization in conjunction with acoustics, is the physical interpretation of structural elements with intermediate densities, e.g. how to interpret an element with 40 % air and 60 % solid. Several methods have been proposed to combat this issue, [13] introduces the concept of a mixed finite element formulation, [6] uses artificial mechanical and acoustic parameters in the non-structural and non-acoustic domains together with self coupling elements and [11] proposes level set based topology optimization.

If we consider the design of loudspeakers from different brands the choice of shape and materials are converging towards similar solutions. This paper will look at the choice of materials in loudspeakers and how these choices can improve the performance. To do this we use advanced numerical optimization techniques in conjunction with a 2D axisymmetric finite element model. This paper is about distributed parameter optimization. Here the mechanical structure is not changeable, and only the material of which it is made of is optimized. This of course limits the design freedom in the sense that new geometries are not created, instead we explore the opportunities of existing mechanical structures.

2 THEORY

Finite element analysis (FEA) is used to calculate the acoustic wave propagation from a vibrating mechanical structure. The model consists of a structural mechanics domain where the governing equation are the dynamic equation of motion and an acoustic domain described with the Helmholtz equation. These domains are discretized into elements with quadratic shape functions. The two domains are coupled together in the interface between the mechanical structure and the acoustic domain, for details see e.g. [5]. Perfectly Matches Layers

(PMLs) are used to mimic exterior acoustic conditions, the details of this method can be found in [4]. The following matrix vector equation is used to calculate mechanical displacements and acoustic pressure

$$\left(\begin{bmatrix} \mathbf{K} & -\mathbf{S}^T \\ \mathbf{0} & \mathbf{K}_F(\omega) \end{bmatrix} - \omega^2 \begin{bmatrix} \mathbf{M} & \mathbf{0} \\ \rho_F \mathbf{S} & \mathbf{M}_F(\omega) \end{bmatrix} \right) \begin{Bmatrix} \mathbf{u}_s \\ \mathbf{p} \end{Bmatrix} = \begin{Bmatrix} \mathbf{f}_s(\omega) \\ \mathbf{0} \end{Bmatrix}, \tag{1}$$

where $\mathbf{K}$ is structural stiffness matrix, $\mathbf{S}$ is the coupling matrix, ω is the harmonic excitation frequency, $\mathbf{M}$ is the structural mass matrix, $\mathbf{u}_s$ is the structural nodal displacements $\mathbf{f}_s(\omega)$ is the externally applied harmonic excitation of the mechanical structure, $\mathbf{K}_F(\omega)$ is the acoustic stiffness matrix that is frequency dependent in the PML region, ρ_f is the density of air, $\mathbf{M}_F(\omega)$ is the acoustic mass matrix which is frequency dependent in the PML region and $\mathbf{p}$ is the nodal pressure in the acoustic domain.

3 DISTRIBUTED PARAMETER OPTIMIZATION

This paper proposes an optimization scheme in which the material distribution within the structure is optimized. The optimization procedure relies on being able to change the element stiffness and density in each individual structural element, which is controlled by the design variable α^e that can take on values between 0 and 1. The following linear interpolation is used in each structural element

$$\rho^e = \rho_{min} + \alpha^e (\rho_{max} - \rho_{min}) \tag{2}$$
$$E^e = E_{min} + \alpha^e (E_{max} - E_{min}), \tag{3}$$

where E^e is the Young's modulus in an element, ρ^e is the element density, ρ_{min} is a lower bound for the element density, ρ_{max} is the upper bound, E_{min} is the lower bound of the element Young's modulus and E_{max} is the upper bound. Young's modulus and density are chosen as the parameters to be changed during the optimization because they are very much linked to the vibration pattern of the mechanical structure. The parameters needs change with some co-dependency (here a linear dependency) such that the achieved material configuration is kept realistic and to avoid trivial solutions.

The system of equations in (1) can be written in a compact form

$$\left(\tilde{\mathbf{K}} - \omega^2 \tilde{\mathbf{M}}\right) \tilde{\mathbf{u}} = \tilde{\mathbf{S}} \tilde{\mathbf{u}} = \tilde{\mathbf{f}}, \tag{4}$$

where $\tilde{(\cdot)}$ indicates that the matrix or vector is written with compact notation.

The full sensitivity analysis is not carried out in this paper, the reader is referred to [7, 6] for a detailed explanation of the derivation of the adjoint sensitivities.

3.1 The Optimization Problem

Figure 1 shows the domain to be optimized, Ω, which resembles a piston-like structure mounted in an infinite baffle. The figure also shows half of the acoustic domain Ω_F, the acoustic domain is also present below the piston, however it is not included in this figure and finally, Ω_A, which is the region with PMLs.

In Figure 1 the region marked by the red rectangle is the region of interest for the optimization. In this region it is desired to enhance the performance of the speaker, consequently, the magnitude of the pressure needs to be increased. This can be cast as a optimization problem

$$\begin{aligned} \max_{\alpha} \quad & \Phi_0 = |\tilde{\mathbf{u}}|^2, \\ \text{s.t.} \quad & \tilde{\mathbf{S}} \tilde{\mathbf{u}} - \tilde{\mathbf{f}} = 0, \\ & 0 \leq \alpha_e \leq 1, \quad e = 1, \ldots, n, \end{aligned} \tag{5}$$

which can be solve using the Method of Moving Asymptotes [12]. It is only the nodal degrees of freedom (DOF) inside the boxed region that should be included in the objective function. Consequently, the diagonal

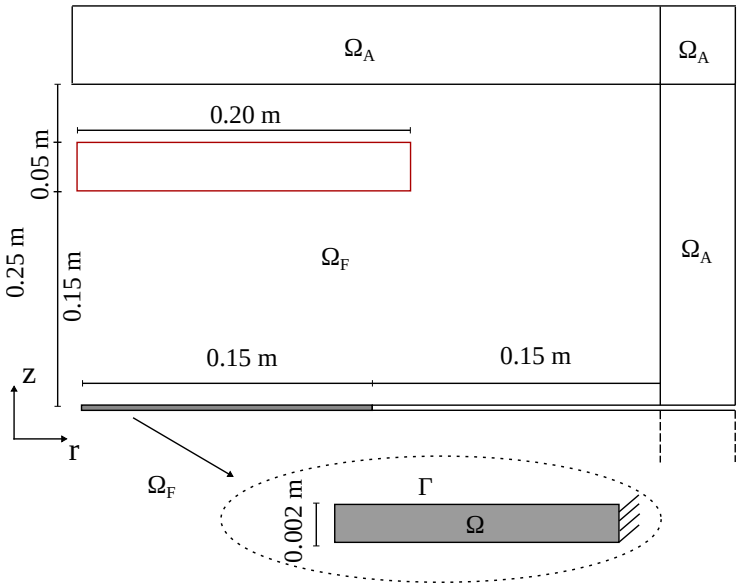

Figure 1. Piston-like-structure mounted in an infinite baffle.

matrix $\mathbf{L}$ is constructed, the matrix contains ones in the diagonal corresponding to the DOF in the boxed region in Figure 1.

$$\Phi_0 = |\tilde{\mathbf{u}}|^2 = |\tilde{\mathbf{u}}|^T \mathbf{L} |\tilde{\mathbf{u}}|. \tag{6}$$

The adjoint equation for this particular optimization problem becomes [7]

$$\tilde{\mathbf{S}}\boldsymbol{\lambda} = -2\mathbf{L}^T\tilde{\mathbf{u}}, \tag{7}$$

the equation should be solved for $\boldsymbol{\lambda}$, which is the adjoint variable that can be used to compute the sensitivities by inserting into:

$$\Phi' = \mathrm{Re}\left(\boldsymbol{\lambda}^T \frac{\partial \tilde{\mathbf{S}}}{\partial \alpha^e}\tilde{\mathbf{u}}\right), \tag{8}$$

where the term $\frac{\partial \tilde{\mathbf{S}}}{\partial \alpha^e}$ is the derivative of the system matrix with respect to the design variable α^e. Evaluating the term yields

$$\frac{\partial \tilde{\mathbf{S}}}{\partial \alpha^e} = \frac{\partial \tilde{\mathbf{K}}}{\partial \alpha^e} - \omega^2 \frac{\partial \tilde{\mathbf{M}}}{\partial \alpha^e}, \tag{9}$$

in which the derivative of the global mass and stiffness matrix is

$$\frac{\partial \tilde{\mathbf{K}}}{\partial \alpha^e} = \begin{bmatrix} \frac{\partial \mathbf{K}}{\partial \alpha^e} & -\frac{\partial \mathbf{S}^T}{\partial \alpha^e} \\ \mathbf{0} & \frac{\partial \mathbf{K}_F}{\partial \alpha^e} \end{bmatrix} = \begin{bmatrix} \frac{\partial E^e}{\partial \alpha^e}\mathbf{K} & \mathbf{0} \\ \mathbf{0} & \mathbf{0} \end{bmatrix} \quad , \quad \frac{\partial \tilde{\mathbf{M}}}{\partial \alpha^e} = \begin{bmatrix} \frac{\partial \mathbf{M}}{\partial \alpha^e} & \mathbf{0} \\ \rho_F \frac{\partial \mathbf{S}}{\partial \alpha^e} & \frac{\partial \mathbf{M}_F}{\partial \alpha^e} \end{bmatrix} = \begin{bmatrix} \frac{\partial \rho^e}{\partial \alpha^e}\mathbf{M} & \mathbf{0} \\ \mathbf{0} & \mathbf{0} \end{bmatrix}, \tag{10}$$

where E^e and ρ^e are determined from (3) and (2), the derivative of the element interpolation functions with respect to the design variable is

$$\frac{\partial E^e}{\partial \alpha^e} = E_{max} - E_{min} \quad , \quad \frac{\partial \rho^e}{\partial \alpha^e} = \rho_{max} - \rho_{min} \tag{11}$$

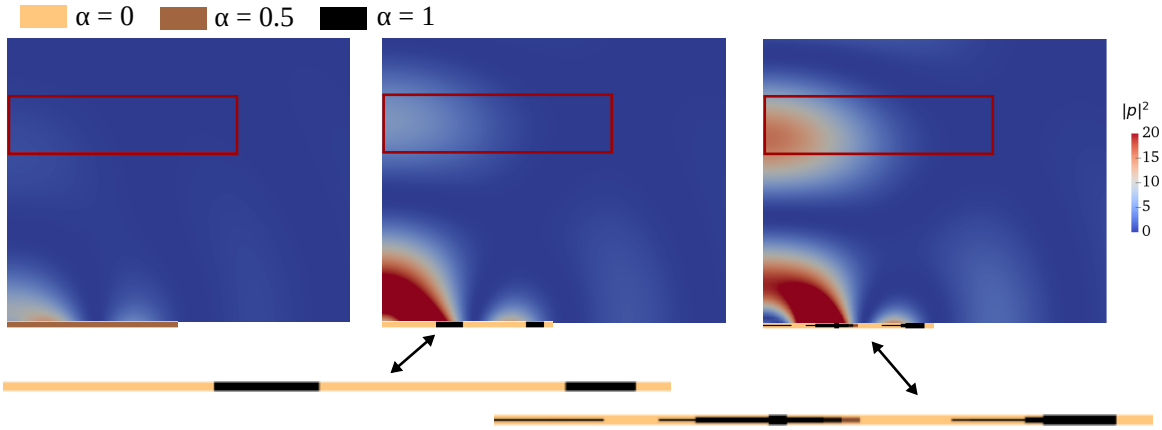

Figure 2. 1500Hz excitation frequency, $|p|^2$ evaluated for the starting guess (left), optimized design with 1 element in the vertical direction (middle) and optimized design with 5 elements in the vertical direction (right).

4 NUMERICAL RESULTS AND DISCUSSION

The optimization problem (5) is solved for the structure presented in Figure 1 at three different excitation frequencies. This structure corresponds to a loudspeaker unit of 12 inches, which is a large bass unit that is used to produce low frequency content. The results in this section is obtained for 1500Hz, 2500Hz and 3500 Hz, these frequencies are well above the operating range of a 12 inch unit. Furthermore the loudspeaker unit is flat and with no dust cap, consequently, the structure does not benefit from geometrical stiffness. These factors makes the optimization problem harder to solve, but solving it might give an indication whether we could extend the operating range of larger units by utilizing optimization techniques.

This section presents the optimized results and these are compared to the original structure with homogeneous material distribution. The vibration pattern of the optimized- and original structures are presented, furthermore the objective functions as function of iteration history are shown. Two optimization results are presented for each excitation frequency, the first result only has one element in the vertical direction and 36 elements in the radial direction. The second result has a higher degree of design freedom, these design consists of 5 elements in the vertical direction and 36 elements ind the radial direction.

Table 1 shows the parameters used to determine the Young's modulus and density in each element.

Table 1. Lower- and upper bound for element stiffness and density

E_{min}:	35 MPa	E_{max}:	105 MPa
ρ_{min}:	1350 kg/m^3	ρ_{max}:	4050 kg/m^3

Figure 2 shows $|p|^2$ for three different structures, all of whom are excited by a tip force of 2N at 1500 Hz. The leftmost structure has a uniform material distribution with $\alpha^e = 0.5$ in all elements. This is the initial design that also serves as a starting guess for the optimization. From the plots of the pressure magnitude, it can be observed that the optimized designs vastly improves the magnitude of the pressure in the desired region. Especially the rightmost design achieves a very good design, which is further validated by looking at the objective function in Figure 8.

The vibration pattern of the structures in Figure 3 shows that the rightmost structure can create larger structural displacements compared to the structure in the middle, it is noted that the overall displacement pattern is similar for the two optimized structures. The structural displacements have been scaled with a factor of 5000 for better visualization.

Figure 3. 1500Hz excitation frequency, vibration pattern for the the starting guess (left), optimized design with 1 element in the vertical direction (middle) and optimized design with 5 elements in the vertical direction (right).

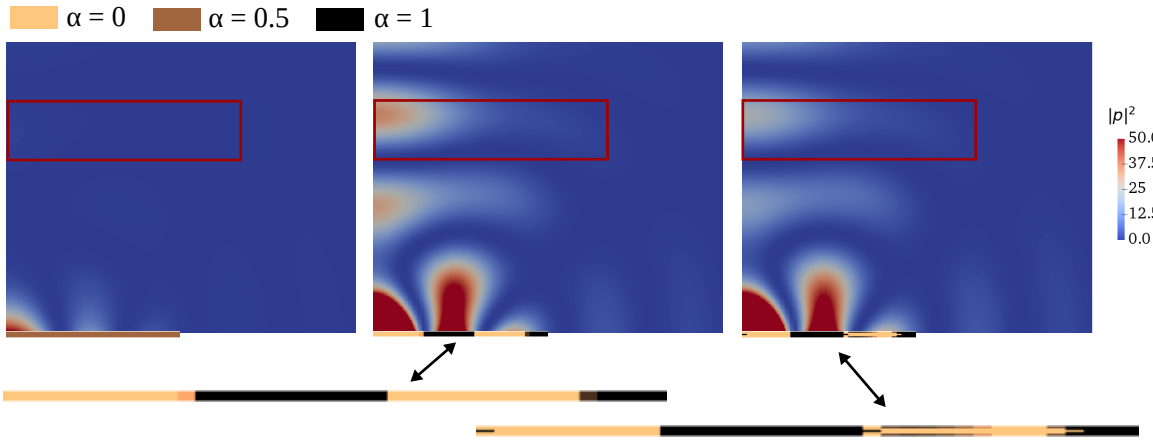

Figure 4. 2500Hz excitation frequency, $|p|^2$ evaluated for the starting guess (left), optimized design with 1 element in the vertical direction (middle) and optimized design with 5 elements in the vertical direction (right).

In Figure 4 the structure is excited with 2N at 2500 Hz. In this figure it is observed that optimized structure in the middle performs slightly better than the rightmost structure. This is surprising since the rightmost structure has larger design freedom and therefore should perform better when optimized, as it was the case in Figure 2. From Figure 8 one can see that the structure containing 5 elements exhibits a strange convergence pattern during the optimization, which might be due to an unfeasible local minimum. The vibration pattern of the structure can be seen in Figure 3.

The structure in Figure 6 is excited at 3500 Hz with a tip force of 2N. It can be seen in the figure that the pressure magnitude is indeed increased, this is however not as significant as the previously shown result. This is supported by Figure 8 that shows that the pressure magnitude in the rectangular area only is increased by a factor of 8. Figure 7 shows the vibration pattern of homogeneous- and optimized structures.

Figure 5. 2500Hz excitation frequency, vibration pattern for the the starting guess (left), optimized design with 1 element in the vertical direction (middle) and optimized design with 5 elements in the vertical direction (right).

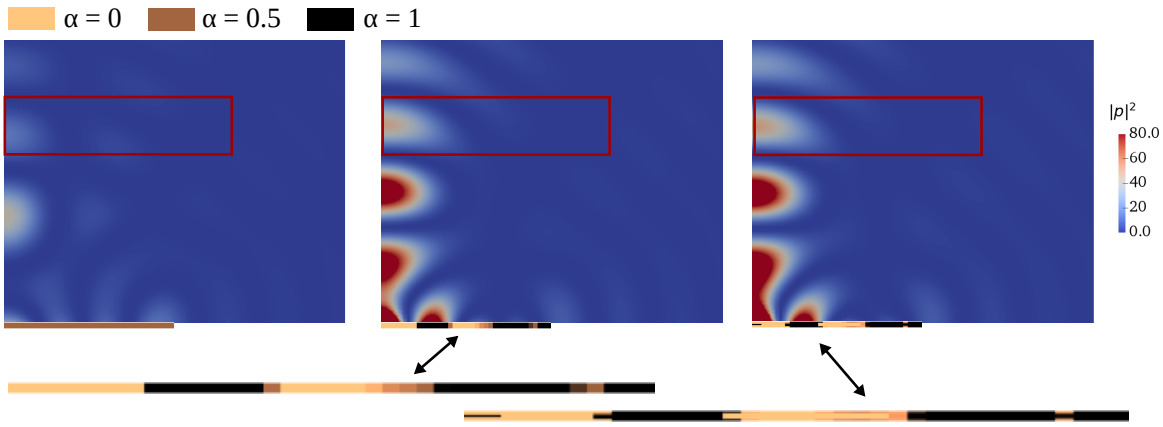

Figure 6. 3500Hz excitation frequency, $|p|^2$ evaluated for the starting guess (left), optimized design with 1 element in the vertical direction (middle) and optimized design with 5 elements in the vertical direction (right).

Figure 7. 3500Hz excitation frequency, vibration pattern for the the starting guess (left), optimized design with 1 element in the vertical direction (middle) and optimized design with 5 elements in the vertical direction (right).

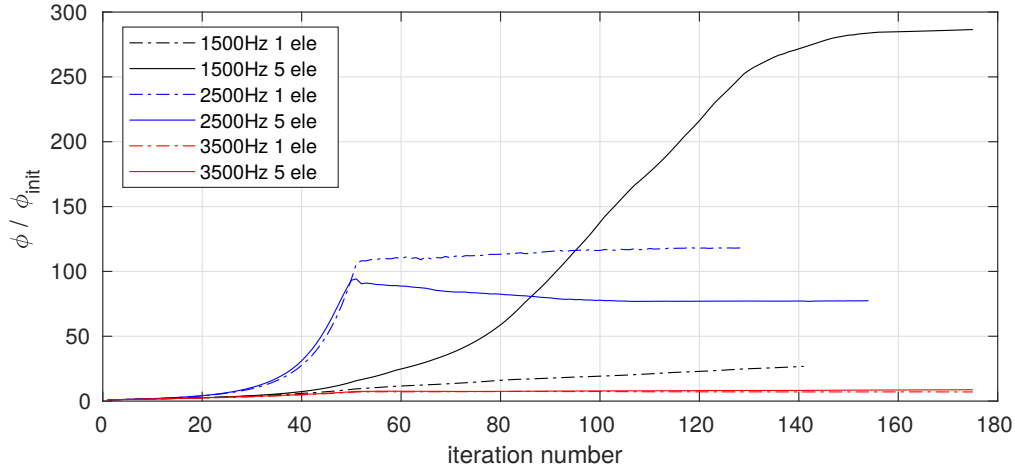

Figure 8. Objective functions evaluated for the optimized designs as function of iteration history.

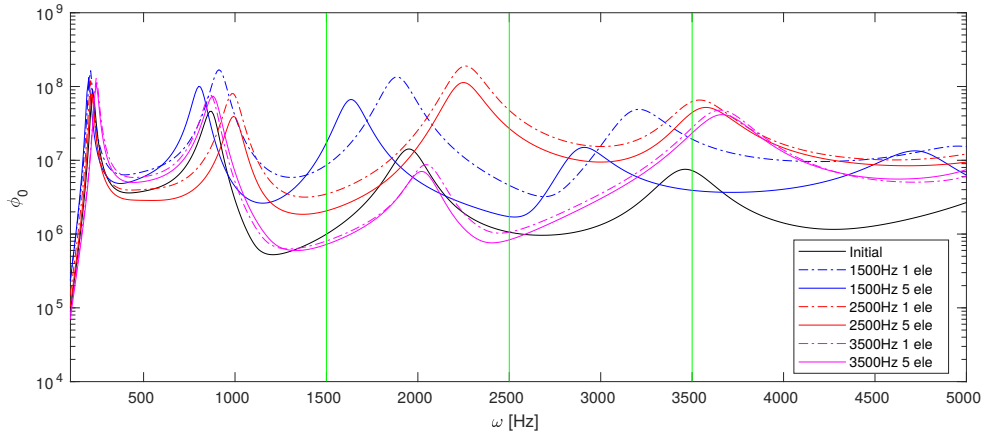

Figure 9. Evaluation of the objective function as a function of frequency for the initial homogeneous solution and for the optimized designs.

Figure 9 shows how the optimized designs performs in the frequency range from 100 Hz to 5000 Hz. The green lines indicate the target frequencies, the blue lines are the performance of the design optimized for 1500 Hz, the red curve is 2500 Hz and the magenta curve is 3500 Hz and the black curve is the initial homogeneous design. The optimizer tries to shift the resonance frequency such that it aligns with the target frequency for the optimization. This is especially pronounced for the blue and red curve where the third resonance frequency of the initial structure is shifted down in frequency for the blue curve and shifted up for the red curve. The first resonance frequency of the initial structure is hardly affected by the optimization whereas the second resonance frequency is affected to some extend. The optimized structure for 2500 Hz actually has a higher objective function value at 3500 Hz than the structure which was optimized for that frequency. This shows the existence of local minimums that can affect the end result of the optimization.

The optimized designs takes advantage of the rather simple objective function by increasing the magnitude of the pressure close to the center axis where it is easiest. This gives a rather uneven pressure response, due to the fact that the pressure on axis is greatly increased relative to the pressure off-axis. If one wants the increase in pressure to be more evenly distributed a more complex objective function should be used; in which the optimization favors the off-axis response over the on-axis response. Another option could be to minimize the standard deviation of the pressure magnitude for the optimized designs presented in this paper.

The designs presented in this paper is optimized for one specific frequency. It was expected that the performance at other frequencies would be sacrificed to achieve optimal performance at the target frequency. This has however not been the case and this could be due to the fact that the optimized structures has regions with lower structural stiffness and thereby larger structural displacements compared to the initial design.

5 CONCLUSION

A 2D axisymmetric numerical framework has been developed and extended to include distributed parameter optimization of mechanical structures coupled to acoustic domains. The optimization is based on well known gradient based methods. The advantage of the method is that it does not require any interpolation scheme, because the interface between fluid and solid is well defined throughout the optimization. The developed method is tested with three simple examples in which the initial design is improved. The design obtained at 1500 Hz shows major improvements when compared to the starting point, the design with 5 vertical elements improves with a factor of 280 when compared to the initial design. This comes to show that large improvements of

existing designs can be obtained by optimizing the material within the structure.

The method can readily be extended to consider more sophisticated objective functions, which i.e. could be used to achieve an even pressure response at higher frequencies. The method should be extended, such that the optimization includes multiple frequencies and thereby making the obtained solutions valid in a broader range.

REFERENCES

[1] N. Aage, E. Andreassen, B. S. Lazarov, and O. Sigmund. Giga-voxel computational morphogenesis for structural design. *Nature*, 550(7674):84–86, 2017.

[2] M. P. Bendsoe and N. Kijuchi. Generating optimal topologies in structural design using a homogenization method. *Computer Methods in Applied Mechanics and Engineering*, 71(2):197–224, 1988.

[3] M. P. Bendsøe and O. Sigmund. *Topology optimization Theory, Methods and Applications*. Springer, Berlin, Heidelberg, New York, 2 edition, 2004.

[4] A. Bermúdez and L. Hervella-Nieto. An optimal finite-element/pml method for the simulation of acoustic wave propagation phenomena. *Variational Formulations in Mechanics: Theory and Applications*, (January), 2006.

[5] R. D. Cook, D. S. Malkus, M. E. Plesha, and R. J. Witt. *Concepts and Applications of Finite Element Analysis*. John Wiley & Sons, 4 edition, 2002.

[6] J. S. Jensen. A simple method for coupled acoustic-mechanical analysis with application to gradient-based topology optimization. *Structural and Multidisciplinary Optimization*, 59(5):1567–1580, 2019.

[7] J. S. Jensen. Adjoint sensitivity analysis for linear dynamic systems with time-harmonic excitation. *Course notes for TopOpt course 2017 Technical University of Denmark*, June 2017.

[8] J. Kook and J. S. Jensen. Topology optimization of periodic microstructures for enhanced loss factor using acoustic–structure interaction. *International Journal of Solids and Structures*, 122-123:59–68, 2017.

[9] S. Marburg. Developments in structural-acoustic optimization for passive noise control. *Archives of Computational Methods in Engineering*, 9(4):291–370, 2002.

[10] D. G. Nielsen, S. D. Pedersen, V. Zhurbenko, V. E. Johansen, O. Sigmund, and N. Aage. Topology optimization and experimental verification of compact e-plane waveguide filters. *Microwave and Optical Technology Letters*, 61(5):1208–1215, 2019.

[11] L. Shu, M. Yu Wang, and Z. Ma. Level set based topology optimization of vibrating structures for coupled acoustic-structural dynamics. *Computers and Structures*, 132:34–42, 2014.

[12] K. Svanberg. The method of moving asymptotes - a new method for structural optimization. *International Journal for Numerical Methods in Engineering*, 1987.

[13] G. H. Yoon, J. S. Jensen, and O. Sigmund. Topology optimization of acoustic-structure interaction problems using a mixed finite element formulation. *International Journal for Numerical Methods in Engineering*, 70(9):1049–1075, 2007.

Paper 3

Seoul inter-noise 2020 23-26 AUGUST

Optimization of the Performance of Small Speaker Systems with Passive Radiators

Daniel Gert Nielsen[1]
Acoustic Technology, Department of Electrical Engineering, Technical University of Denmark
Ørsteds Plads 352, 2800 Kgs. Lyngby, Denmark

Gyeong-Tae Lee
Department of Mechanical Engineering, KAIST
291 Daehak-ro, Yuseong-gu, Daejeon 34141, Korea

Yong-Hwa Park
Department of Mechanical Engineering, KAIST
291 Daehak-ro, Yuseong-gu, Daejeon 34141, Korea

Jakob Søndergaard Jensen
Centre for Acoustic-Mechanical Micro Systems, Technical University of Denmark
Nils Koppels Allé, Bygning 404, 2800 Kgs. Lyngby, Denmark

Finn Thomas Agerkvist
Acoustic Technology, Department of Electrical Engineering, Technical University of Denmark
Ørsteds Plads 352, 2800 Kgs. Lyngby, Denmark

ABSTRACT

Small transportable Bluetooth- and smart/AI speakers are becoming an increasing part of many households. Due to their small size, these speakers have limited output at low frequencies, and typically have a vented port or in some cases a passive radiator to improve the low-frequency performance. In this work, we show how a density based material optimization approach can be used to optimize the frequency response of the system. The passive radiator is placed at the top of a cylinder with a down-firing speaker, driven with a voltage source, which, via a lumped model, is connected to a multi-physics finite element framework. The speaker radiates sound into an unbounded domain, which is realized by using perfectly matched layers. The performance of the speaker is based on a numerical measurement 1 meter away from the speaker. Several optimization results are shown and these are compared with a more generic type of small speaker system.

1. INTRODUCTION

Small compact speakers that can be controlled with voice commands are increasingly becoming a part of many households. Twenty-four percent of Americans owns at least one smartspeaker according

[1]dgniel@elektro.dtu.dk

to a recent report published by Edison Research and NPR [1]. Out of the 60 million Americans owning a smartspeaker 23 % of them use the smartspeaker for the majority of their music listening, a number which increases every year. The quality of the sound of these type of products are therefore increasingly important. The physical size and the limited cabinet space available mean that the reproduction of low frequency content can be lackluster. Presently, there are options available to extend the frequency range of speaker systems, e.g. an EQ that is targeted towards low frequencies can to some extend improve the output, this can lead to distortion if the input voltage is too high, also an overall higher power consumption is to be expected. Other popular options are vented ports or passive radiators. The passive radiator requires less space and does not produce a whistling sound which the vented port systems occasionally are prone to do.

The passive radiator was invented and patented by H. F. Olson in 1934 [2], it was, however, first in 1954 when Olson et. al. published a paper describing the design process of cabinets with 8, 10 and 12 inch loudspeakers where a passive radiator was included in the cabinet [3], that his original idea gained attention. The reason for this being, according to R. H. Small, that the design process was until then not very well described within the literature [4]. In reference [5] R.H. Small gives an in depth description of how a direct-radiator loudspeaker can be designed including a port or passive radiator.

Numerical modelling of vibro-acoustic problems are quite common these days, even complex models of loudspeakers and hearing aids can be modelled with numerical models such as Finite Element (FE) or Boundary Element (BE) models. Within the recent years many advances have been made in applying optimization techniques to improve existing designs or come up with new designs. Topology optimization has been successfully applied to acoustic-structure interaction problems [6, 7] and to the design of acoustic horns [8]. In the recent years generalized shape optimization has also been applied to vibro-acoustic problems [9]. Dilgen et al. compares the aforementioned methods in reference [10]. In reference [11] Bezolla uses parameter-, topology- and shape optimization to improve acoustic elements such as phase plugs in loudspeakers. Recently Nielsen et al. used material optimization to maximize the pressure output from a flat panel loudspeaker [12].

This paper deals with the design of a passive radiator for a small cylindrical speaker. We are utilizing FE modeling combined with a lumped parameter model (LPM) [13] and gradient based optimization techniques. The combination of these methods yields a strong tool for tailoring the frequency response of e.g. a smartspeaker. Subsequent sections will elaborate on the theory required to perform the numerical calculations, then we present the optimization scheme and finally we present and discuss the optimization results.

2. THEORY

This section will describe the model of the smartspeaker used in this paper, along with the FE and optimization theory that is used. The speaker used in this work is inspired from the Amazon Echo speaker configuration, with a down-firing woofer and tweeter. Our model is shown in Figure 1, here we have only included the woofer, since we are only interested in the low frequency output of the speaker. The figure also shows that a passive radiator is placed in the top of the speaker. The figure shows the speaker in 2D with a vertical z-axis and a horizontal r-axis, this implies that the modeling of the speaker utilizes 2D axisymmetry. In this work the woofer is excited with an electrical signal, which is included in the FE model as a lumped addition, this method and the theory required to implement it is thoroughly discussed in reference [13]. The cabinet of the smartspeaker and the acoustic lens is considered rigid.

The speaker system in Figure 1 is shown as a model problem in Figure 2. The smartspeaker is placed in an unbounded domain, here modeled with perfectly matched layers (PMLs) in the domain Ω_A, the rest of the acoustic domain is denoted Ω_a, the structural domains are denoted Ω_s, the interfaces between solid and acoustic domains are called Γ_{as} and finally Γ_a denotes the outer boundaries. The red square pinpoints the listening position 1 meter away from the smartspeaker system. The size of

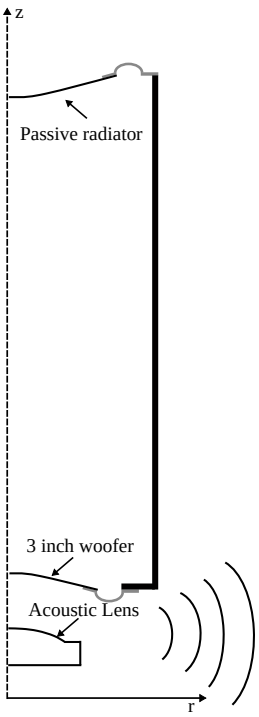

Figure 1: 2D sketch of a cylindrical smartspeaker with a passive radiator

the red square is chosen to be 5x5cm. In this area the preferred objective function is evaluated as a qualitative measure of the speakers performance.

The notation in this paper obeys the following rules; capital bold letters specifies a matrix, small bold letters implies a vector and non bold letters are scalars.

2.1. Finite Element Model

The governing equations for the time-harmonic motion of a linear elastic body where body forces has been neglected are

$$-\rho\omega^2\mathbf{u} - \nabla\cdot\boldsymbol{\sigma}(\mathbf{u}) = 0 \qquad \text{in} \quad \Omega_s \tag{1}$$

$$\boldsymbol{\sigma} = \mathbf{C}\boldsymbol{\epsilon} \tag{2}$$

$$\epsilon = \{\epsilon_r\ \epsilon_\theta\ \epsilon_z\ \gamma_{zr}\}^T \qquad \text{(2D Axisymmetric)} \tag{3}$$

$$\epsilon_r = \frac{\partial u_r}{\partial r},\ \epsilon_\theta = \frac{u_r}{r},\ \epsilon_z = \frac{\partial u_z}{\partial z},\ \gamma_{zr} = \left(\frac{\partial u_r}{\partial z} + \frac{\partial u_z}{\partial r}\right), \tag{4}$$

here ρ is the mass density of the material, ω is the excitation frequency in radians, $\mathbf{u}$ is the structural displacements, $\boldsymbol{\sigma}$ is the stress tensor, Ω_s is the structural domain, $\mathbf{C}$ is the constitutive matrix for an axisymmetric structure, $\boldsymbol{\epsilon}$ is the strain tensor, u_r is the structural displacement in the r-direction and u_z is the displacement in the z-direction.

To obtain the pressure distribution in the acoustic domain, the Helmholtz equation is solved

$$\Delta p + \frac{\omega^2}{c^2}p = 0, \tag{5}$$

here Δ is the Laplace operator in cylindrical coordinates, p is the pressure and c is the speed of sound in air. A modified Helmholtz equation [14, 15] is solved in a truncated PML region (Ω_A), as shown in Figure 2.

$$\frac{1}{\gamma_r}\frac{\partial}{\partial r}\left(\frac{1}{\gamma_r}\frac{\partial p_A}{\partial r}\right) + \frac{1}{\gamma_z}\frac{\partial}{\partial z}\left(\frac{1}{\gamma_z}\frac{\partial p_A}{\partial z}\right) + k^2 p_A = 0, \tag{6}$$

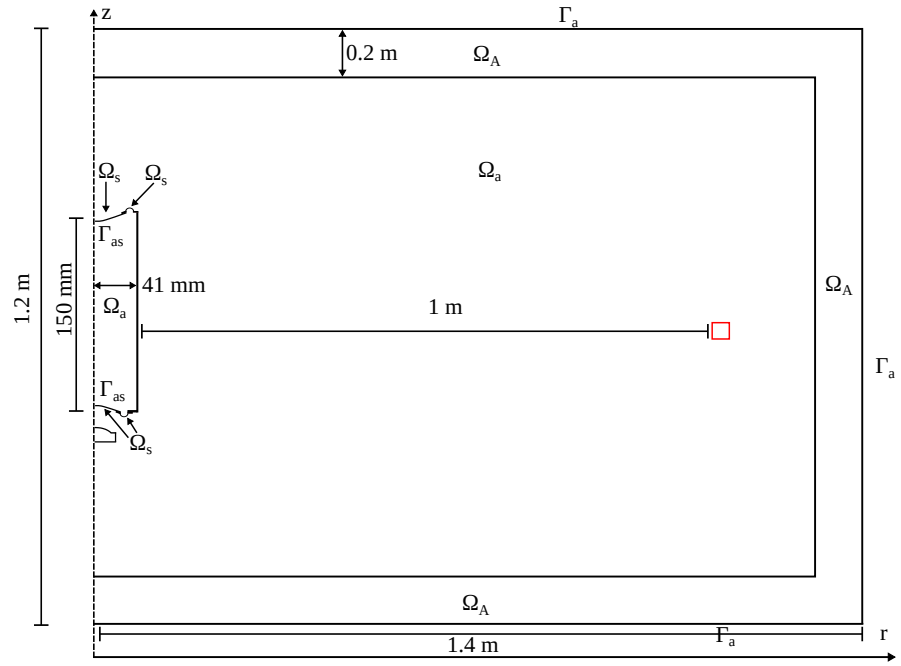

Figure 2: Sketch of the problem to be solved, with definitions of the different domains, interfaces and boundaries.

where p_A is the pressure in the PML region, the formulation of γ is from [16], here extended to accommodate for a PML in both the r- and z direction

$$\gamma_r(r) = 1 - j\kappa\left(\frac{r - r^*}{t}\right)^2 \tag{7}$$

$$\gamma_z(z) = 1 - j\kappa\left(\frac{z - z^*}{t}\right)^2 . \tag{8}$$

Where r^* and z^*, indicate the interface coordinate between the PML/acoustic domain and r and z are the position within the PML, κ is the absorption coefficient with a constant value of 10 and t is half the thickness of the PML which equals 0.1m.

Equation 1 and Equation 5 are to be solved using the FE method. The FE matrices for the elastic body in Equation 1 are

$$\mathbf{K} = \int_{\Omega_s}\int_{-\pi}^{\pi} \mathbf{B}^T\mathbf{C}\mathbf{B}r \, \mathrm{d}\Omega_s \ , \ \mathbf{M} = \int_{\Omega_s}\int_{-\pi}^{\pi} \rho\mathbf{N}^T\mathbf{N}r \, \mathrm{d}\Omega_s. \tag{9}$$

Here $\mathbf{B}$ is the strain-displacement matrix, r is the radial distance to the Gauss point from the center axis z, and $\mathbf{N}$ is a matrix consisting of the quadratic iso-parametric shape functions. Damping in the mechanical components are considered as an isotropic structural loss factor, denoted η, such that $\mathbf{K} = \mathbf{K}(1 + j\eta)$, where j is the imaginary number, η equals 0.45 in the rubber surround and 0.2 in the diaphragm.

The FE matrices required to solve the Helmholtz equation in Equation 5 and the modified Helmholtz equation in Equation 6 are

$$\mathbf{K}_a = \int_{\Omega_a}\int_{-\pi}^{\pi} \left(\mathbf{N}_{a,r}^T\mathbf{N}_{a,r} + \mathbf{N}_{a,z}^T\mathbf{N}_{a,z}\right) r \, \mathrm{d}\Omega_a + \int_{\Omega_A}\int_{-\pi}^{\pi} \left(\frac{\gamma_z}{\gamma_r}\mathbf{N}_{a,r}^T\mathbf{N}_{a,r} + \frac{\gamma_r}{\gamma_z}\mathbf{N}_{a,z}^T\mathbf{N}_{a,z}\right) r \, \mathrm{d}\Omega_A \tag{10}$$

$$\mathbf{M}_a = \int_{\Omega_a}\int_{-\pi}^{\pi} \frac{1}{c^2}\mathbf{N}_a^T\mathbf{N}_a r \, \mathrm{d}\Omega_a + \int_{\Omega_A}\int_{-\pi}^{\pi} \frac{1}{c^2}\gamma_r\gamma_z\mathbf{N}_a^T\mathbf{N}_a r \, \mathrm{d}\Omega_A, \tag{11}$$

where subscript r and z refers, respectively, to the differential operator with respect to global r- and z-coordinates, $\mathbf{N}_a$ is a row vector consisting of the quadratic acoustic shape functions.

At the interface between the mechanical structure and the acoustic domain a coupling matrix, $\mathbf{S}$, is defined such that the structure acts as an acoustic source and the back induced pressure from the air acts as a surface load on the structure

$$\mathbf{S} = \int_{\Gamma_{as}} \int_{-\pi}^{\pi} \mathbf{N}^T \mathbf{n}_a \mathbf{N}_a r \, \mathrm{d}\Gamma_{as}. \tag{12}$$

Here $\mathbf{n}_a$ is the normal vector of the interface between the acoustic and structural boundary pointing outwards from the acoustic boundary.

The entire system of equations then becomes

$$\left(\begin{bmatrix} \mathbf{K} & -\mathbf{S}^T \\ \mathbf{0} & \mathbf{K}_a \end{bmatrix} - \omega^2 \begin{bmatrix} \mathbf{M} & \mathbf{0} \\ \rho\mathbf{S} & \mathbf{M}_a \end{bmatrix} \right) \begin{Bmatrix} \mathbf{u} \\ \mathbf{p} \end{Bmatrix} = \begin{Bmatrix} \mathbf{f} \\ \mathbf{0} \end{Bmatrix}. \tag{13}$$

The above equation are the standard way of solving acoustic-structure interaction problems. However, since we are dealing with loudspeakers the excitation should come from the electric motor system, which is driven with an AC voltage source. Reference [13] suggest an approach in which the electric motor system and parts of the mechanical system is lumped. This lumped system can be added to the FE system of equations in Equation 13 by adding only one equation. As shown in [13] the system of equations can be written as

$$\left(\tilde{\mathbf{K}} + j\omega\tilde{\mathbf{C}} - \omega^2\tilde{\mathbf{M}} \right) \begin{Bmatrix} \mathbf{u} \\ \mathbf{p} \\ i_c \end{Bmatrix} = \begin{Bmatrix} \mathbf{0} \\ \mathbf{0} \\ e_g \end{Bmatrix}. \tag{14}$$

Here $\tilde{\mathbf{C}}$ is the matrix including the velocity proportional terms from the lumped model, i_c is the current in the electric motor system and e_g is applied AC voltage.

Equation 14 is for the duration of this paper written with compact notation as

$$\tilde{\mathbf{S}}\tilde{\mathbf{u}} = \tilde{\mathbf{f}}, \tag{15}$$

2.2. Optimization

We are interested in enhancing the low frequency performance of the smartspeaker in Figure 1. To do this we need to establish a measure of the output of the speaker system, an example could be the pressure squared in a listening area 1m away from the speaker. This can be described in an objective function such as

$$\phi = \tilde{\mathbf{u}}^{\mathbf{T}}\mathbf{L}\bar{\tilde{\mathbf{u}}}, \tag{16}$$

where $\mathbf{L}$ is used to select the pressure degrees of freedom (DOF) related to the 5x5cm boxed region 1m away from the speaker as shown in Figure 2 and $\bar{(\,)}$ is the complex conjugate. The objective function in Equation 16 is beneficial if we purely want to maximize the pressure squared, however, a flat response is more desirable. We therefore propose the following objective function

$$\Phi_0 = \left(Z_D - \tilde{\mathbf{u}}^{\mathbf{T}}\mathbf{L}\bar{\tilde{\mathbf{u}}} \right)^2 \tag{17}$$

here, Z_D is a target value based on the flat output above the fundamental frequency of the woofer. If the difference in Equation 17 is minimized we will obtain a flat response in the desired frequency range. The frequency range will be constructed by specifying a number of discrete frequencies, the objective function, which bears resemblance to a Chebyshev alignment, in Equation 17 is then evaluated for each frequency. This can be cast as a min-max optimization problem, here the optimizer

seeks to minimize the objective function for the discrete frequency with the largest value computed by Equation 17. The optimizer is allowed to change only the material parameters of the passive radiator. The optimization should therefore be able to control stiffness, mass and damping of the passive radiator. The above requirements leads to the following min-max optimization problem

$$\begin{array}{lll} \min\limits_{\mathbf{x}} \quad \max & \Phi_0 = \left(Z_D - \tilde{\mathbf{u}}_k^T \mathbf{L} \tilde{\tilde{\mathbf{u}}}_k\right)^2 \ , & k = 1, \ldots, p \\ \text{s.t.} & \tilde{\mathbf{S}} \tilde{\mathbf{u}}_k - \tilde{\mathbf{f}} = 0 \ , & k = 1, \ldots, p \\ & 0 \leq \mathbf{x}_j \leq 1 \ , & j = 1, \ldots, n \end{array} \tag{18}$$

where p is the number of frequencies, $\mathbf{x}_j$ is the design variables and n is the number of design variables. There are 20 logarithmic spaced frequencies between 90Hz and 170Hz. It is necessary to specify a fine frequency resolution, otherwise the optimizer could exploit the gap between the frequency bins and place unwanted resonances there. The above min-max optimization problem is in practice solved by using a bound formulation and imposing an extra constraints on the problem as shown below

$$\begin{array}{lll} \min\limits_{\mathbf{x},z} & z \ , & z \geq 0 \\ \text{s.t.} & \tilde{\mathbf{S}} \tilde{\mathbf{u}}_k - \tilde{\mathbf{f}} = 0 \ , & k = 1, \ldots, p \\ & \left(Z_D - \tilde{\mathbf{u}}_k^T \mathbf{L} \tilde{\tilde{\mathbf{u}}}_k\right)^2 - z \leq 0 \ , & k = 1, \ldots, p \\ & 0 \leq \mathbf{x}_j \leq 1 \ , & j = 1, \ldots, n \end{array} \tag{19}$$

In the above equations $\mathbf{x}_j$ includes the design variables α, β and ζ, which controls stiffness, mass and damping, respectively. A change in the design variable applies to the whole region to which it is assigned, e.g. if α is assigned to the diaphragm and it increases, the entire stiffness of the diaphragm is increased uniformly. The actual physical stiffness, mass and damping is determined from the design variable with a simple linear interpolation which enforces an upper and lower bound on the physical values

$$\begin{aligned} E &= E_{min} + \alpha \left(E_{max} - E_{min}\right) \\ \rho &= \rho_{min} + \beta \left(\rho_{max} - \rho_{min}\right) \\ \eta &= \eta_{min} + \zeta \left(\eta_{max} - \eta_{min}\right). \end{aligned} \tag{20}$$

Here E is the Young's Modulus, ρ is the density, η is the structural loss factor, the subscript "min" refers to the lower bound and "max" refers to the upper bound. The purpose of the bounds are to avoid completely unrealistic material properties.

The design sensitivities are calculated with the adjoint approach which yields a semi-analytical expression for the gradients of Equation 17

$$\mathbf{S}^T \boldsymbol{\lambda} = -\left(\frac{\partial \Phi_0}{\partial \mathbf{u}_r} - i \frac{\partial \Phi_0}{\partial \mathbf{u}_i}\right)^T = 4 \left(Z_D - \tilde{\mathbf{u}}^{\mathbf{T}} \mathbf{L} \tilde{\tilde{\mathbf{u}}}\right) \mathbf{L} \tilde{\tilde{\mathbf{u}}}, \tag{21}$$

where $\boldsymbol{\lambda}$ is the Lagrange multipliers, subscripts r and i refers to real and imaginary parts of the solution vector, respectively.

The design sensitivities can then be computed as

$$\frac{d\Phi_0}{dx} = \mathrm{Re}\left(\boldsymbol{\lambda}^T \frac{\partial \mathbf{S}}{\partial x} \tilde{\mathbf{u}}\right).$$

The design sensitivities are used in the method of moving asymptotes (MMA) algorithm [17].

Table 1: Material properties for the woofer and initially also the passive radiator

	E [Pa]	ρ [kg/m^3]	η [−]	ν [−]
Diaphragm	10^{10}	1650	0.2	0.3
Surround	$40 \cdot 10^5$	1400	0.25	0.45

Table 2: Lumped parameters used to model the electric motor system, voice coil and spider.

M [kg]	L_E [mH]	n [−]	C_z [m/N]	C_r [m/N]	R [N · s/m]	Bl [T · m]	R_E [Ω]
0.0015	0.05	0.7	$1.0{\cdot}10^{-3}$	$5{\cdot}10^{-5}$	0.75	3.43	3.52

3. RESULTS

This section includes the optimization results for the tuning of the passive radiator. We are considering two cases, one case will only consider tuning the mass of the diaphragm and the damping of the surround, this example will be referred to as "mass tuned". This mimics the traditional lumped approach where one can tune the resonance of the passive radiator, as long as the suspensions is sufficiently compliant, by tuning the mass of the diaphragm. The other approach will allow stiffness, mass and damping to vary independently in the diaphragm and the surround of the passive radiator. This approach has 6 design variables and will be referred to as the 6 variable design.

Table 1 shows the material properties that are used as a starting guess for the optimization, the active loudspeaker also has these material properties. The values are typical values for a paper cone and a rubber surround.

Table 2 shows the values that are used in the LPM to model the 3 inch woofer used in this work. In the table M is the moving mass of the lumped mechanical components, L_E is the voice coil inductance, n is the fractional order derivative used to model the lossy inductor, C_z is the compliance in the z-direction, C_r is the compliance in the r-direction, R is mechanical damping, Bl is the force factor and R_E is the DC resistance in the voice coil wire. The speaker is excited by applying an AC voltage source, e_g, to the lumped circuit. In this work we apply a voltage of 1V.

The material properties of the diaphragm and surround of the passive radiator is determined by an interpolation function which is based on the continuous update of the associated design variable, as shown in Equation 20. These interpolation functions are constrained by a lower and upper bound. The values of these bounds are shown in Table 3.

Figure 3 shows the iteration history of the mass tuned example. The objective function in Figure 3a are normalized with the value of the objective function for the initial guess and it reaches a value of 0.15 after 83 iterations. Figure 3b shows the progression of the two design variables, the starting guess for the optimization is using design variable values such that the material properties corresponds to the values in Table 1. The design variables are only allowed to change 0.01 at each iteration step. Generally we see that that the optimizer increases the mass and lowers the damping. The resulting density and damping can be seen in Table 4a and the frequency response of the optimized smartspeaker are shown in Figure 5

Figure 4 displays the iteration history of the optimization with 6 design variables. In Figure 4a

Table 3: Bounds on the physical values

	E_{min} [Pa]	E_{max} [Pa]	ρ_{min} [kg/m^3]	ρ_{max} [kg/m^3]	η_{min} [−]	η_{max} [−]
Diaphragm	10^8	$40 \cdot 10^9$	1000	4500	0.05	0.9
Surround	$40 \cdot 10^3$	$16 \cdot 10^6$	1000	4500	0.05	0.9

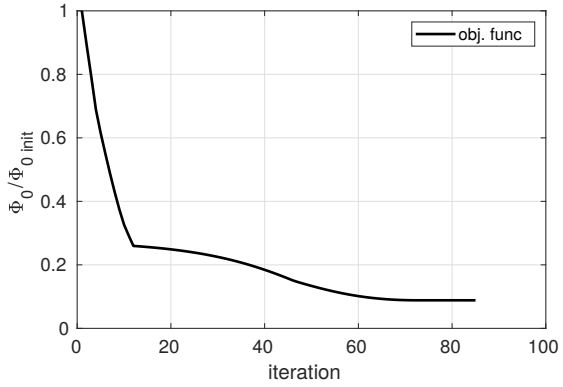

(a) Objective function

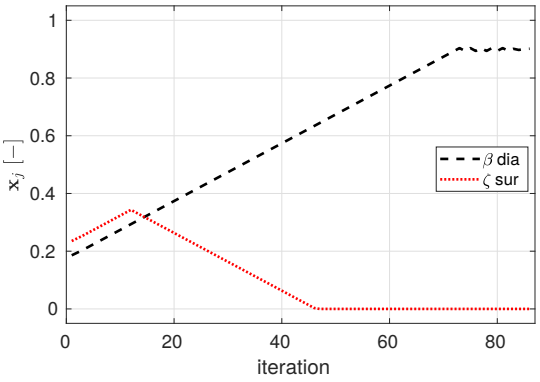

(b) Design variables

Figure 3: Mass case: (a) shows the iteration history of the normalized objective function, (b) shows the design history, here, the black curve relate to the design variable in the diaphragm and the red curve is associated with the surround

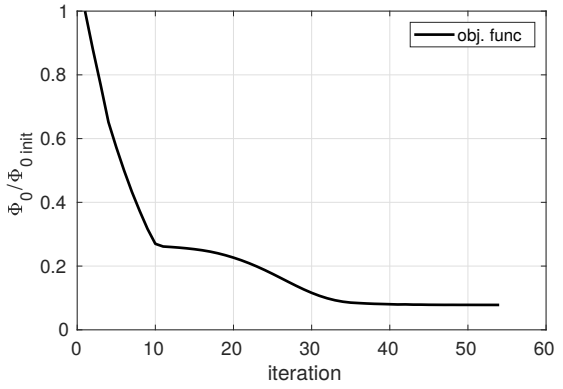

(a) Objective function

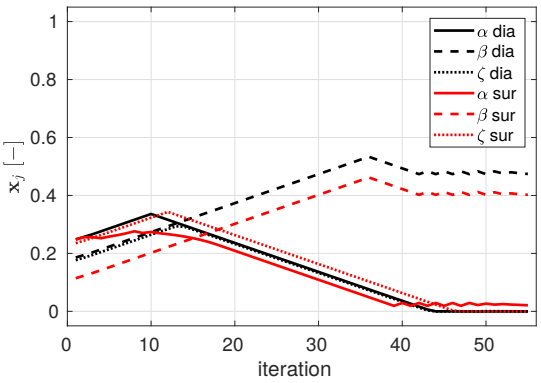

(b) Design Variables

Figure 4: 6 variable case: (a) shows the iteration history of the normalized objective function, (b) shows the design history, here, the black curves relates to the design variables in the diaphragm and the red curves are associated with the surround

one can observe that the pattern of the objective function is similar to that of Figure 3a, however, it uses fewer iterations to converge, here we reach a value of 0.13 after 61 iterations. This configuration of material parameters are therefore slightly better than the previous example. Figure 4b shows the design history. The configuration of stiffness, mass and damping is displaying differences when compared to the configuration in Figure 3b. In Figure 4b we see an increase in mass, as we expect, but the final configuration consists of a lower mass than the mass tuned example. This is due to the fact that the optimizer lowers the stiffness of the surround as the mass increases, it is therefore not necessary to increase the mass of the diaphragm as much as seen in Figure 3b. The material properties for optimized passive radiator are shown in Table 4b, the optimizer finds a material configuration that suggests that the cone of the passive radiator in this example could be made out of aluminum.

The dashed blue line in Figure 5 is the frequency response for the mass tuned passive radiator in Table 4a. This result shows that the optimizer tunes the resonance of the passive radiator such that it is lower and thereby the frequency range of the speaker system is extended. The result is a significant improvement of the output in the targeted range compared with the initial guess. Outside of the frequency range of interest we can see that towards higher frequencies the frequency response is similar to the initial guess, however, towards lower frequencies we see a very steep roll-off and a

Table 4: Material properties obtained with optimization, (a) is the results in Figure 3 and (b) is the results from Figure 4

	ρ [kg/m^3]	η [−]
Diaphragm	4155	-
Surround	-	0.05

(a) Mass and damping

	E [Pa]	ρ [kg/m^3]	η [−]
Diaphragm	10^8	2660	0.05
Surround	$37.2 \cdot 10^4$	2408	0.05

(b) All 6 variables

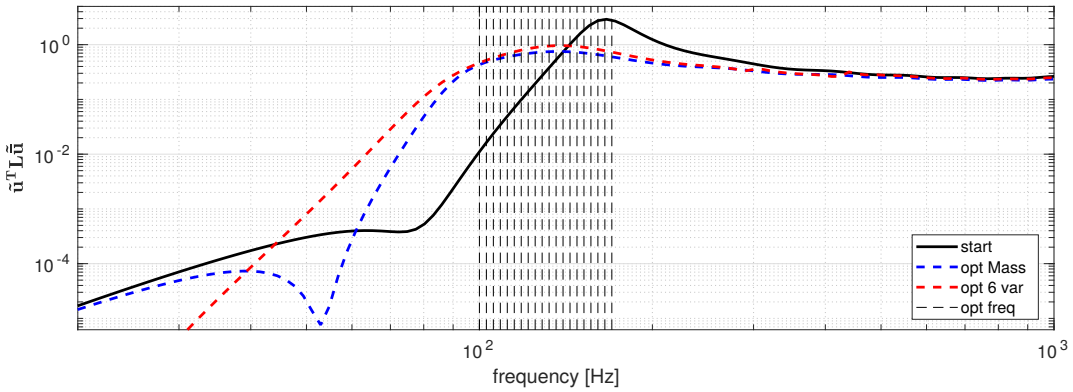

Figure 5: Frequency response function for the initial guess (solid black line), mass tuned passive radiator (dashed blue line) and the 6 variable optimization (dashed red line). The dashed vertical lines indicates the 20 logarithmic spaced discrete frequencies between 90-170Hz.

dip which can be attributed to destructive interference.

The dashed red line in Figure 5 displays the frequency response for the passive radiator for which the optimizer was allowed to tune stiffness, mass and damping in both the diaphragm and the surround. We showed earlier that the optimizer found an optimal solution where the mass was increased and stiffness and damping was decreased. This yields an almost flat line in the entire frequency range of interest, the resonance is not very prominent and the roll-of is not as steep as compared to the dashed blue line. This approach slightly improves the performance of the passive radiator compared to the mass tuned example and yields a 1 dB increase in output in nearly the entire frequency range of interest. We also see a much softer roll-of which means that the output below the frequency range of interest is enhanced compared to both the initial guess but also the dashed blue line. This comes to show that although the tuning of the mass of the diaphragm is important it does not necessarily guarantee the best result, the stiffness of the surround can have a major impact on the low frequency performance of the passive radiator. We show that if the relationship between the stiffness of the surround and the stiffness of the air inside the cabinet is tuned correctly there is more output from the passive radiator to be gained. The trade-off is that the output below 44 Hz is below both the initial guess and the mass tuned passive radiator, however, the reduction at the lowest frequencies is most likely not perceivable when listening.

Figure 6 shows the volume velocity at the surface of the passive radiator for the initial speaker system, the mass tuned system and the system with 6 design variables. From the figure the resonance frequency of the passive radiator can be estimated, the mass tuned example has a resonance frequency of 92 Hz and for the 6 variable case the resonance is 89 Hz. Notice that both the shape and size of the two curves related to the optimized examples are closely related in the frequency range specified in the optimization problem. This explains the similarity in the frequency response seen in Figure 5. The 6 variable optimization has more parameters to tune and the optimizer finds it beneficial to increase the mass and lower the stiffness in a proportional way such that the resonance frequency is

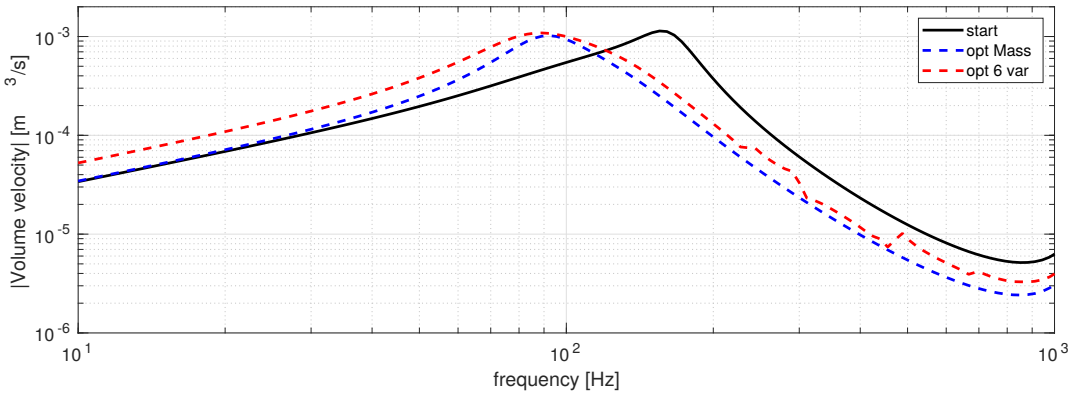

Figure 6: Volume velocity in the z-direction at the surface of the passive radiator for the initial guess (solid black line), mass tuned passive radiator (dashed blue line) and the 6 variable optimization (dashed red line)

situated close to that of the mass tuned example. This leads to an increase in the volume velocity below the resonance peak, as this is attributed to the decrease in the stiffness of the surround. The slight decrease in volume velocity above the fundamental frequency can be attributed to the increase in the mass of the diaphragm and surround. It seems that the 6 variable case is able to tune the passive resonance to be broader, i.e. similar damping but lower Q factor, which giver the system output a bit more at low frequencies.

The the dashed blue line follows the black curve below the resonance which is to be expected since the stiffness here is unchanged. Furthermore we see that the volume velocity above the resonance is the lowest compared to the two other curves due to the fact that the mass tuned example has the highest density of the diaphragm.

There are a few spikes in the volume velocity after the fundamental frequency for the 6 variable optimization case. This is due to the overall decrease in stiffness and damping for the surround and diaphragm, these spikes arise from breakup modes in the surround and diaphragm, the output from these spikes in volume velocity are however barely noticeable in the pressure response in Figure 5.

4. DISCUSSION

In this work we use min-max optimization to formulate an optimization problem to be solved. The formulation always improves the worst performing discrete frequency. This implies that the optimizer is using a lot of effort on the lowest specified frequency since that frequency will, at least at the start of the optimization, be the one with the largest individual value of the objective function. This means that the positive or negative outcome of the optimization is very much dependent on whether the optimizer is successful in raising the output at the lowest frequency. If the optimizer is unsuccessful in improving the lowest frequency the optimization will get stuck and the outcome is not a feasible solution. However, the min-max optimization formulation performs well when the lowest frequency can be improved as shown in this research, here we are able to create an almost flat response. An alternative formulation could be used in which the optimization problem would be an objective function summed over the frequency range of interest. In this case the optimizer will improve the frequencies where it is the most feasible. Such an optimization formulation will also make it possible to specify the frequency range lower than what has been done in this research, since we here at the start of the optimization are relying heavily on the optimizers ability to improve the lowest frequency.

The mass is by far the most influential parameter, since the stiffness of the surround of the passive radiator is sufficiently compliant. The two cases are therefor very close to being identical with regards

to performance in the frequency range of interest. It is seems to be advantageous for the optimizer to lower the stiffness further to decrease the resonance frequency without increasing the mass, this yields a softer roll-of and thereby a higher output at low frequencies. As the surround is becoming softer the stiffness of the air inside the cylinder starts to be important with regards to the resonance frequency of the passive radiator, lowering the stiffness of the surround is, as a consequence, becoming progressively less influential. However, we do show that by tuning the ratio of the stiffness of the surround to the stiffness of the air inside the cabinet of the speaker that we can enhance the low frequency performance of the passive radiator even further when compared to the mass tuned example.

5. CONCLUSION

The work presented utilizes gradient based multi-frequency optimization applied to a numerical model of a cylindrical loudspeaker. The optimization is used to tune the material properties of each individual component for a passive radiator such that the output at low frequencies are improved. We demonstrate the method for two examples. The mass tuned passive radiator where the density of the diaphragm is increased such that a feasible resonance peak is created and as a consequence the frequency range of the speaker unit is extended. The drawback of this method is that destructive interference is created immediately below the frequency range of interest. The second example shows that the optimal configuration of materials in a passive radiator is actually a lighter and less stiff diaphragm and surround when compared to the mass tuned example. This yields a flat response in the entire frequency range of interest which is almost an entire octave. Both examples increase the low frequency performance significantly.

The paper demonstrates the method and the benefits that can be gained from it at low frequencies, but the framework also allows for optimization at higher frequencies, which will be investigated in future work.

6. REFERENCES

[1] Edison Research and NPR, "The Smart Audio Report," tech. rep., 02 2020.

[2] H. F. Olson, "Loud speaker and method of propagating sound." U.S. Patent no. 1988250, application Feb. 1934, patented Jan. 1935.

[3] H. Olson, J. Preston, and E. May, "Recent developments in direct-radiator high-fidelity loudspeakers," *Audio Engineering Society – Journal*, vol. 2, no. 4, pp. 219–227, 1954.

[4] R. H. Small, "Passive-radiator loudspeaker systems .1. analysis," *Journal of the Audio Engineering Society*, vol. 22, no. 8, pp. 592–601, 1974.

[5] R. H. Small, "Direct-radiator loudspeaker system analysis," *IEEE Transactions on Audio and Electroacoustics*, vol. AU-19, no. 4, pp. 269–81, 269–281, 1971.

[6] G. H. Yoon, J. S. Jensen, and O. Sigmund, "Topology optimization of acoustic-structure interaction problems using a mixed finite element formulation," *International Journal for Numerical Methods in Engineering*, vol. 70, no. 9, pp. 1049–1075, 2007.

[7] J. S. Jensen, "A simple method for coupled acoustic-mechanical analysis with application to gradient-based topology optimization," *Structural and Multidisciplinary Optimization*, vol. 59, no. 5, pp. 1567–1580, 2019.

[8] E. Wadbro and M. Berggren, "Topology optimization of an acoustic horn," *Computer Methods in Applied Mechanics and Engineering*, 2006.

[9] C. S. Andreasen, M. O. Elingaard, and N. Aage, "Level set topology and shape optimization by density methods using cut elements with length scale control," *Structural and Multidisciplinary Optimization*, 2020.

[10] C. B. Dilgen, S. B. Dilgen, N. Aage, and J. S. Jensen, "Topology optimization of acoustic mechanical interaction problems: a comparative review," *Structural and Multidisciplinary Optimization*, vol. 60, no. 2, pp. 779–801, 2019.

[11] A. Bezzola, "Numerical optimization strategies for acoustic elements in loudspeaker design," *145th Audio Engineering Society International Convention, Aes 2018*, 2018.

[12] D. G. Nielsen, F. T. Agerkvist, and J. S. Jensen, "Optimization of realistic loudspeaker models with respect to basic response characteristics," *Proceedings of 23rd International Congress on Acoustics*, pp. 6219–6226, 2019.

[13] D. G. Nielsen, P. R. Andersen, J. S. Jensen, and F. T. Agerkvist, "Estimation of optimal values for lumped elements in a finite element -lumped parameter model of a loudspeaker," *Journal of Theoretical and Computational Acoustics*, to appear in 2020.

[14] J. N. Li, S. X. Wang, H. J. Yin, C. H. Dong, and H. M. Chen, "Acoustic wave equation modeling in cylindrical coordinates with convolutional pml," *77th Eage Conference and Exhibition 2015: Earth Science for Energy and Environment*, pp. 4546–4548, 2015.

[15] F. Collino and P. Monk, "The perfectly matched layer in curvilinear coordinates," *Siam Journal of Scientific Computing*, vol. 19, no. 6, pp. 2061–2090, 1998.

[16] J. S. Jensen, "Topology optimization problems for reflection and dissipation of elastic waves," *Journal of Sound and Vibration*, vol. 301, no. 1-2, pp. 319–340, 2007.

[17] K. Svanberg, "The method of moving asymptotes - a new method for structural optimization," *International Journal for Numerical Methods in Engineering*, 1987.

Paper 4

Achieving a flat wide-band frequency response by numerical optimization of a loudspeaker unit with requirements for its directivity

Daniel G. Nielsen,[1, a] Finn T. Agerkvist,[1] and Jakob S. Jensen[2]
[1] *The department of Electrical Engineering, Technical University of Denmark, Ørsteds Plads Building 352, DK-2800 Kgs. Lyngby, Denmark*
[2] *The department of Mechanical Engineering, Technical University of Denmark, Nils Koppels Allé Building 404, DK-2800 Kgs. Lyngby, Denmark*

This paper demonstrates how significant improvement in frequency response and directivity of a loudspeaker may be obtained by optimizing the local properties of the materials for the diaphragm and surround. The limits are investigated as the considered frequency range and off-axis requirements are progressively widened. The results are generated by optimizing the values and layout of stiffness, mass and damping of both the speaker diaphragm and surround. This is accomplished by using a density and gradient-based optimization technique in conjunction with a fully coupled finite element model of the loudspeaker and the surrounding acoustic domain. The targeted frequency range is from 600 Hz up to 10 kHz and the range for the directivity is from 0 to 30 degrees. The results show that a completely flat on-axis response is achievable even for very broad frequency ranges, and that a reasonably flat response over a wide directivity can be obtained as well.

 [https://doi.org(DOI number)]

[XYZ] Pages: 1–10

I. INTRODUCTION

Enhancing the sound quality of loudspeakers is an ever-present research topic. The perceived sound quality is often regarded as being subjective and the quantitative evaluation of the quality of a given transducer can be difficult. However, there are studies that show that humans have certain quantitative preferences, Olive and Welti[1] shows that headphone listeners identified a flat frequency response as the most important criterion when assessing the sound quality of a pair of headphones. Toole[2] highlights that transducers with a flat-on-axis frequency response seem to perform better, however, he stresses that listening to the speaker in a room is important. Evans et al.[3] performs a literature review regarding the directivity pattern of loudspeakers and the influence on the sound quality. The general consensus is that uniformity over frequency is important and that depending on the use case the directivity pattern of the speaker can influence the listening experience. Queen[4] states that the clarity and imaging of home stereos is highly dependent on the directivity, he concludes "A worthy design objective would be to maximize uniformity while minimizing radiation to floor and ceiling where efficiency-reducing absorption may occur" and he continues later with "... a directional loudspeaker providing high uniformity of directional pattern with frequency could also achieve these objectives.". Linkwitz[5] identifies that speakers used in a surround sound setup beside having low distortion, should have a wide dispersion such that the power response can be as even as possible. Bucklein[6] shows that listeners are able to perceive and identify peaks in the frequency response better than dips or valleys.

Loudspeakers are complex to model and are therefore often simplified into lumped parameter models (LPM)s[7,8]. These simplifications come with the disadvantage that the 1-D models become less accurate for mid to high frequencies and do not (in detail) include which materials constitute the loudspeaker, e.g. the diaphragm is assumed rigid. LPMs are used to optimize the material properties of transducers, e.g. by maximizing the on-axis pressure sensitivity by applying sequential quadratic programming to a lumped model of a microspeaker[9]. Nielsen et al.[10] develops a hybrid FE-LPM model specifically aimed at lumping the electrical motor system and parts of the mechanical system, which reduces the complexity of the numerical model while maintaining accuracy. This approach is applied in this paper.

Optimization methods such as a density based approach can be used together with a FE model. With a density-based optimization approach each element can be assigned a number of design variables that e.g. can control stiffness, mass and damping. Density based topology optimization is a method which has been applied in many fields of engineering. One of its applications in acoustics is to generate new designs or improving existing ones[11–13]. Within the recent years topology- and shape optimization is starting to be used on complex multiphysics problems such as loudspeakers[14,15] or for complex acoustic problems such as small resonators with

[a] dgniel@elektro.dtu.dk

losses for improved sound absorption[16]. Density based material optimization on fixed geometries can help determine the optimal material properties. Alfouneh et al.[17] uses optimization to design graded materials to reduce the sound pressure level in a point. A numerical multi-material optimization technique is utilized in reference[18] to maintain the mechanical properties while reducing the weight of the structure. Reference[19] optimizes the material of a passive radiator in a compact speaker to enhance the low frequency performance.

With the recent surge in applying optimization to loudspeakers[14,15] and also loudspeaker enclosures[20], this paper deals with an often overlooked topic, namely the optimization of the very materials that constitute the loudspeaker. The geometry of the loudspeaker used in this paper is a generic 5 inch loudspeaker unit inspired from a common loudspeaker unit shape. This paper utilizes a density based optimization approach that relies on gradient based optimization to optimize the materials in a loudspeaker unit. The results presented in this research assume that complete design and production freedom is available. This entails that the presented designs might not be able to be readily produced with conventional techniques, even though the design consist of commercially available materials. We can gain knowledge and inspiration from the presented designs with regards to what is theoretically achievable and with the continuous rapid development within the fields of e.g. additive manufacturing of elastomeres[21,22] and functionally graded materials[23], these designs could be produced in the not-so-distant future.

We conduct a study based on the literature review above trying to achieve a loudspeaker with a flat frequency response within a desired frequency and angle range. This study is conducted for varying range of angles in order to see how the requirement with regards to uniformity over frequency and space affects the uniformity of the response as the frequency and angle range increases. In the subsequent sections we establish the FE theory, pose the optimization problems and finally we present and discuss the optimized designs.

II. THEORY

This section serves to establish the theory required to compute the radiation of sound from a midrange loudspeaker. The loudspeaker is modelled as 2-D axisymmetric, this assumption generally captures the dominating vibration modes in the speaker except for rocking modes and asymmetric modes in the loudspeaker cone these modes are only effective at relatively high frequencies. The assumption implies that the model complexity is greatly reduced and thereby allows for optimization in broad frequency intervals with a feasible computational time. The loudspeaker unit is radiating into free space, and a truncated computational domain is setup using perfectly matched layers (PML)s. Figure 1 shows the computational domains together with the boundaries and the position of the excitation of the loudspeaker. Figure 2 shows the dimensions of the computational domains together with the placement of the measuring points used to capture and investigate the directivity of the loudspeaker unit.

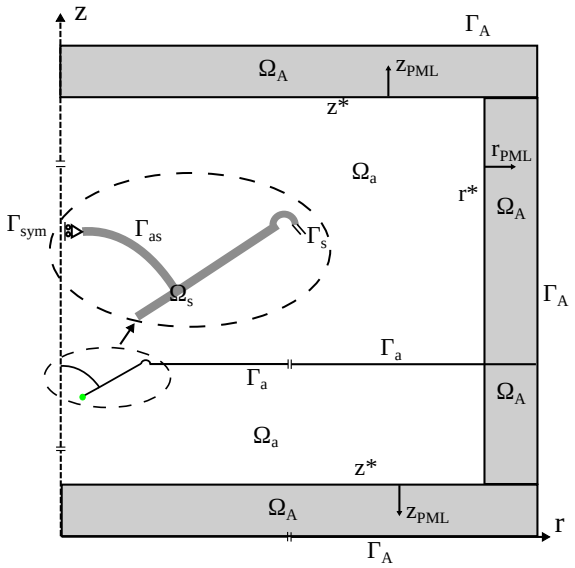

FIG. 1. 2D sketch of the midrange loudspeaker with boundary conditions. The green circle indicates where the LPM is coupled to the FE model.

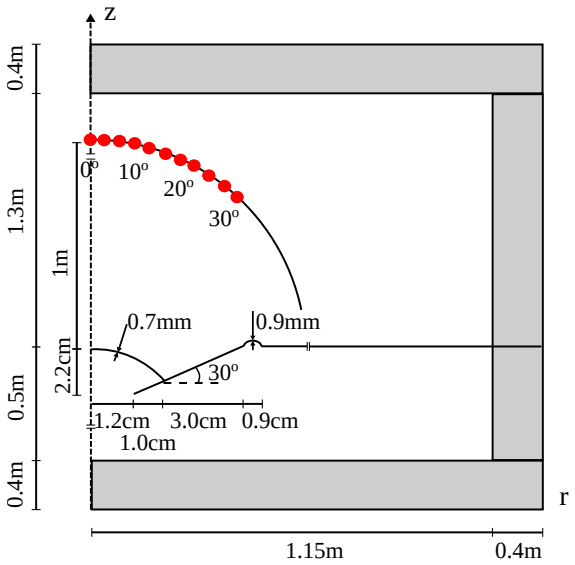

FIG. 2. 2D sketch of the midrange loudspeaker with the dimensions of the computational domains. The red dots indicate where the objective function is measured.

A. Governing equations

The governing equations for the time-harmonic motion of a linear elastic body where body forces have been neglected are

$$\nabla \cdot \boldsymbol{\sigma}(\mathbf{u}) + \rho\omega^2\mathbf{u} = \mathbf{0} \quad \text{in} \quad \Omega_s \tag{1}$$

$$\boldsymbol{\sigma} = \mathbf{C}\boldsymbol{\epsilon} \tag{2}$$

$$\boldsymbol{\epsilon} = \{\epsilon_r \ \epsilon_\theta \ \epsilon_z \ 2\gamma_{zr}\}^T \qquad \text{(2D Axisymmetric)} \tag{3}$$

$$\epsilon_r = \frac{\partial u_r}{\partial r},\ \epsilon_\theta = \frac{u_r}{r},\ \epsilon_z = \frac{\partial u_z}{\partial z},\ \gamma_{zr} = \frac{1}{2}\left(\frac{\partial u_r}{\partial z} + \frac{\partial u_z}{\partial r}\right) \tag{4}$$

$$\mathbf{n}\boldsymbol{\sigma} = p \quad \text{on} \quad \Gamma_{as} \tag{5}$$

$$u = 0 \quad \text{on} \quad \Gamma_s \quad , \quad u_r = 0 \quad \text{on} \quad \Gamma_{sym}, \tag{6}$$

here ρ is the mass density of the material, ω is the excitation frequency in radians, $\mathbf{u}$ is the structural displacements, $\boldsymbol{\sigma}$ is the stress tensor, Ω_s is the structural domain, $\mathbf{C}$ is the constitutive matrix for an axisymmetric structure, $\boldsymbol{\epsilon}$ is the strain tensor, u_r is the structural displacement in the r-direction, u_z is the displacement in the z-direction, on Γ_s the structure is clamped and on Γ_{sym} the symmetry condition means that the structure cannot move in the r-direction.

To obtain the pressure distribution in the acoustic domain, the Helmholtz equation is solved together with a modified Helmholtz equation[24] in the PML region (Ω_A), as shown in Fig. 1

$$\Delta p + \frac{\omega^2}{c^2}p = 0 \quad \text{in} \quad \Omega_a \tag{7}$$

$$\frac{1}{\gamma_r}\frac{\partial}{\partial r}\left(\frac{1}{\gamma_r}\frac{\partial p}{\partial r}\right) + \frac{1}{\gamma_z}\frac{\partial}{\partial z}\left(\frac{1}{\gamma_z}\frac{\partial p}{\partial z}\right) + \frac{\omega^2}{c^2}p = 0 \text{ in } \Omega_A, \tag{8}$$

$$\mathbf{n}\cdot\nabla p = -\omega^2\rho_a\mathbf{n}^T\mathbf{u} \quad \text{on} \quad \Gamma_{as} \tag{9}$$

$$\mathbf{n}\cdot\nabla p = 0 \quad \text{on} \quad \Gamma_a \quad p = 0 \quad \text{on} \quad \Gamma_A \tag{10}$$

here Δ is the Laplace operator in cylindrical coordinates, p is the pressure and c is the speed of sound in air, we apply a hard surface boundary condition on the baffle denoted by Γ_a, a Dirichlect boundary condition is used on the outer boundary, Γ_A, the details of the PML implementation can be seen in[10]

B. Finite element model

Equations (1) and (7) are to be solved using the FE method. The FE matrices are discretized in the usual way[10] yielding the mechanical stiffness matrix $\mathbf{K}$, the mechanical mass matrix $\mathbf{M}$, the acoustic stiffness matrix $\mathbf{K}_a$, acoustic mass matrix $\mathbf{M}_a$ and the coupling matrix $\mathbf{S}$ describing the two-way coupling in the interface between the mechanical and acoustic computational domains.

Combining the matrices yields the entire system of equations

$$\left(\begin{bmatrix}\mathbf{K} & -\mathbf{S}^T\\ \mathbf{0} & \mathbf{K}_a\end{bmatrix} - \omega^2\begin{bmatrix}\mathbf{M} & \mathbf{0}\\ \rho\mathbf{S} & \mathbf{M}_a\end{bmatrix}\right)\begin{Bmatrix}\mathbf{u}\\ \mathbf{p}\end{Bmatrix} = \begin{Bmatrix}\mathbf{f}\\ \mathbf{0}\end{Bmatrix}. \tag{11}$$

Equation (11) constitutes the standard way of solving acoustic-structure interaction problems. However, since we are dealing with loudspeakers the excitation should come from the electric motor system, which is driven with an AC voltage source. Reference[10] suggests an approach in which the electric motor system and parts of the mechanical system is lumped to reduce the complexity of the system to be solved. This lumped system can be added to the FE system of equations in (11) by adding only one equation. The full details can be seen in Ref.[10], here we write the system of equations in a compact format as

$$\left(\tilde{\mathbf{K}} + j\omega\tilde{\mathbf{C}} - \omega^2\tilde{\mathbf{M}}\right)\begin{Bmatrix}\mathbf{u}\\ \mathbf{p}\\ i_c\end{Bmatrix} = \begin{Bmatrix}\mathbf{0}\\ \mathbf{0}\\ e_g\end{Bmatrix}. \tag{12}$$

Here $\tilde{\mathbf{C}}$ is the matrix including the velocity proportional terms from the lumped model, $\tilde{\mathbf{K}}$ and $\tilde{\mathbf{M}}$ are augmented coupled stiffness- and mass matrices, i_c is the current in the electric motor system and e_g is applied AC voltage.

Equation (12) is for the duration of this paper written with compact notation as

$$\tilde{\mathbf{S}}\tilde{\mathbf{u}} = \tilde{\mathbf{f}}, \tag{13}$$

C. Material interpolation strategy

The surround is usually made from elastomers and soft plastics. In Fig. 3 the red areas indicate a thermoplastic elastomer and light blue is a thermoset elastomer, soft plastics are marked dark blue.

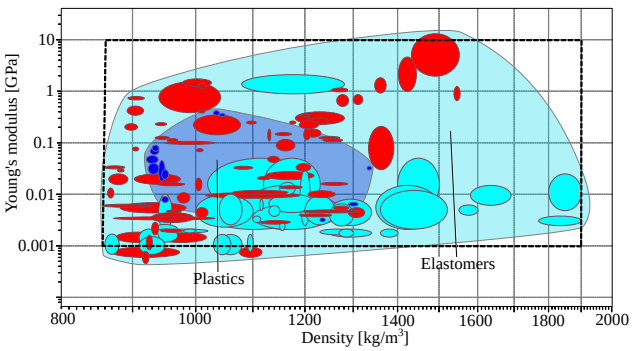

FIG. 3. The range of materials that can be used to manufacture the surround, created with GRANTA EduPack[25]

The loudspeaker diaphragm is usually manufactured from paper, plastics, composites which are mainly either a plastic reinforced with Kevlar, glass or armid fibers, a ceramic matrix with metal in it or metals such as aluminum, magnesium and titanium. The plausible materials for the loudspeaker diaphragm is shown in Fig 4.

In Fig. 3 it is observed that the elastomeres are capable of spanning the same range of Young's modulus with increasing density. As a consequence we will assume that

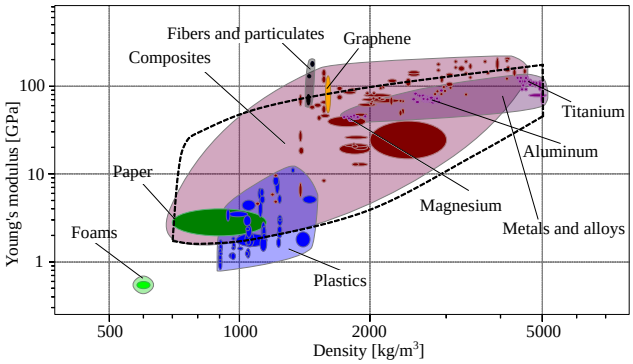

FIG. 4. The available materials that can be used to manufacture a loudspeaker diaphragm, created with GRANTA EduPack[25].

stiffness, mass and also damping can vary independently, corresponding to the full square region in Fig. 3. This is described using the following interpolation functions for the element values of the material properties of the surround

$$\begin{aligned} \rho_e^s &= \rho_{min} + \beta_e \left(\rho_{max} - \rho_{min}\right) \\ E_e^s &= E_{min} + \alpha_e \left(E_{max} - E_{min}\right) \\ \eta_e^s &= \eta_{min} + \zeta_e \left(\eta_{max} - \eta_{min}\right). \end{aligned} \tag{14}$$

Here subscript min and max refers, respectively, to the lower and upper bound of the material property, α_e, β_e and ζ_e are three independent element design variables which are continuous in the interval between 0 and 1 and superscript s indicates that the material properties here are defined for the surround.

From Fig. 4 we construct eq. (15), here the density and stiffness is co-dependent. The interpolation functions approximates the span of the available materials and is indicated by the dashed region in Fig. 4

$$\begin{aligned} \rho_e^d &= \rho_{min} + \beta_e \left(\rho_{max} - \rho_{min}\right) \\ E_e^d &= E_{min} + 1.8 \cdot (0.5\beta_e)^{2.6-2.1\alpha_e} \left(E_{max} - E_{min}\right) \\ \eta_e^d &= \eta_{min} + \zeta_e \left(\eta_{max} - \eta_{min}\right). \end{aligned} \tag{15}$$

Here superscript d express that the material properties here are defined for the diaphragm.

D. Optimization procedure

We have argued that a flat frequency response, preferably with a wide directivity, is one of the key aspects of a good quality loudspeaker. The objective function is chosen such that it is best suited to evaluate this criterion, here we have chosen to minimize the error squared between a desired target and the actual value of the sound pressure level at each angle number n. The desired target is chosen based on the frequency response of the original design in Fig. 5, here a sound pressure level of 74 dB in the frequency range of interest would

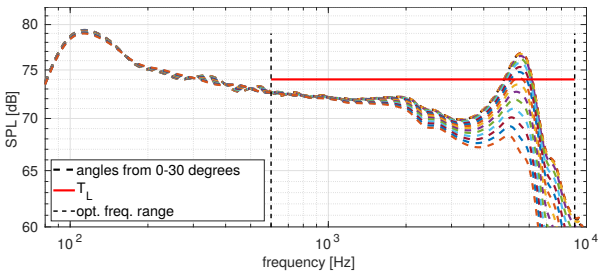

FIG. 5. Initial guess in the frequency range of interest, showing the frequency response for all the angle considered in this paper, together with the target line T_L and the borders of the 50 logarithmic spaced evaluation frequencies.

ensure that the response from 600 Hz an upwards is well aligned with the low frequency response of the unit. The objective function is

$$\phi_0 = \sum_{i=1}^{n} \left(T_L - \mathbf{spl}\boldsymbol{\tau}_n \right)^2. \tag{16}$$

T_L is the desired target, n is the current angle in the objective function, $\mathbf{spl}$ is a row vector containing the sound pressure level for all DOFs with the length l, where l is the amount of DOF in the acoustic domain and $\boldsymbol{\tau}$ is a column vector with equal length in which the DOF corresponding to the measuring point, n, are 1 and all other entries are zero. The sound pressure level is desired to be flat in a wide frequency range, the optimization problem is, as a consequence, posed as a min-max problem in which (16) is evaluated for each frequency in the desired range

$$\begin{aligned} \min_{\mathbf{x}} \quad \max \quad & \phi_{0_k} = \textstyle\sum_{i=1}^{n} \left(T_L - \mathbf{spl}_k\boldsymbol{\tau}_n \right)^2 , && k = 1, \ldots, p \\ \text{s.t.} \quad & \tilde{\mathbf{S}}_k \tilde{\mathbf{u}}_k - \tilde{\mathbf{f}} = 0 , && k = 1, \ldots, p \\ & 0 \leq \mathbf{x}_j \leq 1 , && j = 1, \ldots, m \end{aligned} \tag{17}$$

where p is the number of frequencies, $\mathbf{x}_j$ is the design variables and m is the number of design variables. There are 50 logarithmic evenly spaced frequencies, corresponding to approximately one evaluation frequency per 1/12th octave. These are used to accurately capture the frequency response in the frequency range of interest. A fine resolution of evaluation frequencies is required, since it prevents the optimizer from falsely obtaining a good result by placing peaks in the frequency response between evaluation frequencies. The optimization problem is visualized for the initial design in the frequency range of interest in Fig. 5, where the dashed lines each represent a measured frequency response at an angle. Trailing lines are for increased angle of measurement.

The optimization problem to be solved consists of a large amount of design variables, the adjoint approach is thus applied, which involves the solution of an adjoint

equation

$$\mathbf{S}_k^T \boldsymbol{\lambda}_k = -\left(\frac{\partial \phi_{0_k}}{\partial \tilde{\mathbf{u}}_{r_k}} - j \frac{\partial \phi_{0_k}}{\partial \tilde{\mathbf{u}}_{i_k}} \right)^T. \tag{18}$$

More details regarding the derivation of the analytical gradients can be found in A 1.

With the adjoint solution the design sensitivities can be computed as

$$\frac{\partial \Phi_0}{\partial x_e} = \mathrm{Re}\left(\boldsymbol{\lambda}^T \frac{\partial \tilde{\mathbf{S}}}{\partial x_e} \tilde{\mathbf{u}} \right),$$

where $\frac{\partial \tilde{\mathbf{S}}}{\partial x_e}$ is computed based on the specified interpolation functions.

The design sensitivities are used to solve the optimization problem in Eq. (17) the method of moving asymptotes (MMA)[26].

To avoid high contrast between neighbouring elements a sensitivity filter is employed to smooth the sensitivities and thereby allow for a more even design field. This will affect the performance negatively due to the fact that the sensitivity filter limits the design freedom of the optimizer. However, applying the sensitivity filter will ensure designs which are mesh independent. The sensitivity filter is adapted from Ref.[27] and it accommodates for the unstructured mesh. The filter radius is 1 mm.

III. RESULTS

In this section a study is carried out where we vary both the frequency range and the range of angles for which we measure the sound pressure level, as shown in Fig. 2. The frequency range is from 600 Hz up to a variable upper bound, here the upper bounds are 5, 6, 7, 8, 9 and 10 kHz. The angle from the center axis vary from on-axis response (0 degrees) up to 30 degrees. If the angle is larger than 0 e.g. 12 degrees, the measuring points are spaced 2 degrees apart such that the angles 0, 2, 4, .., 12 are considered in the optimization problem in Eq. (17). The measuring points are all placed 1m away from the speaker.

The optimization starts from a generic 5 inch midrange speaker, Tab. I shows the material properties that are used as a starting guess for the optimization. Notice that the damping in both the diaphragm and surround has a high value in the original design. This implies that the optimizer can simply not use the trivial solution to add damping thus smoothing the response, since this is already included in the initial configuration.

Table II shows the values that are used to model the lumped components of the speaker. Here, M is the moving mass of the lumped mechanical components, L_E is the voice coil inductance, n is the fractional order derivative used to model the lossy inductor, C_z is the compliance in the z-direction, C_r is the compliance in the r-direction, R_M is the mechanical damping, Bl is the force factor and R_E is the DC resistance in the voice coil wire. The speaker is excited by applying an AC voltage source, e_g, to the lumped circuit. Here e_g equals 1V.

The material properties are determined by interpolation functions which are based on the continuous update of the associated design variable, as shown in (14) and (15). These interpolation functions are constrained by a lower and upper bound where the bounds on the density and Young's modulus are determined from Fig. 3 and 4. The values of the bounds are shown in Table III. The limits on the isotropic loss factor in Table III are values that the authors assume are plausible for the given range of materials in Fig. 3 and 4.

A. Study overview

The study amounts to 36 optimization runs, the results of these are presented in Fig. 7 together with the results for the original design in Fig. 6, here the z-axis shows the root-mean-square error (RMSE) with respect to T_L, the x-axis shows the upper frequency limit of the optimization and the y-axis shows the maximum angle covered. The lower bound of the optimization is always 600 Hz. With an increasing angle span, the amount of measuring points per frequency is increased.

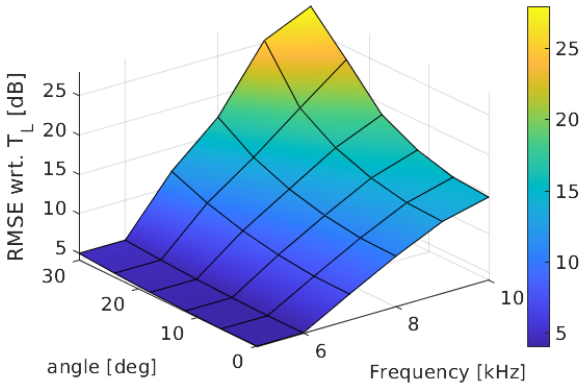

FIG. 6. The RMSE with respect to the target, T_L, for the original design.

It is evident from Fig. 6 and Fig. 7 that the optimized designs provide an improved performance when compared to the original design. The original design with an upper bound of 5-7 kHz on the frequency range exhibits a RMSE between 4.85 dB to 8.05 dB. For the evaluation of the original designs with an upper bound of 8kHz and higher the RMSE increases with a steep slope when frequency range elevated. Figure 7 shows that overall the value of the RMSE is decreased for all of the optimized designs which clearly shows that the proposed method in all cases yields a more flat response. The optimization procedure is able to design loudspeakers with a RMSE below 1 dB from the target line with an angle span of maximum 12 degrees with an upper frequency bound of 5-8 kHz and at 9 kHz the a maximum angle span is 6

TABLE I. Material properties for the original design.

	E [Pa]	ρ [kg/m^3]	η [–]	ν [–]
Diaphragm	$10.0 \cdot 10^9$	1300	0.2	0.3
Surround	$30 \cdot 10^5$	1400	0.25	0.45

TABLE II. Lumped parameters used to model the electric motor system, voice coil and spider.

M [kg]	L_E [mH]	n [–]	C_z [m/N]	C_r [m/N]	R_M [N · s/m]	Bl [T · m]	R_E [Ω]
0.006	3.63	0.77	$4.81 \cdot 10^{-4}$	$5 \cdot 10^{-5}$	0.53	4.81	3.52

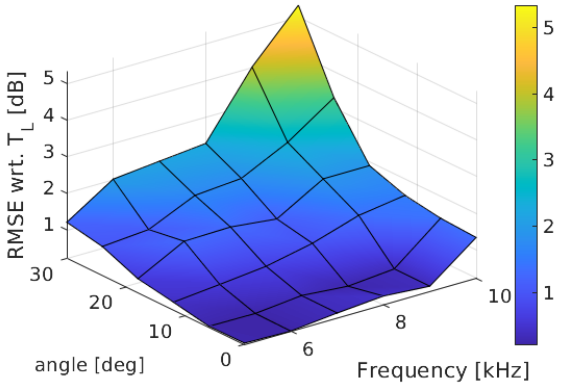

FIG. 7. The RMSE with respect to the target, T_L, for the optimized designs.

degrees. The figure also shows that a RMSE below 2 dB from the target line is achievable with an upper frequency bound of 5-6 kHz with a maximum angle of 30 degrees, at 7-8 kHz the maximum angle is 24 degrees and for 9-10 kHz the maximum angle is 18 degrees..

B. Evaluation of selected designs

This section will show the frequency response and the design of a few selected optimized loudspeaker units such that the performance of the optimized designs presented in Fig. 7 can be related to the performance of the original design shown in Fig. 5.

1. Optimized design at 600 Hz to 8 kHz with angle span of 0-6 degrees

Figure 8 shows the frequency response for the optimized design with a frequency range of 600Hz to 8kHz with angles 0, 2, 4 and 6 degrees included in the optimization. With a RMSE of 0.26 dB with respect to the target line at 74.0 dB this is a design that performs very well compared to the original which has a RMSE of 8.49 dB. The improvement is present in the frequency response, where the SPL output from the loudspeaker at the most deviate 0.4 dB from T_L. One can notice the steep roll-off in the frequency response as soon as 8 kHz is exceeded. This clearly illustrates that the loudspeaker unit is indeed optimized for the specific conditions given.

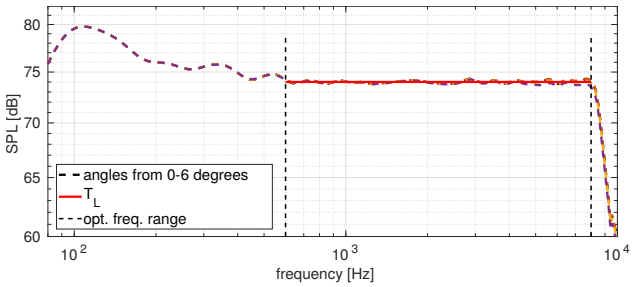

FIG. 8. Frequency response for the optimized design between 600Hz and 8kHz up to an angle of 6 degrees away from the center axis.

Figure 9 illustrates the values of the design variables that gives the frequency response in Fig. 8. Figure 9(a) relates to the design variable α, the β design variables are plotted in Fig. 9(b) finally, the ζ design variables are plotted in Fig. 9(c).

In Fig. 9(b) the bright patches corresponds to a density of 700-1000 kg/m^3 and the orange patches are 1000-1400 kg/m^3. Due to the codependency of the design variables this limits the optimizer in its choice of Young's modulus. In most of the dustcap the Young's modulus is in the range of 1-3 GPa, whereas for the cone the range is between 5-10 GPa. The two black patches on the loudspeaker cone has a Young's modulus of 30-40 GPa. The rubber surround consist of a stiff elastomer in the range of 1-2 GPa close to the connection with the diaphragm of the loudspeaker whereas the rest of the surround is soft with a Young's modulus in the range 0.0015 GPa

TABLE III. Bounds on the physical values

	E_{min} [Pa]	E_{max} [Pa]	ρ_{min} [kg/m^3]	ρ_{max} [kg/m^3]	η_{min} [−]	η_{max} [−]
Diaphragm	$1 \cdot 10^9$	$140 \cdot 10^9$	700	5000	0.05	0.3
Surround	$1 \cdot 10^6$	$10 \cdot 10^9$	850	1900	0.01	0.3

to 0.047 GPa. The values of the density can be placed into three groups in the surround, the light patches are equal to 1000 kg/m^3 the dark brown patches are equal to 1400 kg/m^3 and the black areas are the upper bound of the density which equals 1900 kg/m^3. Figure 9(c) shows that the optimizer elects to have an isotropic loss factor close to the upper bound of 0.3 in the surround and the dustcap whereas lower damping is present in the cone.

2. Optimized design at 600 Hz to 9 kHz with angle span of 0-18 degrees

The response in Fig. 10 is for an optimized design in the frequency range of 600Hz to 9kHz considering the angles from 0 to 18 degrees spaced with a 2 degrees interval. The optimized design has a RMSE from T_L of 1.89 dB making it one of the designs that has the poorest performance, which is to be expected due to the increased demands on the speaker being less directive and the broad frequency range. While this design has one of the higher RMSEs of almost 2 dB it is still a reasonably flat response. The optimized design is improved when compared to the original design which has a RMSE of 13.42 dB for the same frequency range and angle span. We see that this configuration of materials sacrifice some of the performance between 2-3kHz. At higher frequencies the SPL at angles 0-8 degrees for the most part lie above the target line whereas the SPL at 10-18 degrees lies below the target line.

Figure 11 plots the design variables of the optimized design. The layout of the design variables share many similarities with the previous example. The differences are that the loudspeaker cone is slightly stiffer and the surround in this example is divided into clearly defined sections, where the lightest and stiffest section is connected to the loudspeaker cone. The layout of the damping in Fig. 11(c) almost resembles that of Fig. 9(c), however in this configuration the damping is in the range of 0.0 to 0.05 on the right-hand-side of the surround connecting to the baffle. The similarities in the distribution of the damping material indicates that this particular layout of high damping in the dustcap and in the surround seems to yield a good frequency response.

C. Comparison of field variables between the original design and an optimized design

This section will focus on comparing field variables of the original design to the optimized design in sec. III B 1. The directivity pattern of the loudspeaker has been one of the targets in this paper. The directivity pattern of the original speaker is shown in Fig. 12. Here the SPL is measured 1 meter away from the speaker in angles spanning from 0-85 degrees and a frequency range of 500 Hz to 9 kHz. The figure shows that the speaker has varying output, which is especially prominent at 5 to 6 kHz. After 6 kHz the speaker displays quite a sharp roll-off towards a lower SPL output.

Figure 13 shows the directivity of the optimized loudspeaker from Sec. III B 1. The figure shows that the optimization procedure has been able to tune the material properties of the loudspeaker, yielding a more even response. We see that between 5.5 and 6.5 kHz the loudspeaker has increased output for angles larger than 20 degrees when compared to the original design. This is due to the fact that a specification to reduce sound radiation outside of the target angle range is not included in the objective function. The abrupt roll-off can be attributed to that the optimized speaker has a clearly defined side lobe starting from 8 kHz. This emphasizes that the optimizer only controls the response in the specified areas.

In Fig. 14 the vibration pattern of the original loudspeaker and the resulting pressure field near the speaker is shown for the frequency 7600 Hz. We plot the real part of the pressure field together with surface vectors representing magnitude and direction for the real part of the surface velocity. This snapshot shows that the loudspeaker motion is concentrated in the diaphragm, where a break-up mode is present. The resulting pressure field is far from optimal which is illustrated in both the directivity plot in Fig. 12 and by the fact that the amplitude of the pressure field has a reduced size when compared to the optimized design in Fig. 15.

Figure 15 shows the oscillating loudspeaker and the pressure field arising from it at the same frequency as Fig. 14 for the optimized speaker from Sec. III B 1. Here, the surround still contributes to the vibration, making the speaker move up and down. As expected most of the motion happens in the diaphragm. Due to the high frequency the depth of the speaker corresponds to roughly one-half-wavelength, this implies that in order to create a plane wavefront the velocity of the speaker should not be uniform. This is clearly illustrated by the fact that the optimized speaker has a negative pressure situated where the dustcap and the loudspeaker cone intersects. The optimized design is taking into account the physics of the problem-at-hand and is able to tune the break-up

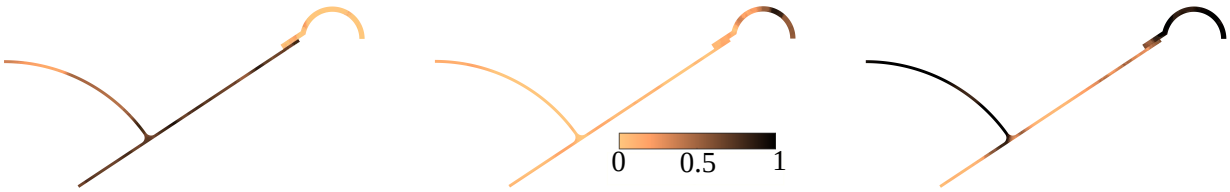

(a) (b) (c)

FIG. 9. Design variables for the optimized design with a frequency range of 600 to 8kHz up to an angle 6 degrees away from the center axis. (a) is stiffness, (α), (b) is density (β) and (c) is damping (ζ)

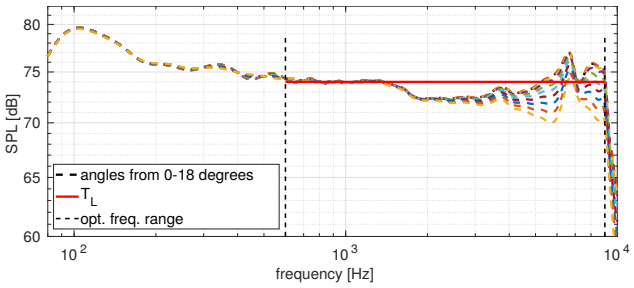

FIG. 10. Frequency response for the optimized design between 600Hz and 9kHz up to an angle of 18 degrees away from the center axis.

mode of the speaker and as a consequence, the optimized speaker is able to keep the pressure constant as a function of frequency.

IV. DISCUSSION

This paper has investigated what it takes from a material properties point-of-view to obtain a flat frequency response over a broad frequency range. It is an interesting objective to investigate due to the fact that it is constantly brought up as one of the key aspects of a loudspeaker. To reach this objective we have developed a solid and versatile material optimization approach which can be utilized to optimize and solve a vast amount of other interesting design cases.

In this paper we have applied a sensitivity filter to avoid a high contrast between neighbouring elements, this reduces the sensitivity to change of the optimized structures and also makes the optimized design mesh independent. With present manufacturing techniques the optimized designs presented in this paper is difficult to realize. If it is desired to manufacture the designs one could add a post-process optimization step with a projection filter. This could yield well defined materials with discrete boundaries between them. With this approach further work should be put into then defining how small are these material patches allowed to be and how should they be connected in the interface between them. A low effort approach if one wants to optimize for a loudspeaker with a more homogeneous material distribution would consists of identifying sections of the loudspeaker that should be homogeneous, i.e. the dustcap can consist of one material, the cone of one material etc. That would essentially mean to apply the work done by the authors in[19] to the example in this paper.

The objective has been to minimize the error between a desired target and the actual frequency response and thus obtaining a flat frequency response in a predefined angle span and frequency range. Several other interesting objectives could be investigated. One could add another term to the current objective function to minimize the output at angles above e.g. 30 degrees such that reflections from the ceiling and floor is reduced. One could also add a term that takes into account the roll-off characteristics of the speaker and thereby make it easier to design a cross-over filter. In connection with cross-over design it would also be interesting to consider the phase of the loudspeaker and possibly optimize it to have a certain behaviour in the frequency range where it should have a cross-over filter.

V. CONCLUSION

The work presented introduces a density based optimization approach where the gradients can be calculated analytically. The method is used to optimize the material properties of a generic 5 inch loudspeaker unit. An investigation of both frequency range and increasing demands to widen the directivity of the loudspeaker unit showed that the applied method is able to significantly improve the optimized designs with at least a factor of 5 when comparing the RMSE from the desired target of the original design. The presented results show a clear bias towards how stiffness, mass and damping ideally should be distributed in a loudspeaker. This can be helpful for generating new ideas or identifying tendencies that were not previously considered.

The presented method is versatile and can be altered to optimize for other objectives and several constraints and filters can be added to make the optimized designs more suitable for manufacturing.

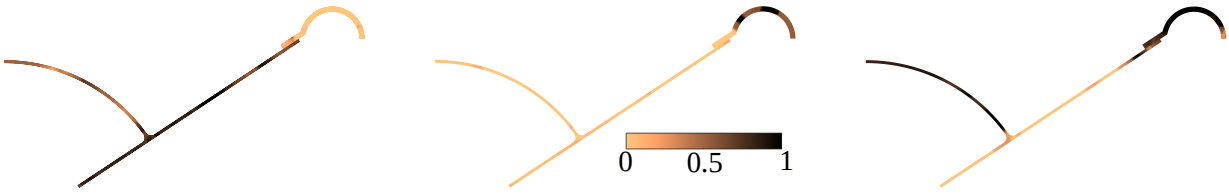

(a) (b) (c)

FIG. 11. Design variables for the optimized design with a frequency range of 600 to 9kHz up to an angle 18 degrees away from the center axis. (a) is stiffness, (α), (b) is density (β) and (c) is damping (ζ)

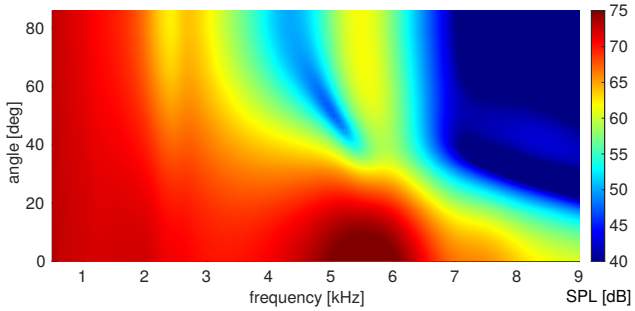

FIG. 12. Directivity sonogram for the original design.

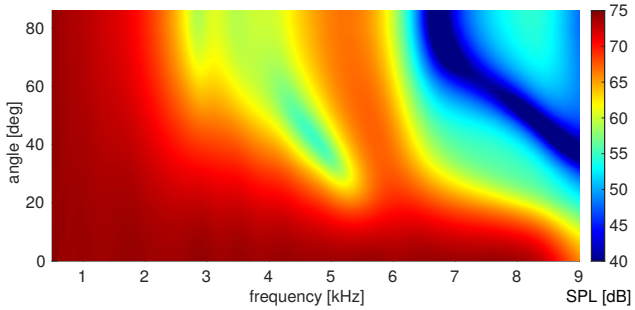

FIG. 13. Directivity sonogram for the optimized design in sec. III B 1

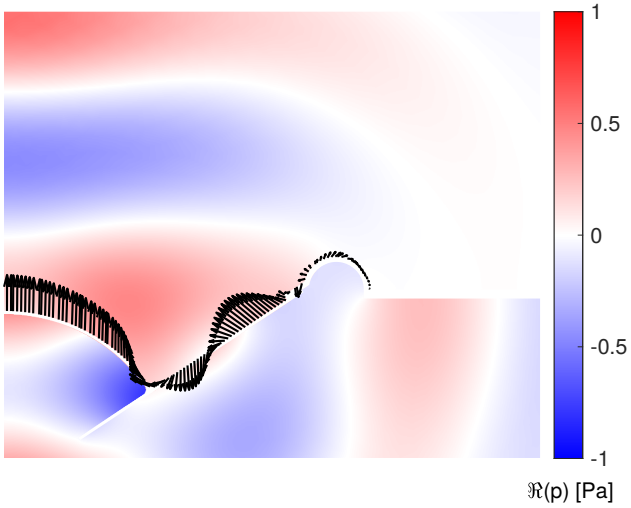

FIG. 14. Arrow plot for the surface velocity of the speaker and the real part of the pressure field for the original design at 7600 Hz.

APPENDIX A:

1. Derivation of the adjoint equation

The following equations are carried out for one angle so $n = 1$ and $\boldsymbol{\tau} = \boldsymbol{\tau}_n$, multiple angles are straightforward to include it requires that the non zero DOF in $\boldsymbol{\tau}$ changes to accommodate for a new angle.

The derivative of (16) with respect to the solution vector $\mathbf{u}$ is

$$\frac{\partial \phi_0}{\partial \mathbf{u}} = 2\left(T_L - \mathbf{spl}\boldsymbol{\tau}\right)\frac{\partial}{\partial \mathbf{u}}\left(-\mathbf{spl}\boldsymbol{\tau}\right). \tag{A1}$$

evaluating $\frac{\partial}{\partial \mathbf{u}}\left(-\mathbf{spl}\boldsymbol{\tau}\right)$ with the chain rule yields

$$\frac{\partial}{\partial \mathbf{u}_{r_k}}\left(-\mathbf{spl}\boldsymbol{\tau}\right) = \frac{-20\boldsymbol{\tau}}{\left(\frac{\sqrt{\mathbf{u}_{r_k}^2+\mathbf{u}_{i_k}^2}}{\sqrt{2}}\right)/p_0 \cdot \ln(10)} \cdot \frac{\sqrt{2}}{4\sqrt{\mathbf{u}_{r_k}^2+\mathbf{u}_{i_k}^2}\,p_0} \cdot 2\mathbf{u}_{r_k}$$

the derivatives of the objective functions then becomes

$$\frac{\partial \phi_{0_k}}{\partial \mathbf{u}_{r_k}} = 2\left(T_L - \mathbf{spl}\boldsymbol{\tau}\right)\frac{-20\mathbf{u}_{r_k}\boldsymbol{\tau}}{\left(\mathbf{u}_{r_k}^2+\mathbf{u}_{i_k}^2\right)\ln(10)} \tag{A2}$$

$$\frac{\partial \phi_{0_k}}{\partial \mathbf{u}_{i_k}} = 2\left(T_L - \mathbf{spl}\boldsymbol{\tau}\right)\frac{-20\mathbf{u}_{i_k}\boldsymbol{\tau}}{\left(\mathbf{u}_{r_k}^2+\mathbf{u}_{i_k}^2\right)\ln(10)} \tag{A3}$$

If there are multiple angles, the above steps should be repeated to yield inputs into $\frac{\partial \phi_{0_k}}{\partial \mathbf{u}_{r_k}}$ and $\frac{\partial \phi_{0_k}}{\partial \mathbf{u}_{i_k}}$.

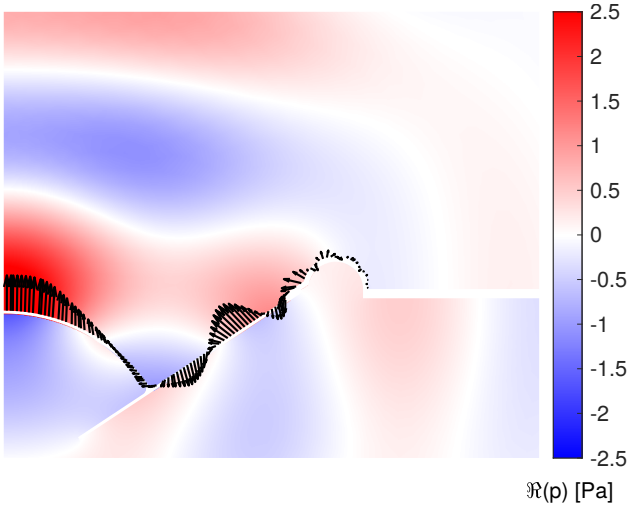

FIG. 15. Arrow plot for the surface velocity of the speaker and the real part of the pressure field for the optimized design at 7600 Hz

Inserting (A2) and (A3) into (18) yields

$$\mathbf{S}_k^T \boldsymbol{\lambda}_k = \frac{-40j\left(20\ln\left(\frac{\sqrt{\mathbf{u}_{r_k}^2+\mathbf{u}_{i_k}^2}\sqrt{2}}{2p_0}\right)\boldsymbol{\tau} - T_L\ln(10)\right)\boldsymbol{\tau}}{(j\mathbf{u}_{r_k} - \mathbf{u}_{i_k})\ln(10)^2}$$

[1] S. E. Olive and T. Welti, "The relationship between perception and measurement of headphone sound quality," 133rd Audio Engineering Society Convention 2012, Aes 2012 **2**, 881–897 (2012).

[2] F. E. Toole, *Sound reproduction: The acoustics and psychoacoustics of loudspeakers and rooms: Third edition* (Taylor and Francis, 2017), pp. 1–490.

[3] W. Evans, J. Dyreby, S. Bech, S. Zielinski, and F. Rumsey, "Effects of loudspeaker directivity on perceived sound quality - a review of existing studies," 126th Audio Engineering Society Convention 2009 **1**, 221–229 (2009).

[4] D. Queen, "Effect of loudspeaker radiation patterns on stereo imaging and clarity," J Audio Eng Soc **27**(5), 368–379 (1979).

[5] S. Linkwitz, "Which loudspeaker parameters are important to create the illusion of a live performance in the living room?," in *Audio Engineering Society Convention 113* (2002), http://www.aes.org/e-lib/browse.cfm?elib=11289.

[6] R. BUCKLEIN, "The audibility of frequency-response irregularities," Journal of the Audio Engineering Society **29**(3), 126–131 (1981).

[7] W. M. Leach Jr., *Introduction to Electroacoustics & Audio Amplifier Design*, 3rd ed. (Kendal/Hunt Publishing Company, 2003).

[8] L. L. Beranek and T. Mellow, *Acoustics: Sound Fields and Transducers* (Elsevier Inc., 2012), pp. Online–Ressource (unknown).

[9] M. R. Bai and R. L. Chen, "Optimal design of loudspeaker systems based on sequential quadratic programming (sqp)," Aes: Journal of the Audio Engineering Society **55**(1-2), 44–54 (2007).

[10] D. G. Nielsen, P. R. Andersen, J. S. Jensen, and F. T. Agerkvist, "Estimation of optimal values for lumped elements in a finite element — lumped parameter model of a loudspeaker," Journal of Theoretical and Computational Acoustics **28**(02), 2050012 (2020) doi: 10.1142/S2591728520500127.

[11] R. E. Christiansen and E. Fernandez Grande, "Design of passive directional acoustic devices using topology optimization - from method to experimental validation," Acoustical Society of America. Journal **140**(5), 3862–3873 (2016) doi: 10.1121/1.4967370.

[12] S. Marburg, "Developments in structural-acoustic optimization for passive noise control," Archives of Computational Methods in Engineering **9**(4), 291–370 (2002) doi: 10.1007/BF03041465.

[13] E. Creixell Mediante, J. S. Jensen, J. Brunskog, and M. Larsen, "Reduced order modeling in topology optimization of vibroacoustic problems," Journal of the Acoustical Society of America **141**(5), 4035–4035 (2017) doi: 10.1121/1.4989307.

[14] A. Bezzola, "Numerical optimization strategies for acoustic elements in loudspeaker design," 145th Audio Engineering Society International Convention, Aes 2018 (2018).

[15] R. Christensen, "Shape and topology optimization of loudspeaker drivers," Comsol Conference Europe 2020 (2020).

[16] P. R. Andersen, V. Cutanda Henríquez, and N. Aage, "Shape optimization of micro-acoustic devices including viscous and thermal losses," Journal of Sound and Vibration **447**, 120–136 (2019) doi: 10.1016/j.jsv.2019.01.047.

[17] M. Alfouneh, J. Ji, and Q. Luo, "Damping design of harmonically excited flexible structures with graded materials to minimize sound pressure and radiation," Engineering Optimization 1–20 (2020) doi: 10.1080/0305215X.2020.1735381.

[18] A. Camberg, Alan, I. Stratmann, and T. Tröster, "Tailored stacked hybrids – an optimization-based approach in material design for further improvement in lightweight car body structures," Technologies for Economical and Functional Lightweight Design 119–131 (2019) doi: 10.1007/978-3-662-58206-0_12,10.1007/978-3-662-58206-0.

[19] D. G. Nielsen, G.-T. Lee, Y.-H. Park, J. S. Jensen, and F. T. Agerkvist, "Optimization of the performance of small speaker systems with passive radiators," Proceedings of 49th International Congress and Exposition on Noise Control Engineering (2020) https://internoise2020.org/.

[20] S. Degraeve and J. Oclee-Brown, "Metamaterial absorber for loudspeaker enclosures," 148th Audio Engineering Society International Convention (2020).

[21] J. Herzberger, J. M. Sirrine, C. B. Williams, and T. E. Long, "Polymer design for 3d printing elastomers: Recent advances in structure, properties, and printing," Progress in Polymer Science **97**, 101144 (2019) doi: 10.1016/j.progpolymsci.2019.101144.

[22] M. Saari, M. Galla, B. Cox, P. Krueger, A. Cohen, and E. Richer, "Additive manufacturing of soft and composite parts from thermoplastic elastomers," Proceedings - 26th Annual International Solid Freeform Fabrication Symposium - an Additive Manufacturing Conference, Sff 2015 949–958 (2020).

[23] A. Toudehdehghan, J. W. Lim, K. E. Foo, M. I. Ma'Arof, and J. Mathews, "A brief review of functionally graded materials," Matec Web of Conferences **131**, 03010 (2017) doi: 10.1051/matecconf/201713103010.

[24] F. Collino and P. Monk, "The perfectly matched layer in curvilinear coordinates," Siam Journal of Scientific Computing **19**(6), 2061–2090 (1998) doi: 10.1137/s1064827596301406.

[25] "Granta edupack" , https://www.ansys.com/products/materials/granta-edupack.

[26] K. Svanberg, "The method of moving asymptotes - a new method for structural optimization," International Journal for Numerical Methods in Engineering (1987).

[27] O. Sigmund, "Morphology-based black and white filters for topology optimization," Structural and Multidisciplinary Optimization **33**(4-5), 401–424 (2007) doi: 10.1007/s00158-006-0087-x.

Paper 5

Shape optimization of compact loudspeakers using free form deformation and the finite element method

Daniel Gert Nielsen[a,*], Peter Risby Andersen[b], Finn Thomas Agerkvist[a]

[a] *The department of Electrical Engineering, Technical University of Denmark, Ørsteds Plads Building 352, DK-2800 Kgs. Lyngby, Denmark*
[b] *GN Audio A/S and Jabra, Audio Research, Lautrupbjerg 7, 2750 Ballerup, Denmark*

Abstract

This paper demonstrates how substantial improvements to a compact speaker's horizontal frequency response may be achieved by optimizing the shape of a dynamic down-firing speaker and an acoustic lens. The capability of the method is tested by using three different starting geometries for the acoustic lens for three different frequency ranges. The numerical model consists of a fully coupled finite element model of the compact speaker and the surrounding acoustic domain. The optimized shapes are obtained by utilizing the principles of free form deformation in conjunction with a multi-frequency design problem based on a minimax formulation. The target frequency range is from 1 kHz up to 8 kHz. The design update is governed by semi-analytical design sensitivities. The study examines a diverse range of starting configurations and the outcome underlines the fact that the starting configuration is essential when striving for obtaining feasible optimized designs. The results show that a flat horizontal frequency response in the entire specified range can be achieved, and the resulting geometries are smooth and uncomplicated.

Keywords: vibro-acoustics, loudspeakers, shape optimization, finite element method, acoustic lens

1. Introduction

The use of compact speakers in homes around the world is increasing. The speakers are controlled with voice commands, making it easy for the user to play their favorite music or listen to podcasts. This convenience translates into the compact speaker gaining market-share over traditional loudspeakers. Ref. [1] recently reported that the number of Americans who use a smart speaker as their primary music listening device increases year by year. Due to the speaker's compact size, the loudspeaker units are often small. The speaker's compact size and the expectation that it should yield good sound quality make for an interesting engineering problem with several sub-problems. Ref. [2] addresses the issue of decreased low frequency performance in compact speakers by optimizing a passive radiator. Compact speakers can be configured with down-firing speakers; in these configurations, an acoustic lens is pivotal to the speaker's ability to yield a desirable sound field in a wide frequency range.

The use of numerical methods allows for simulating the response of loudspeakers and can be a powerful tool that can aid in the design process. The boundary element method is used in [3] to investigate and design an acoustic reflector with a non-trivial shape. The designed reflector is mounted on the treble dome driver, enhancing the driver's performance for high frequencies. In [4] shape and topology optimization are used to design an acoustic horn with a lens design consisting of small scatters. The objective is to obtain high efficiency and even directivity in the frequency range of 250 Hz to 1000 Hz.

*Corresponding author
Email addresses: dgniel@elektro.dtu.dk (Daniel Gert Nielsen), prandersen@jabra.com (Peter Risby Andersen), fa@elektro.dtu.dk (Finn Thomas Agerkvist)

Prior to numerical methods being efficient enough to be used, acoustic lenses were designed based on analytical models and knowledge about geometries and their influence on the frequency response. Ref. [5] proposes an inclined lens design that is tuned to increase the dispersion at 4000 Hz. In [6] an acoustic lens shaped like an ellipsoid is propose to avoid interference between two speakers, thus creating an approximate frequency invariant response as a function of angle. Ref. [7] argues that a radial radiating loudspeaker compared to the traditional front-firing speaker is superior at accurately reproducing mid-to-high frequencies. Radial loudspeakers have the advantage that they radiate sound in the horizontal plane thus it implicitly minimizes reflections from the floor and ceiling. Similarly, an acoustic lens inherently redirects the sound to primarily radiate in the horizontal plane, at least for mid-to-high frequencies.

Shape optimization has proven to be a powerful design tool for coupled vibro-acoustic structures. Contrary to topology optimization, shape optimization always has a well-defined boundary in the interface between the mechanical and acoustic domains. This implies that the physics is well represented throughout the optimization routine. An essential factor for the outcome of shape optimization is the choice of the parameterization method. Typically, parametrization methods can be categorized as discrete parametrization, polynomial and spline parameterization, and free form deformation (FFD) [8]. In this paper, FFD with semi-analytical gradients is used to optimize the shape of an acoustic lens and loudspeaker diaphragm. The FFD implementation is based on the original work by Sederberg and Parry using Bernstein polynomials as the interpolation basis [9]. In FFD shape optimization, the computational mesh is mapped to the underlying volumetric interpolation basis and by changing the location of control points, the mesh can be deformed. Shape optimization naturally is also applicable to the boundary element method; this is demonstrated in Ref. [10], where small resonators with losses were optimized to improve sound absorption. Acoustic shape optimization has been applied by Udawalpola in [11] to investigate the optimization of acoustic horns and brass wind instruments. Several optimization procedures exist for optimizing acoustic-mechanical problems. Dilgen et al. [12] give a comparative review of topology optimization, the level set approach, and bi-directional evolutionary structural optimization.

In recent years, developments in the efficiency of commercial software have paved the way for using numerical methods to optimize loudspeakers' performance. In [13] Bezzola shows several numerical optimization methods aimed towards loudspeakers. The optimization of loudspeaker components is also considered by Christensen in [14]. Degraeve and Oclee-Brown [15] recently published a paper on using a metamaterial absorber in a loudspeaker cabinet to mitigate the influence of the cabinet on the frequency response.

This paper optimizes acoustic lenses for a compact speaker with a down-firing woofer. The objective is to achieve a flat frequency response over a wide frequency range 1 m away from the speaker. This is accomplished by using FFD to alter the geometry of the acoustic lens and the woofer. Subsequent sections will present the necessary theory to model the speaker with finite elements and the optimization procedure using semi-analytical gradients. Finally, results from three different starting guesses are presented, compared, and discussed.

2. Loudspeaker Modeling

The compact speaker in this research is configured with a 3-inch down-firing speaker and a passive radiator as seen in Fig. 1. The geometry allows for modeling the speaker with a 2D axisymmetric model. The assumption of axisymmetry implies that the model does not capture a-symmetric break-up modes at very high frequencies. These high-order modes are usually poor radiators and are associated with degraded sound quality. The impact of higher order modes could be investigated in a full-sized 3D model of the current design. This is, however, deemed beyond the scope of this paper. The assumption reduces the model's complexity, which is vital for reducing the computational task. The speaker is partly lumped, meaning that the electric motor system, voice coil, and spider are contained in a lumped parameter model (LPM), which is coupled to the finite element (FE) model. In this configuration, an acoustic lens is needed to achieve a feasible horizontal output of the speaker. We investigate three lens designs used as starting guesses for the optimization, and these are shown in Fig. 1. The lenses are placed at different distances from the woofer, and this distance is denoted L_D. The compact speaker's walls and the acoustic lens are assumed to be rigid.

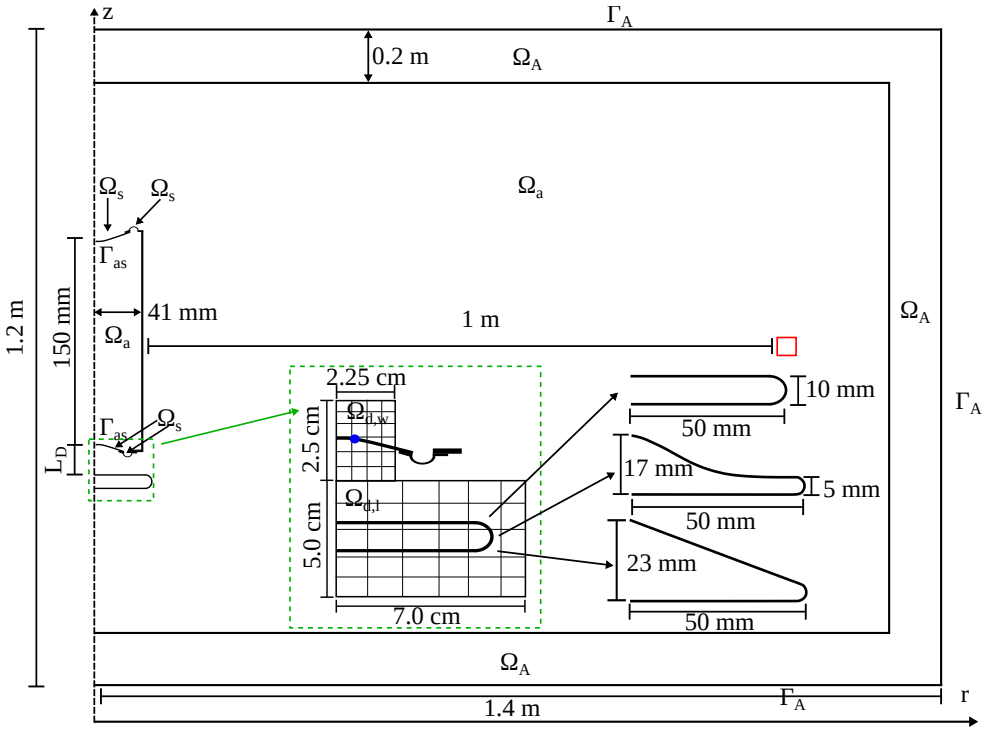

Figure 1: 2D sketch of the compact speaker with domain names and boundary conditions and dimensions. The blue circle indicates where the LPM is coupled to the FE model. The red square is the measurement point where the objective function is evaluated. The two design domains $\Omega_{d,w}$ and $\Omega_{d,l}$ contain the grid of Bernstein Polynomials. The three lens designs used as a starting guess is also shown. They are placed with the distance L_D to the woofer.

The governing equations for the time-harmonic motion of a linear elastic body where body forces has been neglected are

$$\rho\omega^2\mathbf{u} + \nabla\cdot\,\boldsymbol{\sigma}\left(\mathbf{u}\right) = 0 \qquad \text{in} \quad \Omega_s \tag{1}$$

$$\boldsymbol{\sigma} = \mathbf{C}\boldsymbol{\epsilon} \tag{2}$$

$$\epsilon = \left\{\epsilon_r\ \epsilon_\theta\ \epsilon_z\ 2\gamma_{zr}\right\}^T \qquad \text{(2D Axisymmetric)} \tag{3}$$

$$\epsilon_r = \frac{\partial u_r}{\partial r},\ \epsilon_\theta = \frac{u_r}{r},\ \epsilon_z = \frac{\partial u_z}{\partial z},\ \gamma_{zr} = \frac{1}{2}\left(\frac{\partial u_r}{\partial z} + \frac{\partial u_z}{\partial r}\right), \tag{4}$$

$$\mathbf{u} = 0 \quad \text{on} \quad \Gamma_s \quad , \quad \mathbf{u}_r = 0 \quad \text{on} \quad \Gamma_{sym} \tag{5}$$

here ρ is the mass density of the material, ω is the excitation frequency in radians, $\mathbf{u}$ is the structural displacements, $\boldsymbol{\sigma}$ is the stress tensor, Ω_s is the structural domain, $\mathbf{C}$ is the constitutive matrix for an axisymmetric structure, $\boldsymbol{\epsilon}$ is the strain tensor, u_r is the structural displacement in the r-direction, u_z is the displacement in the z-direction, on Γ_s the structure is clamped and on Γ_{sym} the symmetry condition means that the structure can not move in the r-direction.

To obtain the pressure distribution in the acoustic domain, the Helmholtz equation is solved together with a modified Helmholtz equation [16, 17] a truncated PML region (Ω_A), as shown in Fig. 1

$$\Delta p + \frac{\omega^2}{c^2}p = 0 \quad \text{in} \quad \Omega_a \tag{6}$$

$$\frac{1}{\gamma_r}\frac{\partial}{\partial r}\left(\frac{1}{\gamma_r}\frac{\partial p_A}{\partial r}\right) + \frac{1}{\gamma_z}\frac{\partial}{\partial z}\left(\frac{1}{\gamma_z}\frac{\partial p}{\partial z}\right) + \frac{\omega^2}{c^2}p = 0 \text{ in } \Omega_A, \tag{7}$$

$$\mathbf{n}\cdot\nabla p = 0 \quad \text{on} \quad \Gamma_a \tag{8}$$

$$p = 0 \quad \text{on} \quad \Gamma_A \tag{9}$$

$$\mathbf{n}\cdot\nabla p = -\omega^2\rho_a\mathbf{n}^T\mathbf{u} \quad \text{on} \quad \Gamma_{as} \tag{10}$$

here Δ is the Laplace operator in cylindrical coordinates, p is the pressure and c is the speed of sound in air, a Dirichlect boundary conditions is used on the outer boundary, and the formulation of γ is from [18], here extended to accommodate for a PML in both the r- and z direction

$$\gamma_r(r) = 1 - j\kappa\left(\frac{r - r^*}{t}\right)^2 \tag{11}$$

$$\gamma_z(z) = 1 - j\kappa\left(\frac{z - z^*}{t}\right)^2. \tag{12}$$

Where r^* and z^*, indicate the interface coordinate between the PML/acoustic domain and r and z are the position within the PML, κ is the absorption coefficient in the layer with a constant value of 3.5 and t is half the thickness of the PML which equals 0.1m.

2.1. Finite Element Model

Eqs. (1) and (6) are discretized into the usual FE matrices. Damping is included in the mechanical parts with an isotropic loss factor, such that $\mathbf{K} = \mathbf{K}(1 + j\eta)$, where η is the isotropic loss factor and j is the imaginary number. In the interior of the compact speaker, see Fig. 1, standing waves frequently occur due to internal resonances. This greatly affects the response, and we therefore add damping in the interior domain. The damping is mass proportional and is included by defining that $\mathbf{M}_a = \mathbf{M}_a(1 + j\eta_a)$, here η_a is a free parameter that controls the amount of damping. This value was chosen as it supplies a sufficient amount of damping inside the loudspeaker cabinet.

The mechanical and acoustic system is strongly coupled and can be compiled into a system of equations that can be used to solve vibro-acoustic problems

$$\left(\begin{bmatrix}\mathbf{K} & -\mathbf{S}^T\\ \mathbf{0} & \mathbf{K}_a\end{bmatrix} - \omega^2\begin{bmatrix}\mathbf{M} & \mathbf{0}\\ \rho\mathbf{S} & \mathbf{M}_a\end{bmatrix}\right)\begin{Bmatrix}\mathbf{u}\\ \mathbf{p}\end{Bmatrix} = \begin{Bmatrix}\mathbf{f}\\ \mathbf{0}\end{Bmatrix}. \tag{13}$$

It is imperative to include the electrical motor system's contribution when modeling a loudspeaker. The effects of including the motor system are especially pronounced at the first mechanical resonance of the woofer and at higher frequencies where the electrical impedance increases due to the voice coil's inductance. Including the electrical motor system in the FE model will increase the complexity of the model. Therefore, the authors developed a hybrid FE-LPM model where the electric motor system and the spider and voice coil former are included in a lumped model attached to the FE model. The details are described thoroughly in Ref. [19]. The hybrid modeling approach allows us to excite the speaker with an AC voltage source, the system of equations for the hybrid FE-LPM becomes

$$\left(\tilde{\mathbf{K}} + j\omega\tilde{\mathbf{C}} - \omega^2\tilde{\mathbf{M}}\right)\begin{Bmatrix}\mathbf{u}\\ \mathbf{p}\\ i_c\end{Bmatrix} = \begin{Bmatrix}\mathbf{0}\\ \mathbf{0}\\ e_g\end{Bmatrix}. \tag{14}$$

Here $\tilde{\mathbf{C}}$ is the matrix including the velocity proportional terms from the lumped model, i_c is the current in the electric motor system and e_g is applied AC voltage.

Equation (14) is for the duration of this paper written with compact notation as

$$\tilde{\mathbf{S}}\tilde{\mathbf{u}} = \tilde{\mathbf{f}}, \tag{15}$$

3. Parametrization using Free Form Deformation

To handle the deformation of the computational domain, the FEM mesh is mapped in a rectangular region to bivariate Bernstein polynomials using the FFD approach [20]. Cartesian coordinates $\mathbf{q}_{i,j}(s,t)$ within the FFD region can therefore be described as

$$\mathbf{q}_{i,j}(s,t) = \sum_{i}^{l}\sum_{j}^{m} b_i(s)b_j(t)\mathbf{d}_{i,j} \tag{16}$$

where l and n are the order of the Bernstein polynomials, $\mathbf{d}_{i,j}$ are the associated control points, and s and t are local coordinates within the FFD region restricted to $0 \leq s \leq 1$ and $0 \leq t \leq 1$. The Bernstein basis polynomials are given by

$$b_i(s) = \binom{l}{i} s^i (1-s)^{l-s} \quad \text{with} \quad \binom{l}{i} = \frac{l!}{i!(l-i)!} \tag{17}$$

$$b_j(t) = \binom{m}{j} t^j (1-t)^{m-t} \quad \text{with} \quad \binom{m}{j} = \frac{m!}{j!(m-j)!} \tag{18}$$

The design is hereafter altered by changing some of the Cartesian coordinates in $\mathbf{d}_{i,j}$. Fig. 2 shows an example of how the FFD parametrization works when perturbing a control point. Here, the red dots indicate the location of the control points. It should be noted that control points located on the z-axis are only allowed to move in the z-direction. A movement in the negative r-direction will yield a non-physical mesh and a movement in the postive r-direction will create additional unwanted holes in the domain. Additionally, the control points are limited by box constraints to avoid too large deformations. In the FFD regions $\Omega_{d,w}$ and $\Omega_{d,l}$ in Fig. 1 the control points are allowed to move from their initial location $\pm$15 mm and $\pm$ 50 mm, respectively.

4. Optimization problem

The aim of the optimization is to minimize deviations in the acoustic sound pressure level as a function of frequency. Therefore, the optimization problem is stated in terms of a desired target sound pressure level

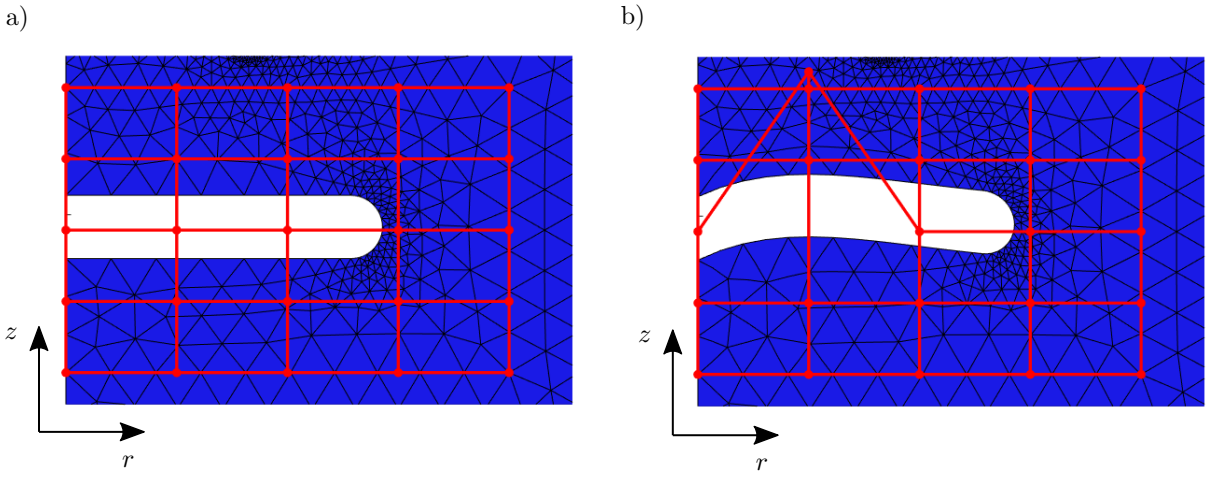

Figure 2: An example of the design region of the one FFD region located around a flat acoustic lens. The location of the control points are indicated with red dots. a) is the initial configuration of the Bernstein polynomials and b) is an example of a change in a control point in the z-direction.

T_L that the sound pressure level ideally is matched to over a range of frequencies. If using an extensive amount of optimization frequencies, it is typically necessary to formulate the optimization problem in terms of a minimax problem, formally stated as

$$\begin{array}{lll} \min\limits_{\mathbf{x}} \quad \max & \phi_k(\mathbf{x}) = \left(T_L - \mathbf{spl}_k \boldsymbol{\tau}\right)^2 \ , & k = 1, \ldots, b \\ \text{s.t.} & \tilde{\mathbf{S}}_k \tilde{\mathbf{u}}_k - \tilde{\mathbf{f}} = 0 \ , & k = 1, \ldots, b \\ & 0 \leq \ x_l \leq 1 \ , & l = 1, \ldots, n \\ & c_i(\mathbf{x}) \leq 0 & i = 1, \ldots, q, \end{array} \tag{19}$$

where $\mathbf{x}$ is the design variables, $\phi_k(\mathbf{x})$ is the objective function evaluated at the frequency k, b is the total number of frequencies used in the optimization, in this work 30 logarithmic spaced frequencies are used, $\boldsymbol{\tau}$ is a zero vector with unity input at the DOF belonging to the measuring point of the objective function, q is the amount of nonlinear constraints, x_l is the l'th design variable with n being the total number of design variables. Furthermore, $\mathbf{c}$ is a vector containing nonlinear element quality constraints, the constraints are introduced in the next section. It should be noted that that the design variables, i.e. the rz-location of the control points in the FFD mapping, is scaled using a linear change of variables so that

$$x_l = \frac{d_{i,j} - L_l}{L_h - L_l} \tag{20}$$

where $d_{i,j}$ is a single control point and L_h and L_l are the upper and lower bounds of the specific control point, respectively.

The three initial lens designs from Fig. 1 are evaluated at the three starting positions as shown in Fig. 3. Moreover, a configuration without an acoustic lens is plotted in Fig. 3a. This figure shows that the loudspeaker has a flat frequency response up to 5 kHz, where a quite steep roll-off is present since the loudspeaker becomes directional at higher frequencies. Therefore, it is desired to design an acoustic lens that can extend the flat frequency response beyond the current limit at 5 kHz. In order to investigate how much the frequency range can be extended, an upper frequency bound of 6 kHz, 7 kHz, and 8 kHz is used in the design problem in Eq. (19). The lower bound on the frequency range is always 1 kHz. As shown in Fig. 3b, 3c and 3d the frequency response below 5 kHz is affected negatively by the introduction of the lens, and it is, therefore, necessary to include this frequency range in the design problem as well.

Using different starting guesses is pivotal to investigate the solution space available for this particular problem. This is because that the design problem is not convex, and therefore many sub-optimal local

minimums exist. By exploring a wider range of initial configurations the chances of achieving high-performing optimized designs are increased. Not only is the geometry of importance but also the distance at which the acoustic lens is placed from the speaker. Fig. 3 features the target line, T_L, the value of the target line is chosen such that if the design is successfully optimized the high frequency response will align with mid frequency response and thus obtaining a flat horizontal frequency response.

4.1. Nonlinear element quality constraints

An issue of concern for shape optimization is element distortion that potentially can lead to an inaccurate numerical model or in the worst case flipped elements. To circumvent such unwanted behaviour, nonlinear element quality constraints are created based on the angles in the elements using an equilateral triangle as the ideal reference triangle. The element angle definition is sketched in Fig. 4. The constraint is separated into angles associated with 60°or 180°. To avoid an extensive amount of constraints in $\mathbf{c}$, angles of the same type in all affected elements are summed using the generalized mean, resulting in the two types of constraints given by

$$\left(\frac{1}{N_{60}}\sum_{l=1}^{N_{60}}\theta_{60,l}^{p_L}\right)^{1/p_L} - c_{60,\max} \leq 0, \tag{21}$$

where the $p_L = 15$ is the penalty factor which means that elements with large angle deviations are dominant in the sum, $\theta_{60,l} = |\theta_l - 60°|$, with θ_l being the angle at a specific node, N_{60} is the total number of angles included in the summation and $c_{60,\max}$ is the allowed deviation from the ideal angle of 60°. In this work the value of $c_{60,\max}$ is equal to 25° which is a conservative choice that ensures high mesh quality.

$$\left(\frac{1}{N_{180}}\sum_{l=1}^{N_{180}}\theta_{180,l}^{p_L}\right)^{1/p_L} - c_{180,\max} \leq 0, \tag{22}$$

here $\theta_{180,l} = |\theta_l - 180°|$, N_{180} is the total number of angles included in the summation and $c_{180,\max}$ is the allowed deviation from the ideal angle of 180°. In this work the value of $c_{180,\max}$ is equal to 10° which again is a conservative choice that ensures high mesh quality.

5. Semi-analytical discrete adjoint sensitivity analysis

The sensitivities are calculated using a semi-analytical discrete adjoint approach where the derivatives on a matrix level are performed with finite difference [21]. The adjoint equation can be formally stated as

$$\tilde{\mathbf{S}}^{\mathrm{T}}\boldsymbol{\lambda} = -\left(\frac{\partial\phi_0}{\partial\tilde{\mathbf{u}}_r} - i\frac{\partial\phi_0}{\partial\tilde{\mathbf{u}}_i}\right)^{\mathrm{T}}, \tag{23}$$

where $\boldsymbol{\lambda}$ is a vector containing the Lagrange multipliers and the subscripts r and i denotes the real and imaginary parts of the state vector, respectively. The adjoint equation is derived analytically as shown in [22]. Hereafter, the sensitivities are obtained as

$$\frac{\mathrm{d}\phi}{\mathrm{d}x_l} = \frac{\partial\phi_0}{\partial x_l} + \Re\left(\boldsymbol{\lambda}^{\mathrm{T}}\left(\frac{\partial\tilde{\mathbf{S}}}{\partial x_l} - \frac{\partial\mathbf{f}}{\partial x_l}\right)\right). \tag{24}$$

The terms $\frac{\partial\phi_0}{\partial x_l}$ and $\frac{\partial\mathbf{f}}{\partial x_l}$ vanishes and the expression is reduced to

$$\frac{\mathrm{d}\phi}{\mathrm{d}x_l} = \Re\left(\boldsymbol{\lambda}^{\mathrm{T}}\left(\frac{\partial\tilde{\mathbf{S}}}{\partial x_l}\right)\right), \tag{25}$$

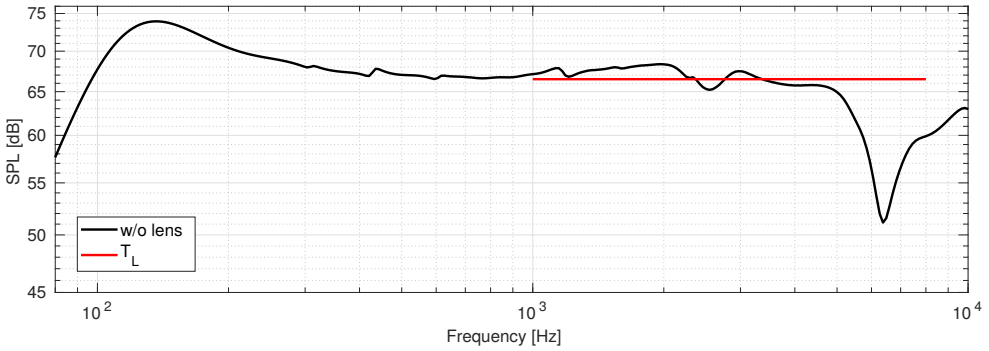

(a) No Lens

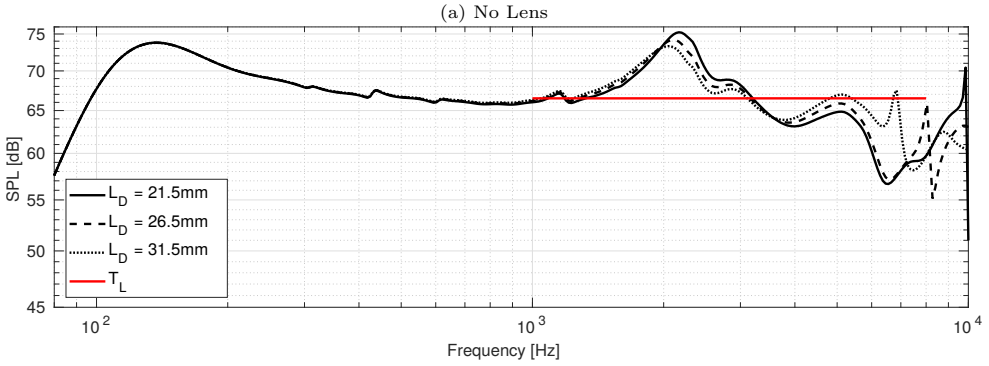

(b) Flat lens

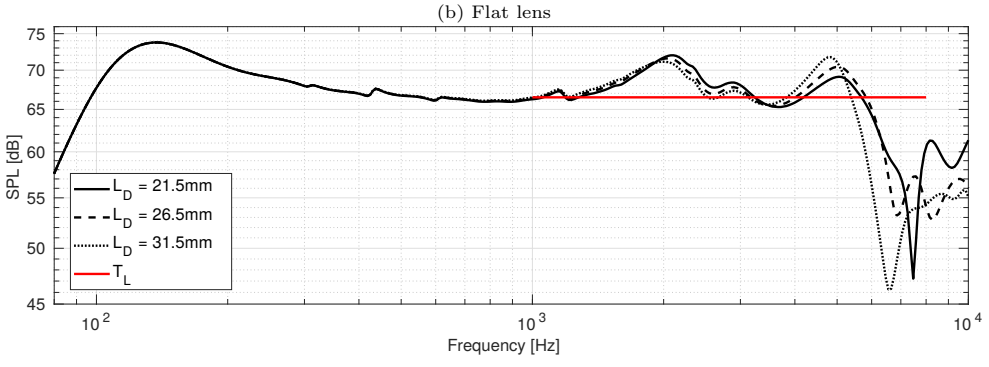

(c) Spatidate-shaped lens

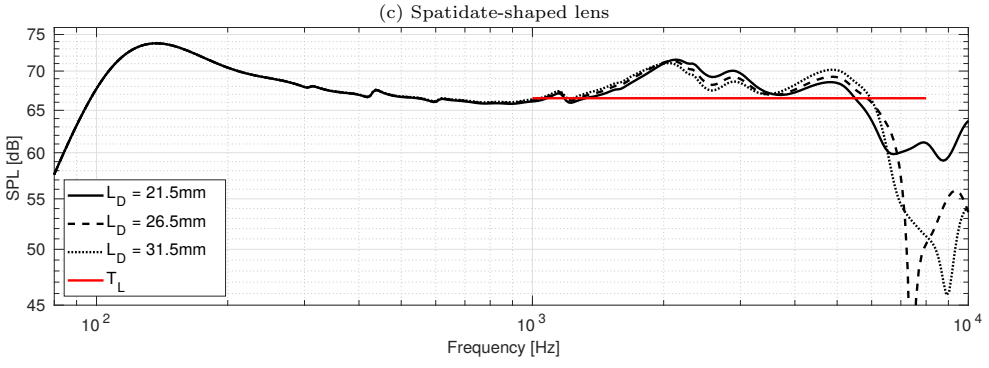

(d) Triangular-shaped lens

Figure 3: Frequency response in the frequency range of 800 Hz to 10 kHz 1 m away from the loudspeaker. (a) is the response for the speaker without a lens (b) is the response for the three starting guesses using a flat lens (c) is the response for the three starting guesses using a spatidate-shaped lens (d) is the response for the three starting guesses using a triangular shaped lens.

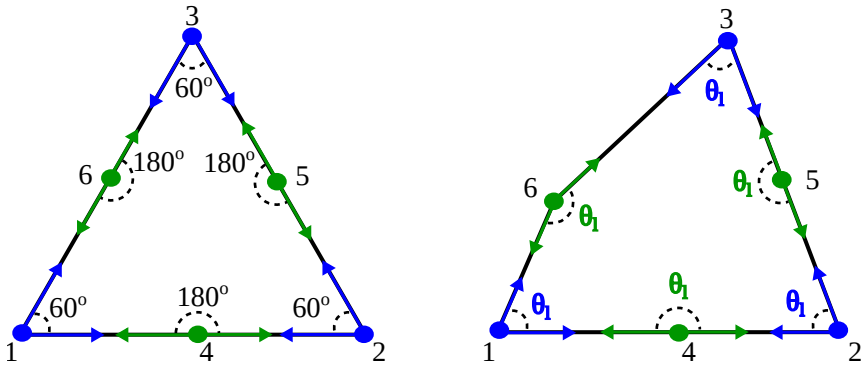

Figure 4: Sketch of an ideal 2nd order triangular element on the left hand side, right hand side shows a slightly deformed element due to a movement in the geometry. The angles that are measured to ensure element quality is shown, blue indicate angles with reference to 60°as and ideal angle and green has a reference angle of 180°.

where

$$\frac{\partial \tilde{\mathbf{S}}}{\partial x_l} = \frac{\partial \tilde{\mathbf{K}}}{\partial x_l} - \omega^2 \frac{\partial \tilde{\mathbf{M}}}{\partial x_l}.$$

The matrix derivative $\frac{\partial \mathbf{S}}{\partial x_l}$ is calculated semi-analytically using finite difference on a matrix level. This is done by perturbing each design variable with an adequately small number, h, here $h = 10^{-5}$ based on a study of the step size. From that, the matrix derivatives of $\tilde{\mathbf{K}}$ and $\tilde{\mathbf{M}}$ can be obtained.

6. Results

The final optimized design has shown to be highly dependent on the starting guess, which is not unusual for shape optimization. In order to find a feasible solution, several starting geometries have been investigated. These geometries are shown in Fig. 1 and consist of a flat lens, a spatidate-shaped lens, and a triangular lens. It was also realized that the optimized solution was dependent on the distance, L_D, from the woofer to the initial configuration of the acoustic lens. For each lens we consider three distances to the woofer, 21.5 mm, 26.5 mm, and 31.5 mm. The distance to the woofer is denoted L_D. Therefore, a study has been carried out to investigate lens designs as a function geometry, distance to the woofer, and frequency range for the design problem in Eq. (19). The lower bound of the frequency range is always 1 kHz. The upper bound, L_{up}, is variable such that we can investigate how wide a frequency range it is possible to achieve high-fidelity sound in. For each value of L_D an upper bound of 6 kHz, 7 kHz, and 8 kHz is used. This amounts to 9 optimizations per start geometry.

The dimensions of the FFD regions with Bernstein polynomials are shown in Fig. 1. The design domain $\Omega_{d,w}$ controls the shape of the down-firing woofer. The grid of control points consists of 5 rows and 10 columns, the control points are linearly spaced. In $\Omega_{d,l}$ the grid of control points consists of 11 columns and 9 rows. The control points on the boundary shared by $\Omega_{d,w}$ and $\Omega_{d,l}$ are inactive to avoid conflict between the two domains, which means that there are 103 active control points. This means that 206 design variables are used for the optimization as each control point has two design variables representing the movement of the point in the r and z-direction.

The material properties used in the FE-model are shown in Tab. 1. The passive radiator's material properties have been optimized to enhance the low frequency performance in [2]. These results are used in this paper.

Tab. 2 shows the values that are used to model the lumped components of the speaker. Here, M is the moving mass of the lumped mechanical components, L_E is the voice coil inductance, n is the fractional order derivative used to model the inductance including the losses in it, C_z is the compliance in the z-direction, C_r is the compliance in the r-direction, R_M is the mechanical damping, Bl is the force factor and R_E is the DC resistance in the voice coil wire. An AC voltage source, e_g, equal to 1V is applied to the speaker.

Table 1

	E [Pa]	ρ [kg/m^3]	η [−]	ν [−]
		Woofer		
Diaphragm	$10 \cdot 10^9$	1650	0.2	0.3
Surround	$40 \cdot 10^5$	1400	0.25	0.45
		Passive radiator		
Diaphragm	$10 \cdot 10^8$	2660	0.05	0.3
Surround	$37.2 \cdot 10^4$	2408	0.05	0.45

Table 2: Lumped parameters used to model the electric motor system, voice coil and spider.

M [kg]	L_E [mH]	n [−]	C_z [m/N]	C_r [m/N]	R [N · s/m]	Bl [T · m]	R_E [Ω]
0.0015	0.05	0.7	$1.0{\cdot}10^{-3}$	$5{\cdot}10^{-5}$	0.75	3.43	3.52

Table 3: Initital values of the objective function for all frequency ranges and starting configurations.

Initial configuration	L_{up}	L_D [mm]		
		21.5	26.5	31.5
Flat	6 kHz	$\phi = 86.97$	$\phi = 72.68$	$\phi = 56.94$
	7kHz	$\phi = 86.22$	$\phi = 72.49$	$\phi = 57.40$
	8 kHz	$\phi = 90.98$	$\phi = 69.04$	$\phi = 58.34$
Traditional	6 kHz	$\phi = 40.21$	$\phi = 33.84$	$\phi = 70.27$
	7kHz	$\phi = 53.33$	$\phi = 115.56$	$\phi = 334.32$
	8 kHz	$\phi = 282.83$	$\phi = 125.42$	$\phi = 293.44$
Inclined	6 kHz	$\phi = 33.90$	$\phi = 32.44$	$\phi = 28.45$
	7kHz	$\phi = 33.67$	$\phi = 50.04$	$\phi = 101.07$
	8 kHz	$\phi = 32.90$	$\phi = 747.10$	$\phi = 167.80$

The optimizations have been run on a cluster in parallel, the entire program is an in-house code that is build in Matlab. Each optimization corresponds to approximately 700 CPU hours. The initial objective function values for all the different starting guesses are shown in Tab. 3. Tab. 4 shows the optimized results and the corresponding objective function values for the design problem in Eq. (19) for the initial configuration with a flat lens. Each picture corresponds to a width of 5.2 cm and height of 5.8 cm in the computational model. In Tab. 5 the optimized results for the spatidate-shaped initial configuration is presented. Tab. 6 displays the optimized designs for the triangular-shaped starting configuration. Generally, the lens is considered a void region with respect to the optimization and is therefore not subject to any constraints. However, not imposing a constraint on the void region can, in some cases, lead to un-physical designs. Some of the designs collapsed, meaning that the top of the lens and the bottom of the lens overlapped. For these designs, the void region was meshed, and a constraint on the element quality was enforced similarly to Eq. (21) and Eq. (22). In Tab. 4 and Tab. 5 these designs are marked with *. The introduction of the meshed void region is avoided where possible as it restricts design freedom, and the mesh is essentially not required since no physics are computed within this region. The value $c_{60,max}$ in the void region are equal to 35 degrees and $c_{180,max}$ is 30 degrees. The collapse of the void region is especially pronounced for the flat lens with a small L_D as it seems to be a difficult design problem, probably caused by the start guess being bad since it is far from the optimal solution in which the lens should be angled.

The results for the flat lens as a starting guess is shown in Tab. 4. The table shows that these designs are affected by the starting guess of the lens. Many of the designs are, to some degree, still flat and are therefore not able to yield as good results as the other initial configurations. Several designs also suffer from collapsing, meaning that the lens's internal region has been meshed to circumvent this behavior. This underlines the fact that this particular starting guess yields a challenging optimization problem to solve, especially when the lens is close to the speaker. However, comparing the objective function values with the initial configurations shows that the optimized designs in all cases are improved with a factor of at least five.

The optimized results in Tab. 5 are made based on the initial configuration being spatidate-shaped. The optimized lens geometries are generally s-shaped and inclined downwards. This particular optimization setup seems to prefer the lens being rather close to the speaker as it is for these designs that the lowest values of ϕ_0 are present. This may be because the starting configuration is inclined where it is closest to the speaker. Generally, we can observe that for the optimized designs that the slope is steeper than for the initial configuration and that it continues along with the geometry. Furthermore, the lens is made shorter during the optimization. The optimized designs are improved significantly from between a factor of 6 up to almost 50. Note that the objective function value is based on the largest value of ϕ_k, so if an evaluation frequency is placed in a deep valley of the frequency response, this will yield a high ϕ_0.

The results in Tab. 6 shows the optimized results for the triangular-shaped initial configuration. The optimized geometries are all inclined, and the lens's length is, in this case, also shortened. Interestingly the designs optimized from the initial configuration with $L_D = 21.5$mm have a very distinct look. Here, a bump is present close to the z-axis. For progressively increasing L_D it is observed that this bump is reduced. The starting guess is giving a good starting point for the optimization, exemplified by the fact that there are no collapsed designs. However, the design in the frequency range of 1 kHz to 8 kHz with $L_D = 26.5$mm is not performing well compared to the other designs. This can be explained from the frequency response in Fig. 3d and the objective function value for this particular set-up in Tab. 3. Here, one evaluation frequency is placed in the profound valley at 7300 Hz, which yields an extraordinary high initial value for ϕ_0. This affects the start of the optimization, and this design has converged into a less feasible local minimum compared to all the other optimized designs. However, the rest of the designs' overall performance shows significant improvements compared to the initial configuration. Here, the objective function is minimized with a factor of 5 to a factor of almost 30.

The results in Tab. 4, 5 and 6 shows that the best performing designs displays a clear bias towards an inclined lens design. Different variations of the inclined lens are shown, such as the s-shaped design seen for most of the designs in Tab. 5, the inclined shape with or without a bump close to the z-axis for the results in Tab. 6. The shape of the woofer also shows a few trends, which seem to be derived from the location of the applied force. Generally, to the right of the applied force, the diaphragm appears to be angled more

Table 4: Optimized designs for flat initial configuration of the lens with three different frequency ranges included in the optimization and with the initial lens design placed at three different distances from the woofer. The red structure is the speaker, the white region below it is the lens and the blue domain is air.

Initial configuration	L_{up}	L_D [mm]		
		21.5	26.5	31.5
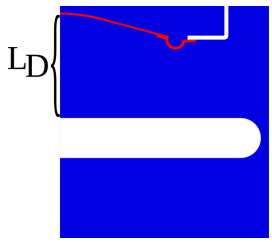	6 kHz	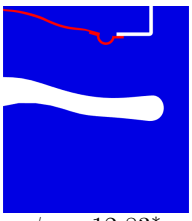 $\phi_0 = 12.83^*$	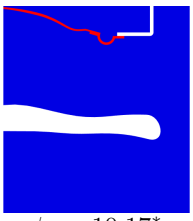 $\phi_0 = 10.17^*$	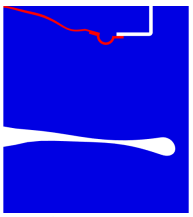 $\phi_0 = 5.89$
	7kHz	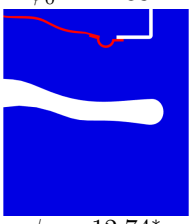 $\phi_0 = 12.74^*$	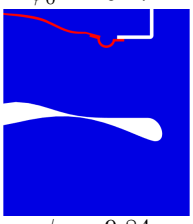 $\phi_0 = 9.84$	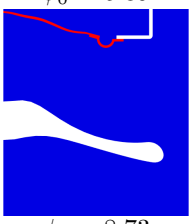 $\phi_0 = 8.73$
	8 kHz	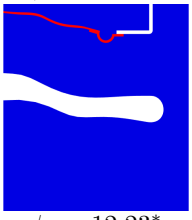 $\phi_0 = 12.23^*$	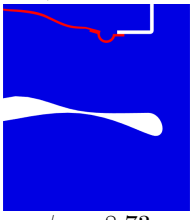 $\phi_0 = 8.73$	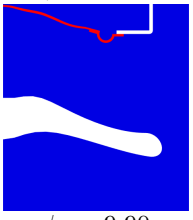 $\phi_0 = 9.90$

Table 5: Optimized designs for the spatidate-shaped initial configuration with three different frequency ranges included in the optimization and with the initial lens design placed at three different distances from the woofer. The red structure is the speaker, the white region below it is the lens and the blue domain is air.

Initial configuration	L_{up}	L_D [mm]		
		21.5	26.5	31.5
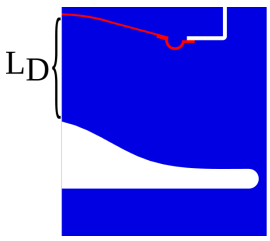	6 kHz	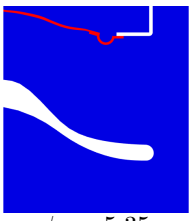 $\phi_0 = 5.35$	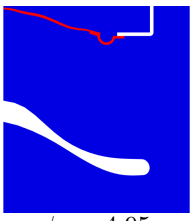 $\phi_0 = 4.95$	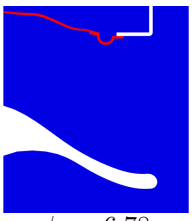 $\phi_0 = 6.78$
	7kHz	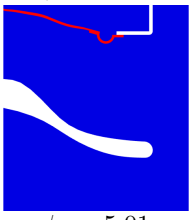 $\phi_0 = 5.01$	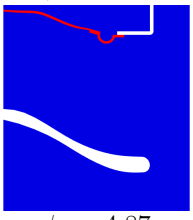 $\phi_0 = 4.87$	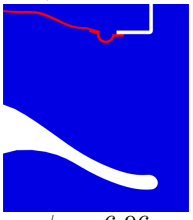 $\phi_0 = 6.96$
	8 kHz	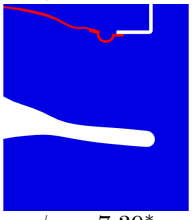 $\phi_0 = 7.39^*$	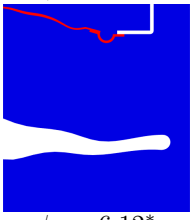 $\phi_0 = 6.12^*$	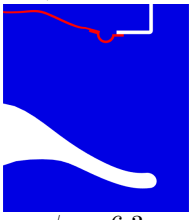 $\phi_0 = 6.3$

Table 6: Optimized designs for the triangular-shaped initial configuration with three different frequency ranges included in the optimization and with the initial lens design placed at three different distances from the woofer. The red structure is the speaker, the white region below it is the lens and the blue domain is air.

Initial configuration	L_{up}	L_D [mm]		
		21.5	26.5	31.5
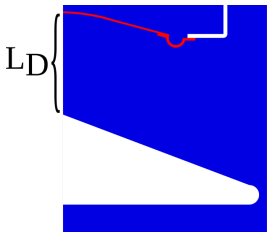	6 kHz	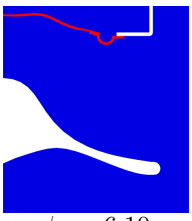 $\phi_0 = 6.10$	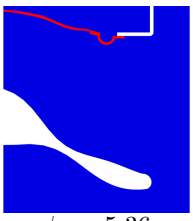 $\phi_0 = 5.36$	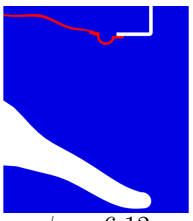 $\phi_0 = 6.12$
	7kHz	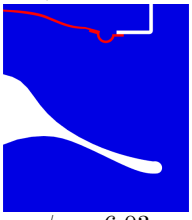 $\phi_0 = 6.03$	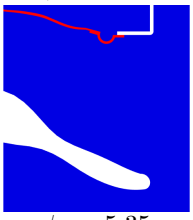 $\phi_0 = 5.35$	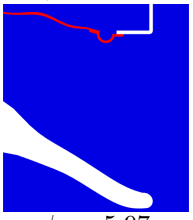 $\phi_0 = 5.97$
	8 kHz	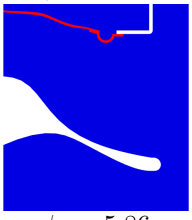 $\phi_0 = 5.86$	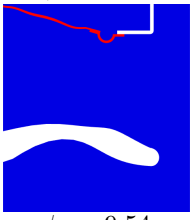 $\phi_0 = 9.54$	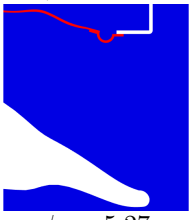 $\phi_0 = 5.27$

downwards, which increases the geometrical stiffness. The speaker is either unchanged or completely flat to the left of the applied force. This suggests that the optimizer tunes the speaker's shape dependent on the lens design or vice-versa.

6.1. Evaluation of Selected Optimized Designs

This section serves to give insight into the performance of the optimized designs, thereby making it possible to relate the objective function value to the designs' behavior in the frequency range for which they are optimized. We therefore examine one design for each frequency of the frequency ranges in Tab. 4, 5 and 6. The best design in the frequency range of 1k Hz to 6 kHz is found in Tab. 5 with $L_D = 26.5$ mm, for the frequency range of 1 kHz to 7 kHz the best design is in Tab. 5 also with $L_D = 26.5$ mm and for 1 kHz to 8 kHz the best design is in Tab. 6 with $L_D = 31.5$ mm.

The three optimized designs are evaluated by performing a frequency sweep. A zoom-in on the frequency range of interest is shown in Fig. 5. The low frequency range has been excluded as the change in the lens and woofer design has not affected the response in this frequency band. The figure shows four different responses. The dashed red curve is the initial speaker without an acoustic lens which serves to give a fair comparison of the quality of the optimized designs. The black curve is for the spatidate-shaped initial configuration with $L_D = 26.5$ mm and an optimization range of 1 kHz to 6 kHz. The black curve dips as it reaches the upper bound of 6 kHz indicated with the dashed black line. Within the frequency range of interest the curve is within ± 2.0 dB of the target line, thus yielding a flat frequency response up to 6 kHz. The blue curve is for a similar starting configuration with a frequency range of 1 kHz to 7 kHz included in the design problem. The coincidence of the blue and black curve's initial configuration manifests itself as the frequency response share many similarities. Interestingly, the blue curve shows the starting guess's full potential as it is revealed that the frequency range can be extended even further. Comparing this response to the black curve underlines the fact that the design problem is optimized for the specific conditions and constraints given. This design is able to yield a frequency response that is ± 2.5 dB from the target line in the range specified. One can note that the response is also well behaved at even higher frequencies. The magenta-colored curve spans a frequency range of 3 octaves (1 kHz to 8 kHz), and the initial shape is triangular with $L_D = 31.5$ mm. Even though this curve is made from a different starting guess it follows the blue curve up to around 2.5 kHz. This could be because they share the same speaker geometry; here the center is flat, as opposed to the black curve where the woofer's shape is closer to the initial configuration. Above 2.5 kHz the magenta curve differs from the two other curves. In the frequency range defined in the optimization, the largest deviations from the target line are ± 2.5 dB.

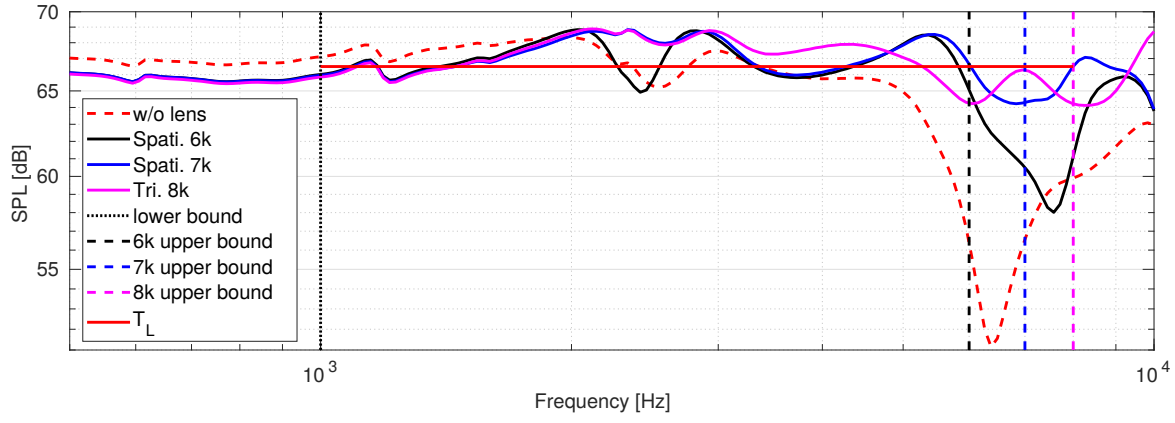

Figure 5: Frequency response of the optimized lenses. The frequency range of the plot is from 500 Hz to 10 kHz. The black curve is the best performing design in the frequency range 1 kHz to 6 kHz, the red curve is the best performing design in the frequency range 1 kHz to 7 kHz and the magenta curve is the best performing design in the frequency range 1 kHz to 8 kHz. The upper bound of each optimization is indicated with the same color scheme as the response curve. The target line used in the objective function is indicated with the red line.

As shown in Fig. 5, the formulated design problem can extend the loudspeaker's frequency range. The evaluated designs are able to maintain a flat frequency response with minor deviations in the ranges specified in the design problem. The improvements of the response yields a frequency response that is ± 2.5 dB from 90 Hz up to 10 kHz with only one 3 inch speaker and a passive radiator.

7. Discussion

The model problem presented in this work is 2D-axisymmetric. This simplification allows for a numerical model with reduced complexity which is necessary to carry out the optimization. The presented method uses 700 CPU hours for each optimization run and an extension of the model into 3D would increase this time tremendously. However, it should be pointed out that this simplified model does not consider asymmetric design features. That means that optimization can only come up with symmetric designs. The 2D-axisymmetric assumption also means that asymmetric vibration modes are not considered in this work. A 3D model would capture these effects and create better solutions, nevertheless, the computational burden is larger. The walls of the compact speaker are assumed rigid, as not to consider the contributions to the sound field from the vibrations of the cabinet. These vibrations would likely interfere with and pollute the frequency response. However, the purpose of this paper is to consider the design of the acoustic lens and the woofer. In that regard, the cabinet vibrations are not considered to be important. Cabinet design is an interesting engineering problem and affects sound quality, and it would be interesting to investigate this in the future.

In this work, different values of L_D is used to test different starting positions of the lens. This is partly due to restrictions regarding the flexibility of the mesh. Large deformations of the lens geometry requires immense efforts by the optimization algorithm in order to obey the implemented constraints on mesh quality. This could be solved with intermediate remeshing and resetting of the parameterization. However, this approach would then introduce inconsistency in the design sensitivities. The different starting guesses also ensures that a larger part of the solution space is investigated. The optimization problem is not convex and it features many nonfeasible local minimums. A diverse set of initial configurations ensures that some of the optimized designs converge to good global minimums. Despite the comprehensive study carried out it is not guaranteed that the best optimized designs are converged to a global minimum.

The presented optimization method relies on a global map between control points and the underlying geometry. This reduces the method's design freedom as the movement of a single point affects the entire geometry. If the optimization relied on a parameterized geometry, the design freedom would be greater as it can change the geometry locally. However, the increased design freedom would imply that more constraints should be imposed on the problem to avoid sharp features, collapsed elements, and collapsed geometries. The method proposed in this paper is, although it relies on a global mapping, able to produce simple, smooth, and well-performing designs.

8. Conclusion

The work presented introduces free form deformation as a tool that can be used for shape optimization of acoustic devices. The method relies on a global map of the underlying geometry to a series of control points, where the mapping is defined by bivariate Bernstein polynomials. The design sensitivities are calculated with a semi-analytical approach, where the adjoint equation is based on an analytically derived expression. The matrix derivatives used to compute design sensitivities are calculated with finite difference. An investigation of the starting guess's influence led to several good designs. It was shown that the final optimized design was highly dependent on the initial guess. The optimized designs for each initial configuration displayed unique features that were not present in optimized designs from different starting guesses. Generally, for this particular problem, it was exemplified that the starting guess needs to be inclined in order to yield a viable solution. The optimized designs showed that the proposed method was able to extend the frequency range of the compact speaker and maintain a flat response in the specified frequency range. The presented results show that it is possible to achieve an excellent wide band performance with different designs.

The proposed design method can be adapted for other types of problems with different configurations. It could be utilized to design an acoustic lens for a tweeter. Another application would be to design waveguides.

References

[1] Edison Research, NPR, The Smart Audio Report, Tech. rep. (02 2020).

[2] D. G. Nielsen, G.-T. Lee, Y.-H. Park, J. S. Jensen, F. T. Agerkvist, Optimization of the performance of small speaker systems with passive radiators, Proceedings of 49th International Congress and Exposition on Noise Control Engineering (2020).
URL https://internoise2020.org/

[3] J. A. Pedersen, G. Munch, Driver directivity control by sound redistribution, Audio Engineering Society Convention 113 (Oct 2002).
URL http://www.aes.org/e-lib/browse.cfm?elib=11277

[4] E. Wadbro, R. Udawalpola, M. Berggren, Shape and topology optimization of an acoustic hornlens combination, Journal of Computational and Applied Mathematics 234 (6) (2010) 1781–1787. doi:10.1016/j.cam.2009.08.028.

[5] E. Geddes, Acoustic lens, their design and application, Audio Eng Soc Prepr for 61st Conv (1980).

[6] M. W. Ferralli, D. Moulton, D. Brugger, J. White, S. Hebrock, Wide dispersion frequency invariant acoustic lens, Audio Engineering Society Preprint (1985).

[7] B. BERLANT, Loudspeaker directionality and the perception of reality, Journal of the Audio Engineering Society 33 (5) (1985) 342–350.

[8] A. Koshakji, A. Quarteroni, G. Rozza, Free form deformation techniques applied to 3d shape optimization problems, École polytechnique fédérale de Lausanne, MATHICSE Technical Report Nr. 44.2013 (2013).

[9] T. Sederberg, Free-form deformation of solid geometric models, Computer Graphics,Volume 20, Issue 4, pp 151-60 (1986).

[10] P. R. Andersen, V. Cutanda Henríquez, N. Aage, Shape optimization of micro-acoustic devices including viscous and thermal losses, Journal of Sound and Vibration 447 (2019) 120–136. doi:10.1016/j.jsv.2019.01.047.

[11] R. Udawalpola, Shape optimization for acoustic wave propagation problems (2010).

[12] C. B. Dilgen, S. B. Dilgen, N. Aage, J. S. Jensen, Topology optimization of acoustic mechanical interaction problems: a comparative review, Structural and Multidisciplinary Optimization 60 (2) (2019) 779–801. doi:10.1007/s00158-019-02236-4.

[13] A. Bezzola, Numerical optimization strategies for acoustic elements in loudspeaker design, 145th Audio Engineering Society International Convention, Aes 2018 (2018).

[14] R. Christensen, Shape and topology optimization of loudspeaker drivers, Comsol Conference Europe 2020 (2020).

[15] S. Degraeve, J. Oclee-Brown, Metamaterial absorber for loudspeaker enclosures, 148th Audio Engineering Society International Convention (2020).

[16] J. N. Li, S. X. Wang, H. J. Yin, C. H. Dong, H. M. Chen, Acoustic wave equation modeling in cylindrical coordinates with convolutional pml, 77th Eage Conference and Exhibition 2015: Earth Science for Energy and Environment (2015) 4546–4548doi:10.3997/2214-4609.201412461.

[17] F. Collino, P. Monk, The perfectly matched layer in curvilinear coordinates, Siam Journal of Scientific Computing 19 (6) (1998) 2061–2090. doi:10.1137/s1064827596301406.

[18] J. S. Jensen, Topology optimization problems for reflection and dissipation of elastic waves, Journal of Sound and Vibration 301 (1-2) (2007) 319–340. doi:10.1016/j.jsv.2006.10.004.

[19] D. G. Nielsen, P. R. Andersen, J. S. Jensen, F. T. Agerkvist, Estimation of optimal values for lumped elements in a finite element — lumped parameter model of a loudspeaker, Journal of Theoretical and Computational Acoustics 28 (02) (2020) 2050012. doi:10.1142/S2591728520500127.

[20] T. W. Sederberg, S. R. Parry, Free-form deformation of solid geometric models, Computer Graphics 20 (4) (1986) 151–60, 151–160. doi:10.1145/15886.15903.

[21] P. R. Andersen, J. Kook, V. Cutanda Henriquez, N. Aage, Towards large-scale acoustic shape optimization for industrial applications using the boundary element method, Noise-con Proceedings (2020).

[22] D. G. Nielsen, P. R. Andersen, J. S. Jensen, F. T. Agerkvist, Achieving a flat wide-band frequency response bynumerical optimization of a loudspeaker unit withrequirements for its directivity, The Journal of the Acoustical Society of AmericaTo appear in 2021 (2021).